MICROBIAL BIOACTIVE LIPIDS: THEIR IDENTIFICATION, BIOSYNTHESIS AND BIOCHEMISTRY

EDITED BY: Yuanda Song, Wanwipa Vongsangnak, Aidil Abdul Hamid and Xiao-Jun Ji

PUBLISHED IN: Frontiers in Nutrition

frontiers Research Topics

ISSN 1664-8714
ISBN 978-2-88976-973-5
DOI 10.3389/978-2-88976-973-5

About Frontiers

Frontiers is more than just an open-access publisher of scholarly articles: it is a pioneering approach to the world of academia, radically improving the way scholarly research is managed. The grand vision of Frontiers is a world where all people have an equal opportunity to seek, share and generate knowledge. Frontiers provides immediate and permanent online open access to all its publications, but this alone is not enough to realize our grand goals.

Frontiers Journal Series

The Frontiers Journal Series is a multi-tier and interdisciplinary set of open-access, online journals, promising a paradigm shift from the current review, selection and dissemination processes in academic publishing. All Frontiers journals are driven by researchers for researchers; therefore, they constitute a service to the scholarly community. At the same time, the Frontiers Journal Series operates on a revolutionary invention, the tiered publishing system, initially addressing specific communities of scholars, and gradually climbing up to broader public understanding, thus serving the interests of the lay society, too.

Dedication to Quality

Each Frontiers article is a landmark of the highest quality, thanks to genuinely collaborative interactions between authors and review editors, who include some of the world's best academicians. Research must be certified by peers before entering a stream of knowledge that may eventually reach the public - and shape society; therefore, Frontiers only applies the most rigorous and unbiased reviews.
Frontiers revolutionizes research publishing by freely delivering the most outstanding research, evaluated with no bias from both the academic and social point of view. By applying the most advanced information technologies, Frontiers is catapulting scholarly publishing into a new generation.

What are Frontiers Research Topics?

Frontiers Research Topics are very popular trademarks of the Frontiers Journals Series: they are collections of at least ten articles, all centered on a particular subject. With their unique mix of varied contributions from Original Research to Review Articles, Frontiers Research Topics unify the most influential researchers, the latest key findings and historical advances in a hot research area! Find out more on how to host your own Frontiers Research Topic or contribute to one as an author by contacting the Frontiers Editorial Office: frontiersin.org/about/contact

MICROBIAL BIOACTIVE LIPIDS: THEIR IDENTIFICATION, BIOSYNTHESIS AND BIOCHEMISTRY

Topic Editors:
Yuanda Song, Shandong University of Technology, China
Wanwipa Vongsangnak, Kasetsart University, Thailand
Aidil Abdul Hamid, National University of Malaysia, Malaysia
Xiao-Jun Ji, Nanjing Tech University, China

Citation: Song, Y., Vongsangnak, W., Hamid, A. A., Ji, X.-J., eds. (2022). Microbial Bioactive Lipids: Their Identification, Biosynthesis and Biochemistry. Lausanne: Frontiers Media SA. doi: 10.3389/978-2-88976-973-5

Table of Contents

frontiers in Nutrition

ORIGINAL RESEARCH
published: 13 October 2021
doi: 10.3389/fnut.2021.756218

Genetic Modification of *Mucor circinelloides* for Canthaxanthin Production by Heterologous Expression of β-carotene Ketolase Gene

Tahira Naz[1†], Junhuan Yang[1†], Shaista Nosheen[1], Caili Sun[1], Yusuf Nazir[1,2], Hassan Mohamed[1,3], Abu Bakr Ahmad Fazili[1], Samee Ullah[1,4], Shaoqi Li[1], Wu Yang[1], Victoriano Garre[5] and Yuanda Song[1]*

[1] Colin Ratledge Center for Microbial Lipids, School of Agricultural Engineering and Food Science, Shandong University of Technology, Zibo, China, [2] Department of Food Sciences, Faculty of Science and Technology, Universiti Kebangsaan Malaysia, Bangi, Malaysia, [3] Department of Botany and Microbiology, Faculty of Science, Al-Azhar University, Assiut, Egypt, [4] University Institute of Diet and Nutritional Sciences, Faculty of Allied Health Sciences, The University of Lahore, Lahore, Pakistan, [5] Departamento de Genética y Microbiología (Unidad asociada al Instituto de Química Física Rocasolano-Consejo Superior de Investigaciones Científicas (IQFR-CSIC)), Facultad de Biología, Universidad de Murcia, Murcia, Spain

OPEN ACCESS

Edited by:
Liguang Xu,
Jiangnan University, China

Reviewed by:
Enrique A. Iturriaga,
University of Salamanca, Spain
Yonghong Meng,
Shaanxi Normal University, China

***Correspondence:**
Yuanda Song
ysong@sdut.edu.cn

[†]These authors have contributed equally to this work

Specialty section:
This article was submitted to Food Chemistry, a section of the journal Frontiers in Nutrition

Received: *10 August 2021*
Accepted: *06 September 2021*
Published: *13 October 2021*

Citation:
Naz T, Yang J, Nosheen S, Sun C, Nazir Y, Mohamed H, Fazili ABA, Ullah S, Li S, Yang W, Garre V and Song Y (2021) Genetic Modification of Mucor circinelloides for Canthaxanthin Production by Heterologous Expression of β-carotene Ketolase Gene. Front. Nutr. 8:756218. doi: 10.3389/fnut.2021.756218

Canthaxanthin is a reddish-orange xanthophyll with strong antioxidant activity and higher bioavailability than carotenes, primarily used in food, cosmetics, aquaculture, and pharmaceutical industries. The spiking market for natural canthaxanthin promoted researchers toward genetic engineering of heterologous hosts for canthaxanthin production. *Mucor circinelloides* is a dimorphic fungus that produces β-carotene as the major carotenoid and is considered as a model organism for carotenogenic studies. In this study, canthaxanthin-producing *M. circinelloides* strain was developed by integrating the codon-optimized β-carotene ketolase gene (*bkt*) of the *Haematococcus pluvialis* into the genome of the fungus under the control of strong promoter *zrt1.* First, a basic plasmid was constructed to disrupt *crgA* gene, a negative regulator of carotene biosynthesis resulted in substantial β-carotene production, which served as the building block for canthaxanthin by further enzymatic reaction of the ketolase enzyme. The genetically engineered strain produced a significant amount (576 ± 28 μg/g) of canthaxanthin, which is the highest amount reported in *Mucor* to date. Moreover, the cell dry weight of the recombinant strain was also determined, producing up to more than 9.0 g/L, after 96 h. The mRNA expression level of *bkt* in the overexpressing strain was analyzed by RT-qPCR, which increased by 5.3-, 4.1-, and 3-folds at 24, 48, and 72 h, respectively, compared with the control strain. The canthaxanthin-producing *M. circinelloides* strain obtained in this study provided a basis for further improving the biotechnological production of canthaxanthin and suggested a useful approach for the construction of more valuable carotenoids, such as astaxanthin.

Keywords: *Mucor circinelloides*, *crgA*, canthaxanthin, β-carotene ketolase, overexpression

INTRODUCTION

Canthaxanthin is a valuable ketocarotenoid, which is naturally present in algae, bacteria, and some fungi (1). Canthaxanthin is also commonly present in wild bird tissue, egg yolk, crustaceans, and fish at low levels. It was first isolated as a major coloring pigment from the edible mushroom *Cantharellus cinnabarinus*, from where it was named canthaxanthin (2). It is formed as an intermediate compound in β-carotene metabolisms to astaxanthin. It has more effective antioxidant potential than β-carotene (3) due to which it is regarded as one among the important xanthophylls of commercial significance and has extensive utilization in industries (4). In the poultry industry, it is used as a feed additive to obtain red color in egg yolks and skins (1), while in the cosmetics industry, it is used as a pigmenting agent for human skin applications.

In the past few decades, the demand for canthaxanthin has increased owing to its beneficial properties on human health such as anticancer, anti-inflammatory, anti-dermatosis, and coloring agent (5). It has been documented as an effective protective agent against skin cancers in the laboratory for the treatment of polymorphous light eruptions and idiopathic photodermatosis (6). It can effectively stimulate the immune defensive system as compared to other carotenoid species (7) and owns excellent medicinal properties for treating rashes and itching. It is anticipated that the natural canthaxanthin market will grow from 75 million to 85 million from 2018 to 2024 with a compound annual growth rate (CAGR) of 3.5% due to change in consumer preferences toward fermentation products instead of synthetic compounds (https://www.gminsights.com/industry-analysis/canthaxanthin-market).

Canthaxanthin is produced by plants, bacteria, microalgae, and halophilic archaeon (*Haloferax alexandrines)* in relatively low concentrations, hence these organisms are unable to compete economically with synthetic canthaxanthin (8). Synthetic canthaxanthin is produced from petrochemicals and is widely preferred due to its low cost. The applicability of plant-based canthaxanthin is also hampered due to geographical, and seasonal variation and marketing. However, microbial production of canthaxanthin by biotechnological approaches is a major development in comparison to chemical synthesis due to safety concerns connected with chemical-based canthaxanthin.

Microbial production of carotenoid using non-native platforms are appealing due to many drawbacks associated with natural hosts such as low abundance and more sophisticated growth requirements, etc. *Mucor circinelloides* is a well-known model organism to study the molecular background of carotene biosynthesis in zygomycetes due to the availability of the whole-genome sequence. *M. circinelloides* has been reported as a natural competent organism compared to other related species and also acts as a good host for heterologous gene expression (9, 10). These attributes make *Mucor* an amenable candidate for genetic modification for desired and high-value products. Although β-carotene is the principal carotenoid of *M. circinelloides*, it has also shown weak β-carotene hydroxylase activity, because it has shown the accumulation of zeaxanthin and β-cryptoxanthin in minute amounts (11). It is possible to produce new carotenoids such as xanthophylls in *Mucor* by exogenous expression of genes involved in carotenogenesis. For example, Papp et al. introduced canthaxanthin-producing genes *crtW* from *Paracoccus* sp. N81106 into *M. circinelloides* (12). The subsequent transformants produced canthaxanthin and astaxanthin but in low amounts, which was attributed to the low copy number of autonomously replicating plasmids. To solve this problem they introduced *crtW* gene into the genome of *Mucor* to get stable expression of the ketolase gene and obtained a higher amount of canthaxanthin with canthaxanthin as the principal carotenoid (13).

The present study attempted to construct a canthaxanthin-producing cell factory by integrating the β-carotene ketolase–encoded gene (*bkt*) from *Haematococcus pluvialis* inside the genome of *M. circinelloides* CBS 277.49. Since precursor accumulation is considered as a prerequisite for xanthophyll production so in the present study higher β-carotene availability as a substrate for β-carotene ketose enzyme was ensured by disrupting the *crgA* locus, which is a negative regulator of the carotene biosynthesis pathway. Then codon-optimized gene of *bkt* from *H. pluvialis* was overexpressed under the control of strong promoter *zrt1*. Integration can be forced by the transformation with linear fragments that have extensive homologous regions at their ends to direct homologous recombination and gene replacement (13). Thus, this study attempted to construct a mutant of *M. circinelloides* CBS 277.49 strain harboring the algal *bkt* gene for canthaxanthin production.

MATERIALS AND METHODS

Strains, Media, and Growth Conditions

The double auxotroph (leucine and uracil) strain MU402 (14), derived from the wild-type *M. circinelloides* CBS277.49 was used as a recipient strain in all the transformation procedures. MU402 was grown on solid YPG media (3 g/L yeast extract, 10 g/L peptone, and 20 g/L glucose) at 28°C for 5–7 days to obtain spores for transformation. Transformants were grown on MMC media (10 g/L casamino acids, 0.5 g/L yeast nitrogen base (w/o amino acids), and 20 g/L glucose). Media were supplemented with uridine (200 μg m/L) when required. The pH was adjusted to 3 and 4.5 for colonial and mycelial growth, respectively.

For carotenoid extraction, all strains were initially grown by inoculating 100 μl of spore suspension ($\sim 10^7$ spores/mL) in 500 ml baffled flasks holding 150 ml Kendrick and Ratledge (K&R) medium for 24 h with 150 rpm at 28°C (15). Then these seed cultures were inoculated at 10% v/v into 2 L fermenters (BioFlo/CelliGen 115, New Brunswick Scientific, Edison, NJ, United States) containing 1.5 L modified K&R medium supplemented with 0.6 g/L of leucine to compensate leucine auxotrophy of transformants. Fermenters were maintained at 28°C with stirring at 700 rpm and aeration of 1 v/v per min and the pH was maintained at 6.0 by automatic addition of 2 M NaOH. All the transformants were cultivated for 4 days under continuous light. *Escherichia coli* strain DH5α was used for maintenance and amplification of recombinant plasmids and

grown in lysogeny broth (LB) containing 100 μg/ml ampicillin at 37°C and 220 rpm (16).

Construction of Recombinant Plasmids

According to the genomic data of *H. pluvialis* available at NCBI, the complete coding sequence of the β-carotene ketolase (GenBank accession No: AF534876.1) was synthesized by GeneWiz (GeneWiz, Suzhou, China). Codon optimization of the *bkt* genes was done according to the genome of *M. circinelloides* CBS 277.49 with the given GenBank accession number MZ020513 to increase the chances of successful expression. The codon-optimized sequence of *bkt* is given in **Supplementary File 1**. The gene sequence was provided in the modified vector, named pMAT1552+*bkt*. To disrupt *crgA* locus, a new basic plasmid was constructed and named pCRC53, which contained *pyrG* gene of *M. circinelloides* as a selection marker surrounded by 1 kb up- and down-stream of *crgA* sequences. The *pyrG* gene encodes orotidine 5′-phosphate decarboxylase and produces uridine to compensate uridine auxotrophy in *Mucor* and allows targeted genomic integration of the whole construct by homologous recombination. pCRC53 was used as a basic plasmid used for the generation of *bkt* overexpressing vector pCRC55. Plasmids used in the present study are listed in **Supplementary Table S1**.

For the construction of pCRC53, *crgA* gene (JGI accession number: 39344) with 1 kb up- and down-stream region was amplified from the genome of *M. circinelloides* CBS 277.49 by PCR using the primer pair F1/R1 (**Supplementary Table S2**). The *crgA* fragment was digested with *SphI* and *SnaBI* and the pUC18 vector was digested with *SmaI* and *SphI* restriction enzymes followed by ligation of these two linear fragments by T4 DNA ligase. From this ligated circular vector, *crgA* coding sequence was deleted by performing reverse PCR (RPCR) using primers F2/R2, resulting in a linear fragment of pUC18 that contained *crgA* up-and down-stream sequences. This linear fragment was then digested with *SpeI* and *SnaBI* restriction endonuclease. The *pyrG* fragment was amplified from the plasmid pMAT1552+bkt using primers F3/R3 and digested with *SmaI* and *SpeI*. Then both the digested fragments were ligated by T4 DNA ligase to make the basic plasmid pCRC53, which was used for the construction of recombinant plasmid pCRC55 carrying the *bkt* gene. For this, the joined *PzrtI* and *bkt* fragment was isolated from modified plasmid pMAT1552+*bkt* using primers F4/R4 as mentioned in **Supplementary Table S2**. Then pCRC53 was digested with *SpeI* and *XhoI*. The PCR amplified product containing joined *Pzrt1* and *bkt* was also digested with *SpeI* and *Xhol* and then ligated by T4 DNA ligase to obtain the final recombinant plasmid pCRC55. The chemically competent *E. coli* DH5α was used for maintaining and propagating recombinant plasmids during gene cloning experiments. The presence of recombinant plasmids in these *E. coli* cells was confirmed by DNA sequencing (Sangon Biotech, Shanghai Co., Ltd, China). The steps of the gene cloning strategy with the complete map of pCRC53 and pCRC55 are presented in **Figure 1**.

Both pCRC53 and pCRC55 were digested with *SmaI* and *AatII* to release 5.45 and 7.29 kb fragments, respectively, containing overexpression cassettes, which were used to transform MU402 double auxotrophic strain as described previously (17). In all the transformation experiments, transformants were selected based on auxotrophy complementation and change in color under dark conditions (18).

Transformation Experiment

For electroporation-mediated transformation, the previously described procedure was followed with some minor modifications (17). Fresh spores of double auxotrophic strain MU402, grown on YPG media for 5–7 days were harvested and nearly 12.5×10^7 spores were inoculated into 25 mL YPG media supplemented with uridine and leucine and placed at 4°C overnight without shaking and then incubated at 28°C at 200 rpm to get germinated spores (2–4 h). Germinated spores were recovered at room temperature by centrifugation at 1,100 rpm for 5 min and then washed with ice-cold phosphate buffer. For protoplast generation, germinated spores were resuspended in 5 ml of PS buffer treated with 0.3 μL chitosanase RD (C0794, Sigma–Aldrich) and 1 mg/mL lysing enzymes (L-1412; Sigma–Aldrich). Removal of the cell wall was assured by using a phase-contrast microscope to monitor the loss of cell wall-associated refringence in the protoplast. Then the prepared protoplasts were suspended in 800 μl of 0.5 M sorbitol, which could be used for electroporation of eight different transformations.

For electroporation, 4–10 μg of linear DNA fragment in a volume of 10–20 μL was added to 100 μL of protoplasts and electric pulse was applied by setting the following condition of electroporator: field strength of 0.8 kV, constant resistance of 400 Ω, and capacitance of 25 μF. After electroporation, 1 ml of ice-cold YPG was added immediately and the solution mixture was incubated at 26°C and 100 rpm for 1 h. Then centrifugation was done to recover protoplasts, followed by resuspension in 500 μl of YNB plus 0.5 M sorbitol and spreading on selective medium (MMC plus 0.5 M sorbitol). These plates were covered with aluminum foil and placed in an incubator at 28°C for 3–4 days.

Molecular Techniques

Extraction and purification of plasmid DNA were performed with the plasmid mini kit and cycle pure kit (Omega-Biotek, Norcross, United States). PCR products were purified using an Exbio PCR Product purification kit according to the instructions of the manufacturer. For the preparation of genomic DNA, mycelium was disrupted with a pestle and mortar in liquid nitrogen, and DNA was extracted using DNA quick Plant system kit (Tiangen Biotech Co., Ltd., Beijing, China) according to the instructions of the manufacturer. DNA fragments were purified from agarose gel using the Gel Extraction Kit (Omega Biotek, Norcross, United States).

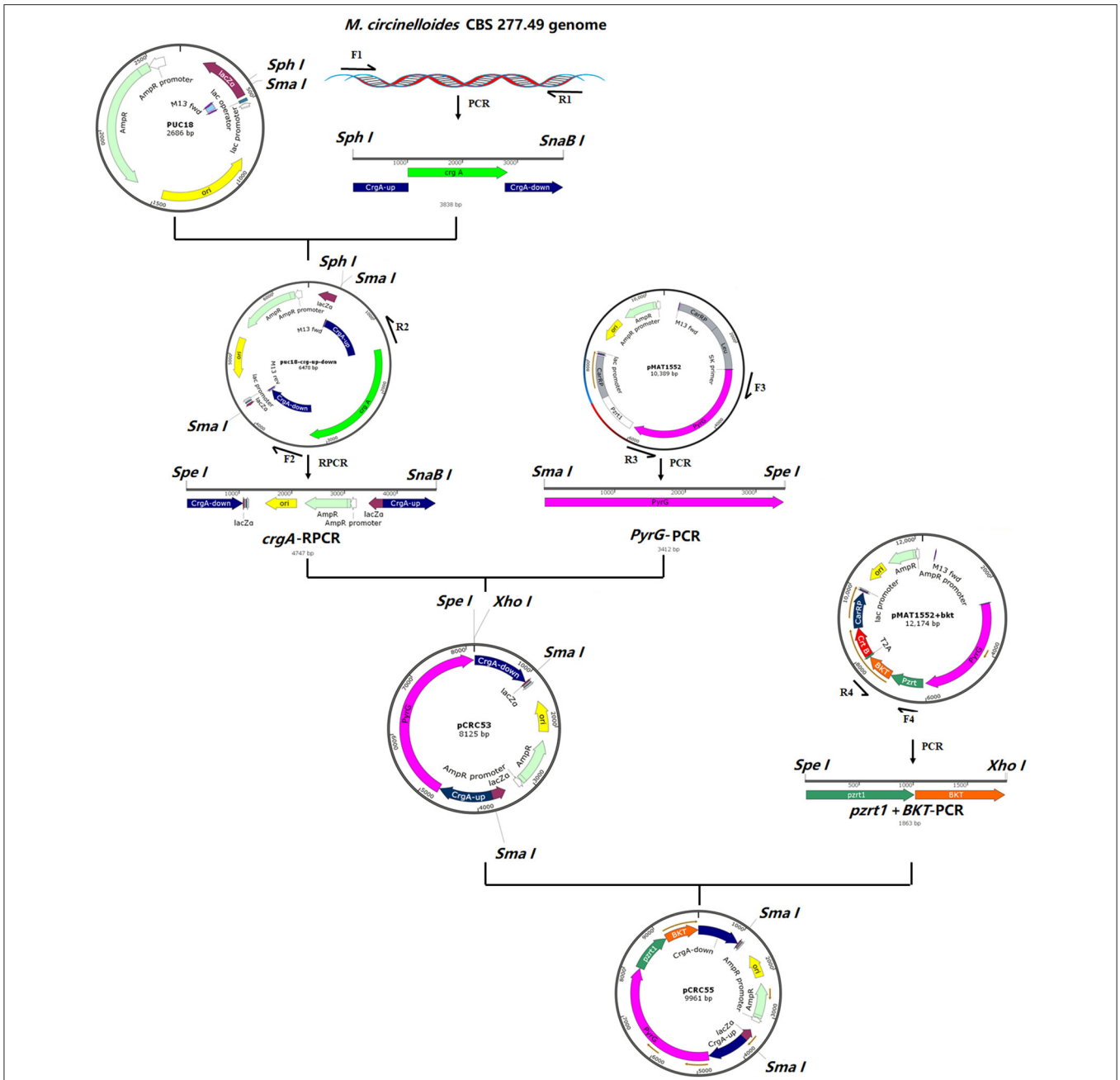

FIGURE 1 | The structure of plasmids pCRC53 and pCRC55. The gene *bkt* was isolated by PCR amplification with specific primers. The PCR fragments were ligated by T4 DNA ligation to generate these plasmids.

Determination of CDW, Glucose, and Nitrogen Concentration

Control and overexpressing strains were grown in a 2 L fermenter containing a 1.5 L modified K&R medium. Mycelia of both strains were collected at 3, 6, 9, 12, 24, 48, 72, and 96 h from the fermenters for analysis. Biomass was harvested on a dried and pre-weighed filter paper by filtration through a Buchner funnel under reduced pressure and washed three times with distilled water, frozen overnight at −80°C, and then freeze dried. The weight of the biomass was determined gravimetrically. A glucose oxidase Peridtest kit was used to determine the concentration of glucose in the culture media according to the instructions of the manufacturer (Shanghai Rongsheng Biotech Co., Ltd.). For ammonium concentration, the indophenol method was used (19).

Carotenoid Extraction and Quantification

Carotenoid was extracted as described in our previous study (20). High-performance liquid chromatography (HPLC) was performed for carotenoid quantification in samples. Samples in a volume of 10 μL were loaded on an infinity Lab Proshell 120 EC-C18 column (4.6 × 150, ODS 4 μm). Two solvents A (96% methanol) and B (100% methyl-terc-butyl ether) were used as mobile phase in the following gradient to analyze carotenoid: min/solvent A%/solvent B% was (0/99/1; 8/60/40; 13/46/54; 15/0/100; 18/0/100; 21/99/1; 25/99/1) at a flow rate of 1 ml/min. Column thermostat temperature was set as 35°C and detection wavelength was set as 450 nm, using a diode-array detector (Agilent Technologies, Santa Clara, CA, United States). The following standards were used to identify the carotenoids in transformants: β-carotene, canthaxanthin, astaxanthin, echinenone (Sigma–Aldrich). The total carotenoids were quantified by a spectrophotometer at 450 nm and measured using an extinction coefficient of 2,500 (A1% = 2,500) as previously described (21).

RNA Extraction and Analysis of Genes Expression

For RNA extraction, Mc-55 was grown in a 2 L fermenter with 1.5 L K&R media, and biomass were collected at 3, 24, 48, and 72 h. Total RNA was extracted by using TRIzol after disruption of biomass in pestle and mortar, using liquid nitrogen as described previously (22). RNA was reverse transcribed using the Prime ScriptRT reagent kit (Takara Biotechnology, Dalian Co., Ltd, Dalian, China) according to the instructions of the manufacturer. To investigate the expression levels of the canthaxanthin biosynthesis gene *bkt*, real-time quantitative PCR (RT-qPCR) was conducted using specifically designed primers (**Supplementary Table S2**) on Light Cycler 96 Instrument (Roche Diagnostics GmbH, Switzerland) with FastStart Universal SYBR Green Master (ROX) Supermix (Roche) according to the instructions of the manufacturer. The mRNA expression level was normalized to levels of actin gene and the results were determined as relative expression levels. The data were quantified by the method of $2-\Delta\Delta^{Ct}$.

Statistical Analysis

The mean values were calculated from the data obtained from three independent experiments. Statistical analysis was conducted by one-/two-way ANOVA with multiple comparison tests wheresoever applicable. These calculations were done by the GraphPad Prism software for Windows (San Diego, CA, United States) and $p < 0.05$ was considered as statistically significant.

RESULTS

Generation of *bkt* Overexpressing Strains of *M. circinelloides*

To overexpress the *bkt* gene in *M. circinelloides* CBS 277.49, an expression vector pCRC55 was constructed to allow targeted integration of *bkt* in the *crgA* locus. The strong promoter *zrt1* was used for the overexpression of *bkt* gene. Basic plasmid pCRC53 was constructed to disrupt *crgA* locus and act as a control plasmid to generate control strain Mc-53. Both basic pCRC53 and recombinant plasmids pCRC55 were digested with *SmaI* and *AatII* to obtain linear fragments. These linear fragments were then used to transform the recipient strain MU402 generating a control strain named Mc-53 and recombinant strain Mc-55, respectively. Two independent *bkt* overexpressing transformants, named Mc-55, Mc-55-1 were selected.

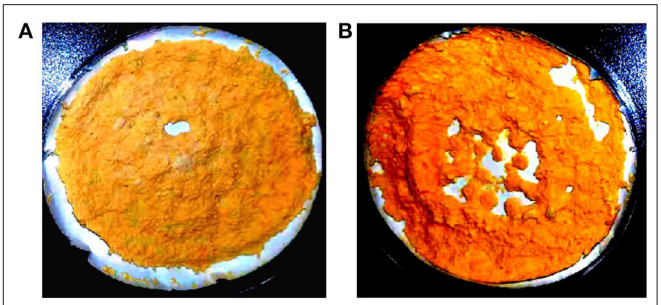

FIGURE 2 | Lyophilized samples of *Mucor circinelloides:* **(A)** control strain Mc-53 and **(B)** *bkt* overexpressing strain Mc-55 grown on K&R media.

Due to the syncytial nature of *Mucor* hyphae, and the multinucleate nature of protoplasts (23), and spores, heterokaryotic transformants were obtained initially. Therefore, transformants were grown on selective media for several consecutive vegetative cycles to obtain stable *pyrG*+ transformants. After more than 10 vegetative cycles, homokaryotic transformants were obtained for both the linear fragments of plasmids pCRC53 and pCRC55. The successful expression of *bkt* gene in *M. circinelloides* was confirmed by the accumulation of ketocarotenoids such as echinenone, canthaxanthin, and astaxanthin in small amounts. Gene replacement in the *crgA* locus resulted in deep yellow colonies that are recognizable among the pale-yellow colonies of wild-type *M. circinelloides* in dark. This color change was an indication of a higher amount of β-carotene accumulation due to disruption of *crgA* gene locus, resulting in deep yellow mycelia for control strain Mc-53 and reddish-orange in case of overexpressing strain Mc-55 in dark (**Figure 2**). Lack of *crgA* function is associated with enhanced production of carotene under both light and dark conditions (24).

The integration of the exogenous gene in all transformants was confirmed by PCR amplification using primers (Ch-F1/R1 and Ch-F2/R2) listed in **Supplementary Table S2**. Genomic DNA was used as a template. The first primer pair (Ch-F1/R1) was designed in such a way that it could amplify few base pairs (bp) beyond *crgA* 1 kb upstream (inside genome) to some portion of *pyrG* (**Figure 3A**). This primer pair amplified the expected size, 1,513 bp sequence from up-streams of *crgA* verifying the presence of marker *PyrG* inside the genome. The same band size was also obtained for Mc-53 as our control strain also contained *pyrG* selection marker (**Figure 3B**). The other primer pair (Ch-F2/R2) was designed to amplify a region of 54 bp beyond *crgA* 1 kb downstream to almost half of the segment of the exogenous *bkt* gene. Amplification reaction produced an expected 1,533 bp

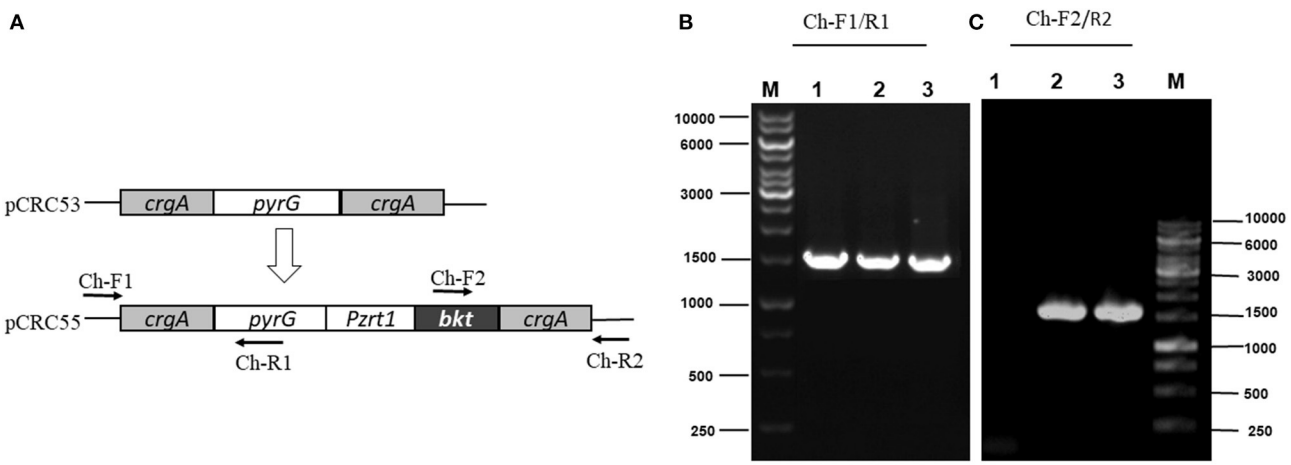

FIGURE 3 | PCR amplification of genomic DNA of control (Mc-53) and recombinant strains (Mc-55) with the indicated primers. Lane 1 representing the control strain and Lane 2, 3 showing the presence of *bkt* in recombinant strains Mc-55 and Mc-55-1, respectively. **(A)** Plasmid structure of pCRC53 and pCRC55 for *bkt* overexpression. **(B)** Verification of the presence of marker *pyrG* inside transformants. Lane M: Marker, 1: control strain, 2-3: Recombinant strains (Ch-F1/R1primers). **(C)** Verification of the presence of *bkt* inside transformants. Lane M: Marker, 1: control strain, 2-3: Recombinant strains (Ch-F2/R2 primers).

fragment as shown in **Figure 3C**, which confirmed the presence of *bkt* gene inside the overexpressing strain Mc-55 while no fragment was amplified for control strain Mc-53 (**Figure 3C**). Thus, PCR amplification results confirmed the integration of the target gene into the genome of the transformants. The presence of a single band indicated the homokaryotic nature of the transformants.

Two overexpression strains Mc-55, Mc-55-1, and one control strain Mc-53 were grown in 150 mL K&R medium for 3–4 days in 500 ml baffled flasks to perform additional screening. Since CDW and canthaxanthin of these two strains were comparable (data not shown), only one strain Mc-55 was selected for further experiments.

Growth of *bkt* Overexpressing Strain

CDW and consumption of ammonium and glucose by Mc-55 were analyzed and compared with control strain Mc-53 as shown in **Figure 4**. In general, both the control and the recombinant strain showed a similar and typical growth profile. Ammonium was completely exhausted in 12–24 h in Mc-55 but it was consumed more rapidly by the control strain Mc-53, while glucose remained in sufficient amount during the entire fermentation time (**Figures 4A,B**). CDW was increased rapidly until 24 h and slowed down (**Figure 4C**). However, cell growth was slightly affected in both strains as compared to wild-type CBS 277.49, which might be attributed to *crgA* disruption in these strains.

Carotenoid Accumulation in *bkt* Overexpressing Strain

Detailed carotenoid profile of recombinant strain is presented in **Table 1**. The mycelia were collected from fermenters at the specified intervals and disrupted using pestle and mortar into fine powder for carotenoid extraction. HPLC analysis showed β-carotene, canthaxanthin, echinenone as major carotenoids in Mc-55. While in the control strain only β-carotene was observed as a major carotenoid, verifying that *bkt* gene was successfully expressed in Mc-55. Nevertheless, the control strain Mc-53 produced an elevated level of β-carotene (2211 ± 47 μg/g of CDW), which was 8-folds higher as compared to recipient strain MU402, that could only produce 275 ± 13 μg/g of β-carotene under the same cultivation condition (data not shown). This substantial increase in β-carotene production could be possible due to *crgA* disruption in Mc-53 since disruption of *crgA* caused over-accumulation of β-carotene even in dark by increasing the mRNA levels of *carB* and *carRP* (24).

Overexpression of the algal *bkt* in the Mc-55 gene led to the production of ketoderivatives (**Figure 5**). The accumulation of canthaxanthin started at 6 h and substantially increased with the progress of cultivation time. Mc-55 produced the maximum amount of canthaxanthin at 72 h. Other measured carotenoids and total carotenoids also showed the same trend. The highest amount of canthaxanthin (576 ± 28 μg/g) and echinenone (410 ± 29 μg/g) and a comparatively small amount of astaxanthin (41 ± 2.3 μg/g) were produced, which corresponded to 32, 23, and 3% of total carotenoid in Mc-55 at 72 h, respectively. This significant amount of canthaxanthin production might be possible in the current study due to the availability of a higher amount of β-carotene substrate as it is the closest intermediate to canthaxanthin in the introduced pathway (**Figure 5**).

The Expression Level of *bkt* Gene in Overexpressing Strain

The mRNA expression level of *bkt* in overexpressing strain Mc-55 was analyzed by RT-qPCR at specified intervals. In control strain Mc-53, the mRNA level of *bkt* was undetectable throughout the culture time. The mRNA expression level of Mc-55 was considered as 1 at 3 h, and by comparing with this value the

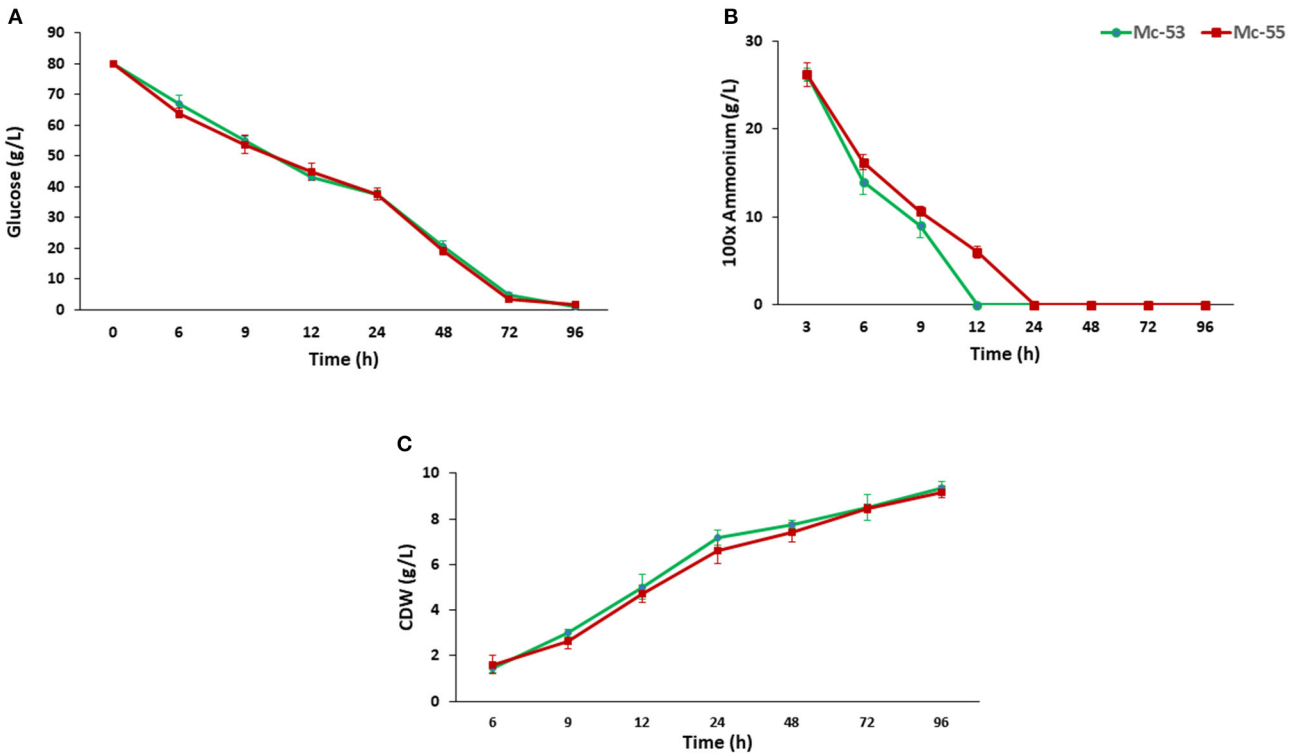

FIGURE 4 | Determination of glucose and nitrogen consumption and cell CDW in recombinant strain Mc-55 and control strain Mc-53 at indicated time intervals. **(A)** Glucose concentration, **(B)** ammonium concentration, and **(C)** CDW. Values were the mean of three independent experiments. Error bars represent the standard deviation of the data.

TABLE 1 | Total carotenoid content and major carotenoid composition of control Mc-53 and recombinant Mc-55 strains.

Time (h)	β-Carotene	Echinenone	Canthaxanthin	Astaxanthin	Total carotenoids
Mc-53					
6	169 ± 13	–	–	–	254 ± 44
9	290 ± 28	–	–	–	388 ± 28
12	523 ± 16	–	–	–	701 ± 16
24	952 ± 25	–	–	–	1197 ± 73
48	1,673 ± 40	–	–	–	1877 ± 45
72	2211 ± 47	–	–	–	2495 ± 56
96	2167 ± 16	–	–	–	2424 ± 37
Mc-55					
6	33 ± 14	61 ± 9	63 ± 13	2 ± 0.9	291 ± 48
9	54 ± 22	87 ± 15	105 ± 22	5 ± 1	440 ± 36
12	118 ± 12	143 ± 8	178 ± 29	8 ± 1.3	611 ± 32
24	207 ± 22	244 ± 30	381 ± 23	14 ± 1.4	985 ± 26
48	324 ± 21	359 ± 25	507 ± 12	27 ± 1.8	1470 ± 54
72	422 ± 23	410 ± 29	576 ± 28	41 ± 2.3	1789 ± 47
96	391 ± 14	403 ± 25	556 ± 13	38 ± 2.2	1743 ± 31

The indicated amounts are average values in μg/g of cell dry weight from the data of three independent experiments. Carotenoid extraction was carried out after cultivation of the strains in K&R media for 4 days at 28°C under continuous light.

expression level was determined at other time intervals. The expression level of Mc-55 was quickly increased at the start of fermentation till 24 h but showed a decreasing trend afterward. It was observed that the expression level of *bkt* was increased by 5.3-, 4.1-, and 3-folds at 24, 48, and 72 h, respectively, and maintained at elevated levels throughout the cultivation

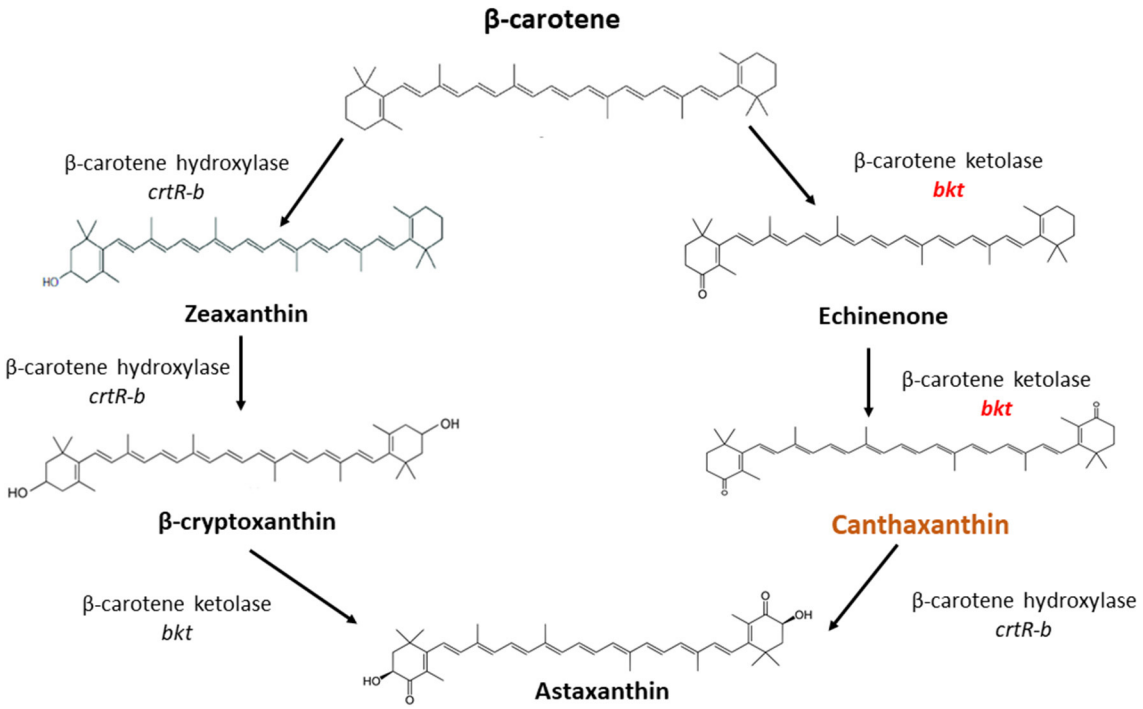

FIGURE 5 | The possible pathway for conversion of β-carotene to canthaxanthin and astaxanthin in *M. circinelloides* as proposed by Misawa et al. (25).

time, suggesting that it was overexpressed successfully in Mc-55 (**Figure 6**).

DISCUSSION

In *M. circinelloides* β-carotene is produced as a major carotenoid *via* the mevalonate pathway along with a lower amount of zeaxanthin and β-cryptoxanthin due to weak hydroxylase activity. However, no astaxanthin could be produced due to the absence of ketolase enzymes (11). β-carotene can be further converted into canthaxanthin by β-carotene ketolase encoded by gene *bkt* in algae and *crtW* in bacteria, which add keto group in the ring of β-carotene at 4,4-position. The efficient conversion of β-carotene into canthaxanthin depends on the ketolase enzyme with higher catalytic activity. *Haematococcus pluvialis* is a marine, astaxanthin producing algae, in which the conversion of β-carotene to astaxanthin is carried out by the enzymes β-carotene ketolase and hydroxylase with canthaxanthin as an intermediate compound (**Figure 5**). *Haematococcus pluvialis*, being a natural source of valuable xanthophylls, is grown for ketocarotenoid production, but commercial-scale cultivation of this algae is embedded with few drawbacks. For example, high light requirement, slow growth at room temperature, as well as vulnerable to contamination by other algae (26). Over the past two decades, *M. circinelloides* has been successfully engineered for various useful metabolites by either overexpressing indigenous genes or by introducing the exogenous biosynthetic genes (11, 27–30).

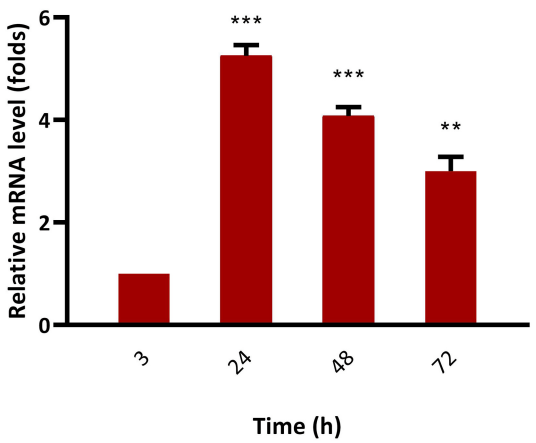

FIGURE 6 | Determination of expression levels of *bkt* genes by RT-qPCR in the overexpressing strains Mc-55. Values were the mean of three independent experiments. Error bars represent the standard deviation of the data. Asterisks indicate that the difference is significant.***$p < 0.001$ in comparison between 3, 24, and 48 h, and **$p < 0.01$ in comparison between 24, 48, and 72 h of growth.

In the present study, *bkt* gene from *H. pluvialis* was successfully overexpressed in *M. circinelloides* under the control of strong promoter *zrt1* to construct the canthaxanthin biosynthesis pathway. The successful integration of *bkt* was indicated by the accumulation of ketocarotenoid in Mc-55,

producing ∼576 ± 28 μg/g canthaxanthin, which is the highest titer of canthaxanthin ever reported in *M. circinelloides*. This amount was almost 3-folds more than the canthaxanthin content of the wild-type strain of *Gordonia jacobaea* (200 μg/g) (31), but almost comparable with 600 μg/g of canthaxanthin *in Brevibacterium* KY-4313 (32), both of them are considered as a natural source of canthaxanthin. Similarly, the bacterium *Dietza natronolimnaea* HS-1 was reported to produce a maximum of 8,923 ± 18 μg/L canthaxanthin in a fed-batch process (33). Previously, Papp et al. had successfully engineered *crtW* gene in *M. circinelloides* from marine bacterium but the amount of canthaxanthin produced was very low, i.e., 6–13 μg/g (12). The transformants obtained in our study accumulated a significantly higher amount of canthaxanthin than that obtained by a previous study in which a maximum of 443 ± 71 μg/g canthaxanthin was produced by *Mucor* after co-expression of *crtW and crtZ* and cultivation of the mutant strain on the combination of glucose and dihydroxyacetone (34). Similarly, in another report overexpression of *crtW* gene from *Paracoccus* into *M. circinelloides* produced a maximum amount of canthaxanthin in the range of 100–240 μg/g after genetic modification and medium optimization (13). Csernetics et al. also introduced two genes *crtR* and *crtS* from the yeast *Xanthophyllomyces dendrorhous* in *M. circinelloides,* which are responsible for the conversion of β-carotene to astaxanthin. After laborious genetic modification, a maximum of 190 μg/g of canthaxanthin was produced in a mutant strain of *M. circinelloides* (29). So, the higher production of canthaxanthin could be attributed to the higher catalytic efficiency of *bkt* from an algal source in comparison to its bacterial and yeast counterpart.

However, control strain Mc-53 in the present study showed superior production of β-carotene up to 2211 ± 47 μg/g in the fermenter at 72 h with increased total carotenoid as compared to *bkt* overexpressing strain Mc-55 (**Table 1**). In overexpressing strain Mc-55, the concentration of β-carotene was drastically reduced to 422 ± 23 at 72 h which might be attributed to the conversion of β-carotene into ketocarotenoids such as echinenone and canthaxanthin. This could also be explained as a possible feedback effect of β-carotene and its derivatives produced during the β-carotene biosynthesis. So, it might be possible that β-carotene production has decreased in Mc-55 due to its conversion into canthaxanthin and affected the functioning of genes involved in carotenogenesis (13).

The successful overexpression of the *bkt* gene from an algal source was also verified by RT-qPCR. The result showed that mRNA levels of the *bkt* gene remained elevated throughout the fermentation time. The expression level of *bkt* showed maximum expression reaching up to 5.3-folds at 24 h after which a decrease in the expression level was observed. However, the maximum production of canthaxanthin was achieved in our study at 72 h, which might be explained as *bkt* gene regulated the canthaxanthin accumulation by post-transcriptional or post-translational regulatory processes (35).

In our study, the higher canthaxanthin production might be possible because of two reasons (1): The expression of codon-optimized *bkt* gene under the control of strong promoter *zrt1*; (2): Availability of a high amount of β-carotene precursor, achieved by the disruption of *crgA*, a well-known repressor of carotenogenesis (24). Codon optimization of the algal *bkt* gene was done with the codon preference of *M. circinelloides.* Zhou et al. also used codon-optimized genes for astaxanthin synthesis by *Saccharomyces cerevisiae* and found increased expression levels of *bkt* and *crtZ* (36) as compared to the non-optimized aforementioned gene sequence. Moreover, it is well-known from the literature that initial astaxanthin synthesis utilizes the existing β-carotene as a precursor, so the production of the bulk astaxanthin esters depends on *de novo* β-carotene synthesis (37). *CrgA* is identified as a repressor of carotenoid biosynthesis in *M. circinelloides* because disruption of *crgA* caused over-accumulation of β-carotene even in dark by increasing the mRNA levels of structural carotenogenic genes, that is, *carB* and *carRP* (24). The *crgA* gene suppresses carotenoid biosynthesis in *Mucor* by proteolysis-independent mono-ubiquitilation and di-ubiquitilation of white collar *wc-1b*, which triggers the transcription of *carB* and *carRP* genes when non-ubiquitilated (38). A previous study has also shown that the deletion of *crgA* resulted in higher lycopene accumulation in mutant *M. circinelloides* strain (39). Similarly, Zhang et al. found that disruption of *crgA* caused over-accumulation of β-carotene in mutant strains of *M. circinelloides* (18).

The canthaxanthin-producing strain of *M. circinelloides* obtained in our study can be a strong putative candidate for industrial production because of two main reasons; first, the fermentation process using *M. circinelloides* would be much simpler than the complicated growth requirement of *H. pluvialis*. Second, dimorphic nature favors its biotechnological application. The highest canthaxanthin production of 576 ± 28 μg/g was achieved in *Mucor*, which is the maximum reported canthaxanthin in *Mucor* to date. This study can be regarded as a good extension of previous genetic modifications done in *M. circinelloides* for canthaxanthin production. In conclusion, canthaxanthin production in our recombinant strain could be further augmented by improving cultivation conditions or by employing a fed-batch process to enhance the biomass productivity for the volumetric production of canthaxanthin. Genetic engineering of early steps of the mevalonate pathway to increase the supply of rate-limiting precursor, suppressing the competitive fatty acid and sterol biosynthesis pathway, and improving the fermentation process could be attractive strategies for future improvement of canthaxanthin production in the obtained recombinant strains of *M. circinelloides.*

DATA AVAILABILITY STATEMENT

All data generated or analyzed during this study are included in this published article and its **Supplementary Material**.

AUTHOR CONTRIBUTIONS

TN and JY performed the experiments and manuscript writing. SN worked in experimental design. CS reviewed the initial draft and helped in editing. YN and HM were involved in the experimental design and data analysis. AF and SL helped with

the HPLC analysis and quantification. SU helped in statistical analysis. WY helped in drawing images. VG involved in results interpretations. YS proposed the project and was involved in data analysis, and review of the final draft. All authors read and approved the final manuscript.

FUNDING

This work was supported by the National Natural Science Foundation of China (Grant Nos. 31670064 and 31972851), the TaiShan Industrial Experts Program tscy 20160101, and the Shandong provincial key technology R&D plan (2018GNC110039, 2018GSF121013).

ACKNOWLEDGMENTS

We would like to thank Faiza Asghar, Kiren Mustafa, Hafiy Halim, and Pranesha for their assistance during fermentation and RNA extraction and Atif Taj for careful reading of the manuscript and discussions.

SUPPLEMENTARY MATERIAL

The Supplementary Material for this article can be found online at: https://www.frontiersin.org/articles/10.3389/fnut.2021.756218/full#supplementary-material

REFERENCES

1. Esatbeyoglu T, Rimbach G. Canthaxanthin: from molecule to function. *Mol Nutr Food Res.* (2017) 61:1600469. doi: 10.1002/mnfr.201600469
2. Haxo F. Carotenoids of the mushroom *Cantharellus cinnabarinus*. *Bot Gaz.* (1950) 112:228–32. doi: 10.1086/335653
3. Naguib Y. Pioneering astaxanthin. *Nutr Sci News.* (2001) 1–6. Available online at: https://chiro.org/nutrition/FULL/Pioneering_Astaxanthin.shtm
4. Perera CO, Yen GM. Functional properties of carotenoids in human health. *Int J Food Prop.* (2007) 10:201–30. doi: 10.1080/10942910601045271
5. Chan KC, Mong MC, Yin MC. Antioxidative and anti-inflammatory neuroprotective effects of astaxanthin and canthaxanthin in nerve growth factor differentiated PC12 cells. *J Food Sci.* (2009) 74:H225–31. doi: 10.1111/j.1750-3841.2009.01274.x
6. Santamaria L, Bianchi A, Arnaboldi A, Ravetto C, Bianchi L, Pizzala R, et al. Chemoprevention of indirect and direct chemical carcinogenesis by carotenoids as oxygen radical quenchers. *Ann NY Acad Sci.* (1988) 534:584–96. doi: 10.1111/j.1749-6632.1988.tb30149.x
7. Jyonouchi H, Sun S, Mizokami M, Gross MD. Effects of various carotenoids on cloned, effector-stage T-helper cell activity. *Nutr Cancer.* (1996) 26:313–24. doi: 10.1080/01635589609514487
8. Sanchez S, Ruiz B, Rodríguez-Sanoja R, Flores-Cotera LB. Microbial production of carotenoids. In: McNeil B, Archer D, Giavasis I, Harvey L, editors. *Microbial Production of Food Ingredients, Enzymes and Nutraceuticals*. Mexico: Elsevier; Woodhead Publishing (2013). p. 194–233.
9. Iturriaga EA, Díaz-Mínguez JM, Benito EP, Alvarez MI, Eslava AP. Heterologous transformation of *Mucor circinelloides* with the *Phycomyces blakesleeanus leul* gene. *Curr Genet.* (1992) 21:215–23. doi: 10.1007/BF00336844
10. Garre V, Barredo JL, Iturriaga EA. Transformation of *Mucor circinelloides f. lusitanicus* Protoplasts. In: *Genetic Transformation Systems in Fungi*. Cham: Springer (2015). p. 49–59.
11. Csernetics Á, Nagy G, Iturriaga EA, Szekeres A, Eslava AP, Vágvölgyi C, et al. Expression of three isoprenoid biosynthesis genes and their effects on the carotenoid production of the zygomycete *Mucor circinelloides*. *Fungal Genet Biol.* (2011) 48:696–703. doi: 10.1016/j.fgb.2011.03.006
12. Papp T, Velayos A, Bartók T, Eslava AP, Vágvölgyi C, Iturriaga EA. Heterologous expression of astaxanthin biosynthesis genes in *Mucor circinelloides*. *Appl Microbiol Biotechnol.* (2006) 69:526–31. doi: 10.1007/s00253-005-0026-6
13. Papp T, Csernetics Á, Nagy G, Bencsik O, Iturriaga EA, Eslava AP, et al. Canthaxanthin production with modified *Mucor circinelloides* strains. *Appl Microbiol Biotechnol.* (2013) 97:4937–50. doi: 10.1007/s00253-012-4610-2
14. Benito EP, Díaz-Mínguez JM, Iturriaga EA, Campuzano V, Eslava AP. Cloning and sequence analysis of the *Mucor circinelloides* pyrG gene encoding orotidine-5′-monophosphate decarboxylase: use of *pyrG* for homologous transformation. *Gene.* (1992) 116:59–67. doi: 10.1016/0378-1119(92)90629-4
15. Kendrick A, Ratledge C. Desaturation of polyunsaturated fatty acids in Mu*cor circinelloides* and the involvement of a novel membrane-bound malic enzyme. *Eur J Biochem.* (1992) 209:667–73. doi: 10.1111/j.1432-1033.1992.tb17334.x
16. Hanahan D. Studies on transformation of *Escherichia coli* with plasmids. *J Mol Biol.* (1983) 166:557–80. doi: 10.1016/S0022-2836(83)80284-8
17. Gutiérrez A, López-García S, Garre V. High reliability transformation of the basal fungus *Mucor circinelloides* by electroporation. *J Microbiol Methods.* (2011) 84:442–6. doi: 10.1016/j.mimet.2011.01.002
18. Zhang Y, Navarro E, Cánovas-Márquez JT, Almagro L, Chen H, Chen YQ, et al. A new regulatory mechanism controlling carotenogenesis in the fungus *Mucor circinelloides* as a target to generate β-carotene over-producing strains by genetic engineering. *Microb Cell Fact.* (2016) 15:1–14. doi: 10.1186/s12934-016-0493-8
19. Chaney AL, Marbach EP. Modified reagents for determination of urea and ammonia. *Clin Chem.* (1962) 8:130–2.
20. Naz T, Nazir Y, Nosheen S, Ullah S, Halim H, Fazili ABA, et al. Redirecting metabolic flux towards the mevalonate pathway for enhanced β-carotene production in *M. circinelloides* CBS 277.49. *Biomed Res Int.* (2020) 2020:8890269. doi: 10.1155/2020/8890269
21. Scott KJ. Detection and measurement of carotenoids by UV/VIS spectrophotometry. *Curr Protoc food Anal Chem.* (2001), (1): F2–2.
22. Nosheen S, Yang J, Naz T, Nazir Y, Ahmad MI, Fazili ABA Li S, et al. Annotation of AMP-activated protein kinase genes and its comparative transcriptional analysis between high and low lipid producing strains of *Mucor circinelloides. Biotechnol Lett.* (2020) 43:1–10.
23. Binder U, Navarro-Mendoza MI, Naschberger V, Bauer I, Nicolas FE, Pallua JD, Lass-Flörl C, Garre V. Generation of a *Mucor circinelloides* reporter strain—A promising new tool to study antifungal drug efficacy and mucormycosis. *Genes (Basel).* (2018), 9(12): 613. doi: 10.3390/genes9120613
24. Navarro E, Lorca-Pascual J, Quiles-Rosillo M, Nicolás F, Garre V, Torres-Martínez S, et al. negative regulator of light-inducible carotenogenesis in *Mucor circinelloides*. *Mol Genet Genomics.* (2001) 266:463–70. doi: 10.1007/s004380100558
25. Misawa N, Satomi Y, Kondo K, Yokoyama A, Kajiwara S, Saito T, et al. Structure and functional analysis of a marine bacterial carotenoid biosynthesis gene cluster and astaxanthin biosynthetic pathway proposed at the gene level. *J Bacteriol.* (1995) 177:6575–84. doi: 10.1128/jb.177.22.6575-6584.1995
26. Masojídek J, Torzillo G. "Mass Cultivation of Freshwater Microalgae," in *Encyclopedia of Ecology, Five-Volume Set* doi: 10.1016/B978-008045405-4.00830-2
27. Khan MAK, Yang J, Hussain SA, Zhang H, Liang L, Garre V, Song Y. Construction of DGLA producing cell factory by genetic modification of *Mucor circinelloides*. *Microb Cell Fact.* (2019), 18(1): 1–8. doi: 10.1186/s12934-019-1110-4
28. Yang J, Khan MAK, López-García S, Nosheen S, Nazir Y, Zhang H, et al. Improved SDA production in high lipid accumulating strain of *Mucor circinelloides* WJ11 by genetic modification. *Am J Biochem Biotechnol.* (2020) 16:138–47. doi: 10.3844/ajbbsp.2020.138.147

29. Csernetics Á, Tóth E, Farkas A, Nagy G, Bencsik O, Vágvölgyi C, et al. Expression of Xanthophyllomyces dendrorhous cytochrome-P450 hydroxylase and reductase in *Mucor circinelloides*. *World J Microbiol Biotechnol.* (2015) 31:321–36. doi: 10.1007/s11274-014-1784-z
30. Hussain SA, Hameed A, Khan MAK, Zhang Y, Zhang H, Garre V, et al. Engineering of fatty acid synthases (FASs) to boost the production of medium-chain fatty acids (MCFAs) in *Mucor circinelloides*. *Int J Mol Sci.* (2019) 20:786. doi: 10.3390/ijms20030786
31. Veiga-Crespo P, Blasco L, Do Santos FR, Poza M, Villa TG. Influence of culture conditions of Gordonia jacobaea MV-26 on canthaxanthin production. *Int Microbiol.* (2005) 8:55–8. doi: 10.2436/im.v8i1.9498
32. Nelis HJ, De Leenheer AP. Reinvestigation of *Brevibacterium* sp. strain KY-4313 as a source of canthaxanthin. *Appl Environ Microbiol.* (1989) 55:2505–10. doi: 10.1128/aem.55.10.2505-2510.1989
33. Nasrabadi MRN, Razavi SH. Enhancement of canthaxanthin production from *dietzia natronolimnaea HS-1* in a fed-batch process using trace elements and statistical methods. *Brazilian J Chem Eng.* (2010) 27:517–29. doi: 10.1590/s0104-66322010000400003
34. Csernetics Á, Tóth E, Farkas A, Nagy G, Bencsik O, Manikandan P, et al. Expression of a bacterial ß-carotene hydroxylase in canthaxanthin producing mutant *Mucor circinelloides* strains. *Acta Biol Szeged.* (2014) 58:139–46. Available online at: http://abs.bibl.u-szeged.hu/index.php/abs/articleview/2830
35. Zhao Y, Yue C, Geng S, Ning D, Ma T, Yu X. Role of media composition in biomass and astaxanthin production of *Haematococcus pluvialis* under two-stage cultivation. *Bioprocess Biosyst Eng.* (2019) 42:593–602. doi: 10.1007/s00449-018-02064-8
36. Zhou P, Ye L, Xie W, Lv X, Yu H. Highly efficient biosynthesis of astaxanthin in *Saccharomyces cerevisiae* by integration and tuning of algal crtZ and bkt. *Appl Microbiol Biotechnol.* (2015) 99:8419–28. doi: 10.1007/s00253-015-6791-y
37. Han D, Li Y, Hu Q. Astaxanthin in microalgae: Pathways, functions and biotechnological implications. *Algae.* (2013) 28:131–47. doi: 10.4490/algae.2013.28.2.131
38. Silva F, Navarro E, Peñaranda A, Murcia-Flores L, Torres-Martínez S, Garre V, et al. RING-finger protein regulates carotenogenesis *via* proteolysis-independent ubiquitylation of a White Collar-1-like activator. *Mol Microbiol.* (2008) 70:1026–36. doi: 10.1111/j.1365-2958.2008.06470.x
39. Nicolás-Molina FE, Navarro E, Ruiz-Vázquez RM. Lycopene over-accumulation by disruption of the negative regulator gene *crgA* in *Mucor circinelloides*. *Appl Microbiol Biotechnol.* (2008) 78:131–7. doi: 10.1007/s00253-007-1281-5

Conflict of Interest: The authors declare that the research was conducted in the absence of any commercial or financial relationships that could be construed as a potential conflict of interest.

frontiers in Nutrition

ORIGINAL RESEARCH
published: 21 October 2021
doi: 10.3389/fnut.2021.746342

Characterization of NAD$^+$/NADP$^+$-Specific Isocitrate Dehydrogenases From Oleaginous Fungus *Mortierella alpina* Involved in Lipid Accumulation

Xin Tang[1,2], *Xiaoqi Sun*[1,2], *Xuxu Wang*[1,2], *Hao Zhang*[1,2,3,4], *Yong Q. Chen*[1,2,3,4], *Jianxin Zhao*[1,2], *Haiqin Chen*[1,2*] *and Wei Chen*[1,2,3,5]

[1] State Key Laboratory of Food Science and Technology, Jiangnan University, Wuxi, China, [2] School of Food Science and Technology, Jiangnan University, Wuxi, China, [3] National Engineering Research Center for Functional Food, Jiangnan University, Wuxi, China, [4] Wuxi Translational Medicine Research Center and Jiangsu Translational Medicine Research Institute Wuxi Branch, Wuxi, China, [5] Beijing Innovation Centre of Food Nutrition and Human Health, Beijing Technology and Business University (BTBU), Beijing, China

Mortierella alpina has a strong capacity for lipid accumulation. Isocitrate dehydrogenase (IDH) plays an important role in affecting the flow of intracellular carbon sources and reducing power NADPH for lipid biosynthesis. In this study, the effect of various IDHs (NAD$^+$- and NADP$^+$-specific) in *M. alpina* on the lipid accumulation was investigated through homologous overexpression. The results showed that the transcription level and enzyme activity of the IDHs from *M. alpina* (MalDHs) in homologous overexpressing strains were higher than those of the control strain, but that their biomass was not significantly different. Among the various NAD$^+$-specific MalDH1/2/3 overexpression, NAD$^+$-MalDH3 reduced total lipid content by 12.5%, whereas overexpression NAD$^+$-MalDH1 and NAD$^+$-MalDH2 had no effect on fatty acid content. Intracellular metabolites analysis indicated that the overexpression NAD$^+$-MalDH3 strain had reduced the fatty acid accumulation, due to its greater carbon flux with the tricarboxylic acid cycle and less carbon flux with fatty acid biosynthesis. For the NADP$^+$-MalDH4/5/6 recombinant strains overexpressing only NADP$^+$-MalDH4 enhanced the total fatty acid content by 8.2%. NADPH analysis suggested that this increase in lipid accumulation may have been due to the great reducing power NADPH is produced in this recombinant strain. This study provides theoretical basis and guidance for the analysis of the mechanism of IDH function and the potential to improve lipid production in *M. alpina*.

Keywords: ***Mortierella alpina*, isocitrate dehydrogenase, homologous overexpression, lipid accumulation, mechanism**

OPEN ACCESS

Edited by:
Yuanda Song,
Shandong University of Technology, China

Reviewed by:
Parmanand Malvi,
Yale University, United States
Baris Binay,
Gebze Technical University, Turkey
He Huang,
Nanjing Normal University, China
Seraphim Papanikolaou,
Agricultural University of Athens, Greece

***Correspondence:**
Haiqin Chen
haiqinchen@jiangnan.edu.cn
orcid.org/0000-0002-2359-2622

Specialty section:
This article was submitted to Food Chemistry, a section of the journal Frontiers in Nutrition

Received: *23 July 2021*
Accepted: *21 September 2021*
Published: *21 October 2021*

Citation:
Tang X, Sun X, Wang X, Zhang H, Chen YQ, Zhao J, Chen H and Chen W (2021) Characterization of NAD$^+$/NADP$^+$-Specific Isocitrate Dehydrogenases From Oleaginous Fungus Mortierella alpina Involved in Lipid Accumulation. Front. Nutr. 8:746342. doi: 10.3389/fnut.2021.746342

INTRODUCTION

Mortierella alpina has strong fatty acid synthesis ability and can synthesize a variety of biologically active polyunsaturated fatty acids (PUFAs), including arachidonic acid (AA) and eicosapentaenoic acid (EPA) (1). *Mortierella alpina* is an industrialized strain that produces AA (2), which is an essential nutrient for early human development. At present, AA synthesized by *M. alpina* has become an important additive for infant milk powder (3–5).

Isocitrate dehydrogenase (IDH) is an enzyme that plays an important role in energy metabolism, amino acid synthesis and vitamin synthesis. It catalyzes the oxidative dehydrogenation of isocitrate to form the intermediate product, oxalosuccinic acid, followed by oxidative decarboxylation to produce 2-oxoglutarate (6). IDH has been found in almost all organisms, including animals (7), plants (8), fungi (9), and bacteria (10). IDH can be divided into NAD^+-specific isocitrate dehydrogenase (NAD^+-IDH, EC 1.1.1.41) which has NAD^+ as an electron acceptor and $NADP^+$-specific isocitrate dehydrogenase ($NADP^+$-IDH, EC 1.1.1.42) which has $NADP^+$ as an electron acceptor. NAD^+-IDH is generally localized in the mitochondrial matrix and is the rate-limiting enzyme of the tricarboxylic acid (TCA) cycle, which is an important metabolic pathway affecting fatty acid synthesis (11). $NADP^+$-IDH is mainly localized in eukaryotic chloroplasts (12), mitochondria (13), peroxisomes (14), cytoplasm (15), and prokaryotic cells (16), and serves as one of the sources of NADPH. It plays a crucial role in cell defense against oxidative damage (17–19). Many enzymes are cofactor dependent and they frequently require NADH or NADPH in stoichiometric quantities for their catalytic function (20–22).

Previous studies had shown that isocitrate dehydrogenase is related to lipid accumulation in microorganisms (23–25). When the nitrogen source in culture medium is depleted, the activity of intracellular adenosine monophosphate (AMP) deaminase (AMPD) increases rapidly, catalyzing the conversion of AMP to inosine monophosphate (IMP), and releasing NH_4^+ to supplement the nitrogen source. The activity of NAD^+-IDH depends on the concentration of intracellular AMP (26, 27); decrease in AMP concentration leads to decrease in the activity of NAD^+-IDH, which in turn inhibits the tricarboxylic acid cycle. Subsequently, the proliferation rate of oleaginous microbial cells reduces and they start entering the lipid accumulation phase. Under nitrogen-limiting conditions, the decrease in NAD^+-IDH activity in mitochondria reduces the conversion rate of isocitrate to α-ketoglutaric acid, and isocitrate accumulates in mitochondria producing citric acid via aconitate hydratase. The citrate in the mitochondria is then transported to the cytoplasm via the citrate transporter where it is decomposed by the ATP citrate lyase (ACL) to form oxaloacetate and acetyl-CoA (25, 28). Acetyl-CoA is used as a substrate for lipid biosynthesis in oleaginous microorganisms. In the cytoplasm, $NADP^+$-IDH catalyzes a reaction similar to that of NAD^+-IDH in the mitochondria, and mediates oxidative decarboxylation of isocitrate to form α-ketoglutaric acid. However, unlike NAD^+-IDH, which produces NADH, $NADP^+$-IDH can reduce $NADP^+$ in the cytoplasm to produce reducing power NADPH, which together with the malic enzyme and pentose phosphate pathways for fatty acid synthase in lipid-producing microorganisms.

In this study, various isozymes of IDH from *M. alpina* (MaIDH) were investigated for their effect on lipid biosynthesis. This is conducive to improving our understanding the mechanism of lipid accumulation in *M. alpina*, and provides theoretical support for concepts to follow-up on and further improve the efficiency of lipid production in *M. alpina*. Moreover, the research results could be applied to other lipid-producing microorganisms, enhancing its scientific significance and application value.

MATERIALS AND METHODS

Strain, Media, and Culture Conditions

Mortierella alpina ATCC 32222 was purchased from the American Type Culture Collection, and the uracil auxotrophic strain CCFM 501 was constructed by our laboratory and used as a recipient strain for transformation (29). The uracil-recovering strain CCFM 505 was used as the control strain for the experiments. *Escherichia coli* Top 10 was used to preserve the constructed recombinant plasmid. *Agrobacterium tumefaciens* CCFM 834 was used for the mediated transformation of *M. alpina* and the plasmid pBIG2-ura5s-ITs contained kanamycin resistance and uracil screening markers was used as an expression vector for genetic manipulation. The *E. coli* Top 10 strain for plasmid storage and construction was cultivated at 37°C in lysogeny broth (LB) medium (10 g/L tryptone, 5 g/L yeast extract, and 10 g/L NaCl). *A. tumefaciens* CCFM 834 was grown on yeast extract-peptone (YEP) medium (10 g/L tryptone, 10 g/L yeast extract, and 5 g/L NaCl) at 28°C. The uracil-auxotrophic *M. alpina* strain CCFM 501 and wild-type *M. alpina* ATCC 32222 were maintained on glucose-yeast extract (GY) solid medium (30 g/L glucose, 5 g/L yeast extract, 2 g/L KNO_3, 1 g/L NaH_2PO_4, 0.3 g/L $MgSO_4{\cdot}7H_2O$, and 15 g/L agar), supplemented with 0.1 g/L uracil when necessary. For flask culture, *M. alpina* spores were inoculated into the broth medium (20 g/L glucose, 5 g/L yeast extract, 10 g/L KNO_3, 1 g/L KH_2PO_4, and 0.25 g/L $MgSO_4{\cdot}7H_2O$) at 28°C for 48 h and transferred into a new broth medium (1%, v/v). This was repeated for three generations, and mycelium cultured in the 100 mL modified Kendrick medium (50 g/L glucose, 2.0 g/L diammonium tartrate, 7.0 g/L KH_2PO_4, 2.0 g/L Na_2HPO_4, 1.5 g/L $MgSO_4{\cdot}7H_2O$, 1.5 g/L yeast extract, 0.1 g/L $CaCl_2{\cdot}2H_2O$, 8 mg/L $FeCl_3{\cdot}6H_2O$, 1 mg/L $ZnSO_4{\cdot}7H_2O$, 0.1 mg/L $CuSO_4{\cdot}5H_2O$, 0.1 mg/L $Co(NO_3)_2{\cdot}6H_2O$, and 0.1 mg/L $MnSO_4{\cdot}5H_2O$) held in 250 mL flasks for 7 days at 28°C, with agitation at a shaft speed of 200 rpm.

Construction of the Recombinant Strain

Specific primers were designed based on the *M. alpina* IDH nucleic acid sequence; the primers are listed in **Supplementary Table S1**. *Mortierella alpina* cDNA was used as a template, and specific amplification of the target gene was used for PCR amplification to obtain the target fragment. The PCR amplification reaction was carried out using a KOD high-fidelity enzyme system as per manufacturer's instructions. After the PCR amplification product was verified by nucleic

acid electrophoresis, the PCR product was subjected to gelation recovery and purification. Meanwhile, *E. coli* Top 10 contained the plasmid pBIG2-ura5s-ITs was cultured overnight in an LB liquid medium contained Kanamycin, and the plasmid was extracted using plasmid extraction kit as per manufacturer's instructions. The purified PCR product and the extracted plasmid were digested with the same restriction endonucleases, according to specified reaction conditions for each enzyme, subsequently, the digested products were purified using a gel recovery purification kit and the ligation reaction was prepared according to the specifications of T4 ligase to enable the ligation of the target gene to the expression vector pBIG2-ura5-ITs. *E. coli* Top 10 was used to prepare competent cells, and 5 μL of the ligation product was added to the competent cells for electroporation. In this experiment, the target gene fragment on the original plasmid pBIG2-ura5s-ITs was replaced with the recombinant gene fragment, to construct a recombinant binary expression vector. The recombinant plasmid was named pBIG2-ura5s-MaIDH1/2/3/4/5/6 and transformed into *E. coli* Top 10 for preservation.

A. tumefaciens-Mediated Transformation (ATMT)

ATMT was performed as previously described (1, 29). *A. tumefaciens* stored at −80°C were activated on the YEP screening plates. After picking up single colonies, the cells were inoculated in YEP liquid medium contained Kanamycin and Rifampicin, and cultured at 28°C and 200 rpm for 36–48 h in the dark, until the medium became bright orange. The minimum medium (MM) was inoculated at 1% bacterial solution and cultured. When the OD_{600} value of the bacterial solution in the MM medium reached 1.2–1.5, it was inoculated into 20 mL of inducing medium (IM) supplemented with acetosyringone. The initial OD_{600} was adjusted between 0.15 and 0.20, and incubated at 28°C and 200 rpm away light until the OD_{600} was ∼0.8. The uracil-deficient spores of *M. alpina* CCFM 501 were collected in a sterile 50 mL centrifuge tube with broth liquid medium, and incubated at 28°C for 24 h. The *A. tumefaciens* liquid and *M. alpina* spore solution were mixed and applied to IM solid medium coated with cellophane, and cultured at 28°C for 48 h in the dark. After a layer of hyphae grew on the surface of the IM, the membrane on the IM was transferred to the uracil-free synthetic-complete medium with cefotaxime and spectinomycin (SC-CS), and the culture was allowed to incubate at 28°C. After 3 days, the new colonies grew. The newly grown colonies were picked and cultured on fresh SC-CS medium for three consecutive cycles, and the transformants were stably cultured on the SC-CS plates. The compositions of IM, MM, and SC-CS were described previously (30, 31). The recombinant binary expression vector was transformed into uracil auxotrophic *M. alpina* by *A. tumefaciens* CCFM 834 to complete the development of the recombinant strain. The recombinant strains were named *M. alpina-MaIDH1/2/3/4/5/6*.

Preparation of Genomic DNA

Suspected positive transformants were picked and inoculated in broth liquid medium for further culturing. The cells were collected, and genomic DNA was extracted using the Biospin Fungal Genomic DNA Extraction Kit (BioFlux Cat #BSC14M1).

Bioinformatic Analysis of MaIDH

A BLAST local library was constructed using *M. alpina* genome-wide data (32), and the MaIDH sequence was screened and further sequenced with the isocitrate dehydrogenase submitted to NCBI; the functional domain search was performed using NCBI BLASTp analysis. Transcription-level analysis of MaIDH was performed according to transcriptomic data for *M. alpina* ATCC 32222, which was initially determined by the laboratory (33). Subcellular localization prediction analysis and signal peptide analysis of MaIDH in *M. alpina* were performed using the online analysis website TargetP1.1 Server (http://www.cbs.dtu.dk/services/TargetP/). The transmembrane structure prediction analysis of MaIDH in *M. alpina* was carried out using the online analysis website TMHMM Server v. 2.0, (http: //www. cbs. dtu. dk/services/TMHMM/). Throughout the above description of bioinformatics data, the function of each MaIDH isozyme in *M. alpina* was predicted and further investigated.

Transcript-Level Analysis

Total RNA was extracted using the Trizol lysis method, and 1 μg of total RNA was used as a template to obtain cDNA by reverse transcription according to the instructions of PrimeScript™ RT reagent Kit with gDNA Eraser (Takara Reverse Transcription Kit, RR047A). The cDNA obtained was quantified and stored at −80°C until further use. The cDNA obtained by reverse transcription was used as a template, and the reaction system was prepared in accordance with the instructions of SYBR Green SuperMix. Primer pairs used for quantitative reverse transcription PCR (RT-qPCR) are listed in **Supplementary Table S2**. RT-qPCR was carried out using the Bio-Rad CFX Connect™ system, to determine the level of expression of the target gene. The 18S rDNA of *M. alpina* was used as the internal reference gene, and the cDNA from prototrophic strain CCFM 505 was used as the control. The relative transcription levels of the target genes were analyzed using the $2^{-\Delta\Delta Ct}$ method.

Determination of Biomass and Fatty Acid Content of the MaIDH Homologous Overexpressing Strain

The cultured *M. alpina* were collected, the wet cells were washed three times with deionized water, and the excess water that remained on the cells was absorbed using a sheet of filter paper. The cells were placed in a vacuum freeze dryer and lyophilized, and the dry weight of the cells was obtained for calculation of the biomass of the recombinant strain. The weighed cells were ground to a powder in a mortar, and fatty acids were extracted by the methanol chloroform method using pentadecanoic acid (C15:0) as an internal standard. Derivatization was performed using methanolic hydrochloric acid. The extracted fatty acid methyl ester was detected using gas chromatography–mass spectrometry (GC-MS) (32).

Determination of Enzyme Activity of the Recombinant MaIDH Strain

Extraction of the crude enzyme solution was performed as described by Wynn et al. (34). The mycelia of the cultured *M. alpina* recombinant strain were collected and washed three times with deionized water. Subsequently, the mycelium was obtained by suction filtration using a Buchner funnel, was quickly frozen in liquid nitrogen, placed in a mortar with liquid nitrogen, and ground to a powder form. The powder was placed in a centrifuge tube, and enzyme extraction buffer was added. The tube was centrifuged at 10,000 × g for 10 min at 4°C, and the supernatant was aspirated into a new centrifuge tube. The above procedure was repeated twice, and the supernatant was obtained as a crude enzyme solution. A standard curve was prepared using bovine serum albumin as a standard, and the protein concentration of the crude enzyme solution sample was determined using the BCA method. The enzyme activity assay was performed at 30°C according to the method of Wynn et al. (34). The standard reaction system was maintained at 82.2 mmol/L Tris-HCl, pH 8.0, 1.2 mmol/L NAD^+ or 0.6 mmol/L $NADP^+$, 50 mmol/L DL-isocitrate, and 3 mmol/L $MgCl_2$. The catalytic activity of IDH was monitored by the generation of NADH or NADPH at 340 nm.

Extraction and Analysis of Metabolites of the MaIDH-Homologous Overexpressing Strain

The mycelia of the cultured *M. alpina* recombinant strain were collected and washed three times with physiological saline. Then, the mycelium was obtained by suction filtration using a Buchner funnel, and the mycelium was quenched in liquid nitrogen for 10 s, placed in a mortar that was pre-cooled in advance, and ground to a powder form by adding liquid nitrogen. Approximately 50 mg of ground powder was weighed into a 1.5 mL centrifuge tube and 0.6 mL of aqueous methanol (1:1, v/v) was added. Precisely, 50 μL of 2 mg/mL heneicosanoic acid (C21:0) internal standard was added and left to stand for 30 min at −80°C, then centrifuged at 12,000 × g for 15 min. The supernatant was collected and transferred to a new pre-cooled 1.5 mL centrifuge tube. 0.6 mL aqueous methanol solution (1:1, v/v) was added to the precipitate, the supernatant was extracted twice, and the two supernatants were combined. The collected supernatant was concentrated and dried in vacuum for 4–6 h, and 100 μL of pyridine contained 10 mg/mL methoxyamine hydrochloride was added, followed by a metal bath at 37°C for 90 min. Derivatization was continued by adding 40 μL of MSTFA + 1% TMS and a metal bath at 37°C for 30 min. The derivatized product was analyzed using GC-MS.

Statistical Analysis

The mean values and the standard errors were calculated from three biological replicates. A statistical analysis of the data was performed by SPSS 24.0 for Windows. One-way analysis of variance (ANOVA) with Duncan's test was conducted on the data, and $p < 0.05$ was considered to indicate that the data were significantly different.

RESULTS AND DISCUSSION

Bioinformatic Analysis of MaIDH

According to the genome-wide information of *M. alpina* ATCC 32222 (32), six nucleic acid sequences encoding IDH were identified in the genome of *M. alpina*, and named MaIDH1/2/3/4/5/6. Among them, MaIDH1/2/3 are NAD^+-specific IDHs, and MaIDH4/5/6 are $NADP^+$-specific IDHs. IDH is a class of basal metabolic enzymes widely found in bacteria, fungi, animals, plants, and other organisms. To further investigate the functional structure of MaIDH, their conserved domain was analyzed, revealing that all MaIDH belong to the isocitrate dehydrogenase superfamily. Among them, MaIDH1/2/3 were annotated as mitochondrial NAD^+-specific IDH, suggesting that its subcellular localization may occur in mitochondria. The mitochondrial NAD^+-specific IDH of eukaryotes functions in a similar manner to $NADP^+$-specific IDH and 3-isopropylmalate dehydrogenase (NAD^+-specific enzymes) in prokaryotes. It is closely tied to basic metabolism, energy production, and amino acid transport in the cell, and is usually an α(2)-β-γ heterotetramer. MaIDH4/5/6 were annotated as eukaryotic NADP-specific IDHs, which may be present in cytoplasm, mitochondria, and chloroplasts, but their amino terminus was very similar to that of the cytoplasmic form, indicating that they may be located in the cytoplasm.

Predictive analysis of the subcellular localization of MaIDH was performed according to the TargetP1.1 Server online analysis website. Mitochondrial targeting peptide results indicate that NAD^+-specific MaIDH1/2/3 may be highly likely to be localized in mitochondria, and $NADP^+$-specific MaIDH4/5/6 is highly likely to be localized in the cytoplasm due to the absence of specific signal peptides. In addition, the transmembrane structure of MaIDH protein was predicted based on online analysis at TMHMM Server v.2.0. The results showed that there was no transmembrane structure in MaIDH1/2/3/4/5/6 indicating that MaIDH is not a transmembrane protein localized on the biofilm. Specific information is listed in **Table 1**.

Genes with expression levels that change before and after nitrogen depletion may be key regulators in fatty acid synthesis, and their changes in transcription levels may be responsible for the transformation of *M. alpina* from cell proliferation to lipid accumulation. The transcription level of each MaIDH isozyme was analyzed based on the transcriptome data for *M. alpina*, which was determined in our previous study (33). The time point E, where the nitrogen source was exhausted, was used as a control. As shown in **Figure 1**, the transcriptional levels of MaIDH genes at different time points during the fermentation process varied. MaIDH1 and MaIDH6 did not change significantly during the entire fermentation process. The FPKM value of MaIDH1 was maintained between 50 and 100, while that of MaIDH6 was always below 35. Compared to the other four MaIDHs, their transcription levels were lower, and were not regulated by the levels of the nitrogen source during fermentation. The transcription levels of MaIDH2 and MaIDH3 after nitrogen depletion were ∼5 times lower than before nitrogen depletion (point E to point K), but the FPKM value of *MaIDH3* was always higher than that of MaIDH2. MaIDH5 was

TABLE 1 | Information for the isocitrate dehydrogenases from *M. alpina* (MaIDHs).

Gene name	*M. alpina* genome number	Length (bp)	Coenzyme dependence	Subcellular localization prediction
MaIDH1	MA-00067-296	1086	NAD^+	Mitochondria
MaIDH2	MA-00073-258	1077	NAD^+	Mitochondria
MaIDH3	MA-00153-313	1137	NAD^+	Mitochondria
MaIDH4	MA-00090-236	1233	$NADP^+$	Cytoplasm
MaIDH5	MA-00184-263	1248	$NADP^+$	Cytoplasm
MaIDH6	MA-00297-491	1191	$NADP^+$	Cytoplasm

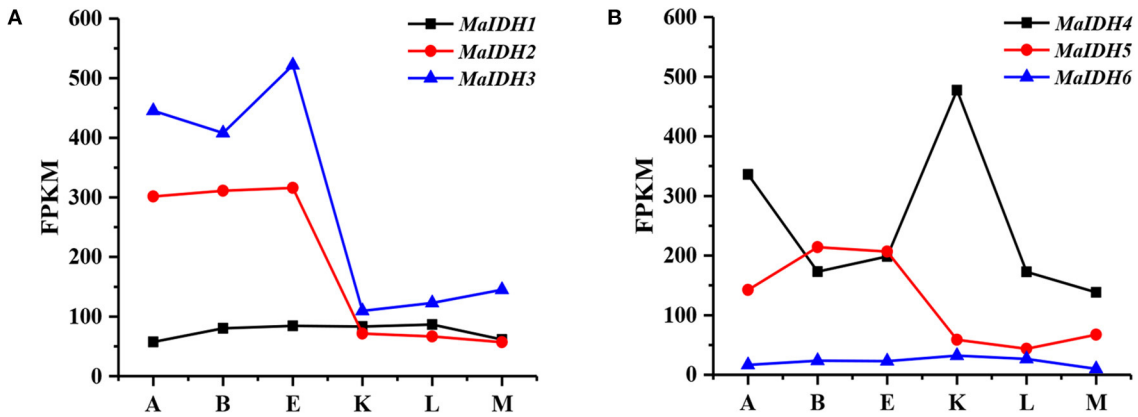

FIGURE 1 | Transcriptome level analysis of isocitrate dehydrogenases from *M. alpina* (MaIDHs) at different time points during the fermentation process. A–K indicate various time points prior to and after nitrogen exhaustion, A: −12 h, B: −2 h, E: −30 min, K: +1 h, L: +12 h, and M: +48 h. **(A)** FPKM of NAD^+-MaIDHs, **(B)** FPKM of $NADP^+$-MaIDHs.

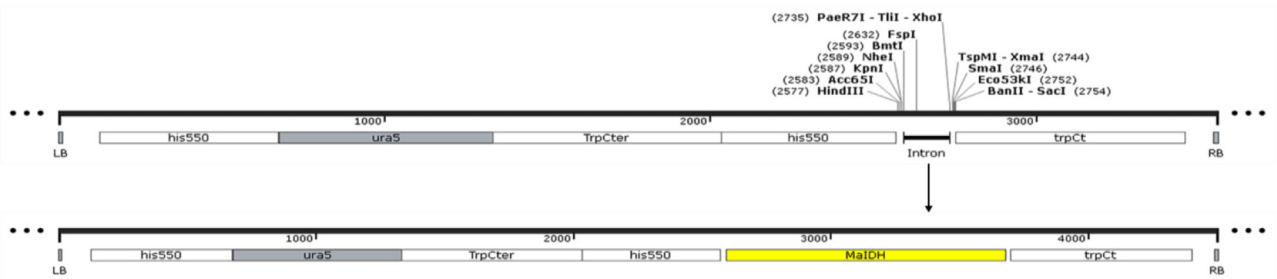

FIGURE 2 | Construction of the vector overexpressing isocitrate dehydrogenases from *M. alpina* (MaIDHs).

downregulated 3.5-fold, and MaIDH4 was the only MaIDH that was up-regulated after nitrogen-restricted; its transcription level was up-regulated 2.5-fold compared to point E.

Generation of MaIDH-Overexpressing Strains of *M. alpina* by Genetic Engineering

Using the *M. alpina* cDNA as a template, the target gene was subjected to PCR amplification using specific primers for MaIDH1/2/3/4/5/6. The obtained target fragment of MaIDH1/2/3/4/5/6 was ligated to the binary expression vector pBIG2-ura5s-ITs, and the construction process of each recombinant vector of MaIDH is shown in **Figure 2**. Successfully constructed recombinant binary expression vectors were transformed into *E. coli* Top 10, and positive transformants were selected on the screening plates and verified using the universal primer Hispro F1/TrpCR 1 of pBIG2-ura5s-ITs. The universal primer binds to the same promoter (his550) and terminator (trpCT) in the T-DNA region of the binary expression vector. Thus, two fragments of the uracil nutritional complement sequence ura5 (818 bp) and the target gene (MaIDH) were amplified. The results in **Figure 3** showed that the nucleic acid electrophoresis gel pattern showed bright and clear bands at 818 bp and the position of the

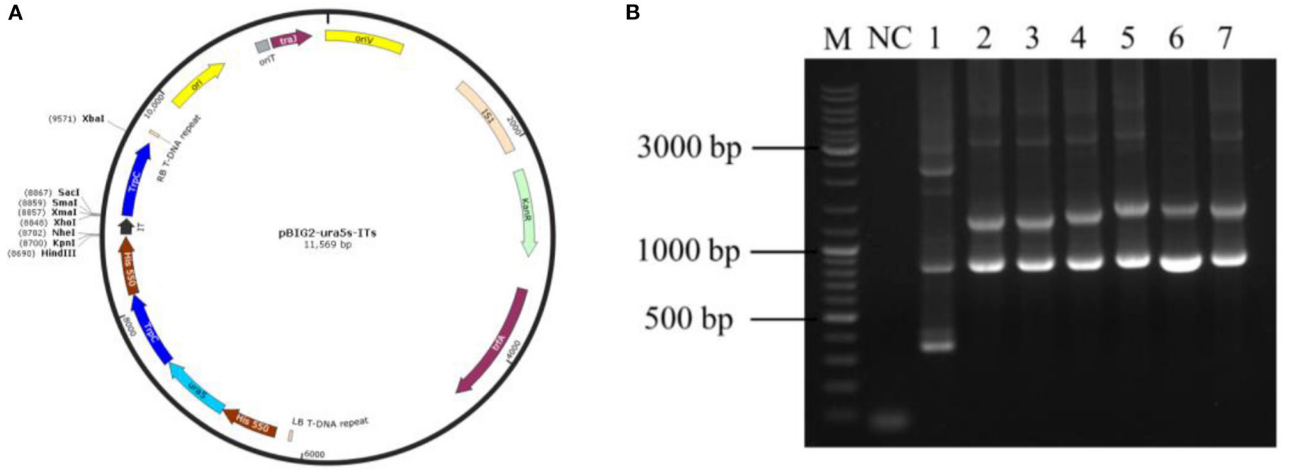

FIGURE 3 | Polymerase chain reaction (PCR) verification of the vector overexpressing isocitrate dehydrogenases from *M. alpina* (MaIDHs). **(A)** pBIG2-ura5s-ITs plasmid map, **(B)** *E. coli* colony PCR assay, M, Marker; NC, Negative control; 1, Empty vector; 2∼7, *MaIDH1/2/3/4/5/6* overexpression vectors.

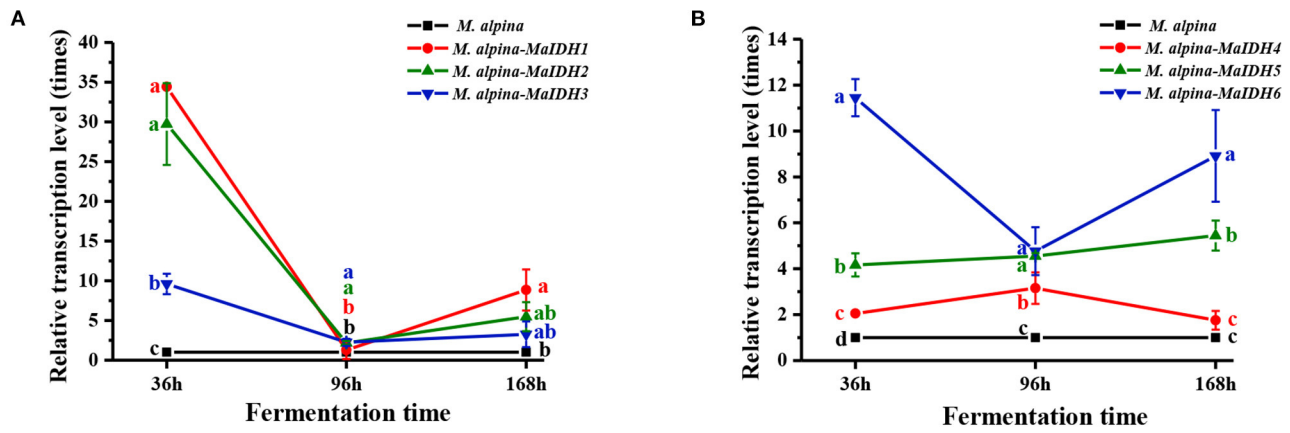

FIGURE 4 | Transcriptional levels of various MaIDHs recombinant strains of *M. alpina* at different time points (36, 96, and 168 h). **(A)** Transcriptional levels of NAD^+-MaIDHs, **(B)** transcriptional levels of $NADP^+$-MaIDHs.

target gene, which was consistent with the theoretical value. The recombinant binary expression vector of MaIDH was successfully constructed and transferred into *E. coli* Top 10 for preservation. The constructed binary expression vectors were named pBIG2-ura5s-MaIDH1/2/3/4/5/6.

Agrobacterium tumefaciens-mediated transformation experiments of *M. alpina* were carried out, and six strains of MaIDH1/2/3/4/5/6 homologous overexpression strains were successfully constructed. Each transformant grew normally after three serial cycles on SC-CS screening medium, indicating that the characteristic traits of the transformants were genetically stable.

Expression Levels and Enzyme Activity of MaIDH in the Overexpressing Strain

The transcription levels of each MaIDH in the overexpressed recombinant strain was higher than that in the control group at 36 h, indicating that the MaIDH was successfully overexpressed in the recombinant strain (**Figure 4**). As an oxidoreductase with in *vivo* regulatory functions, IDH plays an important role in energy metabolism and has a significant impact on the life activities of organisms. Because the expression of genes in the cell is divided into two levels of transcription and translation, the time and location of transcription and translation of eukaryotic genes are different. The formation of active proteins in the post-transcriptional translation process requires further processing and modification. Sometimes, when the protein level reaches its peak, its mRNA is degraded, so the transcription level of the gene is not entirely consistent with the expression level of the protein. Levitan et al. (35) found no change in the transcriptional level of malic enzyme after nitrogen limitation, but its protein expression level was significantly increased. Therefore, the transcript level results can preliminarily determine whether a gene plays a role, but

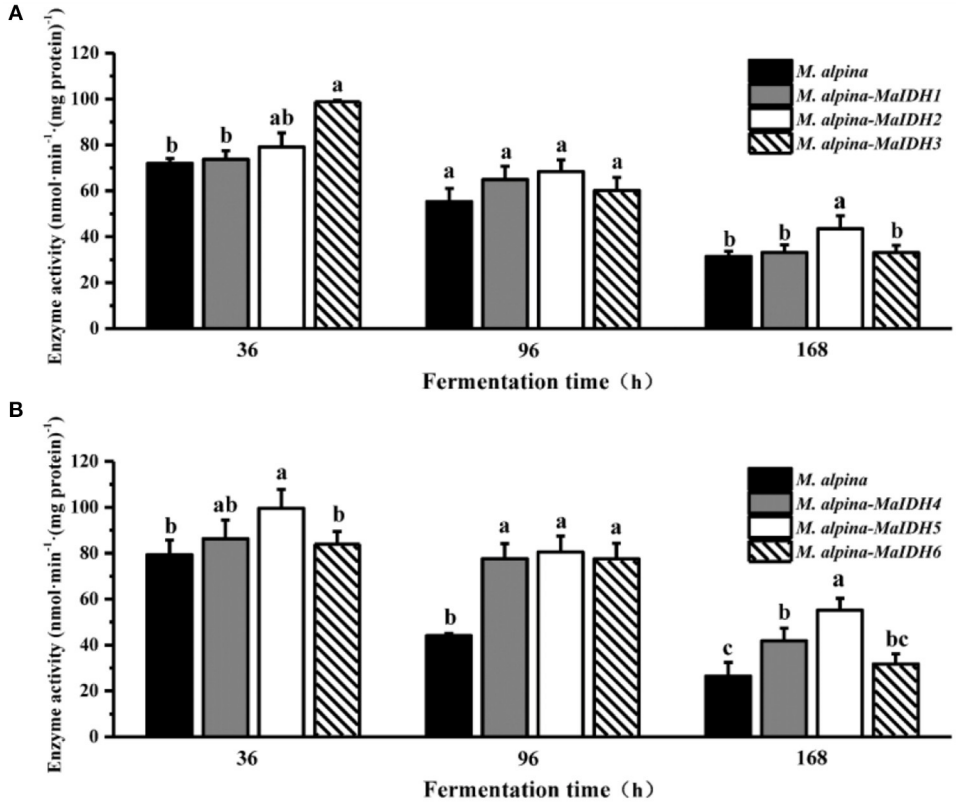

FIGURE 5 | Enzyme activity of isocitrate dehydrogenases from *M. alpina* (MaIDHs) expressed by recombinant strains at different time points (36, 96, and 168 h). **(A)** Changes in enzyme activity of NAD^+-MaIDHs, **(B)** changes in enzyme activity of $NADP^+$-MaIDHs. Different letters indicate significant differences, $p < 0.05$.

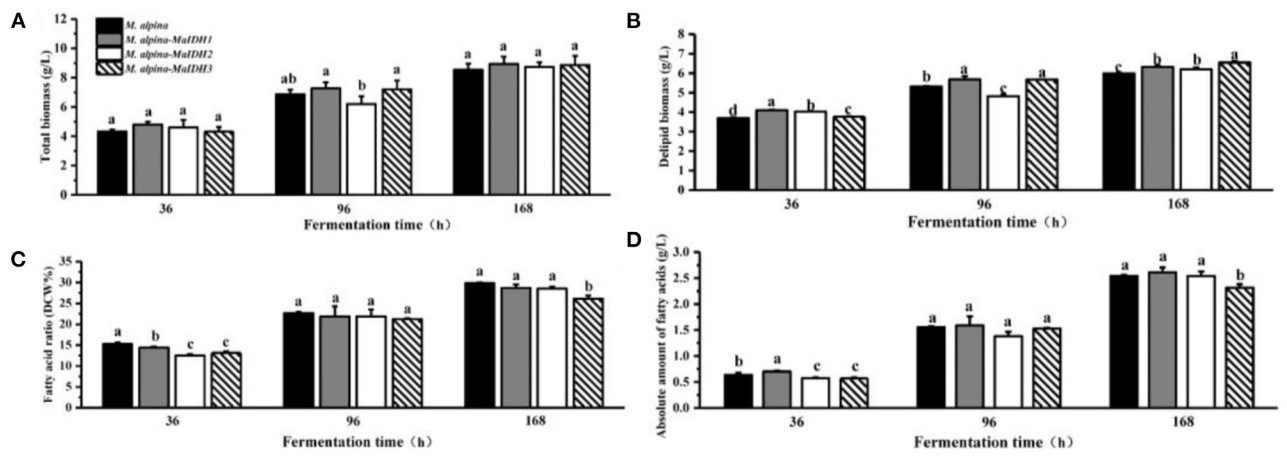

FIGURE 6 | Biomass and lipid accumulation of recombinant strains overexpressing NAD^+-MaIDH at different time points (36, 96, and 168 h). Different letters indicate significant differences, $p < 0.05$. **(A)** Total biomass, **(B)** delipid biomass, **(C)** fatty acid ratio, and **(D)** absolute amount of fatty acids.

further research is needed to understand its impact on the biological phenotype.

The effects of overexpressing MaIDH in the recombinant strain of *M. alpina* were further investigated at the protein level by measuring the enzymatic activity of MaIDH in the recombinant strain (**Figure 5**). The enzyme activity of MaIDH in all recombinant strains gradually decreased over prolonged fermentation, but was still higher than that of the control group. During the fermentation process, the enzyme activity of the NAD^+-MaIDH3 recombinant strain decreased from 98.8

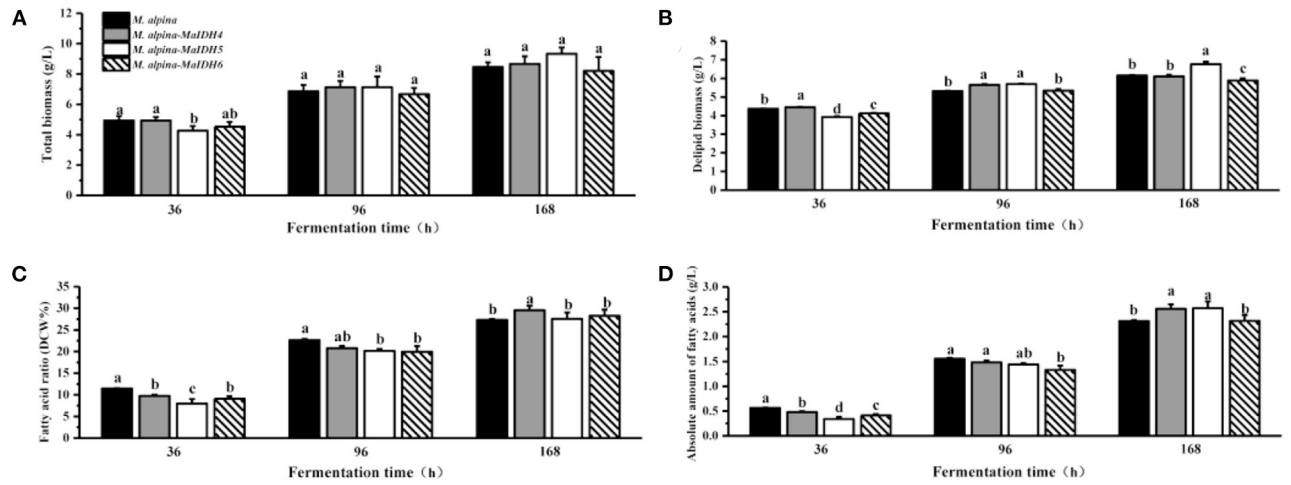

FIGURE 7 | Biomass and lipid accumulation of recombinant strains overexpressing NADP$^+$-MalDH at different time points (36, 96, and 168 h). Different letters indicate significant differences, $p < 0.05$. **(A)** Total biomass, **(B)** delipid biomass, **(C)** fatty acid ratio, and **(D)** absolute amount of fatty acids.

nmol·min^{-1}·(mg protein)$^{-1}$ at 36 h to 60.1 nmol·min^{-1}·(mg protein)$^{-1}$ at 96 h, a 39.2% reduction. However, the changes in the enzymatic activity of NAD$^+$-MaIDH1 and NAD$^+$-MaIDH2 recombinant strains were not significant. This may be due to the fact that NAD$^+$-MaIDH3 is more dependent on AMP concentration than NAD$^+$-MaIDH1 and NAD$^+$-MaIDH2; thus, its activity is more obviously decreased with nitrogen exhaustion. Previous studies have shown that different IDHs have different degrees of dependence on AMP. The Ratledge team conducted a preliminary investigation of mitochondrial NAD$^+$-IDH in oil-producing and non-oil-producing yeast (23). The results showed that the activity of mitochondrial NAD^{+-}IDH in oleaginous yeast was dependent on AMP, but that in non-oil producing yeast was not dependent on AMP. Furthermore, our previous study also indicated that the activity of the mitochondrial NAD$^+$-IDH in the oleaginous filamentous fungus *Mucor circinelloides* is only dependent on AMP at low isocitrate concentrations, and its activity is not fully regulated by AMP (24). Our results showed that the enzyme activities of NADP$^+$-MaIDH4/5/6 were obviously higher than those of the control strain, especially at 96 h. As *M. alpina* enters the lipid accumulation phase, it requires an intracellular supply of large amounts of NADPH for lipid synthesis, and the increased activity of NADP$^+$-MaIDH is beneficial to lipid accumulation.

Growth and Lipid Accumulation in the MaIDH Homologous Overexpressing Strain

To further investigate the effects of various isozymes of MaIDH on the growth and lipid accumulation in the recombinant strains, the biomass and fatty acid content at different time points in the fermentation process were determined (**Figures 6**, **7**). As a result, it was found that the total biomass of each MaIDH homologous overexpressing strain during the fermentation did not change significantly compared with the control group and the values ranged from 8.5 to 9.3 g/L at the end of 168 h fermentation (**Figures 6A**, **7A**).

According to the data on the fatty acid content of each recombinant strain, it can be seen that the recombinant strains of MaIDH have different effects on lipid accumulation. As shown in **Figure 6C**, the homologous overexpression of NAD$^+$-MaIDH3 resulted in a significant decrease in fatty acid content in the recombinant strain, compared to the control group, which had decreased by 12.5% at 168 h. In contrast, overexpression of NAD$^+$-MaIDH1 and NAD$^+$-MaIDH2 had no effect on the fatty acid content. The results indicated that NAD$^+$-MaIDH3 may play a major role in the three NAD$^+$-MaIDH isoenzymes, a phenomenon that is also present in other proteins with isoenzymes and is a widespread self-protection and regulation mechanism in organisms (36). In addition, Yang et al. heterologously expressed NAD$^+$-IDH from the oil-producing microorganism *Rhodosporidium toruloides* in *Saccharomyces cerevisiae* knocked out of IDH, and found that the fatty acid content of the recombinant strain was higher than that of the wild-type strain; which also indicated that NAD$^+$-IDH can indeed affect lipid synthesis (37).

As shown in **Figure 7C**, among the recombinant strains overexpressing NADP$^+$-MaIDH4/5/6, only NADP$^+$-MaIDH4 enhanced the total fatty acid content at the end of fermentation for 168 h, which increased by 8.2%. Combined with the transcriptome data of *M. alpina* (33), it was found that the transcription level of MaIDH4 was upregulated after the nitrogen source was depleted, and its FPKM value was maintained at a high level throughout the fermentation process. Notably, overexpression of NADP$^+$-MaIDH4 has a more pronounced effect on lipid accumulation than NADP$^+$-MaIDH5/6, which may be related to its high transcription level. NADP$^+$-IDH can provide the reducing power NADPH for fatty acid

TABLE 2 | Fatty acid composition (%, w/w of total fatty acids) of the recombinant strains during the fermentation.

Strains	Fatty acid composition (%, w/w of total fatty acids)							
(at different time)	C 16:0	C 18:0	C 18:1	C 18:2	C 18:3	C 20:3	C 20:4	Others
M. alpina (36 h)	14.7 ± 0.3	12.9 ± 0.1	11.7 ± 0.4	5.3 ± 0.1	5.6 ± 0.1	4.3 ± 0.1	38.6 ± 0.3	6.8 ± 0.1
M. alpina (96 h)	14.1 ± 0.3	12.2 ± 0.2	11.2 ± 0.5	9.7 ± 0.4	5.1 ± 0.1	3.3 ± 0.1	37.5 ± 1.1	6.9 ± 0.2
M. alpina (168 h)	15.9 ± 1.6	14.0 ± 1.5	13.5 ± 1.2	13.6 ± 2.1	4.8 ± 0.5	2.9 ± 0.2	28.8 ± 1.7	6.5 ± 0.1
M. alpina-MaIDH1 (36 h)	14.6 ± 0.1	12.3 ± 0.2	14.0 ± 0.1	5.6 ± 0.1	5.3 ± 0.1	4.5 ± 0.1	37.5 ± 0.2	6.3 ± 0.1
M. alpina-MaIDH1 (96 h)	15.1 ± 0.1	12.7 ± 0.5	14.0 ± 0.1	9.9 ± 0.4	5.0 ± 0.1	3.4 ± 0.1	33.4 ± 0.1	6.5 ± 0.2
M. alpina-MaIDH1 (168 h)	15.3 ± 0.3	14.3 ± 0.5	15.4 ± 1.1	13.5 ± 0.6	4.6 ± 0.1	3.0 ± 0.1	27.5 ± 1.2	6.4 ± 0.1
M. alpina-MaIDH2 (36 h)	14.4 ± 0.1	11.5 ± 0.6	13.5 ± 0.1	6.3 ± 0.3	5.2 ± 0.1	4.5 ± 0.2	38.0 ± 0.4	6.6 ± 0.1
M. alpina-MaIDH2 (96 h)	15.1 ± 0.3	11.6 ± 0.3	13.6 ± 0.3	11.5 ± 0.7	4.4 ± 0.1	3.1 ± 0.1	33.7 ± 0.6	7.0 ± 0.2
M. alpina-MaIDH2 (168 h)	15.5 ± 0.3	13.1 ± 0.3	14.9 ± 0.1	14.0 ± 0.3	4.1 ± 0.1	2.8 ± 0.1	28.9 ± 0.4	6.7 ± 0.1
M. alpina-MaIDH3 (36 h)	14.4 ± 0.3	12.6 ± 0.4	12.1 ± 0.3	5.7 ± 0.2	5.4 ± 0.1	4.6 ± 0.1	39.0 ± 0.8	6.1 ± 0.1
M. alpina-MaIDH3 (96 h)	14.6 ± 0.2	12.2 ± 0.4	12.1 ± 0.1	10.0 ± 0.2	5.2 ± 0.1	3.4 ± 0.1	35.9 ± 0.2	6.7 ± 0.1
M. alpina-MaIDH3 (168 h)	15.1 ± 0.1	13.6 ± 0.4	14.0 ± 1.1	13.8 ± 0.9	4.6 ± 0.1	3.0 ± 0.1	29.4 ± 0.7	6.6 ± 0.2
M. alpina-MaIDH4 (36h)	16.5 ± 0.4	14.0 ± 0.5	16.9 ± 0.4	6.4 ± 0.2	5.3 ± 0.2	3.9 ± 0.1	29.7 ± 1.0	7.1 ± 0.1
M. alpina-MaIDH4 (96 h)	14.8 ± 0.4	11.5 ± 0.1	12.7 ± 0.5	12.9 ± 0.7	4.9 ± 0.1	2.8 ± 0.1	33.4 ± 1.3	7.2 ± 0.1
M. alpina-MaIDH4 (168 h)	15.2 ± 1.1	14.0 ± 0.8	14.8 ± 0.1	14.2 ± 0.3	4.9 ± 0.2	2.7 ± 0.1	27.6 ± 1.6	6.7 ± 0.2
M. alpina-MaIDH5 (36 h)	19.8 ± 0.6	16.0 ± 0.3	20.0 ± 0.4	4.7 ± 0.1	5.8 ± 0.3	4.9 ± 0.1	22.3 ± 0.9	6.6 ± 0.1
M. alpina-MaIDH5 (96 h)	17.2 ± 0.3	11.6 ± 0.1	16.4 ± 0.2	11.6 ± 0.2	5.1 ± 0.1	3.4 ± 0.1	28.5 ± 0.4	6.3 ± 0.1
M. alpina-MaIDH5 (168 h)	16.2 ± 0.2	13.3 ± 0.3	17.3 ± 0.2	13.8 ± 0.2	4.9 ± 0.2	3.1 ± 0.1	25.3 ± 0.1	6.1 ± 0.3
M. alpina-MaIDH6 (36 h)	17.9 ± 0.1	15.3 ± 0.1	19.5 ± 0.2	5.0 ± 0.1	5.9 ± 0.2	4.9 ± 0.1	26.1 ± 0.2	5.4 ± 0.1
M. alpina-MaIDH6 (96 h)	15.7 ± 0.9	14.9 ± 0.4	24.5 ± 1.0	7.5 ± 0.5	5.1 ± 0.4	3.3 ± 0.1	23.6 ± 1.5	5.4 ± 0.1
M. alpina-MaIDH6 (168 h)	16.1 ± 0.9	15.1 ± 0.1	19.0 ± 3.6	10.9 ± 0.6	5.2 ± 0.3	3.0 ± 0.1	25.2 ± 1.4	5.5 ± 0.2

biosynthesis (38). Thus, our study indicated that $NADP^+$-MaIDH4 may influence lipid synthesis by affecting intracellular NADPH content. In addition, the fatty acid composition in the recombinant strains was analyzed, and the results showed that overexpressed $NADP^+$-IDH slightly decreased the ARA content in total fatty acids compared with the control strain (**Table 2**).

Analysis of Intracellular Metabolites in the MaIDH-Overexpressing Strain

As MaIDH is not directly involved in fatty acid synthesis (e.g., fatty acid synthase, fatty acid desaturase), its regulation of lipid synthesis is carried out by intracellular citric acid content or the reducing power of NADPH. Therefore, the effect of each MaIDH isoenzyme on intracellular lipid metabolism can be further explored by assaying the substrates and products associated with MaIDH in the recombinant strain.

Citric acid is a key substrate that provides acetyl-CoA for fatty acid biosynthesis, and other metabolites from the TCA cycle also play critical roles in the lipid accumulation of filamentous fungi (24). In this study, the main metabolites from the TCA cycle in the recombinant strain overexpressing NAD^+-MaIDH3 were analyzed at 168 h of fermentation. It can be seen from **Table 3** that the citric acid content was increased, while isocitric acid, succinic acid, fumaric acid, malic acid, and pyruvic acid content in the recombinant strain was decreased compared to that in the control strain. These observations indicate that the overexpression of the NAD^+-MaIDH3 strain resulted neither in greater carbon flux to the TCA cycle nor fatty acid biosynthesis. This is consistent with the result that overexpression of the NAD^+-MaIDH3 strain had a low content of fatty acid accumulation.

TABLE 3 | Changes in related metabolite of NAD^+-MaIDH recombinant strains.

Metabolite	Relative amount (*M. alpina-MaIDH3*/*M. alpina*)
Citric acid	1.16 ± 0.04
Isocitric acid	0.90 ± 0.07
α-ketoglutarate	1.00 ± 0.05
Succinic acid	0.64 ± 0.08
Fumaric acid	0.86 ± 0.09
Malic acid	0.93 ± 0.03
Pyruvic acid	0.61 ± 0.04

TABLE 4 | NADPH production in *M. alpina-MaIDH4* recombinant strains.

Strains	NADPH/(NADPH+$NADP^+$) (%)
M. alpina	36.5 ± 6.2
M. alpina-MaIDH4	50.3 ± 3.9

With there being eight condensations reactions needed to produce a C18-fatty acyl-CoA, then 16 mol NADPH are needed. The source of this NADPH is then one of the major metabolic challenges in elucidating lipid biosynthesis in

oleaginous microorganisms (39). According to the measurements of intracellular NADPH reducing power, the overexpression of $NADP^+$-MaIDH4 in *M. alpina* could effectively increase intracellular NADPH content. As shown in **Table 4**, the NADPH content in the $NADP^+$-MaIDH4 overexpressing strain increased from 36.5 to 50.3% compared to the control strain. The results showed that $NADP^+$-MaIDH4 could effectively regulate intracellular NADPH content and increase lipid accumulation. Similar results were reported in previous studies. The study of Hao et al. found that overexpression of malic enzyme had a significant effect on NADPH production and lipid biosynthesis in *M. alpina* (29). Hao et al. also studied the source of NADPH in *M. alpina* and the results indicated that overexpression of the enzymes from pentose phosphate pathway could enhance NADPH contributor and increases fatty acid production (31).

CONCLUSION

In this study, we constructed isoenzyme-overexpressing strains of MaIDH to explore their roles in lipid synthesis in *M. alpina*. Overexpressing NAD^+-MaIDH3 reduced total lipid content due to its greater carbon flux with the tricarboxylic acid cycle and less carbon flux with fatty acid biosynthesis. While $NADP^+$-MaIDH4 enhanced the total fatty acid content may be due to the great reducing power NADPH is produced in the overexpression strain. Our results provide theoretical support for the analysis of the lipid synthesis mechanism in *M. alpina*.

DATA AVAILABILITY STATEMENT

The original contributions presented in the study are included in the article/**Supplementary Material**, further inquiries can be directed to the corresponding author/s.

AUTHOR CONTRIBUTIONS

XT and XS: carried out the experiments and drafted the manuscript. XT, XS, and XW: analyzed the data and helped to draft the manuscript. HZ, YC, JZ, HC, and WC: conceived and designed the study and revised the manuscript. All authors contributed to the article and approved the submitted version.

FUNDING

This research was supported by the National Natural Science Foundation of China (31901659 and 31722041), the project funded by China Postdoctoral Science Foundation (2017M611701), the Postdoctoral Science Foundation of Jiangsu Province (1701061C), the National First-class Discipline Program of Food Science and Technology (JUFSTR20180102), and the Jiangsu Province Collaborative Innovation Center for Food Safety and Quality Control.

SUPPLEMENTARY MATERIAL

The Supplementary Material for this article can be found online at: https://www.frontiersin.org/articles/10.3389/fnut.2021.746342/full#supplementary-material

REFERENCES

1. Tang X, Chang L, Gu S, Zhang H, Chen YQ, Chen H, et al. Role of beta-isopropylmalate dehydrogenase in lipid biosynthesis of the oleaginous fungus *Mortierella alpina*. *Fungal Genet Biol.* (2021) 152:103572. doi: 10.1016/j.fgb.2021.103572
2. Sakuradani E. Advances in the production of various polyunsaturated fatty acids through oleaginous fungus breeding. *Biosci Biotechnol Biochem.* (2010) 74:908–17. doi: 10.1271/bbb.100001
3. Nobuhiro K, Shigenobu K, Kenichi N, Rokuro M, Makoto M, Satoshi O, et al. Calpinactam, a new anti-mycobacterial agent, produced by *Mortierella alpina* FKI-4905. *J Antibiotics.* (2010) 63:183–6. doi: 10.1038/ja.2010.14
4. Eiji S, Sakayu S. Single cell oil production by *Mortierella alpina*. *J Biotechnol.* (2009) 144:31–6. doi: 10.1016/j.jbiotec.2009.04.012
5. Dyal SD, Narine SS. Implications for the use of Mortierella fungi in the industrial production of essential fatty acids. *Food Res Int.* (2005) 38:445–67. doi: 10.1016/j.foodres.2004.11.002
6. Domínguez-Martín MA, López-Lozano A, Diez J, Gómez-Baena G, Rangel-Zúñiga OA, García-Fernández JM. Physiological regulation of isocitrate dehydrogenase and the role of 2-oxoglutarate in *Prochlorococcus sp.* strain PCC 9511. *PLoS ONE.* (2014) 9:e103380. doi: 10.1371/journal.pone.0103380
7. Nekrutenko A, Hillis DM, Patton JC, Bradley RD, Baker RJ. Cytosolic isocitrate dehydrogenase in humans, mice, and voles and phylogenetic analysis of the enzyme family. *Mol Biol Evol/.* (1998) 15:1674. doi: 10.1093/oxfordjournals.molbev.a025894
8. Abiko T, Obara M, Ushioda A, Hayakawa T, Hodges M, Yamaya T. Localization of NAD-isocitrate dehydrogenase and glutamate dehydrogenase in rice roots: candidates for providing carbon skeletons to NADH-glutamate synthase. *Plant &Cell Physiol.* (2005) 46:1724. doi: 10.1093/pcp/pci188
9. Minard KI, Mcalisterhenn L. Antioxidant function of cytosolic sources of NADPH in yeast. *Free Rad Biol Med.* (2001) 31:832–43. doi: 10.1016/S0891-5849(01)00666-9
10. Choi IY, Sup KI, Kim HJ, Park JW. Thermosensitive phenotype of *Escherichia coli* mutant lacking NADP+-dependent isocitrate dehydrogenase. *Redox Rep Commun Free Rad Res.* (2003) 8:51. doi: 10.1179/135100003125001251
11. Suzuki K, Takada Y. Characterization of NADP(+)-dependent isocitrate dehydrogenase isozymes from a psychrophilic bacterium, *Colwellia psychrerythraea* strain 34H. *Biosci Biotechnol Biochem.* (2016) 80:1492. doi: 10.1080/09168451.2016.1165602
12. Martínez-Rivas JM, Vega JM. Purification and characterization of chloroplastic NADP-isocitrate dehydrogenase from *Chlamydomonas reinhardtii*. *Physiol Plantarum.* (2010) 118:157–63. doi: 10.1034/j.1399-3054.2003.00082.x
13. Kil IS, Park JW. Regulation of mitochondrial NADP+-dependent isocitrate dehydrogenase activity by glutathionylation. *J Biol Chem.* (2005) 280:10846–54. doi: 10.1074/jbc.M411306200
14. Corpas FJ, Barroso JB, Sandalio LM, Palma JM, Río LAD. Peroxisomal NADP-dependent isocitrate dehydrogenase. characterization and activity

regulation during natural senescence. *Plant Physiol.* (1999) 121:921–8. doi: 10.1104/pp.121.3.921
15. Chen R, Le Maréchal P, Vidal J, Jacquot JP, Gadal P. Purification and comparative properties of the cytosolic isocitrate dehydrogenases (NADP) from pea (*Pisum sativum*) roots and green leaves. *Febs J.* (2010) 175:565–72. doi: 10.1111/j.1432-1033.1988.tb14229.x
16. Muro-Pastor MI, Florencio FJ. Purification and properties of NADP-isocitrate dehydrogenase from the unicellular cyanobacterium *Synechocystis sp.* PCC 6803. *Febs J.* (1992) 203:99–105. doi: 10.1111/j.1432-1033.1992.tb19833.x
17. Sun YK, Park JW. Cellular defense against singlet oxygen-induced oxidative damage by cytosolic NADP + -dependent isocitrate dehydrogenase. *Free Rad Res Commun.* (2003) 37:309–16. doi: 10.1080/1071576021000050429
18. Su ML, Koh HJ, Park DC, Song BJ, Huh TL, Park JW. Cytosolic NADP-dependent isocitrate dehydrogenase status modulates oxidative damage to cells. *Free Rad Biol Med.* (2002) 32:1185–96. doi: 10.1016/S0891-5849(02)00815-8
19. Jo SH, Son MK, Koh HJ, Lee SM, Song IH, Kim YO, et al. Control of mitochondrial redox balance and cellular defense against oxidative damage by mitochondrial NADP+-dependent isocitrate dehydrogenase. *J Biol Chem.* (2001) 276:16168–76. doi: 10.1074/jbc.M010120200
20. Alpdagtas S, Binay B. Nadp+-dependent formate dehydrogenase: a review. *Biocatal Biotransform.* (2021) 39:260–8. doi: 10.1080/10242422.2020.1865933
21. Alpdagtaş S, Yücel S, Kapkaç HA, Liu S, Binay B. Discovery of an acidic, thermostable and highly NADP+ dependent formate dehydrogenase from *Lactobacillus buchneri* NRRL B-30929. *Biotechnol Lett.* (2018) 40:1135–47. doi: 10.1007/s10529-018-2568-6
22. Alpdagtaş S, Çelik A, Ertan F, Binay B. DMSO tolerant NAD (P) H recycler enzyme from a pathogenic bacterium, *Burkholderia dolosa* PC543: effect of N-/C-terminal His Tag extension on protein solubility and activity. *Eng Life Sci.* (2018) 18:893–903. doi: 10.1002/elsc.201800036
23. Wynn JP, Hamid AA, Li Y, Ratledge C. Biochemical events leading to the diversion of carbon into storage lipids in the oleaginous fungi *Mucor circinelloides* and *Mortierella alpina*. *Microbiology.* (2001) 147:2857–64. doi: 10.1099/00221287-147-10-2857
24. Tang X, Chen H, Chen YQ, Chen W, Garre V, Song Y, et al. Comparison of biochemical activities between high and low lipid-producing strains of *Mucor circinelloides*: an explanation for the high oleaginicity of strain WJ11. *PLoS ONE.* (2015) 10:e0128396. doi: 10.1371/journal.pone.0128396
25. Ling FZ, Tang X, Zhang H, Chen YQ, Zhao JX, Chen HQ, et al. Role of the mitochondrial citrate-oxoglutarate carrier in lipid accumulation in the oleaginous fungus *Mortierella alpina*. *Biotechnol Lett.* (2021) 43:1455–66. doi: 10.1007/s10529-021-03133-x
26. Li X, Wang P, Ge Y, Wang W, Abbas A, Zhu G. NADP+-Specific isocitrate dehydrogenase from oleaginous yeast *Yarrowia lipolytica* CLIB122: biochemical characterization and coenzyme sites evaluation. *Appl Biochem Biotechnol.* (2013) 171:403–16. doi: 10.1007/s12010-013-0373-1
27. Tang W, Zhang S, Wang Q, Tan H, Zhao ZK. The isocitrate dehydrogenase gene of oleaginous yeast *Lipomyces starkeyi* is linked to lipid accumulation. *Can J Microbiol.* (2009) 55:1062–9. doi: 10.1139/W09-063
28. Yang W, Dong SQ, Yang JH, Mohamed H, Shah AM, Nazir Y, et al. Molecular mechanism of citrate efflux by the mitochondrial citrate transporter CT in filamentous fungus *Mucor circinelloides* WJ11. *Front Microbiol.* (2021) 12:673881. doi: 10.3389/fmicb.2021.673881
29. Hao G, Chen H, Wang L, Gu Z, Song Y, Zhang H, et al. Role of malic enzyme during fatty acid synthesis in the oleaginous fungus *Mortierella alpina*. *Appl Environ Microbiol.* (2014) 80:2672–8. doi: 10.1128/AEM.00140-14
30. Chang LL, Tang X, Lu HQ, Zhang H, Chen YQ, Chen HQ, et al. Role of adenosine monophosphate deaminase during fatty acid accumulation in oleaginous fungus *Mortierella alpina*. *J Agric Food Chem.* (2019) 67:9551–9. doi: 10.1021/acs.jafc.9b03603
31. Hao G, Chen H, Gu Z, Zhang H, Chen W, Chen YQ. Metabolic engineering of *Mortierella alpina* for enhanced arachidonic acid production through the NADPH supplying strategy. *Appl Environ Microbiol.* (2016) 82:3280–8. doi: 10.1128/AEM.00572-16
32. Lei W, Wei C, Yun F, Yan R, Zhennan G, Haiqin C, et al. Genome characterization of the oleaginous fungus *Mortierella alpina*. *PLoS ONE.* (2011) 6:e28319. doi: 10.1371/journal.pone.0028319
33. Chen H, Hao G, Wang L, Wang H, Gu Z, Liu L, et al. Identification of a critical determinant that enables efficient fatty acid synthesis in oleaginous fungi. *Sci Rep.* (2015) 5:11247. doi: 10.1038/srep11247
34. Wynn JP, Kendrick A, Ratledge C. Sesamol as an inhibitor of growth and lipid metabolism in *Mucor circinelloides* via its action on malic enzyme. *Lipids.* (1997) 32:605–10. doi: 10.1007/s11745-997-0077-1
35. Levitan O, Dinamarca J, Zelzion E, Lun DS, Guerra LT, Kim MK, et al. Remodeling of intermediate metabolism in the diatom *Phaeodactylum tricornutum* under nitrogen stress. *Proc Natl Acad Sci USA.* (2015) 112:412–7. doi: 10.1073/pnas.1419818112
36. Ishikawa K, Makanae K, Iwasaki S, Ingolia NT, Moriya H. Post-translational dosage compensation buffers genetic perturbations to stoichiometry of protein complexes. *PLoS Genet.* (2017) 13:e1006554. doi: 10.1371/journal.pgen.1006554
37. Yang F, Zhang S, Zhou YJ, Zhu Z, Lin X, Zhao ZK. Characterization of the mitochondrial NAD+ -dependent isocitrate dehydrogenase of the oleaginous yeast *Rhodosporidium toruloides*. *Appl Microbiol Biotechnol.* (2012) 94:1095–105. doi: 10.1007/s00253-011-3820-3
38. Lina Z, Huaiyuan Z, Liping W, Haiqin C, Chen YQ, Wei C, et al. (13)C-metabolic flux analysis of lipid accumulation in the oleaginous fungus *Mucor circinelloides*. *Bioresour Technol.* (2015) 197:23–9. doi: 10.1016/j.biortech.2015.08.035
39. Ratledge C. The role of malic enzyme as the provider of NADPH in oleaginous microorganisms: a reappraisal and unsolved problems. *Biotechnol Lett.* (2014) 36:1557–68. doi: 10.1007/s10529-014-1532-3

Conflict of Interest: The authors declare that the research was conducted in the absence of any commercial or financial relationships that could be construed as a potential conflict of interest.

frontiers in Nutrition

ORIGINAL RESEARCH
published: 09 December 2021
doi: 10.3389/fnut.2021.802231

Tricarboxylate Citrate Transporter of an Oleaginous Fungus *Mucor circinelloides* WJ11: From Function to Structure and Role in Lipid Production

Wu Yang[1†], *Aabid Manzoor Shah*[1†], *Shiqi Dong*[2], *Caili Sun*[1], *Huaiyuan Zhang*[1], *Hassan Mohamed*[1,3], *Xiuzhen Gao*[1], *Huirong Fan*[2*] *and Yuanda Song*[1*]

[1] *Colin Ratledge Center for Microbial Lipids, School of Agriculture Engineering and Food Sciences, Shandong University of Technology, Zibo, China,* [2] *Tianjin Key Laboratory of Radiation Medicine and Molecular Nuclear Medicine, Institute of Radiation Medicine, Chinese Academy of Medical Sciences and Peking Union Medical College, Tianjin, China,* [3] *Department of Botany and Microbiology, Faculty of Science, Al-Azhar University, Assiut, Egypt*

OPEN ACCESS

Edited by:
Marcello Iriti,
University of Milan, Italy

Reviewed by:
Csilla Szebenyi,
University of Szeged, Hungary
Yana Sergeeva,
Kurchatov Institute, Russia

***Correspondence:**
Yuanda Song
ysong@sdut.edu.cn
Huirong Fan
fanhr99@163.com

[†] These authors have contributed equally to this work and share first authorship

Specialty section:
This article was submitted to Food Chemistry, a section of the journal Frontiers in Nutrition

Received: *26 October 2021*
Accepted: *15 November 2021*
Published: *09 December 2021*

Citation:
Yang W, Shah AM, Dong S, Sun C, Zhang H, Mohamed H, Gao X, Fan H and Song Y (2021) Tricarboxylate Citrate Transporter of an Oleaginous Fungus Mucor circinelloides WJ11: From Function to Structure and Role in Lipid Production. Front. Nutr. 8:802231. doi: 10.3389/fnut.2021.802231

The citrate transporter protein (CTP) plays an important role in citrate efflux from the mitochondrial matrix to cytosol that has great importance in oleaginous fungi. The cytoplasmic citrate produced after citrate efflux serves as the primary carbon source for the triacylglycerol and cholesterol biosynthetic pathways. Because of the CTP's importance, our laboratory has extensively studied its structure/function relationships in *Mucor circinelloides* to comprehend its molecular mechanism. In the present study, the tricarboxylate citrate transporter (Tct) of *M. circinelloides* WJ11 has been cloned, overexpressed, purified, kinetically, and structurally characterized. The Tct protein of WJ11 was expressed in *Escherichia coli*, isolated, and functionally reconstituted in a liposomal system for kinetic studies. Our results showed that Tct has a high affinity for citrate with Km 0.018 mM. Furthermore, the *tct* overexpression and knockout plasmids were created and transformed into *M. circinelloides* WJ11. The mitochondria of the *tct*-overexpressing transformant of *M. circinelloides* WJ11 showed a 49% increase in citrate efflux, whereas the mitochondria of the *tct*-knockout transformant showed a 39% decrease in citrate efflux compared to the mitochondria of wild-type WJ11. To elucidate the structure-function relationship of this biologically important transporter a 3D model of the mitochondrial Tct protein was constructed using homology modeling. The overall structure of the protein is V-shaped and its 3D structure is dimeric. The transport stability of the structure was also assessed by molecular dynamics simulation studies. The activity domain was identified to form hydrogen bond and stacking interaction with citrate and malate upon docking. Tricarboxylate citrate transporter has shown high binding energy of −4.87 kcal/mol to citric acid, while −3.80 kcal/mol to malic acid. This is the first report of unraveling the structural characteristics of WJ11 mitochondrial Tct protein and understanding the approach of the transporting toward its substrate. In

conclusion, the present findings support our efforts to combine functional and structural data to better understand the Tct of *M. circinelloides* at the molecular level and its role in lipid accumulation.

Keywords: *Mucor circinelloides*, tricarboxylate citrate transporter, molecular dynamics, citrate efflux, molecular modeling

INTRODUCTION

Citrate, an intermediate of Krebs cycle, is a precursor to lipid and cholesterol biosynthesis as well as a nexus point between glucose and lipid pathways (1–4). In oleaginous fungi, extra citrate in the mitochondria had to be transported into the cytosol and metabolized by ATP-citrate lyase to form acetyl-CoA, an important precursor for lipid biosynthesis (5, 6). Intracellular citrate influences the activity of key enzymes in fatty acid (FA) oxidation and glycolysis (7). Citrate products, such as malonyl CoA, play important signaling roles in energy expenditure regulation (8). Citrate cannot diffuse through the mitochondrial membrane therefore transport process is facilitated by mitochondrial citrate transport system (7). The ability of transporters to bind to their specific substrate is a major mechanism for modifying transport activity (9). To better understand the citrate binding potential to the tricarboxylate citrate transporter (Tct) in oleaginous *Mucor circinelloides*, its Tct binding properties must be known. *M. circinelloides* is a dimorphic Zygomycete fungus, a model organism for lipid studies that has been researched for the last 35 years (10, 11). Its biotechnological interest as a major source of carotenes and lipids especially γ-linolenic acid has gained the interest of researchers all over the world (6).

In the Zygomycota phylum, *M. circinelloides* has the most diverse repertoire of molecular tools (12, 13). This includes self-replicating plasmid-mediated genetic transformation, *Agrobacterium*-mediated integrative transformation, the generation of knockout mutants, and the use of RNAi-based procedures to suppress gene function (12). The known *Mucor* genome sequence aids in the identification and study of genes and proteins involved in the aforementioned processes, as well as the production of lipids useful in the production of biodiesel (13).

For decades, computational methods for predicting protein structure and ligand-protein interactions have been used successfully in biochemical research. Five transporters involved in mitochondrial citrate transportation were discovered in *M. circinelloides* based on their predicted function in the TCDB. These included a citrate transporter (Ct), also known as CiC, a tricarboxylate carrier (Tct), that was found transporting citrate out of mitochondria, and a malate transporter (Mt), which may be involved in malate translocation (14, 15). Recently, it was reported that the overexpressing of Tct in *M. circinelloides* resulted in a 68% increase in lipid production (16), implying that Tct facilitated citrate transport from mitochondria in *M. circinelloides*, which was associated with high lipid biosynthesis. Tricarboxylate carrier protein of *M. circinelloides* when blasted, was found as Tct (Mtc family) belongs to the mitochondrial carrier large family (MC) that have a specific character contains three times tandemly repeated 100 residue domain, with two hydrophobic segments and a signature sequence motif PX [D/E]XX [K/R]X [K/R] (20–30 residues) [D/E]GXXXX [W/Y/F][K/R]G (PFAM03820) (17, 18).

In this study, we examined the genome of *M. circinelloides* WJ11 a high lipid-producing strain to identify homology modeling, molecular docking, molecular dynamics, and citrate efflux of tricarboxylate carrier (Tct) involved in the citrate transport system. In order to gain a better understanding of the functions of the Tct transporter in the mitochondrial citrate transport system, general properties such as protein sequence identity and domain structure were studied *in silico* as well as their expression profiling *in vitro*. Our study confirmed that Tct contributes to the efflux of citrate from mitochondria that provide enough carbon sources for cell utilization thus have a significant impact on lipid accumulation.

MATERIALS AND METHODS

Strains, Media, and Culture Conditions

Competent *Escherichia coli* BL21 (DE3) cells were used for *tct* gene heterologous expression (19). For fungal transformation experiments, *M. circinelloides* WJ11 (CCTCC No. M2014424; China Center for Type Culture Collection) was used as the recipient strain for *tct* gene overexpression and knockout.

Mucor circinelloides cultures were inoculated at approximately 10^6-10^7 spores/ml into 150 ml K&R seed medium (1 L flask with baffles) and incubated at 28°C for 24 h in an incubator shaker with 150 rpm (revolution/min). The 10% seed culture was then inoculated into a 1.5 L modified K&R fermentation medium in a 2 L bioreactor (BioFlo/CelliGen115, New Brunswick Scientific, Edison, NJ, USA) (20). At 72 h, culture samples of transformed strain were taken for further experimentation (5, 15, 21).

Transport Activity Determination of Tct Reconstituted Liposomes

Heterologous Expression and Purification

The entire *tct* gene sequence was optimized (according to *E. coli* codon usage), synthesized, and subcloned into the expression vector pET30a(+). The plasmid pET30a(+)-*tct* was made using the following cloning strategy: pET30a-NdeI-ATG-ct-Histag-Stop codon-HindIII-pET30a.The heat-shock method was used for transformation in the BL21 (DE3) strain. The pET30a-*tct* recombinant strain BL21 (DE3) was inoculated into LB broth medium supplemented with kanamycin incubated at 37°C for 16 h (22). Pre-inoculum (1 ml) was inoculated into 100 ml LB_{kan} and culture was grown at 37 °C until OD600 was reached 1.2. The expression of pET30a-tct were induced by IPTG at 15°C for 16 h before being harvested by centrifugation (5,000 g for 10 min). Cell

pellets were resuspended in lysis buffer (50 mM Tris, 150 mM NaCl, 5% glycerol, pH 8.0), then sonicated for 10 min. Urea was then used to dissolve the precipitate. Denatured protein was obtained in a single step using a Ni-column purification method (23). The target protein was renatured and sterilized by passing it through a 0.22 μm filter. Isolated pure protein was dissolved in 1X PBS (Phosphate-buffered saline), pH 7.4, 10% glycerol, and 0.5 M L-arginine. The concentration was determined using the Bradford protein assay, which used BSA (Bovine serum albumin) as the standard. SDS-PAGE and Western blot (GenScript, Cat. No. A00186) were used to analyze samples of whole cell lysate, supernatant, and debris. Standard SDS-PAGE and western blot confirmation were used to determine protein purity and molecular weight (**Supplementary Figure 1**).

Tct Liposome Reconstitution and Transport Assay

The liposomes were prepared by adding 232, 58, and 94 mg of soybean lecithin, cholesterol, Tween 80, respectively, in 15 ml mixture of chloroform: methanol (3:1). This mixture was dried by rotavapor at 50°C followed by the addition of 20 ml of 20 mM phosphate buffer. The resulting solution was placed in the ultrasonic bath for 10 min.

The solubilized recombinant protein was reconstituted into liposomes after being diluted three times with a buffer containing 3% Triton X-114 (w/v), 20 mM Na_2SO_4, and 10 mM piperazine-1,4-bisethanesulfonic acid (PIPES, pH 7.0). The liposome system was designed as follows: 1% TritonX-114, ultrasound-prefabricated liposome, 20 mM PIPES, 0.8 mg cardiolipin, and water replenishment to a final volume of 700 μl. These components were gently mixed, and the mixture was recycled 13 times before being passed through a hydrophobic chromatography column (Bio-Rad Beads SM-2). The substrates and 10 mM PIPES (pH 7.0) were used to pre-equilibrate the columns (24–26). The substrate in this case is to be embedded in a liposome that exchanges citrate. Except for the passages through the column, which were performed at room temperature, all other operations were carried out at 4°C. The amount of purified protein reconstructed into the liposome was determined using the method described by Vito et al. (27), and 11.2% of the protein was added to the reconstructed mixture. Immediately before transport, a given proteoliposomal sample was thawed, sonicated on ice, and passed through Sephadex G-75 columns pre-equilibrated with buffer (10 mM PIPES and 50 mM NaCl pH 7.0) to remove the external citrate and other substrates.

To begin transport at 25°C, radioactive [^{14}C] citrate (PerkinElmer Life Sciences) was added to either substrate-loaded (exchange) or empty proteoliposomes. The reaction was stopped by adding 20 mM pyridoxal 5'-phosphate, which completely and rapidly inhibits the activity of several MCTs (28, 29). The inhibitor was added together with the [^{14}C] citrate at the start of the controls using the "inhibitor-stop" method (24). Finally, Sephadex G-75 was used to remove the external radioactivity from the protein liposomes, and the radioactivity of the protein liposomes was measured using a Liquid Scintillation Analyzer (PerkinElmer, Tri-carb 4910TR) (26, 30). The linear regression analysis of the transport results yielded the Km-values.

Mitochondrial Transport Properties of Tct Mutants in WJ11

Construction of Over-Expression and Knockout Recombinant Mutants

The previous research work of our lab designed plasmids pMAT2085 and pMAT2060 for *tct* gene over-expression and knockout, respectively (unpublished data). The strain MU65, a uridine auxotrophic strain derived from WJ11 were transformed with pMAT2085 and pMAT2060 (31). To create the knockout strain, a plasmid carrying a selectable marker (pyrF) flanked by 1 kb of the tct gene's up and downstream regions was constructed. The selectable marker pyrF was amplified from M. circinelloides WJ11 strain. The three fragments (UP stream of tct, Downstream of tct and pyrF) were joined by overlap extension polymerase and the resultant fragment was cloned in pMAT2060. Restriction fragments from plasmid containing the pyrF gene, used as a selective marker, flanked by 1 kb sequences of the adjacent regions of the tct gene to allow homologous recombination were used to transform the MU65 strain, which is auxotrophic for uracil. After many vegetative cycles in the selective medium, transformed strains were selected and validated by PCR.

Mitochondrial Isolation

Transformed *M. circinelloides* were grown for 72 h in fermenter and the cell biomass was filtered, washed, and the mitochondria were isolated by the method as discussed in our previous research (17).

Viability Test for Isolated Mitochondria

To detect the mitochondrial viability, NADH and fumarate were added to the mitochondria suspension [100 μl NADH (0.5 mmol), 20 μl fumarate (7 mmol), 70 μl 1× PBS buffer (pH 7.4), and 10 μl mitochondria]. After 20 min of incubation, the absorbance of the biochemical reaction mixture was measured with a microporous plate absorbance spectrophotometer (Bio-Rad xMark^{TM}) at 340 nm using the enzymatic kinetic method (21).

Measuring Mitochondrial Transport Activity

The mitochondrial suspension was pre-incubated in a 30°C water bath for 3 min to "load" the mitochondria with [^{14}C] citrate before adding the substrate (21). The reaction is started by adding malate or α-ketoglutarate at the same time, and it is stopped by rapid centrifugation. The incorporation of [^{14}C] citrate radiolabel into mitochondrial pellets and the disappearance of [^{14}C] citrate radiolabel from incubations were used to determine citrate uptake. To achieve a final volume of 1.0 ml, 10 mM substrates were added simultaneously. After 5 min, the reactions were stopped by rapidly separating the mitochondria from the incubation mixture using the same centrifugation conditions.

Sequence and Structure Analysis of tct Gene

Tricarboxylate citrate transporter amino acid sequences were obtained from Uniprot and physicochemically predicted

using ProtParam (http://web.expasy.org/protparam/), while hydrophobicity was predicted using ProtScale (http://web.expasy.org/protscale/). Gene annotations were used to identify putative mitochondrial transporter genes in *M. circinelloides* WJ11 using databases such as the Kyoto Encyclopedia of Genes and Genomes (KEGG), the National Center for Biotechnology Information (NCBI), non-redundant proteins (NR), protein families (Pfam), and the transporter classification database (TCDB). The amino acid sequences of Cts of yeasts that resemble *Mucor* and mitochondrial transporter family members whose crystal structures have been determined were aligned with our sequenced Tct using the NCBI-PubMed database search results. Pairwise Sequence Alignment was used to analyze the homology of the sequences, which were then aligned with ClustalW and ESPript.

Homology Modeling and Model Quality Evaluation

LOMETS searched the PDB database (www.pdb.org) for proteins with similar topology to the target protein sequences that had already been resolved experimentally (32). The protein structures with a high Z-Score were chosen from the search results as the template structures for subsequent modeling calculations, and the results are shown in **Supplementary Table 1**.

The Tct protein structure was predicted by the protein topological similarity principle using the obtained template protein 3D structure files and sequence comparison files. Tricarboxylate citrate transporter protein structures were predicted separately using the I-TASSER threading method to obtain the target proteins' 3D structures. During the prediction calculation, five different target protein structures were generated, and each target protein structure was evaluated for plausibility using the C-score, target protein model with the highest score being chosen for further calculations.

Gromacs 4.6 kinetics software was used to optimize the target protein structure, either for the amino acid side chain, a segment of the structure, or the protein as a whole (33). To achieve the best results and get the target protein structure as close to the real structure as possible, it was necessary to optimize the protein structure as a whole using energy minimization. All structures were optimized in a periodic boundary water box using the Gromacs 4.6 force field, with a Steepest Decent optimization of 5,000 steps followed by a conjugate gradient optimization of 2,000 steps. This parameter configuration ensures that the protein structure was completely optimized. Unreasonable dihedral angles, side-chain structures, and excessively close contacts are eliminated during optimization, resulting in a more rational protein structure.

Tricarboxylate citrate transporter templates cannot be used directly for multimer modeling predictions due to their poor homology. As a result, molecular docking was used to predict the Tct multimeric structure model. The multimers are all dimeric, according to the template protein structure. As a result, molecular docking predicted a direct binding model of the two Tct subunits to construct dimers. The dimeric Tct protein structure was also optimized using the Gromacs 4.6 kinetics software, yielding the optimized Tct dimeric protein 3D structure.

Molecular Docking and Molecular Dynamics Simulations

Tricarboxylate citrate transporter protein was set as the receptor and the citric acid and malic acid small molecules as the ligands in AutodockTools (34). The binding modes of citric acid and malic acid at the Tct active site were searched for using molecular docking calculations, and the lowest energy binding mode was chosen for visualization with the PyMol program to provide insight into the binding interactions of different ligands with proteins during the transport process.

Simulation of kinetics: Citric acid (CIT) and malic acid (MAL) small molecule three-dimensional structure files were created using Chemdraw and combined with molecular docking results, and the energy minimum conformation of the protein-citric acid complex was calculated and output for molecular dynamics simulations. Gromacs 2018 created the initial model structure for the transmembrane molecular dynamics simulation; first, the cell membrane-protein-small molecule composite system was built based on the energy minimum complex conformation obtained through docking, and the cell membrane was a phospholipid bilayer of DOPC and DOPG (7:3). The cell membrane-transport protein-small molecule complex model was then subjected to a 30 ns molecular dynamics simulation in an aqueous environment system using a Gromacs-based solvent model. The force field Gromos 53A6 was used, and the water model was SPC. The simulated system employs a standard cubic box that is wrapped around the model and other molecules, with the complex in the center of the box. Before subjecting the model to a completely free kinetic simulation, the complex was optimized for 2,000 steps using the steepest descent method to eliminate possible atomic collisions. Following that, the protein was positioned and molecular dynamics simulations for the solvent were performed for 100 picoseconds (ps); then the protein backbone and ligand were restricted for 100 ps; finally, the restriction was removed and the simulation was performed for 100 ps, i.e., the pre-procedure. The simulated system's long-range van der Waals forces were set to 1.4 nm, and the classical interactions were calculated using the spherical "cut-off" radius method. The simulations were run in steps of 2 fs, with one conformation output every 100 ps, using periodic boundary conditions in all directions. Gromacs 2018 was used to trace the simulations, and PyMol and vmd were used to visualize them. The root mean square deviation (RMSD) can approximate the system's relative change in conformation and is an important criterion for determining whether the simulated system converges. As a result, RMSD is used in this research work to determine and judge the system's equilibrium moment.

Statistical Analysis

All statistical data from three independent values were analyzed by one-way analysis of the variance (ANOVA) with multiple comparison tests (Tukey's) using SPSS 16.0.

The data is presented as mean standard deviation (SD). The differences were statistically significant at $P < 0.05$.

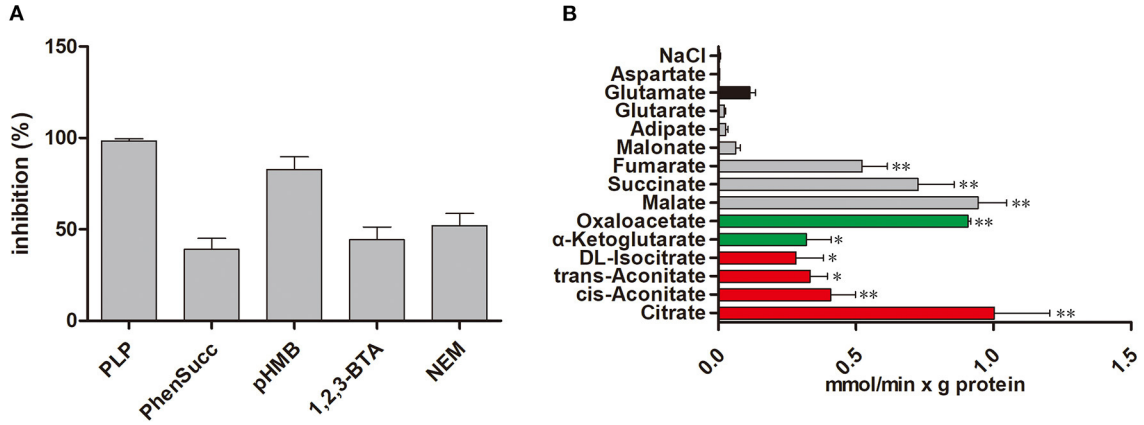

FIGURE 1 | Transport properties of Tct. **(A)** Effect on citrate/citrate exchange of Tct by inhibitors. Liposomes were reconstituted with Tct and preloaded internally with 10 mM citrate. Transport was initiated by the addition of 0.01 mM [^{14}C] citrate and terminated after 2 min. The concentrations of the inhibitors were 20 mM (PLP, pyridoxal 5′-phosphate), 2 mM (phesucc, phenylsuccinate), 0.1 mM (pHMB, p-hydroxymercuribenzoate), 2 mM (1,2,3-BTA, 1,2,3-benzenetricarboxylate), 1 mM (NEM, N-ethylmaleimide) **(B)** Tct transport activity is substrate dependent. Tct-reconstructed liposomes were preloaded internally with 20 mM substrates (Red: tricarboxylic acids. Green color: α-ketodicarboxylic acids. Gray color: dicarboxylic acids. Black color: other compounds). Transport was initiated by the addition of external 0.01 mM [^{14}C] citrate. The values are means ± SEM of three independent experiments. *represents significant difference $p < 0.05$ while as **represents $p < 0.01$.

RESULTS

Experimental Validation of Tct

Our previous research on mitochondrial transporters revealed the presence of two MCTs (Tct and Ct) in oleaginous *M. circinelloides* WJ11, which are associated with high lipid accumulation (15, 17). The molecular investigation of citrate efflux from the mitochondria by Tct in *M. circinelloides* was first investigated in this study. For the mechanistic study of Tct, and the citrate transporter gene (*tct* of WJ11) was expressed and purified in *E. coli*. The protein's citrate transport activity was investigated in Tct reconstituted liposomes.

We examine the impact of certain MCT inhibitors on the recombinant Tct-catalyzed [^{14}C] citrate/citrate exchange reaction (**Figure 1A**). Pyridoxal-5'-phosphate (PLP) and pHMB strongly inhibit Tct transport activity, that is why PLP was utilized as a reaction termination inhibitor. The homo-exchange activity of Tct at internal and external concentrations of 10 μM and 10 mM of [^{14}C] citrate and citrate, respectively, were inhibited by PLP. The highest absorption activity of [^{14}C] citrate in proteoliposomes was achieved by internal citrate, malate, oxaloacetate, succinate, and fumarate. [^{14}C] citrate is also exchanged, to a less extent, with internal α-ketoglutarate, isocitrate, and aconitate (**Figure 1B**). Our results showed that Tct has a high efficiency value for [^{14}C] citrate/citrate exchange with Km 0.018 mM at 25 °C. Furthermore, the *tct* overexpression and knockout plasmids were created and transformed into *M. circinelloides* WJ11. A modified K & R medium with glucose as the sole carbon source was used to grow these engineered strains. The mitochondria of transformed strain were isolated, and their transport activity was investigated. The current study used ^{14}C metabolic flux analysis on recombinant *M. circinelloides* strains to examine the effects of *tct* gene overexpression or knockout on metabolic fluxes using calculated extracellular flux values. In the presence of 10 mM malate, the mitochondria of the *tct*-overexpressing transformant showed a 49% increase in [^{14}C] citrate efflux, whereas the mitochondria of the *tct*-knockout transformant showed a 39% decrease in citrate efflux compared to the mitochondria of wild-type WJ11 (**Figure 2**). These findings support the importance of Tct in citrate efflux from the oleaginous fungus *M. circinelloides*, which is associated with high lipid accumulation.

Tct Sequence Characteristics

The *tct* genes of WJ11 encode protein with a total of 321 amino acid residues. The sequence similarities between Tct and Ct proteins were found to be 39.6%. The Tct protein was found to contain 12.1% of positively charged amino acid residues (Arg+His+Lys) and 7.8% of negatively charged amino acid residues (Asp+Glu). The hydrophobic residues in Tct protein were high ≈50.6% which provided a foundation for the stable embedding of transmembrane proteins into non-polar lipid membrane (**Figure 3**). The significant hydrophobicity (total average hydrophilic value of 0.089) of Tct protein provides a basis for embedding in the cell membrane and functioning as a stable transporter protein in biological cells.

Homology Modeling Analysis

Models were created by manually aligning Tct protein sequence of WJ11 to each of the available templates. Although the protein sequence comparison with the other template sequences in NCBI revealed low homology that prevents reliable alignment. As a result, cycles of computerized modeling followed by manual alignment improvement were performed until a model that satisfies data and constraints was generated. Based on the 10 selected Protein Data Bank (PDB) structures, the 3D structure prediction of Tct was performed. The template sequences all covered the entire Tct sequence provides a basis for structure

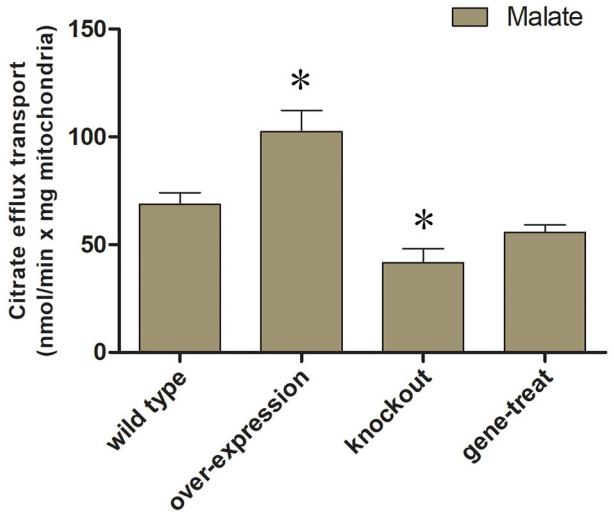

FIGURE 2 | Mitochondrial transport activity of transformed *M. circinelloides* strains. Mitochondria from the wild-type transformants, overexpressed and knockout were preloaded with 0.01 mM [14C] citrate. For exchange malate were added as substrates (10 mM malate) outside of mitochondria. Error bars represent standard deviations ($n = 3$). *represents significant difference $p < 0.05$.

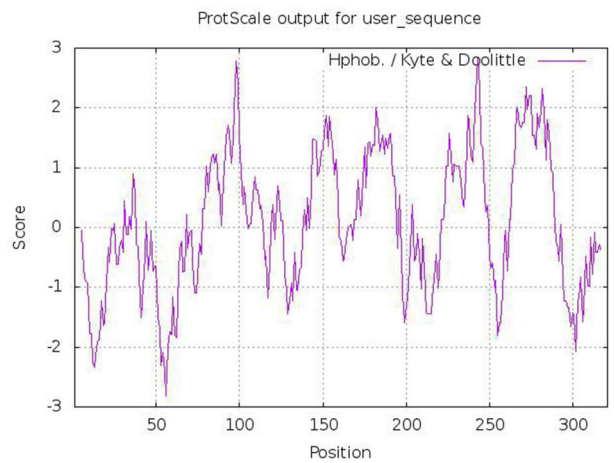

FIGURE 3 | Predicted hydrophobicity analysis of Tct protein heavy chains (>0 indicates hydrophobicity; <0 indicates hydrophilicity).

prediction by the threading method (fold recognition), which improves the accuracy of the predicted structures. Because of the low sequence homology models based solely on sequence alignment were not expected to produce good results. Manual alignment optimization avoided this issue to some extent and enabled the generation of an acceptable model for Tct protein.

Tricarboxylate citrate transporter is a transmembrane protein that facilitates the transport of molecules therefore its transmembrane structure prediction is of great significance. The results of the transmembrane structure prediction of Tct by TMHMM (http://www.cbs.dtu.dk/services/TMHMM) are shown in **Figure 4**. Tricarboxylate citrate transporter contains

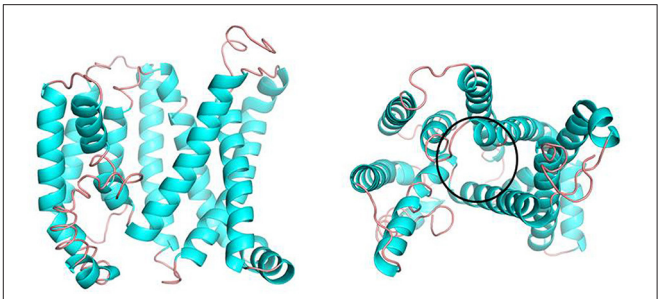

FIGURE 4 | Side view (left) and top view (right) of the 3D structure of the Tct model.

three transmembrane structures (i.e., 141–163, 178–195, and 262–284), while the chain structures 75–125 and 225–250 also have a 50% probability of being transmembrane structures. The overall structure of the protein is V-shaped and intra-membrane.

Figure 5 depicts the three-dimensional structure of the Tct dimeric protein. Tricarboxylate citrate transporter's two subunits dimerize in a spatially complementary manner, with the lateral helical chains inserted into each other's subunit vacancies, forming good spatial complementarity. The electrostatic surface of the Tct monomer, with the positively charged region in blue, the negatively charged region in red, and the white region (large portion) is the non-charged or very low charge region, i.e., the non-polar region; thus, the Tct surface is densely packed with hydrophobic residues. The two subunits aggregate via hydrophobic interactions on the subunit surface, promoting multimer aggregation and binding stability. **Figure 5** also depicts the binding electrostatic surface of Tct's two subunits. Tricarboxylate citrate transporter's binding interface is only in the non-polar hydrophobic region, according to the electrostatic analysis of the binding interface.

3D Structure Prediction and Active Site Analysis

The Ramachandran plot of amino acid residues obtained from PROCHECK program evaluated the constructed Tct protein structure as shown in **Figure 6**. The model Tct structure contains 70.7% of the amino acids in the core region, 23.3% of the amino acid residues in the allowed region, 4.2% of the amino acid residues in the maximum allowed region, and only 1.8% of the amino acid residues in the forbidden region of the torsion angle. Although the Tct whole protein chain segment model contains five residues in the forbidden region of the torsion angle, this is due to the greater flexibility of this region of the protein. Because the protein as a whole follows the stereochemical energy rules, the constructed protein model has a reasonably accurate stereological structure.

The higher the Overall quality factor value, the better the result, generally up to one for high resolution crystal structures and only around 91% for average resolution. **Figure 7** shows the results of the ERRAT analysis for the Tct protein, with an ERRAT value of 91.374 indicating the high accuracy of the model generated by the structure prediction. The two error limits

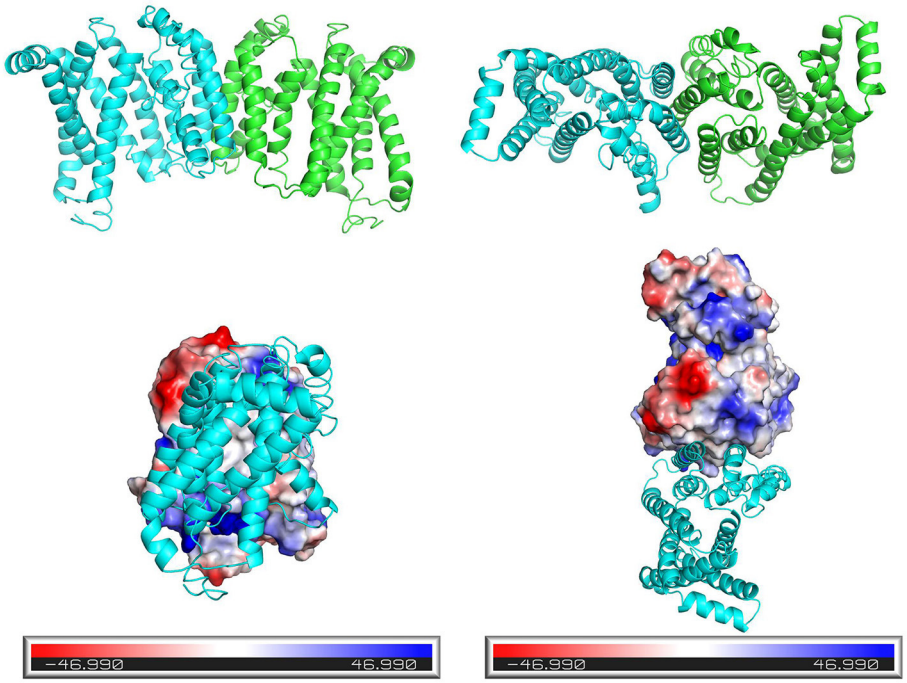

FIGURE 5 | Side view (left) and top view (right) of the three-dimensional structure of the dimer formed by the two subunits of Tct, and electrostatic surface view of the monomeric protein.

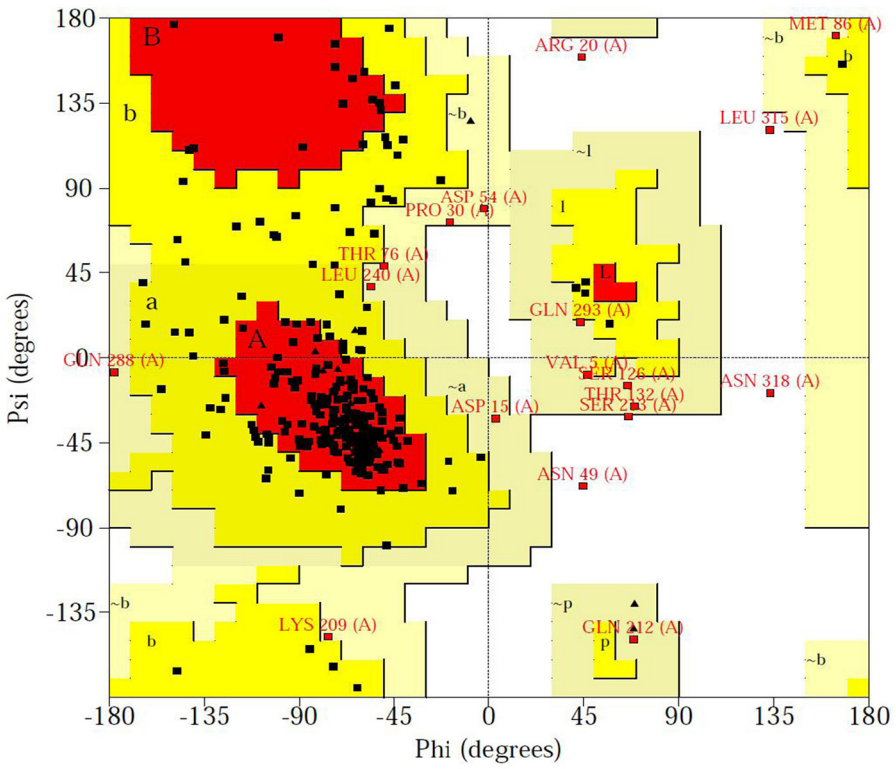

FIGURE 6 | Ramachandran plot of Tct protein structure obtained from Procheck program.

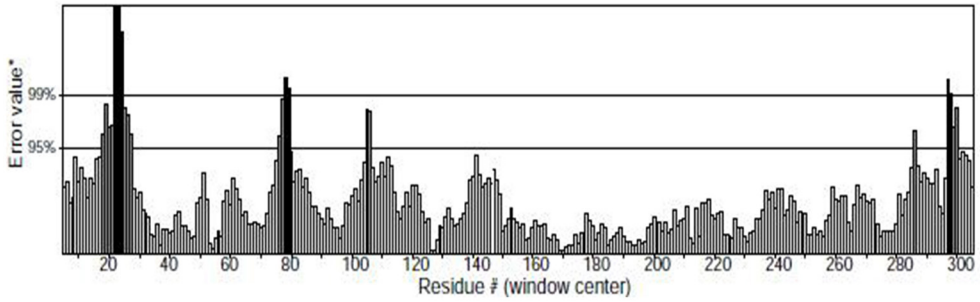

FIGURE 7 | ERRAT diagram of the Tct protein model.

present in the graph indicate how likely it is that the region above the line is problematic, and below the error, line indicates a protein structure with high resolution. Based on this result, it can be seen that the ERRAT values for amino acid residues near residues 21–28 in the Tct protein chain segment are above the two error lines due to the high flexibility of this region due to the Loop; the rest of the structures are below the error lines.

Molecular Docking With Citrate and Malate

Using Autodock's molecular docking, the interaction of citric acid and malic acid with Tct transporter proteins was investigated at the molecular level. Tricarboxylate citrate transporter had binding energy of −4.87 kcal/mol to citric acid, while −3.80 kcal/mol to malic acid. The lower the binding energy, the more stable is the binding of a molecule to the protein. Citric acid was found more stable binding than malic acid.

Figure 8 show the binding patterns of citric and malic acids in the Tct protein active site. As can be seen from **Figure 8**, citric and malic acids can be stably bound in the Tct transporter protein active pocket by interaction with residues after deprotonation. Comparative analysis revealed that citric acid can interact with key residues ARG22, LYS65, LYS177, and PHE222 in the Tct active site by hydrogen bonding, with double hydrogen-bonding interactions with ARG22 and LYS177, allowing citric acid to be stably bound at the bottom of the active pocket, providing for its transport. In contrast, malic acid can also hydrogen-bond with ARG22, LYS65, LYS177, and the key residue PHE222 in its binding in the Tct active site, but only the double hydrogen-bonding interaction with LYS177 is present, resulting in a slightly less stable binding than that of citric acid. This is one of the reasons why malic acid has a higher docking binding energy than citric acid.

The electrostatic matching of citric and malic acids with Tct is depicted in **Figure 8**. The electrostatic surface distribution map of Tct shows that the majority of the interior of the Tct transporter protein's active cavity is a positively charged region, which provides the electrostatic environment for stable binding of citric and malic acids after deprotonation. As a result of the deprotonation of the citric and malic acid carboxyl groups, the polycarboxyl functional groups are negatively charged and can bind strongly electrostatically to the positive region at the active site's bottom. Because citric acid contains three deprotonated carboxyl groups, the electrostatic binding interaction with Tct proteins is stronger, improving binding stability and lowering binding energy, providing a theoretical explanation for the small molecule transport mechanism and transport efficiency.

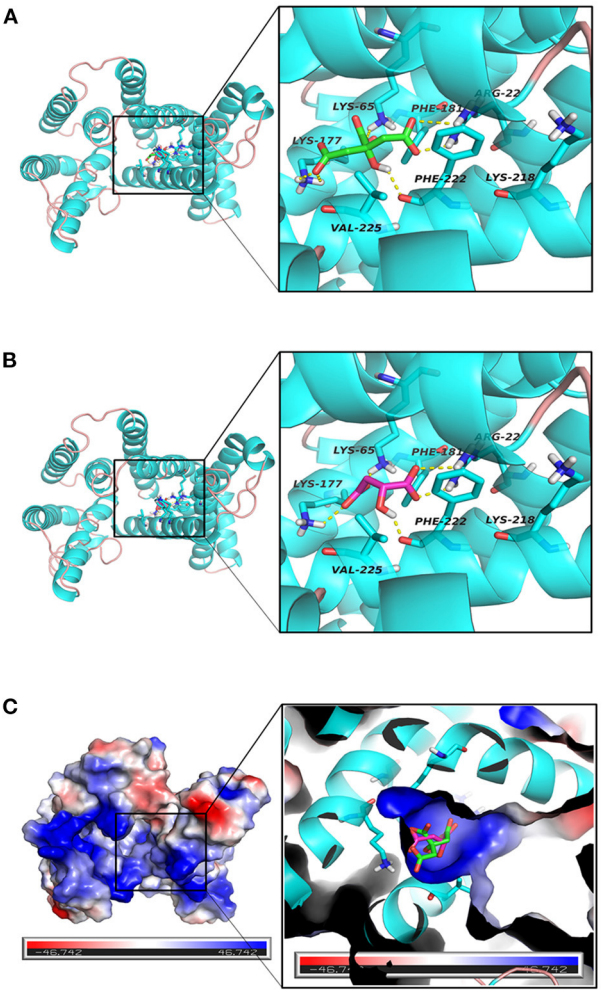

FIGURE 8 | (A–C) Tct Transport Protein (Cyan), citrate (green), malate (red) binding interaction diagram and three-dimensional structure diagram of the active site.

Molecular Dynamics Simulation of Tct Protein Interacting Small Molecules

The initial RMSD of the complexes fluctuated considerably due to the protein-small molecule cell membrane interactions, the adjustment and adaptation of the systems to the solvent effect; after 10 ns, both the Tct-CIT and Tct-MAL systems reached equilibrium and the RMSD of the systems stabilized at around 0.4–0.5 nm, fluctuating within 0.1 nm. The molecular dynamics simulations in the solvent systems were all stable. The kinetic simulations for the Tct-CIT and Tct-MAL systems were carried out to extract the conformational structures for a more detailed comparative analysis, and the results are shown in **Figures 9–11**. As can be seen from **Figure 10** the Tct-CIT system showed some degree of fluctuation in protein structure during the kinetic process due to the effect of cell membrane and solubilization. During the kinetic simulation, the helical chain of Tct underwent helicalization, followed by unhelicalization and post-helicalization (**Figure 10**). However, the overall structure of Tct did not change much and was relatively stable, while the Tct-MAL system was relatively stable during the kinetic simulations, with no significant changes in the overall tertiary structure of the protein (**Figure 11**). At the same time, the binding of CIT and MAL, respectively, to Tct remained relatively stable during the kinetic simulations, and there was no dissociation. To further determine the binding of CIT and MAL to Tct, the minimum distances between the small molecules and Tct during the kinetic simulations were analyzed, and it was found that the minimum distances between the small molecules and the protein were both stable at around 0.17 nm (**Figure 12**), with little difference. The distance is just one hydrogen bond distance, i.e., the two are more stable in the transport protein and there is no dissociation.

The radius of gyration trajectories of the proteins can indicate the stability of the proteins during the kinetic process, and also the degree of protein tightness. As can be seen from **Figure 12B**, the radius of gyration of the translocated proteins in the Tct-CIT and Tct-MAL systems was essentially constant throughout the kinetic simulations under the interaction of solubilization and cell membranes; the Rg of the same protein was also essentially constant in the simulations calculated for different systems. The Rg of Tct in the Tct-CIT and Tct-MAL systems was also relatively small after equilibration, at around 2.2 nm, and fluctuations can also be small. Thus, solubilization and cell membrane interactions did not lead to any adjustment of the protein structure and did not affect the transport process of small molecules, thus allowing efficient transport of small molecules with good activity.

Figure 12 shows the secondary structure content of Tct in the Tct-CIT and Tct-MAL systems during the kinetic simulations; in the Tct-CIT system, there was a significant increase in the Helix content of Tct, with significant fluctuations (**Figure 12E**), due to the unfolding of the Sheet content into helical chains, while the random loop Coil content was largely unchanged. In contrast, in the Tct-MAL system, the Sheet chain unfolded to a lesser extent,

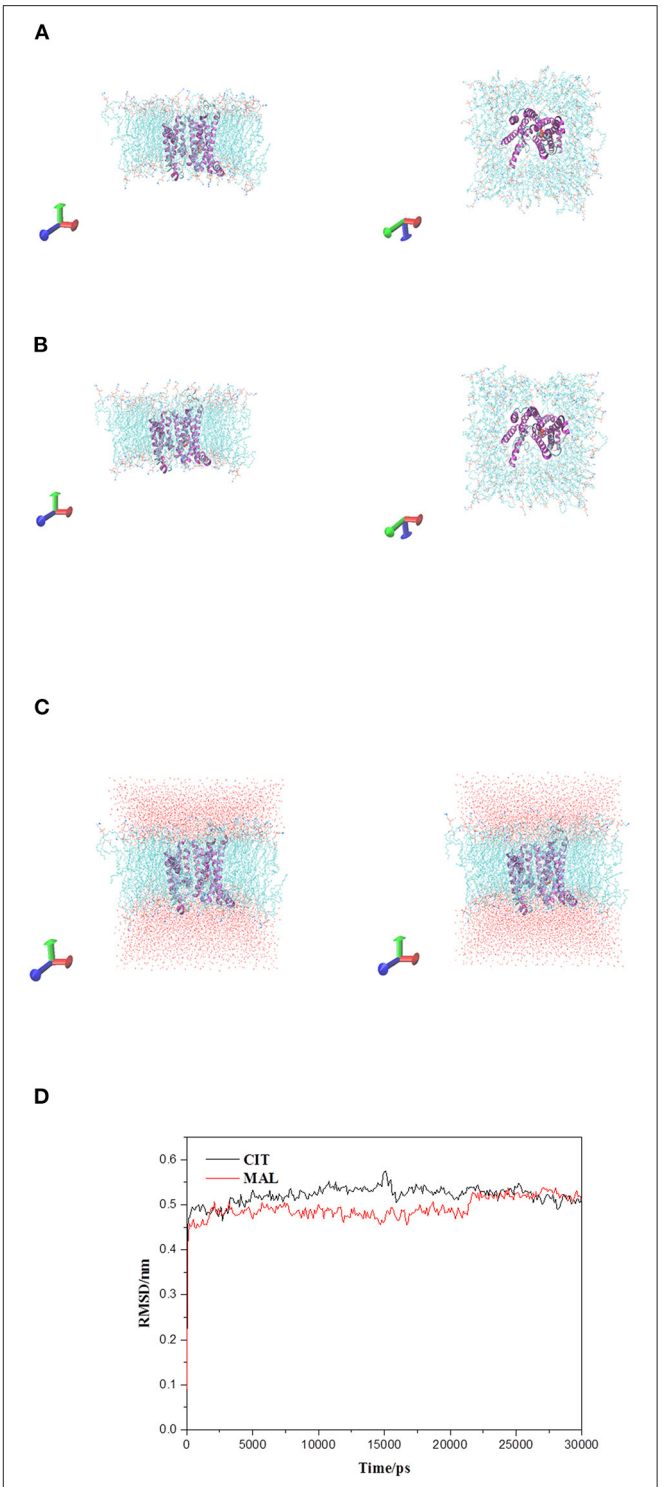

FIGURE 9 | Tct protrin and substrates complex and membrane system. **(A)** Tct-CIT was complex and membrane system. **(B)** Tct-MAL was complex and membrane system. **(C)** The solvation model of Tct-CIT (left) and Tct-MAL (right) system. **(D)** RMSD of backbone vs. simulation time. Side view left and top view right for **(A)** and **(B)**.

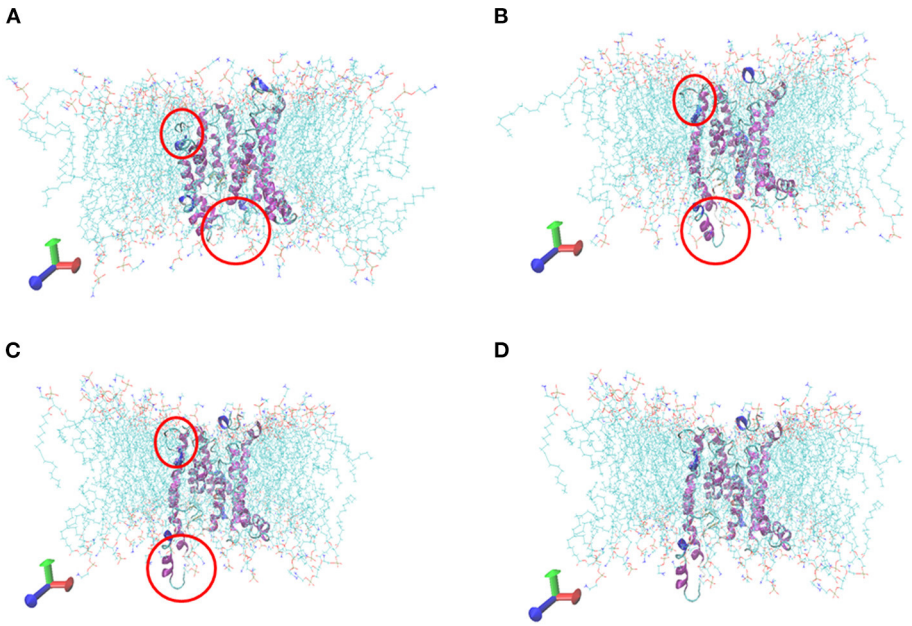

FIGURE 10 | Comformations of Tct-CIT system vs. MD simulation time. **(A)** 0 ns, **(B)** 10 ns, **(C)** 20 ns, **(D)** 30 ns, Tct was in cartoon, membrane in line, ligand in ball.

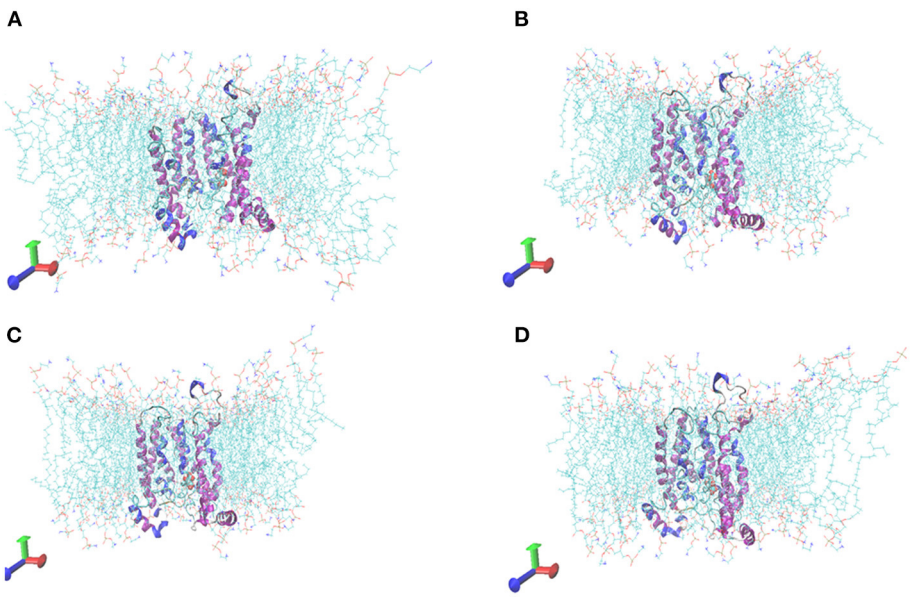

FIGURE 11 | Comformations of Tct-MAL system vs. MD simulation time. **(A)** 0 ns, **(B)** 10 ns, **(C)** 20 ns, **(D)** 30 ns, Tct was in cartoon, membrane in line, ligand in ball.

resulting in a less pronounced increase in Helix, while the other chain segments remained essentially unchanged (**Figure 12F**). Thus, although there is some change in the secondary structure of Tct in both systems, there is also no increase in flexibility and the overall structural stability of the protein is relatively good, resulting in high transport efficiency.

DISCUSSION

Oleaginous microorganisms have high lipid content and are thought to be potential cell factories for the production of high-value FAs (35, 36). These microbes have become industrial targets for lipid products and are amenable to

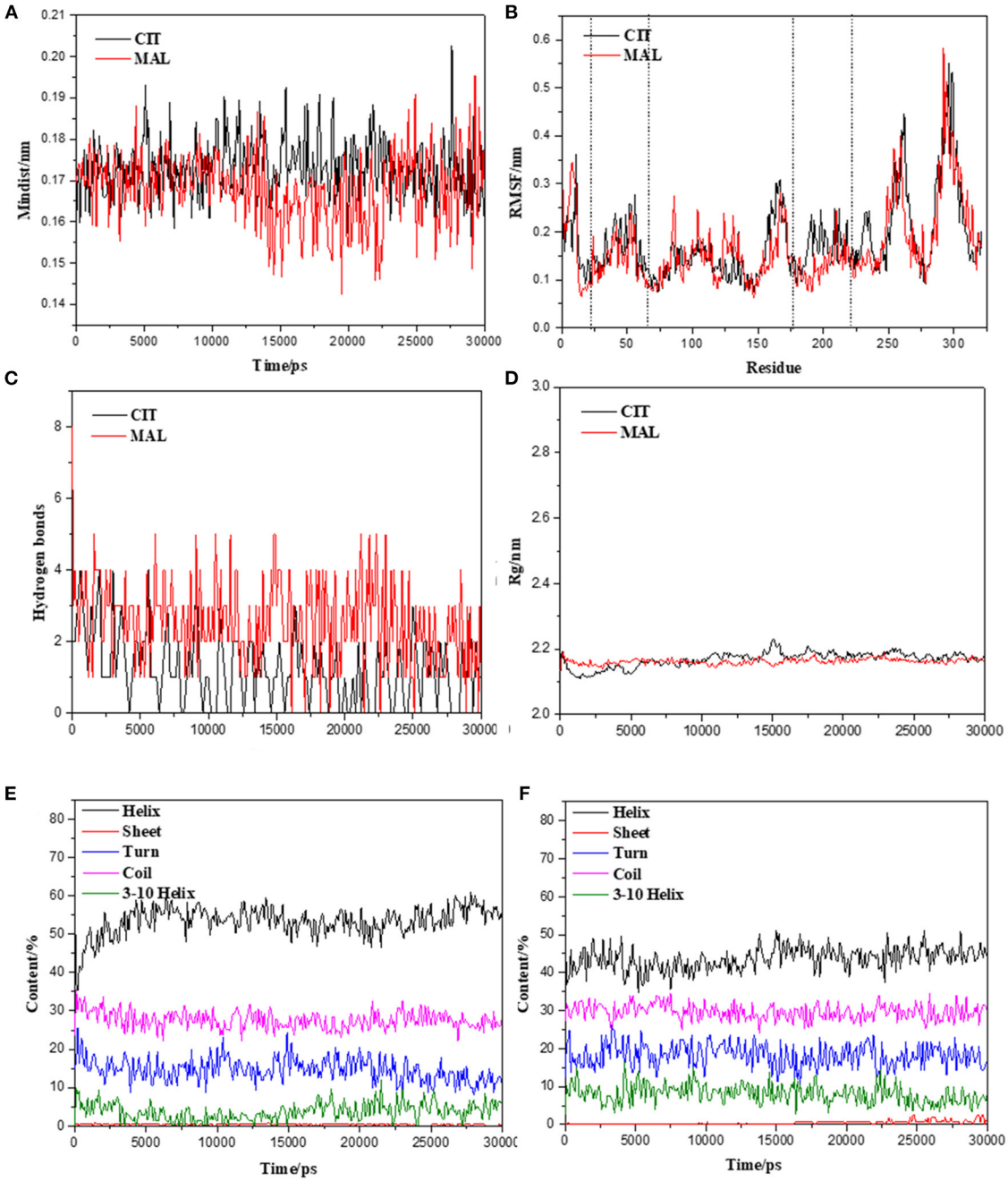

FIGURE 12 | Molecular dynamics simulation stability assessment of Tct protein interacting small molecules complex system. **(A)** Min-distance of skeletal muscle myosins multimer vs. simulation time of Tct-CIT and Tct-MAL. **(B)** RMSF of protein in the complex system vs. simulation time. **(C)** Intramolecular hydrogen bonds between protein and ligand vs. simulation time. **(D)** Radius of gyration of skeletal muscle myosins multimer vs. simulation time. Secondary structure content of Tct during the simulation with and without electric field vs. simulation time, **(E)** for citrate and **(F)** for malate.

metabolic engineering to increase their FA content (37, 38). Various studies proved that FA synthesis is triggered by citrate accumulation in the mitochondria, the relationships between lipid production and the activities of related enzymes in the TCA cycle and glycolysis have been extensively studied (39–41). Furthermore, the mitochondrial citrate transport system is expected to play a significant role in lipid production by controlling the citrate between mitochondria and the cytoplasm. As a result, it was necessary to investigate the mitochondrial citrate transport system that will be the key targets for metabolic engineering that in turn will help to understand the mechanism of lipid accumulation in oleaginous

microorganisms. However, only a few reports on mitochondrial Cts in microbes have been published, and little is known about the mechanism of the mitochondrial citrate transport system in oleaginous microorganisms (42). *Mucor circinelloides* WJ11 that accumulates higher levels of lipids has been used as a model organism to study citrate transport system. In our ongoing research on mitochondrial transporters, we identified 51 transporter genes that were predicted to be involved in a variety of important metabolic pathways, including oxidative phosphorylation, the citric acid cycle, FA oxidation, and amino acid degradation (15). WJ11, a high lipid-producing strain of *M. circinelloides*, was shown to have higher citrate flux from the mitochondria to the cytoplasm than CBS 277.49, a low lipid-producing strain (43). In WJ11, five genes were identified coding for transporters of the mitochondrial citrate transport system (15). In previous research, we found that CT of WJ11 contributes to the efflux of citrate from mitochondria and supply enough carbon sources for cell utilization in normal physiological processes and lipid biosynthesis (17). In the present work, we targeted *tct* gene that was overexpressed and its roles in FA accumulation and related metabolic pathways under nitrogen limitation were investigated. In WJ11, *tct* was successfully overexpressed and their FA content was increased while as knock out of *tct* resulted in slight decrease of lipid production. These findings supported the hypothesis that CTP overexpression increased lipid accumulation in *M. circinelloides* (16). Lipid accumulation is efficient when citrate is present in the cytosol of oleaginous microorganisms (39). The efflux of citrate from the mitochondria to the cytoplasm is a key event during lipogenesis in oleaginous microorganisms (5, 6). In theory, overexpression of citrate carriers promotes citrate transport from the mitochondria to the cytoplasm, thereby hastening the formation of the cytoplasmic citrate pool (44).

In the present study, the transporter Tct of *M. circinelloides* WJ11 has been cloned, overexpressed purified, kinetically and structurally characterized. The Tct protein was expressed in *E. coli*, isolated, and functionally reconstituted in a liposomal system. The Km-value of Tct for the citrate was found to be 0.018 mM. Based on Km-values, our findings showed that Tct's affinity to citrate was significantly higher than as previously reported in *S. cerevisiae* Yhm2p for citrate and oxoglutarate were about 0.16 and 1.2 mM, respectively (42).

The mitochondria of the *tct*-overexpressing transformant of *M. circinelloides* WJ11 showed a 49% increase in citrate efflux, whereas the mitochondria of the *tct*-knockout transformant showed a 39% decrease in citrate efflux compared to the mitochondria of wild-type WJ11. Our results are in confirmation with previous research that showed overexpression of MT in *M. circinelloides* resulted in increased citrate efflux from mitochondria (43). A higher citrate pool serves as an acetyl-CoA donor, promoting FA synthesis. The molecular mechanism by which the mitochondrial citrate transport system increases citrate efflux from the mitochondria and its role in FA synthesis is still under investigation.

The lack of an experimentally determined structure is one of the difficulties in studying Tct. To develop tool compounds in structure-based ligand discovery, a thorough understanding of the substrate binding site is required. The use bioinformatics in Tct are sufficient to identify the intrinsic role of the Tct in *M. circinelloides* that demonstrated a strategy for selecting candidate genes for further functional investigation. This will allow for further research and development of future Tct. As a result, we modeled Tct with new alignment and template structures and investigated their potential utility in small molecule discovery. A 3D model of the yeast mitochondrial Tct protein was also constructed using homology modeling. The WJ11 genes *tct* encode proteins with a total of 321 amino acid residues that contains 12.1% of positively charged amino acid residues and 7.8% of negatively charged amino acid residues. Most mitochondrial carrier family proteins (MCF) are small, with a length of around 300 amino acids and a molecular weight ranging from 30 to 35 kDa (45). The hydrophobic residues in Tct protein were high ≈50.6% with an average hydrophilic value of 0.089. The transmembrane structure prediction of Tct contains three transmembrane structures (i.e., 141–163, 178–195, and 262–284), while the chain structures 75–125 and 225–250 also have a 50% probability of being transmembrane structures. The overall structure of the protein was found V-shaped and its 3D structure is dimeric. It is now thought that MCs exist and function as monomers. The only carrier that has been proven to exist as a homodimer is the human aspartate-glutamate carrier (with two isoforms: AGC1 and AGC2) (46, 47). When eel liver mitochondria were solubilized with the mild detergent digitonin, the dimeric form of the Tct protein was discovered (48). Molecular docking and molecular dynamics were also used to investigate molecular interactions and the mode of binding between Tct and citrate. Tricarboxylate citrate transporter had binding energy of −4.87 kcal/mol to citric acid vs. −3.80 kcal/mol to malic acid. The molecular dynamics analyses revealed that the complexes had certain conformational stability, which was due to the significant interactions between Tct and citrate, which were consistent with the docking study interactions.

CONCLUSION

MCTs are so important in cellular bioenergetics, our group has been studying their structure-based mechanism. Tricarboxylate citrate transporter overexpression boosted citrate transport from the mitochondria to cytosol, which is one of the reasons of high lipid accumulation in the oleaginous fungus *M. circinelloides* WJ11. Tricarboxylate citrate transporter appears to play a key role in citrate transport in *M. circinelloides*, based on kinetics data collected in this study in conjunction with our homology-modeled Tct structure. The findings of this study show the significance of the *tct* gene as a target gene for genetic engineering to improve citrate transport in oleaginous fungus, hence opening up new perspectives for improving *M. circinelloides* WJ11 for commercial lipid production.

DATA AVAILABILITY STATEMENT

The original contributions presented in the study are included in the article/**Supplementary Material**,

further inquiries can be directed to the corresponding author/s.

AUTHOR CONTRIBUTIONS

WY and AS planned the experiments, carried out the experimental work, and generated the figures. SD, CS, and HZ did additional experimental work and participated in writing of the article. HM, XG, and HF participated in the writing of the article. YS supervised the work and participated in the writing of the article. All authors contributed to the article and approved the submitted version.

FUNDING

This work was supported by National Science Foundation of China (grant nos. 31972851 and 31670064), TaiShan Industrial Experts Programme (tscy no. 20160101), Shandong Provincial Key Technology R&D Plan (nos. 2018GNC110039 and 2018GSF121013).

ACKNOWLEDGMENTS

The authors acknowledge the University of Murcia, Spain for providing the plasmids vector (pUC18 and pMAT2075), the Tianjin Key Laboratory of Radiation Medicine, and Molecular Nuclear Medicine for providing the ^{14}C experiment platform.

SUPPLEMENTARY MATERIAL

The Supplementary Material for this article can be found online at: https://www.frontiersin.org/articles/10.3389/fnut.2021.802231/full#supplementary-material

REFERENCES

1. Endemann G, Goetz PG, Edmond J, Brunengraber H. Lipogenesis from ketone bodies in the isolated perfused rat liver. Evidence for the cytosolic activation of acetoacetate. *J Biol Chem.* (1982) 257:3434–40. doi: 10.1016/S0021-9258(18)34796-3
2. Conover TE. Does citrate transport supply both acetyl groups and NADPH for cytoplasmic fatty acid synthesis? *Trends Biochem Sci.* (1987) 12:88–9. doi: 10.1016/0968-0004(87)90042-9
3. Athenaki M, Gardeli C, Diamantopoulou P, Tchakouteu SS, Sarris D, Philippoussis A, et al. Lipids from yeasts and fungi: physiology, production and analytical considerations. *J Appl Microbiol.* (2018) 124:336–67. doi: 10.1111/jam.13633
4. Liu H, Marsafari M, Deng L, Xu P. Understanding lipogenesis by dynamically profiling transcriptional activity of lipogenic promoters in Yarrowia lipolytica. *Appl Microbiol Biotechnol.* (2019) 103:3167–79. doi: 10.1007/s00253-019-09664-8
5. Evans CT, Scragg AH, Ratledge C. A comparative study of citrate efflux from mitochondria of oleaginous and non-oleaginous yeasts. *Eur J Biochem.* (1983) 130:195–204. doi: 10.1111/j.1432-1033.1983.tb07136.x
6. Ratledge C, Wynn JP. The biochemistry and molecular biology of lipid accumulation in oleaginous microorganisms. *Adv Appl Microbiol.* (2002) 51:1–52. doi: 10.1016/S0065-2164(02)51000-5
7. Iacobazzi V, Infantino V. Citrate–new functions for an old metabolite. *Biol Chem.* (2014) 395:387–99. doi: 10.1515/hsz-2013-0271
8. Paumen MB, Ishida Y, Muramatsu M, Yamamoto M, Honjo T. Inhibition of carnitine palmitoyltransferase I augments sphingolipid synthesis and palmitate-induced apoptosis. *J Biol Chem.* (1997) 272:3324–9. doi: 10.1074/jbc.272.6.3324
9. Alberts B, Johnson A, Lewis J, Raff M, Roberts K, Walter P. *Carrier proteins and active membrane transport. Molecular Biology of the Cell. 4th ed*. New York, NY: Garland Science (2002).
10. Khan M, Kabir A, Yang J, Hussain SA, Zhang H, Garre V, et al. Genetic modification of Mucor circinelloides to construct stearidonic acid producing cell factory. *Int J Mol Sci.* (2019) 20:1683. doi: 10.3390/ijms20071683
11. Yuan SF, Alper HS. Metabolic engineering of microbial cell factories for production of nutraceuticals. *Microb Cell Fact.* (2019) 18:1–1. doi: 10.1186/s12934-019-1096-y
12. Nyilasi I, Ács K, Papp T, Nagy E, Vágvölgyi C. *Agrobacterium tumefaciens*-mediated transformation of *Mucor circinelloides*. *Fol Microbiol.* (2005) 50:415–20. doi: 10.1007/BF02931423
13. Tang X, Zhao L, Chen H, Chen YQ, Chen W, Song Y, et al. Complete genome sequence of a high lipid-producing strain of *Mucor circinelloides* WJ11 and comparative genome analysis with a low lipid-producing strain CBS 277.49. *PLoS ONE*. (2015) 10:e0137543. doi: 10.1371/journal.pone.0137543
14. Zhao L, Cánovas-Márquez JT, Tang X, Chen H, Chen YQ, Chen W, et al. Role of malate transporter in lipid accumulation of oleaginous fungus *Mucor circinelloides*. *Appl Microbiol Biotechnol.* (2016) 100:1297–305. doi: 10.1007/s00253-015-7079-y
15. Yang J, Khan MA, Zhang H, Zhang Y, Certik M, Garre V, et al. Mitochondrial citrate transport system in the fungus *Mucor circinelloides*: identification, phylogenetic analysis, and expression profiling during growth and lipid accumulation. *Curr Microbiol.* (2020) 77:220–31. doi: 10.1007/s00284-019-01822-5
16. Yang J, Li S, Kabir Khan MA, Garre V, Vongsangnak W, Song Y. Increased lipid accumulation in *Mucor circinelloides* by overexpression of mitochondrial citrate transporter genes. *Ind Eng Chem Res.* (2019) 58:2125–34. doi: 10.1021/acs.iecr.8b05564
17. Yang W, Dong S, Yang J, Mohamed H, Shah AM, Nazir Y, et al. Molecular mechanism of citrate efflux by the mitochondrial citrate transporter CT in filamentous fungus *Mucor circinelloides* WJ11. *Front Microbiol.* (2021) 12:947. doi: 10.3389/fmicb.2021.673881
18. Palmieri F. Mitochondrial carrier proteins. *FEBS Lett.* (1994) 346:48–54. doi: 10.1016/0014-5793(94)00329-7
19. Deininger P. *Molecular Cloning: A Laboratory Manual*. (in 3 volumes). Edited by Sambrook J, Fritsch EF, Maniatis T. Cold Spring Harbor, NY: Cold Spring Harbor Laboratory Press (1989).
20. Kendrick A, Ratledge C. Desaturation of polyunsaturated fatty acids in *Mucor circinelloides* and the involvement of a novel membrane-bound malic enzyme. *Eur J Biochem.* (1992) 209:667–73. doi: 10.1111/j.1432-1033.1992.tb17334.x
21. Christopher TE, Scragg AH, Ratledge C. Regulation of citrate efflux from mitochondria of oleaginous and non-oleaginous yeasts by long-chain fatty acyl-CoA esters. *Eur J Biochem.* (1983) 132:617–22. doi: 10.1111/j.1432-1033.1983.tb07408.x
22. Studier FW. Protein production by auto-induction in high-density shaking cultures. *Protein Expr Purif.* (2005) 41:207–34. doi: 10.1016/j.pep.2005.01.016
23. Larentis AL, Nicolau JF, dos Santos Esteves G, Vareschini DT, de Almeida FV, dos Reis MG, et al. Evaluation of pre-induction temperature, cell growth at induction and IPTG concentration on the expression of a leptospiral protein in *E. coli* using shaking flasks and microbioreactor. *BMC Res Notes.* (2014) 7:1–3. doi: 10.1186/1756-0500-7-671
24. Palmieri F, Indiveri C, Bisaccia F, Iacobazzi V. [25] Mitochondrial metabolite carrier proteins: purification, reconstitution, and transport studies. *Meth Enzymol.* (1995) 260:349–69. doi: 10.1016/0076-6879(95)60150-3
25. Monné M, Daddabbo L, Gagneul D, Obata T, Hielscher B, Palmieri L, et al. Uncoupling proteins 1 and 2 (UCP1 and UCP2) from *Arabidopsis thaliana*

are mitochondrial transporters of aspartate, glutamate, and dicarboxylates. *J Biol Chem.* (2018) 293:4213–27. doi: 10.1074/jbc.RA117.000771
26. Yuzbasheva EY, Agrimi G, Yuzbashev TV, Scarcia P, Vinogradova EB, Palmieri L, et al. The mitochondrial citrate carrier in *Yarrowia lipolytica*: its identification, characterization and functional significance for the production of citric acid. *Metab Eng.* (2019) 54:264–74. doi: 10.1016/j.ymben.2019.05.002
27. Vito P, Fiermonte G, Longo A, Palmieri F. The human gene SLC25A29, of solute carrier family 25, encodes a mitochondrial transporter of basic amino acids. *J Biol Chem.* (2014) 289:13374–84. doi: 10.1074/jbc.M114.547448
28. Marobbio CM, Agrimi G, Lasorsa FM, Palmieri F. Identification and functional reconstitution of yeast mitochondrial carrier for S-adenosylmethionine. *EMBO J.* (2003) 22:5975–82. doi: 10.1093/emboj/cdg574
29. Marobbio CM, Di Noia MA, Palmieri F. Identification of a mitochondrial transporter for pyrimidine nucleotides in *Saccharomyces cerevisiae*: bacterial expression, reconstitution and functional characterization. *Biochem J.* (2006) 393:441–6. doi: 10.1042/BJ20051284
30. Palmieri L, Lasorsa FM, Iacobazzi V, Runswick MJ, Palmieri F, Walker JE. Identification of the mitochondrial carnitine carrier in *Saccharomyces cerevisiae*. *FEBS Lett.* (1999) 462:472–86. doi: 10.1016/S0014-5793(99)01555-0
31. Rodríguez-Frómeta RA, Gutiérrez A, Torres-Martínez S, Garre V. Malic enzyme activity is not the only bottleneck for lipid accumulation in the oleaginous fungus *Mucor circinelloides*. *Appl Microbiol Biotechnol.* (2013) 97:3063–72. doi: 10.1007/s00253-012-4432-2
32. Zaheer UH, Saeed M, Halim SA, Khan W. 3D structure prediction of human β1-adrenergic receptor via threading-based homology modeling for implications in structure-based drug designing. *PLoS ONE.* (2015) 10:e0122223. doi: 10.1371/journal.pone.0122223
33. Mark JA, Murtola T, Schulz R, Páll S, Smith JC, Hess B, et al. GROMACS: high performance molecular simulations through multi-level parallelism from laptops to supercomputers. *SoftwareX.* (2015) 1:19–25. doi: 10.1016/j.softx.2015.06.001
34. Morris GM, Huey R, Lindstrom W, Sanner MF, Belew RK, Goodsell DS, et al. AutoDock4 and AutoDockTools4: automated docking with selective receptor flexibility. *J Comp Chem.* (2009) 30:2785–91. doi: 10.1002/jcc.21256
35. Ykema A, Verbree EC, Nijkamp HJ, Smit H. Isolation and characterization of fatty acid auxotrophs from the oleaginous yeast *Apiotrichum curvatum*. *Appl Microbiol Biotechnol.* (1989) 32:76–84. doi: 10.1007/BF00164826
36. Shah AM, Mohamed H, Zhang Z, Song Y. Isolation, characterization and fatty acid analysis of *Gilbertella persicaria* DSR1: a potential new source of high value single-cell oil. *Biomass Bioenergy.* (2021) 151:106156. doi: 10.1016/j.biombioe.2021.106156
37. Chutrakul C, Jeennor S, Panchanawaporn S, Cheawchanlertfa P, Suttiwattanakul S, Veerana M, et al. Metabolic engineering of long chain-polyunsaturated fatty acid biosynthetic pathway in oleaginous fungus for dihomo-gamma linolenic acid production. *J Biotechnol.* (2016) 218:85–93. doi: 10.1016/j.jbiotec.2015.12.003
38. Zhang Y, Luan X, Zhang H, Garre V, Song Y, Ratledge C. Improved γ-linolenic acid production in *Mucor circinelloides* by homologous overexpressing of delta-12 and delta-6 desaturases. *Microb Cell Factories.* (2017) 16:1–9. doi: 10.1186/s12934-017-0723-8
39. Ratledge C. Fatty acid biosynthesis in microorganisms being used for single cell oil production. *Biochimie.* (2004) 86:807–15. doi: 10.1016/j.biochi.2004.09.017
40. Lina Z, Tang X, Luan X, Chen H, Chen YQ, Chen W, et al. Role of pentose phosphate pathway in lipid accumulation of oleaginous fungus *Mucor circinelloides*. *RSC Adv.* (2015) 5:97658–64. doi: 10.1039/C5RA20364C
41. Zhang H, Zhang L, Chen H, Chen YQ, Chen W, Song Y, et al. Enhanced lipid accumulation in the yeast *Yarrowia lipolytica* by over-expression of ATP: citrate lyase from *Mus musculus*. *J Biotechnol.* (2014) 192:78–84. doi: 10.1016/j.jbiotec.2014.10.004
42. Castegna A, Scarcia P, Agrimi G, Palmieri L, Rottensteiner H, Spera I, et al. Identification and functional characterization of a novel mitochondrial carrier for citrate and oxoglutarate in *Saccharomyces cerevisiae*. *J Biol Chem.* (2010) 285:17359–70. doi: 10.1074/jbc.M109.097188
43. Zhao L, Zhang H, Wang L, Chen H, Chen YQ, Chen W, et al. 13C-metabolic flux analysis of lipid accumulation in the oleaginous fungus *Mucor circinelloides*. *Bioresour Technol.* (2015) 197:23–9. doi: 10.1016/j.biortech.2015.08.035
44. Chihiro K, Izumitsu K, Onoue M, Okutsu K, Yoshizaki Y, Takamine K, et al. Mitochondrial citrate transporters CtpA and YhmA are required for extracellular citric acid accumulation and contribute to cytosolic acetyl coenzyme A generation in *Aspergillus luchuensis* mut. *Kawachii Appl Environ Microbiol.* (2019) 85:e03136–e03118. doi: 10.1128/AEM.03136-18
45. Toleco MR, Naake T, Zhang Y, Heazlewood JL, Fernie AR. Plant mitochondrial carriers: molecular gatekeepers that help to regulate plant central carbon metabolism. *Plants.* (2020) 9:117. doi: 10.3390/plants9010117
46. Palmieri L, Pardo B, Lasorsa FM, Del Arco A, Kobayashi K, Iijima M, et al. Citrin and aralar1 are Ca2+-stimulated aspartate/glutamate transporters in mitochondria. *EMBO Rep.* (2001) 20:5060–9. doi: 10.1093/emboj/20.18.5060
47. Lasorsa FM, Pinton P, Palmieri L, Fiermonte G, Rizzuto R, Palmieri F. Recombinant expression of the Ca2+-sensitive aspartate/glutamate carrier increases mitochondrial ATP production in agonist-stimulated Chinese hamster ovary cells. *J Biol Chem.* (2003) 278:38686–92. doi: 10.1074/jbc.M304988200
48. Kim DH, Park S, Kim DK, Jeong MG, Noh J, Kwon Y, et al. Direct visualization of single-molecule membrane protein interactions in living cells. *PLoS Biol.* (2018) 16:e2006660. doi: 10.1371/journal.pbio.2006660

Conflict of Interest: The authors declare that the research was conducted in the absence of any commercial or financial relationships that could be construed as a potential conflict of interest.

Publisher's Note: All claims expressed in this article are solely those of the authors and do not necessarily represent those of their affiliated organizations, or those of the publisher, the editors and the reviewers. Any product that may be evaluated in this article, or claim that may be made by its manufacturer, is not guaranteed or endorsed by the publisher.

frontiers in Nutrition

ORIGINAL RESEARCH
published: 14 December 2021
doi: 10.3389/fnut.2021.795651

Development of an Efficient Gene Editing Tool in *Schizochytrium* sp. and Improving Its Lipid and Terpenoid Biosynthesis

Peng-Wei Huang[1], *Ying-Shuang Xu*[1], *Xiao-Man Sun*[1]*, *Tian-Qiong Shi*[1], *Yang Gu*[1], *Chao Ye*[1] *and He Huang*[1,2]

[1] School of Food Science and Pharmaceutical Engineering, Nanjing Normal University, Nanjing, China, [2] College of Biotechnology and Pharmaceutical Engineering, Nanjing Tech University, Nanjing, China

Schizochytrium sp. HX-308 is a marine microalga with fast growth and high lipid content, which has potential as microbial cell factories for lipid compound biosynthesis. It is significant to develop efficient genetic editing tool and discover molecular target in *Schizochytrium* sp. HX-308 for lipid compound biosynthesis. In this study, we developed an efficient gene editing tool in HX-308 which was mediated by *Agrobacterium tumefaciens* AGL-1. Results showed that the random integration efficiency reached 100%, and the homologous recombination efficiency reached about 30%. Furthermore, the metabolic pathway of lipid and terpenoid biosynthesis were engineered. Firstly, the acetyl-CoA *c*-acetyltransferase was overexpressed in HX-308 with a strong constitutive promoter. With the overexpression of acetyl-CoA c-acetyltransferase, more acetyl-CoA was used to synthesize terpenoids, and the production of squalene, β-carotene and astaxanthin was increased 5.4, 1.8, and 2.4 times, respectively. Interestingly, the production of saturated fatty acids and polyunsaturated fatty acids also changed. Moreover, three Acyl-CoA oxidase genes which catalyze the first step of β-oxidation were knocked out using homologous recombination. Results showed that the production of lipids increased in the three knock-out strains. Our results demonstrated that the *A. tumefaciens*-mediated transformation method will be of great use for the study of function genes, as well as developing *Schizochytrium* sp. as a strong cell factory for producing high value products.

Keywords: *Schizochytrium* sp., *Agrobacterium tumefaciens*, genetic manipulation, terpenoids, lipid

OPEN ACCESS

Edited by:
Yuanda Song,
Shandong University of Technology, China

Reviewed by:
Shiu Cheung Lung,
The University of Hong Kong, Hong Kong SAR, China
Yefu Chen,
Tianjin University of Science and Technology, China

***Correspondence:**
Xiao-Man Sun
xiaomansun@njnu.edu.cn

Specialty section:
This article was submitted to Food Chemistry, a section of the journal Frontiers in Nutrition

Received: *15 October 2021*
Accepted: *24 November 2021*
Published: *14 December 2021*

Citation:
Huang P-W, Xu Y-S, Sun X-M, Shi T-Q, Gu Y, Ye C and Huang H (2021) Development of an Efficient Gene Editing Tool in Schizochytrium sp. and Improving Its Lipid and Terpenoid Biosynthesis. Front. Nutr. 8:795651. doi: 10.3389/fnut.2021.795651

INTRODUCTION

Oleaginous microalgae can accumulate up to 30% of lipids, which are valuable commercial resources (1). These lipids can be divided into two categories: saturated fatty acids with 14–16 carbons can be used as biodiesel fuel; polyunsaturated fatty acids with more than 20 carbons can be used as health care products (2, 3). *Schizochytrium* sp. HX-308 (CCTCC M 209059) is a marine microalga which belongs to thraustochytrids genera, and it was isolated from seawater with fast growth and high lipid yields (4, 5). Previously, our studies have reported that the lipid yield and the cell dry weight (CDW) of HX-308 can reach 80.14 g/L and 134.5 g/L, respectively (1, 5–7). However, manipulation of fermentation conditions to promote the productivity of target products seems

to have reached choke point. With the development of molecular biology technologies, genetic engineering is becoming more and more common strategies for improving the production of high value products in microalgae (8–12). Thus, it is of great importance to develop efficient gene editing tools in HX-308 for constructing it as a better cell factory.

It has been reported that electroporation is the main approach to introduce exogenous DNA into *Schizochytrium* (13). However, the efficiency of homologous recombination is very low after electroporation. Sakaguchi et al. tried to knockout the Δ5 desaturase gene in *Thraustochytrium aureum* ATCC 34304 but only destroyed one allele in the first round of electroporation (13). They had to carry a second round of electroporation to knockout the other allele, which cost them more time and money. Apart from electroporation, *Agrobacterium tumefaciens* mediated transformation (ATMT) can also be used to transform DNA into other organisms (14). *Agrobacterium tumefaciens* was widely applied for the transformation of plant cells. *Agrobacterium tumefaciens* can transform the T-DNA on the Ti plasmid into plant cells, and the T-DNA was then integrated into the nuclear chromosomes randomly (15, 16). In recent years, ATMT has also been widely used for the transformation of fungi, including yeasts and filamentous fungi (17–19). In addition, it was reported that ATMT can lead to homologous recombination and thus promote the efficiency of gene knockout (20). Therefore, ATMT may also be a promising approach for efficient gene editing in *Schizochytrium*.

In this study, an efficient gene editing tool in HX-308 was constructed based on ATMT. Firstly, a *NeoR* resistance expression cassette was constructed and transformed into HX-308 successfully. Then, the gene acetyl-CoA *c*-acetyltransferase (*AACT*) was overexpressed under the control of the promoter of the endogenous gene acetyl-CoA carboxylase (*ACCase*), and more acetyl-CoA was pulled into the mevalonate (MVA) pathway to improve the productivity of terpenoids. Furthermore, three genes associated with β-oxidation which were named acyl-CoA oxidases (*Acox*) were knocked out using homologous recombination to improve total fatty acids. This study would facilitate the genetic engineering of other thraustochytrids for the production of more high value products.

MATERIALS AND METHODS

Strains and Culture Media

Schizochytrium sp. HX-308 (CCTCC M 209059) is a microalga which was isolated from seawater and stored in the China Center for Type Culture Collection (CCTCC) (1). The strain was stored at −80°C in 20% (v/v) glycerol. The seed culture medium and batch culture medium were the same as those described in our previous study (5). The seed of HX-308 was cultured for three passages and then 10 mL of the seed was transferred to 500-mL shake flasks containing 100 mL of medium for batch culture. HX-308 was cultured at 28°C with a rotation speed of 170 rpm. The strain *A. tumefaciens* AGL-1 and the plasmid pZPK were kind gifts from Dr. Sheng Yang (CAS Center for Excellence in Molecular Plant Science).

Plasmid Construction

A binary vector named pZPK was used to carry the DNA elements which were used in this study (21). The vector pZPK-P_{GAPDH}-NeoR-T_{GAPDH} was constructed by inserting a 2.3-kb neomycin resistance (*NeoR*) gene expression cassette into the *EcoRI-XbaI* site of pZPK. The 2.3-kb *NeoR* resistance cassette contained a 1-kb promoter of the endogenous gene glyceraldehyde-3-phosphate dehydrogenase (*GAPDH*), a 0.8-kb *NeoR* gene, and a 0.5-kb terminator of *GAPDH* (**Figure 1A**). The plasmid pZPK-AACT was constructed by inserting an *AACT* expression cassette into the *HindIII* site of pZPK-P_{GAPDH}-NeoR-T_{GAPDH}. The *AACT* expression cassette contained a 1-kb promoter of the endogenous gene acetyl-CoA carboxylase (*ACCase*), the gene *AACT*, and the *Trpc* terminator (**Figure 2**). The plasmid pZPK-Acox1 was constructed by inserting a 4.3-kb targeted knock-out sequence into the *EcoRI-XbaI* site of pZPK. The sequence contained a 1-kb region in the upstream of the *acox1*, the *NeoR* resistance cassette, and a 1-kb region in the downstream of the *acox1*. The vector pZPK-Acox2 and pZPK-Acox3 were constructed the same way as pZPK-Acox1. The primers described above were listed in **Supplementary Table S1**.

The Transformation of HX-308 Mediated by *A. tumefaciens* AGL-1

The transformation method of HX-308 used was a modification of that of Cheng et al. (20). HX-308 was cultured overnight in seed medium, and then was inoculated to fresh seed medium and grown to a logarithmic phase. Cells were harvested by centrifugation at 1000g for 5 min, and then were washed with sterile water for two times. The *A. tumefaciens* harboring plasmids was cultured at 28°C with a rotation speed of 220 rpm overnight in YEB medium supplemented with 50 μg/mL of kanamycin (pH 7.5). Cells were harvested by centrifugation at 4000g for 5 min, and then were resuspended in liquid induction medium (IM) supplemented with 50 μg/mL of kanamycin and 200 μM acetosyringone (pH 5.4). After 8 h of pre-induction at 28°C with a rotation speed of 220 rpm, *A. tumefaciens* was harvested by centrifugation at 4000g for 5 min, and then was washed with sterile water for two times. For transformation, 1×10^7 HX-308 cells and 1×10^8 *A. tumefaciens* cells were mixed and then were spread on IM plates supplemented with 50 μg/mL of kanamycin and 200 μM acetosyringone (pH 5.4). After 48 h of induction at 28°C, the cocultures were washed with sterile water and then were selected on GPYS (10 g yeast extract, 20 g tryptone, 20 g sea life, 50 g glucose, 20 g agar per liter) plates supplemented with 300 μg/mL of cefotaxime sodium and 500 μg/mL of G418 at 28°C for three to five days.

PCR Analysis of the Transformants

The transformants were cultured for at least two passages before PCR analysis. The genomic DNA of the transformants were isolated. Primer sets NeoR-test-F/R were used to verify the incorporation of the NeoR resistance gene. Primer sets P2520-F and Trpc-R were used to verify the incorporation of the *AACT* gene. Primer sets ACOX1-test1-F/R, ACOX1-test2-F/R, ACOX2-test1-F/R, ACOX2-test2-F/R, ACOX3-test1-F/R, and ACOX3-test2-F/R were used to verify the disruption of the *ACOX1*,

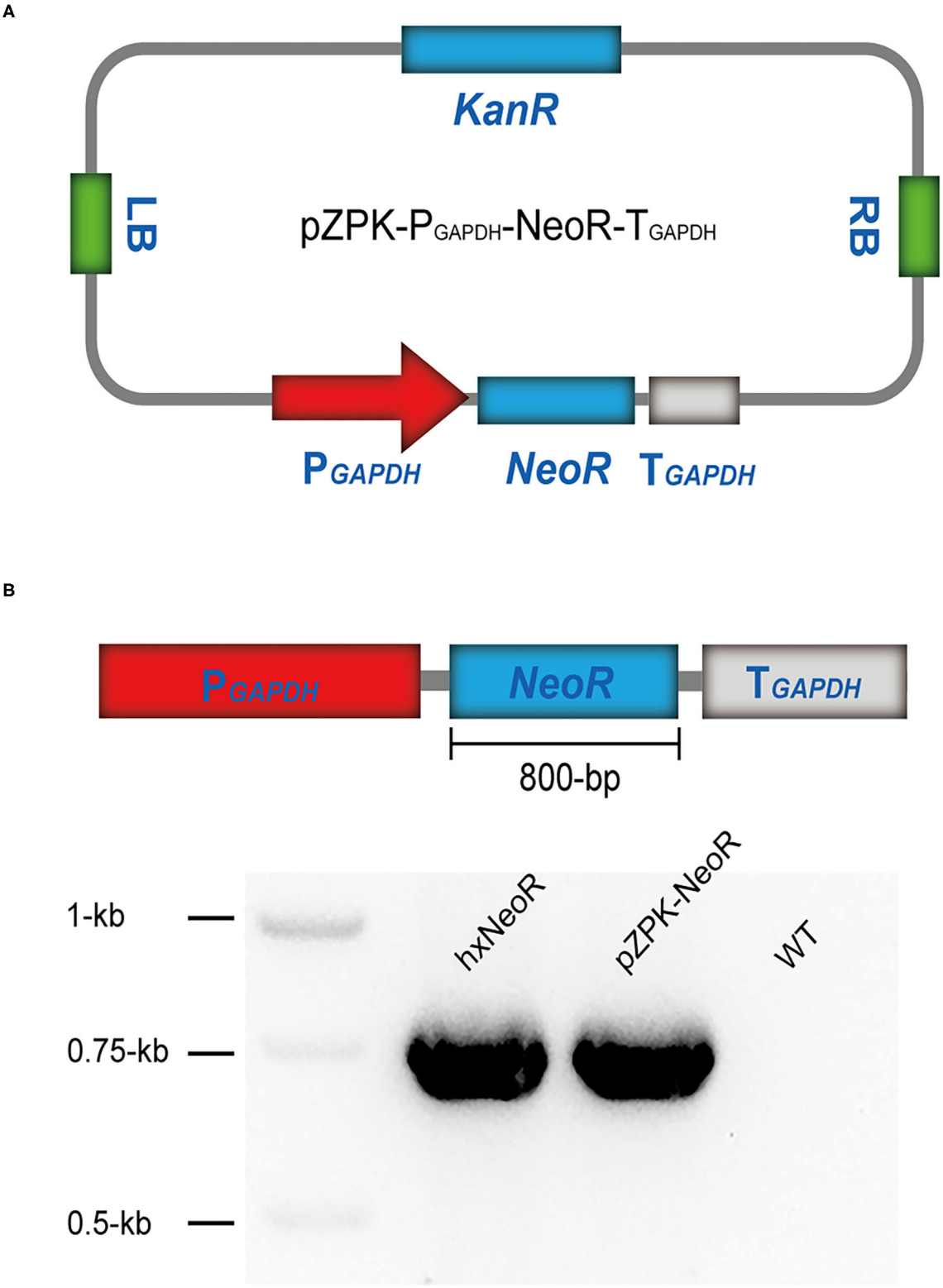

FIGURE 1 | The construction of the plasmid pZPK-P_{GAPDH}-NeoR-T_{GAPDH} and the transformation of HX-308. **(A)** Map of the plasmid pZPK-P_{GAPDH}-NeoR-T_{GAPDH}. **(B)** The schematic diagram of the *NeoR* expression cassette and diagnostic PCR validation of the *NeoR* gene.

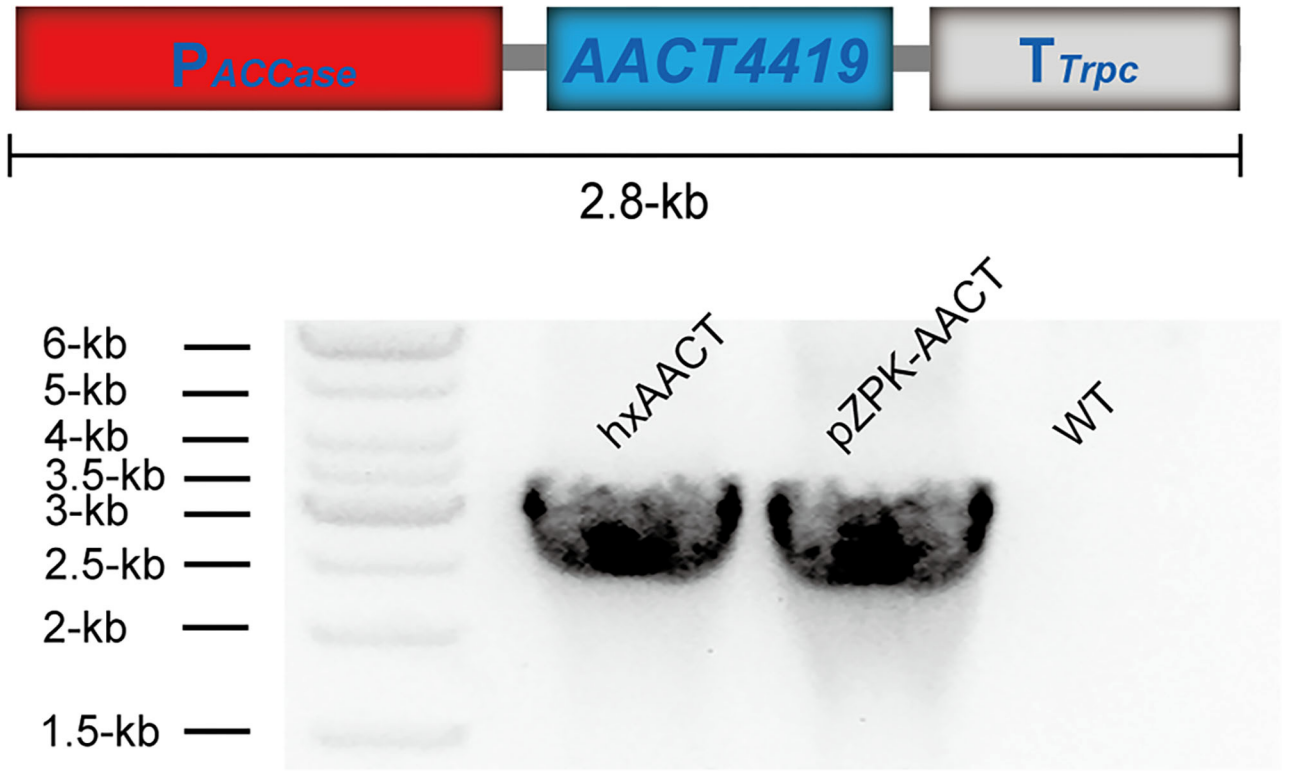

FIGURE 2 | The schematic diagram of the *AACT4419* expression cassette and the diagnostic PCR validation of the *AACT4419* expression cassette.

ACOX2, and *ACOX3* gene. The primers described above were listed in **Supplementary Table S2**.

Determination of Biomass, Glucose, and Lipid Production

To measure CDW, 10 mL of the culture was harvested by centrifugation at 5000g for 5 min. The sediments were dried at 60°C for 48 h to constant weight, and was then used for gravimetric analysis. For extracellular glucose and the production of total lipids, they were measured according to our previous study (4, 5).

Fatty Acids and Terpenoids Analysis

To determine fatty acids, 0.1 g of biomass was used to prepare fatty acid methyl esters (FAMEs). The preparation methods used were according to our previous study (4). And the FAMEs were then analyzed using the gas chromatography system (GC-2014; Shimadzu, Japan) equipped with a 60 m × 0.22 mm capillary column (DB-23; Agilent, USA) and a flame ionization detector (FID). The carrier gas was nitrogen. The detection methods used were according to our previous study (5). Authentic FAMEs reference standards were purchased from Sigma-Aldric, USA.

To determine terpenoids, one gram of biomass was firstly freeze-dried at −20°C for 48 h. The residue was ground at 60 Hz, and then be extracted with 1 mL of hexane. β-carotene and astaxanthin contents were quantitated using the high performance liquid chromatography (1260 Infinity II; Agilent, USA) equipped with a 4.6 mm × 150 mm column (Eclipse XDB-C18; Agilent, USA). The analytical condition was a modification of that of Harnkarnsujarit et al. (22). A gradient solvent system of MeCN/H_2O (90/10, v/v) (solvent A) and MeOH/IPA (60/40, v/v) (solvent B) were used: 100% solvent A and 0% solvent B was used firstly, then solvent A was decreased to 10% and solvent B was increased to 90% within 15 min and retained from 15 to 30 min. The detection wavelength was 470 nm, and the flow rate was 1.0 mL/min. Authentic β-carotene and astaxanthin reference standards were purchased from Sigma-Aldric, USA.

Statistical Analysis

This study carried out analyses on the glucose consumption, CDW, total fatty acids, squalene productivity, β-carotene productivity, astaxanthin productivity and the percentage of fatty acids. The analyses were performed by GraphPad Prism 8, and the results of the quantification were presented as the mean value ± standard deviation from at least three replicates.

RESULTS AND DISCUSSION

Optimization of the Selection Condition of *Schizochytrium* sp. HX-308 and the Construction of G418 Resistant Expression Cassette

It was reported that G418 could inhibit the growth of *Schizochytrium* sp. strain SEK 579 (13). However, the inhibition

data of G418 to the strain HX-308 was unknown. Thus, the sensitivity of HX-308 to G418 was determined and then been used to select transformants. The results appeared that 300 μg/mL or higher concentration of G418 was able to inhibit the growth of HX-308 on GPYS solid plates (**Supplementary Figure S1**). Thus, to avoid false positive results, GPYS solid plates supplemented with 500 μg/mL of G418 and 300 μg/mL of cefotaxime sodium were used to select HX-308 transformants in the next studies. The cefotaxime sodium was used to kill *A. tumefaciens* which was used to transform DNA into HX-308 after transformation (23).

The gene *NeoR* encodes the enzyme neomycin phosphotransferase, which could confer resistance to the aminoglycoside antibiotic G418 in HX-308 transformants (24). Thus, a *NeoR* expression cassette should be constructed under the control of a promising promoter. The promoter of a housekeeping gene *GAPDH* which expresses constantly was chosen as a candidate (25). The coding sequence of the endogenous gene *GAPDH* in HX-308 was found according to the annotation of the genome sequence. The 1-kb promoter of *GAPDH* (P_{GAPDH}) in HX-308 was cloned and been used to drive the expression of the gene *NeoR*. Thus, the *NeoR* expression cassette driven by P_{GAPDH} was inserted into the vector pZPK, resulting in a new vector pZPK-P_{GAPDH}-NeoR-T_{GAPDH} (**Figure 1A**). Luckily, the results in the next studies appeared that the promoter P_{GAPDH} worked successfully in HX-308. Some other promoters such as P_{TEF-1}, P_{AOX1}, and P_{EF-1} were also reported to work in *Schizochytrium* sp. ATCC 20888 (8). However, the promoters were not the endogenous promoters, expression intensity maybe not be enough in HX-308. Thus, more promoters should be characterized by the β-Galactosidase reporter system or the EGFP reporter system in the future (8).

Transformation of *Schizochytrium* sp. HX-308 Mediated With *A. tumefaciens* AGL-1

The *A. tumefaciens* AGL-1 containing the plasmid pZPK-P_{GAPDH}-NeoR-T_{GAPDH} was used to transform the *NeoR* expression cassette into HX-308. In a previous study, Cheng et al. transformed an *egfp* gene into *Schizochytrium* and green fluorescence was observed successfully (20). To improve the contact between *Agrobacterium* and *Schizochytrium*, they treated the *Schizochytrium* with DTT and lysing enzymes to weaken the cell wall (20). In this study, we abolished the pretreatment of HX-308 to simplify the transformation procedures. *Agrobacterium tumefaciens* AGL-1 were mixed with HX-308 and spread on IM plates which were supplemented with 200 μM acetosyringone. Acetosyringone was used to induce *A. tumefaciens* AGL-1 to integrate the T-DNA containing the *NeoR* expression cassette into the HX-308 genome (26). After induction, the cocultures were selected on GPYS plates supplemented with cefotaxime sodium and G418. The results appeared that *A. tumefaciens* AGL-1 could also attach to HX-308 even without weakening the cell wall of *Schizochytrium*.

The colonies were grown on GPYS plates supplemented with cefotaxime sodium and G418 for at least three generations, and the transformants were then used to extract genomic DNA for PCR analysis. The insertion of the *NeoR* gene in the transformants was confirmed by diagnostic PCR. The transformants generated an expected ∼800-bp band, but the *NeoR* gene could not be detected in the wild type (WT) (**Figure 1B**), indicating that the *NeoR* gene was integrated into the genome of HX-308. Our results demonstrated that the ATMT method we developed was a promising strategy to transform HX-308.

Overexpression of the Acetyl-CoA *c*-Acetyltransferase Gene in *Schizochytrium* sp. HX-308 for Enhancing the Terpenoid Biosynthesis

The successful expression of the *NeoR* gene suggested that the ATMT method can be used to overexpress functional genes in HX-308. In our previous study, HX-308 can produce over 80 g/L lipid during fed-batch culture, which indicated that it can produce high level of acetyl-CoA as the precursor for lipid biosynthesis (5, 27). Similarly, acetyl-CoA is also the precursor of terpenoids. And it was reported that *Schizochytrium sp.* could synthesize some terpenoids such as squalene, β-carotene and astaxanthin during fermentation (28–30). However, the productivity of terpenoids in *Schizochytrium sp.* was quite low. In recent years, genetic engineering strategies are commonly being used to increase terpenoids production in microalgae (31). Thus, it would be hopeful to pull some acetyl-CoA from the biosynthesis of lipids to enhance the biosynthesis of these valuable terpenoids in HX-308 through genetic manipulation. In nature, all terpenoids can be synthesized via the MVA pathway or the methylerythritol phosphate (MEP) pathway, and HX-308 utilizes the MVA pathway to synthesize terpenoids. In this study, the gene acetyl-CoA c-acetyltransferase (*AACT4419*) was overexpressed to increase terpenoid productivity in HX-308. It catalyzes the condensation of two molecules of acetyl-CoA, and a molecule of acetoacetyl-CoA is formed (31). This is the first step of the MVA pathway. The strong promoter P_{ACCase} was chosen to drive the expression of the gene *AACT4419*, resulting the strain hxAACT (**Figure 2**). ACCase is a constitutive enzyme which catalyzes the carboxylation of acetyl-CoA during the biosynthesis of fatty acids in *Schizochytrium* (8). Thus, the promoter of the gene *ACCase*, P_{ACCase}, would be a promising promoter to express the gene *AACT4419*, and thus synthesizing more acetoacetyl-CoA to synthesize terpenoids in the strain hxAACT.

The strains hxAACT4419 and WT were subjected to fed-batch culture for 120 h. What surprised us was that the growth and glucose consumption of hxAACT decreased a lot when compared with WT. By the end of fermentation, the glucose consumption of hxAACT was 148.5 g/L, which was 55% lower than that of the WT (**Figure 3A**). And the total fatty acids and CDW of hxAACT decreased 71% and 35% respectively when compared with WT (**Figures 3B,C**). Moreover, as shown in **Table 1**, the lipid composition of hxAACT also changed significantly. The percentage of 14:0 and docosapentaenoic acid (DPA) remained

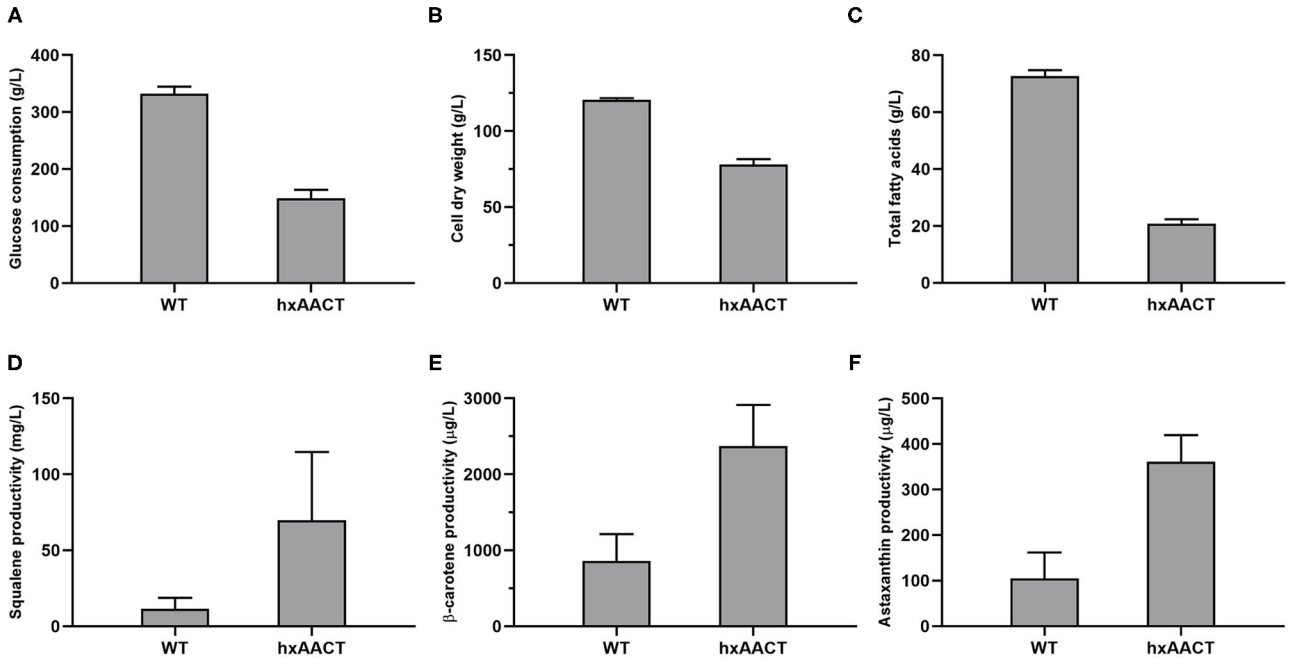

FIGURE 3 | Comparison of cell growth, the accumulation of lipids, and the synthesis of terpenoids between the strain WT and the strain hxAACT at 120 h in 500-mL shake flasks. **(A)** Glucose consumption, **(B)** CDW, **(C)** Lipid productivity, **(D)** Squalene productivity, **(E)** β-carotene productivity, **(F)** Astaxanthin productivity. Values and error bars represent the means and standard deviations from triplicate experiments.

TABLE 1 | The percentage of fatty acids (w/w%) in WT and hxAACT at 24, 48, 72, 96, 120 h in 500-mL shake flasks.

Time	Strains	C14:0	C16:0	EPA	DPA	DHA
24 h	WT	11.24 ± 1.11	26.8 ± 0.99	1.66 ± 0.08	14.27 ± 0.22	44.84 ± 1.80
	hxAACT	18.91 ± 2.01	13.96 ± 0.25	0.93 ± 0.89	18.77 ± 0.87	42.87 ± 2.53
48 h	WT	12.67 ± 0.59	25.06 ± 1.15	1.27 ± 0.06	15.06 ± 0.40	44.58 ± 1.97
	hxAACT	25.54 ± 0.83	14.63 ± 0.26	0.75 ± 0.22	20.47 ± 0.37	20.47 ± 0.37
72 h	WT	10.95 ± 0.08	22.55 ± 1.35	1.07 ± 0.08	15.99 ± 0.06	45.00 ± 1.06
	hxAACT	25.95 ± 1.19	12.60 ± 0.21	1.01 ± 0.14	19.06 ± 0.78	32.88 ± 1.15
96 h	WT	9.49 ± 0.24	20.75 ± 1.41	0.90 ± 0.00	16.84 ± 0.38	46.61 ± 1.30
	hxAACT	23.15 ± 1.11	12.04 ± 0.76	0.71 ± 0.09	21.22 ± 1.37	34.40 ± 1.54
120 h	WT	9.58 ± 0.12	22.36 ± 0.53	0.79 ± 0.04	16.98 ± 0.20	44.45 ± 0.35
	hxAACT	22.61 ± 1.19	11.99 ± 0.30	0.77 ± 0.03	21.13 ± 0.54	33.81 ± 1.03

Values and error represent the means and standard deviations from triplicate experiments.

higher in hxAACT than that in WT throughout the fermentation. The highest percentage of 14:0 was obtained at 72 h in hxAACT, which was 15% higher than that in WT. Similarly, the percentage of DPA in hxAACT remained around 20%, which was 4 to 5% higher than that in WT. In contrast to 14:0 and DPA, the percentage of 16:0 and DHA remained lower in hxAACT than that in WT throughout the fermentation. The percentage of DHA in WT remained around 45%. However, the percentage of DHA in hxAACT decreased rapidly from 42.87 to 20.47% during 24–48 h, and then increased from 20.47 to around 33% during 72–120 h.

We speculated that the integration site of foreign genes may affect the growth phenotype of HX-308 (**Figure 3**). Thus, inverse PCR was performed to find out the integration site of the *AACT4419* expression cassette (32). The PCR reagent was sent to be sequenced, and the *AACT4419* expression cassette was found to be integrated about 1.2-kb downstream in the coding sequence of the gene which was named *A3018*, resulting in insertional inactivation of the gene *A3018* (**Supplementary Figure S2**). The amino acid sequences of the gene *A3018* was then submitted to NCBI for basic local alignment. The results suggested that the gene *A3018* encoded the enzyme UDP-D-xylose: ribitol-5-phosphate beta1,4-xylosyltransferase (TMEM5). TMEM5 was reported to be critical for the biosynthesis of *O*-mannosyl glycan, which is responsible for the biosynthesis of cell wall (33). Further studies can be conducted to knockout the gene *TMEM5* to

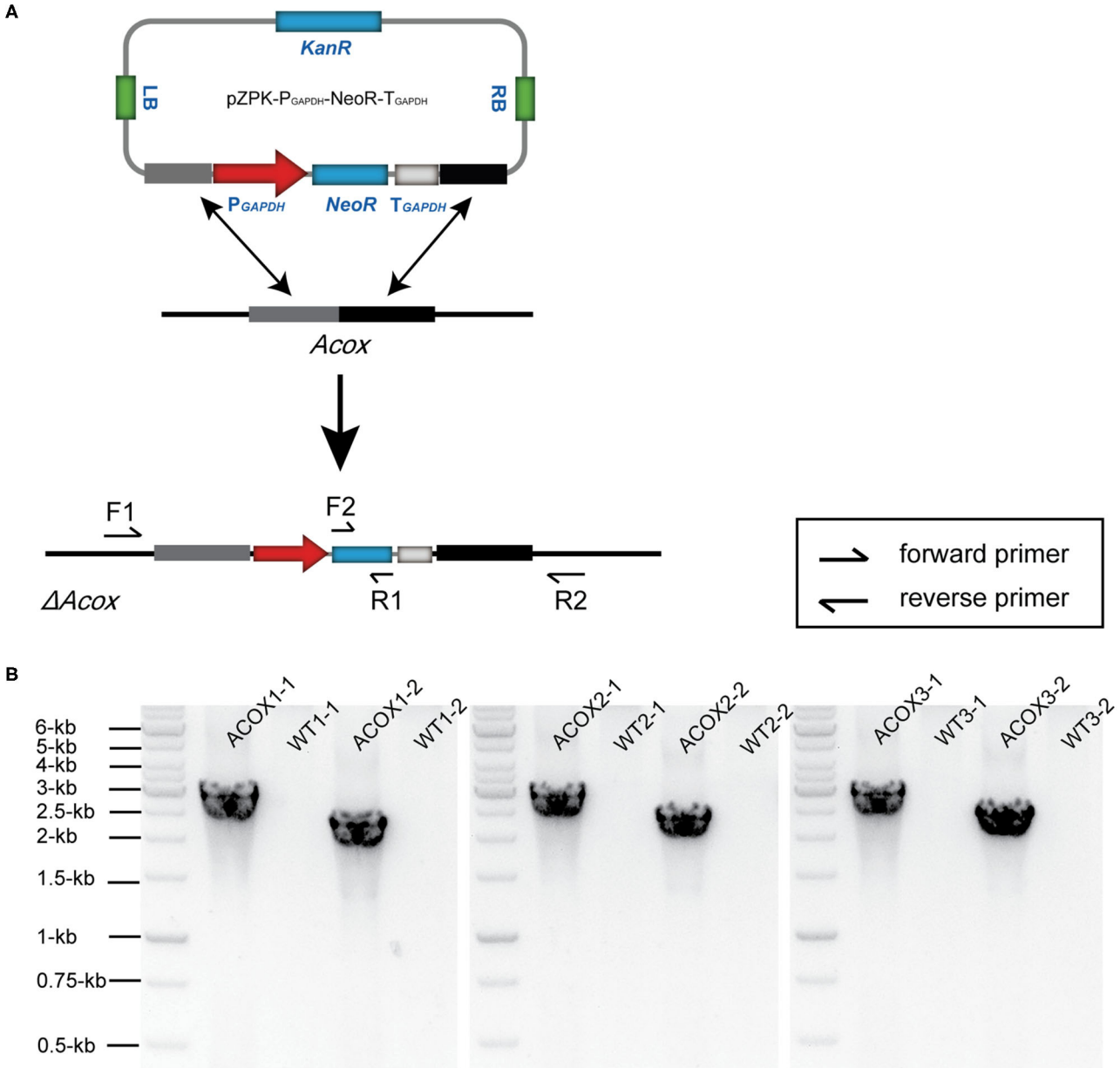

FIGURE 4 | Disruption of the genes *Acox1-3* in HX-308. **(A)** The schematic diagram of the disruption of the genes *Acox1-3*. **(B)** Diagnostic PCR confirmation of the mutants ACOX1, ACOX2, and ACOX3.

verify the effect of the gene *A3018* on the growth of HX-308 in the future.

The overexpression of *AACT4419* was aimed to improve the biosynthesis of terpenoids. Thus, the productivity of these three valuable terpenoids in HX-308 were detected. As was expected, the productivity of squalene in the strain hxAACT was increased from 11 mg/L to 70 mg/L, representing a 5.4-fold increase than that of the WT (**Figure 3D**). Similarly, with the overexpression of the gene *AACT4419* in hxAACT, the production of β-carotene and astaxanthin were increased 1.8 times and 2.4 times, respectively (**Figures 3E,F**). These findings indicated that the overexpression of *AACT4419* increased terpenoids production in hxAACT, probably by increasing the supply of acetyl-CoA and acetoacetyl-CoA.

Disruption of *Acox1-3* in HX-308 for Enhancing the Lipid Biosynthesis

β-Oxidation is the process of the metabolism of fatty acids which takes place in both mitochondria and peroxisomes. Thus, the inhibition of β-oxidation may facilitate the accumulation of lipids (34). It was reported that disrupting the gene associated with β-oxidation (*Acox*) could reduce the degradation of fatty

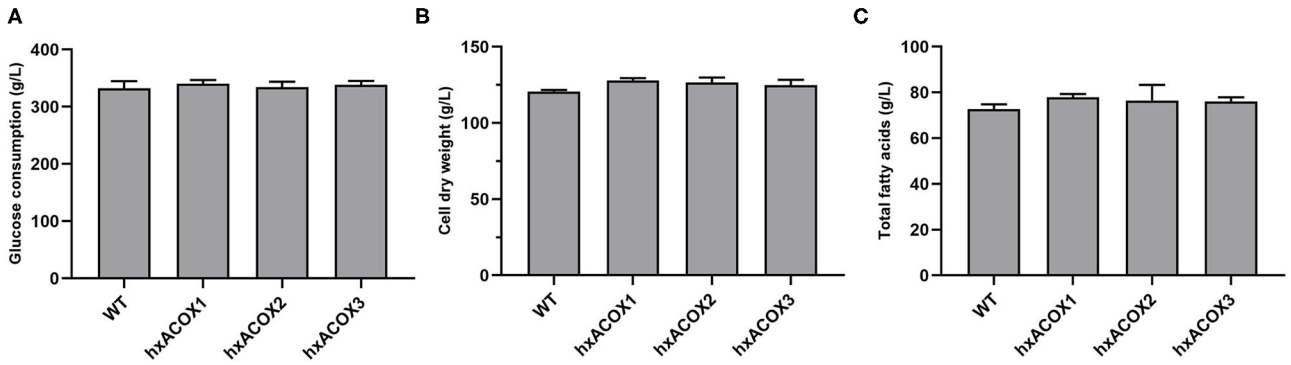

FIGURE 5 | Comparison of cell growth and the accumulation of lipids between the strain WT and the strains ACOX1-3 at 120 h in 500-mL shake flasks. **(A)** Glucose consumption, **(B)** CDW, **(C)** Lipid productivity. Values and error bars represent the means and standard deviations from triplicate experiments.

acids, and thus increased the accumulation of total lipids in *Aurantiochytrium* sp. (10). Acox catalyzes the transformation of acyl-CoA into trans-2, 3-dehydroacyl-CoA (35). It is the first step of β-oxidation in peroxisome. Thus, knocking out of *Acox* could break the process of β-oxidation, resulting in lipid accumulation. In this study, we identified and knocked out the three *Acox* genes in HX-308 in order to increase the lipid biosynthesis. Three plasmids named pZPK-Acox1-3 were constructed based on the sequences of *Acox1-3*, and then were transformed into HX-308 respectively. During diagnostic PCR, two primer pairs F1/R1 and F2/R2 were used to screen the genome edited transformants of each gene. The primers F1 and R2 were located in the genome of HX-308, outside of the homologous arms of the plasmids pZPK-Acox1-3. The primers F2 and R1 were located in the coding sequence of *NeoR* on the plasmids pZPK-Acox1-3. The mutants generated an expected ∼2.9-kb band and an expected 2.4-kb band, but no bands could be generated when WT was used as templates (**Figure 4**). The results demonstrated that the genes *Acox1-3* were disrupted successfully, and the strains were named hxACOX1, hxACOX2 and hxACOX3. During verification, what surprised us was that the knock-out efficiency of *Acox1*, *Acox2*, and *Acox3* was about 20% (2 mutants in 10 transfromants), 30% (3 mutants in 10 transfromants), and 16.7% (2 mutants in 12 transfromants) respectively. It was much higher than that in other fungi such *Aspergillus sojae* and *Aspergillus oryzae* with an efficiency of ∼5% (36). A previous study also reported that ATMT lead to homologous recombination and facilitated gene knock-out in *Aspergillus carbonarius* (37). Thus, the ATMT method we constructed would be promising for gene disruption in HX-308.

The strains hxACOX1, hxACOX2, hxACOX3, and WT were subjected to fed-batch culture for 120 h. By the end of fermentation, the glucose consumption of the four strains has no significant difference (**Figure 5A**). However, the CDW of the strains hxACOX1-3 increased about 6.1, 5.1, and 3.7% when compared with WT (**Figure 5B**). Accordingly, the total fatty acids of the strains hxACOX1-3 increased about 7.1, 5.1, and 4.7% respectively (**Figure 5C**). The results appeared that the disruption of *Acox1-3* inhibited the process of β-oxidation, and thus increased the biosynthesis of lipids in HX-308. The Acox1-3 were three isoenzymes which were expressed by HX-308. The disruption of one *Acox* gene can be complemented by other *Acox* genes (38). To further improve the accumulation of lipids in HX-308, the cre-*loxP* system can be constructed in the future to disrupt *Acox1*, *Acox2*, and *Acox3* simultaneously (39).

CONCLUSION

In conclusion, we have firstly established an efficient ATMT method for the genetic manipulation in the *Schizochytrium* sp. HX-308. The gene *AACT4419* was overexpressed and the genes *Acox1-3* were disrupted in HX-308 to improve the productivity of terpenoids and lipids. A strong constitutive promoter P_{ACCase} was used to drive the expression of *AACT4419*, and the squalene, β-carotene and astaxanthin yields of the resulting strain hxAACT were increased 5.4, 1.8 and 2.4 times compared to the WT. When disrupting the genes associated with β-oxidation, the resulting strains hxACOX1, hxACOX2, and hxACOX3 reached a CDW of 127.9, 126.7, and 124.9 g/L. And the lipid yields of hxACOX1, hxACOX2, and hxACOX3 were increased 7.1, 5.1, and 4.7% respectively. In the future, the ATMT method we constructed would be beneficial to studying functional genes as well as producing high value products in HX-308.

NUCLEOTIDE SEQUENCE ACCESSION NUMBERS

The accession numbers of the sequences reported in this article deposited in GenBank: OK641580 (*GAPDH*), OK641581 (*AACT*), OK641582 (*ACOX1*), OK641583 (*ACOX2*), OK641584 (*ACOX3*), OK641585 (*ACCase*).

DATA AVAILABILITY STATEMENT

The original contributions presented in the study are included in the article/**Supplementary Material**, further inquiries can be directed to the corresponding author.

AUTHOR CONTRIBUTIONS

P-WH carried out the experiments and drafted the manuscript. Y-SX and X-MS analyzed the data and helped to draft the manuscript. T-QS, YG, CY, and HH conceived and designed the study and revised the manuscript. All authors read and approved the final manuscript.

FUNDING

This work was supported by the Nature Science Foundation of Jiangsu Province (No. BK20190706), the National Natural Science Foundation of China (Nos. 21908112 and 22038007).

SUPPLEMENTARY MATERIAL

The Supplementary Material for this article can be found online at: https://www.frontiersin.org/articles/10.3389/fnut.2021.795651/full#supplementary-material

REFERENCES

1. Ren L, Sun L, Zhuang X, Qu L, Ji X, Huang H. Regulation of docosahexaenoic acid production by *Schizochytrium* sp: effect of nitrogen addition. *Bioproc Biosyst Eng.* (2014) 37:865–72. doi: 10.1007/s00449-013-1057-5
2. Sun X, Ren L, Zhao Q, Zhang L, Huang H. Application of chemicals for enhancing lipid production in microalgae-a short review. *Bioresource Technol.* (2019) 293:122135. doi: 10.1016/j.biortech.2019.122135
3. Patel A, Sarkar O, Rova U, Christakopoulos P, Matsakas L. Valorization of volatile fatty acids derived from low-cost organic waste for lipogenesis in oleaginous microorganisms-a review. *Bioresour Technol.* (2021) 321:124457. doi: 10.1016/j.biortech.2020.124457
4. Ren L, Huang H, Xiao A, Lian M, Jin L, Ji X. Enhanced docosahexaenoic acid production by reinforcing acetyl-CoA and NADPH supply in *Schizochytrium* sp. HX-308. *Bioproc Biosyst Eng.* (2009) 32:837–43. doi: 10.1007/s00449-009-0310-4
5. Sun X, Ren L, Bi Z, Ji X, Zhao Q, Huang H. Adaptive evolution of microalgae *Schizochytrium* sp. under high salinity stress to alleviate oxidative damage and improve lipid biosynthesis. *Bioresource Technol.* (2018) 267:438–44. doi: 10.1016/j.biortech.2018.07.079
6. Sun X, Ren L, Bi Z, Ji X, Zhao Q, Jiang L, et al. Development of a cooperative two-factor adaptive-evolution method to enhance lipid production and prevent lipid peroxidation in *Schizochytrium* sp. *Biotechnol Biofuels.* (2018) 11:65. doi: 10.1186/s13068-018-1065-4
7. Ren L, Sun X, Ji X, Chen S, Guo D, Huang H. Enhancement of docosahexaenoic acid synthesis by manipulation of antioxidant capacity and prevention of oxidative damage in *Schizochytrium* sp. *Bioresource Technol.* (2017) 223:141–8. doi: 10.1016/j.biortech.2016.10.040
8. Han X, Zhao Z, Wen Y, Chen Z. Enhancement of docosahexaenoic acid production by overexpression of ATP-citrate lyase and acetyl-CoA carboxylase in *Schizochytrium* sp. *Biotechnol Biofuels.* (2020) 13:131. doi: 10.1186/s13068-020-01767-z
9. Zhang S, He Y, Sen B, Chen X, Xie Y, Keasling JD, et al. Alleviation of reactive oxygen species enhances PUFA accumulation in *Schizochytrium* sp. through regulating genes involved in lipid metabolism. *Metab Eng Commun.* (2018) 6:39–48. doi: 10.1016/j.meteno.2018.03.002
10. Watanabe K, Perez CMT, Kitahori T, Hata K, Aoi M, Takahashi H, et al. Improvement of fatty acid productivity of thraustochytrid, *Aurantiochytrium* sp. by genome editing. *J Biosci Bioeng.* (2021) 131:373–80. doi: 10.1016/j.jbiosc.2020.11.013
11. Wang F, Bi Y, Diao J, Lv M, Cui J, Chen L, et al. Metabolic engineering to enhance biosynthesis of both docosahexaenoic acid and odd-chain fatty acids in *Schizochytrium* sp. S31. *Biotechnol Biofuels.* (2019) 12:141. doi: 10.1186/s13068-019-1484-x
12. Wang S, Lan C, Wang Z, Wan W, Cui Q, Song X. PUFA-synthase-specific PPTase enhanced the polyunsaturated fatty acid biosynthesis via the polyketide synthase pathway in *Aurantiochytrium*. *Biotechnol Biofuels.* (2020) 13:152. doi: 10.1186/s13068-020-01793-x
13. Sakaguchi K, Matsuda T, Kobayashi T, Ohara J, Hamaguchi R, Abe E, et al. Versatile transformation system that is applicable to both multiple transgene expression and gene targeting for *Thraustochytrids*. *Appl Environ Microb.* (2012) 78:3193–202. doi: 10.1128/AEM.07129-11
14. Krenek P, Samajova O, Luptovciak I, Doskocilova A, Komis G, Samaj J. Transient plant transformation mediated by *Agrobacterium tumefaciens*: principles, methods, and applications. *Biotechnol Adv.* (2015) 33:1024–42. doi: 10.1016/j.biotechadv.2015.03.012
15. Binns AN, Zhao J. The MexE/MexF/AmeC efflux pump of *Agrobacterium tumefaciens* and its role in Ti plasmid virulence gene expression. *J Bacteriol.* (2020) 202:e00609–19. doi: 10.1128/JB.00609-19
16. Barton IS, Eagan JL, Nieves-Otero PA, Reynolds IP, Platt TG, Fuqua C. Co-dependent and Interdigitated: dual quorum sensing systems regulate conjugative transfer of the Ti plasmid and the At megaplasmid in *Agrobacterium tumefaciens* 15955. *Front Microbiol.* (2020) 11:605896. doi: 10.3389/fmicb.2020.605896
17. de Groot MJ, Bundock P, Hooykaas PJ, Beijersbergen AG. *Agrobacterium tumefaciens*-mediated transformation of filamentous fungi. *Nat Biotechnol.* (1998) 16:839–42. doi: 10.1038/nbt0998-839
18. Dai Z, Deng S, Culley DE, Bruno KS, Magnuson JK. *Agrobacterium tumefaciens*-mediated transformation of oleaginous yeast *Lipomyces* species. *Appl Microbiol Biotechnol.* (2017) 101:6099–110. doi: 10.1007/s00253-017-8357-7
19. Hooykaas P, van Heusden G, Niu X, Reza RM, Soltani J, Zhang X, et al. *Agrobacterium*-mediated transformation of yeast and fungi. *Curr Top Microbiol Immunol.* (2018) 418:349–74. doi: 10.1007/82_2018_90
20. Cheng R, Ma R, Li K, Rong H, Lin X, Wang Z, et al. *Agrobacterium tumefaciens* mediated transformation of marine microalgae *Schizochytrium*. *Microbiol Res.* (2012) 167:179–86. doi: 10.1016/j.micres.2011.05.003
21. Wang Y, Lin X, Zhang S, Sun W, Ma S, Zhao ZK. Cloning and evaluation of different constitutive promoters in the oleaginous yeast *Rhodosporidium toruloides*. *Yeast.* (2016) 33:99–106. doi: 10.1002/yea.3145
22. Harnkarnsujarit N, Charoenrein S, Roos YH. Reversed phase HPLC analysis of stability and microstructural effects on degradation kinetics of beta-carotene encapsulated in freeze-dried maltodextrin-emulsion systems. *J Agric Food Chem.* (2012) 60:9711–8. doi: 10.1021/jf303452c
23. Li D, Wei X, Liu T, Liu C, Chen W, Xuan YH, et al. Establishment of an *Agrobacterium tumefaciens*-mediated transformation system for *Tilletia foetida*. *J Microbiol Meth.* (2020) 169:105810. doi: 10.1016/j.mimet.2019.105810
24. Nash MA, Platsoucas CD, Wong BY, Wong PM, Cottler-Fox M, Otto E, et al. Transduction of rIL-2 expanded $CD4^+$ and $CD8^+$ ovarian TIL-derived T cell lines with the G1Na (neor) replication-deficient retroviral vector. *Hum Gene Ther.* (1995) 6:1379–89. doi: 10.1089/hum.1995.6.11-1379
25. Barber RD, Harmer DW, Coleman RA, Clark BJ, GAPDH. as a housekeeping gene: analysis of GAPDH mRNA expression in a panel of 72 human tissues. *Physiol Genomics.* (2005) 21:389–95. doi: 10.1152/physiolgenomics.00025.2005

26. Harighi B. Role of CheY1 and CheY2 in the chemotaxis of *A. tumefaciens* toward acetosyringone. *Curr Microbiol.* (2008) 56:547–52. doi: 10.1007/s00284-008-9120-1
27. Kong F, Romero IT, Warakanont J, Li-Beisson Y. Lipid catabolism in microalgae. *New Phytol.* (2018) 218:1340–8. doi: 10.1111/nph.15047
28. Hoang L, Nguyen HC, Le TT, Hoang T, Pham VN, Hoang M, et al. Different fermentation strategies by *Schizochytrium mangrovei* strain pq6 to produce feedstock for exploitation of squalene and omega-3 fatty acids. *J Phycol.* (2018) 54:550–6. doi: 10.1111/jpy.12757
29. Bindea M, Rusu B, Rusu A, Trif M, Leopold LF, Dulf F, et al. Valorification of crude glycerol for pure fractions of docosahexaenoic acid and beta-carotene production by using *Schizochytrium limacinum* and *Blakeslea trispora*. *Microb Cell Fact.* (2018) 17:97. doi: 10.1186/s12934-018-0945-4
30. Du H, Liao X, Gao Z, Li Y, Lei Y, Chen W, et al. Effects of Methanol on carotenoids as well as biomass and fatty acid biosynthesis in *Schizochytrium limacinum* B4D1. *Appl Environ Microbiol.* (2019) 85:e01243–19. doi: 10.1128/AEM.01243-19
31. Huang PW, Wang LR, Geng SS, Ye C, Sun XM, Huang H. Strategies for enhancing terpenoids accumulation in microalgae. *Appl Microbiol Biotechnol.* (2021) 105:4919–30. doi: 10.1007/s00253-021-11368-x
32. Green MR, Sambrook J. Inverse Polymerase Chain Reaction (PCR). *Cold Spring Harb Protoc.* (2019) 2019. doi: 10.1101/pdb.prot095166
33. Manya H, Yamaguchi Y, Kanagawa M, Kobayashi K, Tajiri M, Akasaka-Manya K, et al. The muscular dystrophy gene TMEM5 encodes a ribitol beta1,4-xylosyltransferase required for the functional glycosylation of dystroglycan. *J Biol Chem.* (2016) 291:24618–27. doi: 10.1074/jbc.M116.751917
34. Reddy JK, Hashimoto T. Peroxisomal beta-oxidation and peroxisome proliferator-activated receptor alpha: an adaptive metabolic system. *Annu Rev Nutr.* (2001) 21:193–230. doi: 10.1146/annurev.nutr.21.1.193
35. Zhang X, Feng L, Chinta S, Singh P, Wang Y, Nunnery JK, et al. Acyl-CoA oxidase complexes control the chemical message produced by *Caenorhabditis elegans*. *Proc Natl Acad Sci U S A.* (2015) 112:3955–60. doi: 10.1073/pnas.1423951112
36. Huang PW, Yang Q, Zhu YL, Zhou J, Sun K, Mei YZ, et al. The construction of CRISPR-Cas9 system for endophytic *Phomopsis liquidambaris* and its PmkkA-deficient mutant revealing the effect on rice. *Fungal Genet Biol.* (2020) 136:103301. doi: 10.1016/j.fgb.2019.103301
37. Weyda I, Yang L, Vang J, Ahring BK, Lubeck M, Lubeck PS, et al. comparison of *Agrobacterium*-mediated transformation and protoplast-mediated transformation with CRISPR-Cas9 and bipartite gene targeting substrates, as effective gene targeting tools for *Aspergillus carbonarius*. *J Microbiol Methods.* (2017) 135:26–34. doi: 10.1016/j.mimet.2017.01.015
38. Eastmond PJ, Hooks M, Graham IA. The arabidopsis acyl-CoA oxidase gene family. *Biochem Soc Trans.* (2000) 28:755–7. doi: 10.1042/bst0280755
39. Kos CH. Cre/loxP system for generating tissue-specific knockout mouse models. *Nutr Rev.* (2004) 62:243–6. doi: 10.1301/nr2004.jun243-246

Conflict of Interest: The authors declare that the research was conducted in the absence of any commercial or financial relationships that could be construed as a potential conflict of interest.

frontiers in Nutrition

ORIGINAL RESEARCH
published: 23 December 2021
doi: 10.3389/fnut.2021.793795

Transcriptomic Responses of *Cordyceps militaris* to Salt Treatment During Cordycepins Production

Gongbo Lv[1], *Yue Zhu*[1], *Xiaojie Cheng*[2], *Yan Cao*[3], *Bin Zeng*[1,4], *Xinping Liu*[1] *and Bin He*[1]*

[1] *Jiangxi Key Laboratory of Bioprocess Engineering and Co-innovation Center for in-vitro Diagnostic Reagents and Devices of Jiangxi Province, College of Life Sciences, Jiangxi Science and Technology Normal University, Nanchang, China,* [2] *College of Life Sciences, Sichuan Normal University, Chengdu, China,* [3] *Information Institute of Sichuan Academy of Agricultural Sciences, Chengdu, China,* [4] *College of Pharmacy, Shenzhen Technology University, Shenzhen, China*

Cordycepin is a major bioactive compound found in *Cordyceps militaris* (*C. militaris*) that exhibits a broad spectrum of biological activities. Hence, it is potentially a bioactive ingredient of pharmaceutical and cosmetic products. However, overexploitation and low productivity of natural *C. militaris* is a barrier to commercialization, which leads to insufficient supply to meet its existing market demands. In this study, a preliminary study of distinct concentrations of salt treatments toward *C. militaris* was conducted. Although the growth of *C. militaris* was inhibited by different salt treatments, the cordycepin production increased significantly accompanied by the increment of salt concentration. Among them, the content of cordycepin in the 7% salt-treated group was five-fold higher than that of the control group. Further transcriptome analysis of samples with four salt concentrations, coupled with Gene Ontology (GO) analysis and Kyoto Encyclopedia of Genes and Genomes (KEGG) pathway enrichment, several differentially expressed genes (DEGs) were found. Finally, dynamic changes of the expression patterns of four genes involved in the cordycepin biosynthesis pathway were observed by the quantitative real-time PCR. Taken together, our study provides a global transcriptome characterization of the salt treatment adaptation process in *C. militaris* and facilitates the construction of industrial strains with a high cordycepin production and salt tolerance.

Keywords: cordycepin, *Cordyceps militaris*, salt treatment, molecular mechanism, transcriptome

OPEN ACCESS

Edited by:
Wanwipa Vongsangnak, Kasetsart University, Thailand

Reviewed by:
Rúbia Carvalho Gomes Corrêa, Cesumar University - UniCesumar, Brazil
Yanchun Shao, Huazhong Agricultural University, China

***Correspondence:**
Bin He
hebin.li@foxmail.com

Specialty section:
This article was submitted to Food Chemistry, a section of the journal Frontiers in Nutrition

Received: *12 October 2021*
Accepted: *24 November 2021*
Published: *23 December 2021*

Citation:
Lv G, Zhu Y, Cheng X, Cao Y, Zeng B, Liu X and He B (2021) Transcriptomic Responses of Cordyceps militaris to Salt Treatment During Cordycepins Production. Front. Nutr. 8:793795. doi: 10.3389/fnut.2021.793795

INTRODUCTION

Cordyceps militaris (*C. militaris*), or known as North *Cordyceps sinensis*, is an entomogenous fungus belonging to the *Ascomycota*, *Hypocreales*, and *Ergotacea*e, as spores are produced internally inside a sac, called ascus (1). It is a well-known edible and medicinal fungus and one of the most important traditional Chinese medicines. Contrary to *Cordyceps sinensis* (DongChongXiaCao) in Chinese herbs, which is unique to China, *C. militaris* is a worldwide species and is also distributed in almost all provinces and regions in China. Its soporophore can parasitize larvae or grow on the pupae of lepidopteran insects. These insects are located on the scales half-buried on the forest floor or under the layer of deciduous branches from spring to autumn (2). *C. militaris* has been extensively used as a folk medicine in areas of East Asia for the revitalization of various systems of the body from ancient times, and currently it is also widely used in Western countries (3). Since *C. militaris* produces a variety of bioactive compounds with functional properties, it has long been utilized as a

dietary supplement (tonic food) or herbal medicine for the pharmaceutical and cosmetics industries for many years (4, 5). Various bioactive metabolites isolated from *C. militaris*, such as cordycepin (3′-deoxyadenosine) (6), cordycepic acid, carotenoid, ergosterol, and cordyceps polysaccharide (7), have been explored extensively for extending its applications; particularly, several of them are extracted and made into tablets and capsules (8). In addition, fermentation and downstream processes or other bioprocess developments have permitted a prospect in the production of these specific bioactive metabolites as functional ingredients for diversified applications (9).

Among the aforementioned bioactive metabolites, the cordycepin (3′-deoxyadenosine) has attracted the most attention in *C. militaris*, and its potential therapeutic effect has been mostly mentioned and investigated for clinical trials against cancer (10). As the main bioactive ingredient of *C. militaris*, cordycepin is used as a transcription inhibitor for its lack of hydroxyl moiety at the C3 position. When cordycepin is integrated into the RNA chain, it will lead to the termination of transcription (11). Moreover, it has been reported that cordycepin can inhibit cell proliferation and induce cell apoptosis *via* binding signaling molecules, which resulted in anti-inflammatory action (12–14). Cordycepin and adenosine have a similar structure, except for the lack of a 3′ hydroxyl group on cordycepin. Even with such a tiny difference, cordycepin and adenosine exhibit completely distinct biological activity, and cordycepin is reported to interfere with many molecular and cellular processes within cells. Furthermore, extensive research results showed that cordycepin has many other diversified biological activities, such as a very potent anti-cancer, anti-ischemic, and anti-oxidant protective effect. Exactly, cordycepin binds the A3 adenosine receptor, which results in activating G protein (inhibitory regulative guanine nucleotide-binding protein). Afterward, the cAMP formation was inhibited, then the serine/threonine kinase glycogen synthase kinase (GSK)-3β/β-catenin signaling pathway and subsequently cell division were indirectly inactivated and suppressed, respectively (15). Additionally, it has been also documented that cordycepin effects on inhibiting platelet aggregation, inducing steroid formation, and with broad-spectrum antibiotic activity by inhibiting NAD^+-dependent DNA ligase (13, 16, 17).

With over seven-decade-long historical investigations of cordycepin, it was first isolated from *C. militaris* in 1950 (6), and the chemical structure of cordycepin was confirmed to be 3′-deoxyadenosine *via* mass spectrometry data, infrared spectroscopy, and nuclear magnetic resonance spectroscopy data, combined with the characteristics of the ultraviolet absorption spectrum (18, 19). Meanwhile, the cordycepin biosynthetic pathway has been exploited for over half-centuries. Though several hypotheses concerning cordycepin biosynthetic pathways were proposed, clear experimental evidence to clarify "how cordycepin is produced" was lacking. With the completion of the whole genome sequencing of *C. militaris*, Xia et al. first identified the gene cluster responsible for the cordycepin biosynthesis, and the cordycepin biosynthesis pathway was further fulfilled in 2017 (20, 21). There were four genes (*Cns1*–*Cns4*) physically linked as the cordycepin biosynthetic gene cluster and encoded proteins with distinct conserved domains, which differently mediated cordycepin metabolism. Among them, *Cns1* (CCM_04436) contains the oxidoreductase/dehydrogenase domain, and *Cns2* (CCM_04437) possesses the HDc family of metal-dependent phosphohydrolase domain. There were two functional domains contained in *Cns3* (CCM_04438): an N-terminal nucleoside/nucleotide kinase (NK) and a C-terminal HisG family of ATP phosphoribosyltransferases. Lastly, *Cns4* (CCM_04439) was identified as a member of the putative pleiotropic drug resistance (PDR) family of ATP-binding cassette (ABC) transporters (20). According to the finding of Xia et al., cordycepin biosynthesis begins at adenosine, and the hydroxyl phosphorylation is catalyzed by *Cns3* to produce adenosine-3′-monophosphate (3′AMP). Subsequently, 3′AMP was dephosphorylated to 2′-carbonyl-3′-deoxyadenosine (2′-C-3′-dA) by phosphohydrolase activity of *Cns2* (21). Finally, the 2′-C-3′-dA was converted to cordycepin *via* oxidoreduction reactions mediated by *Cns1*. Simultaneously, it was noteworthy that pentostatin (PTN, 2′-deoxycoformycin), an irreversible inhibitor of adenosine deaminase, was yielded in coupling with cordycepin by phosphoribosyltransferase domain of *Cns3* (22). Consequently, this process inhibited the deamination of cordycepin to 3′-deoxyinosine to maintain the stability of cellular cordycepin through the bacterium protector-protégé strategy (23). Furthermore, when cordycepin accumulation reaches a high (toxic) intracellular level, such PTN will be pumped out of the cell by the *Cns4* transporter for neutralizing cordycepin to nontoxic 3′-deoxyinosine (24).

To meet the existing and increasing market demand of cordycepin production, strategies for the enhancement of this medical component production in *Cordyceps* spp. are warranted. Plentiful literature has been reported on diversified approaches which focused on the improvement of cordycepin content, such as *C. militaris* strain mutagenesis, optimization of medium composition, culture conditions, and extraction methods. Among them, optimization of medium composition is usually the first choice to increase the content of cordycepin. Growth supplements and additives, such as sugar, amino acids (L-alanine, glycine, casein hydrolysate, and glutamine), vitamins, inorganic salts (ferrous sulfate and sodium selenite), nucleoside analog (hypoxanthine and adenosine), porcine liver extracts, or vegetable oils (peanut and cottonseed oil), were proved to be successful (8, 25–30). Moreover, ways of genetic and metabolic engineering are noteworthy, and two main methods are mentioned as follows, the overexpression and disruption of the gene on the cordycepin biosynthetic cluster. It has been reported that the production of cordycepin was increased by 25% by deletion of *Cns3* when compared with the control (21). Meanwhile, overexpression of the single *Cns1*, *Cns2*, and *Cns3* along with the *Cns1*/*Cns2* fusion gene was also performed *via* individually transformed the control strain of *C. militaris*. It was observed that in contrast to the wild-type strain, the yield of cordycepin in the transformant was engineered with the *Cns1*/*Cns2* fusion gene that was increased 2.7-fold, whereas no obvious differences were found between the control and transformants engineered with single genes.

Moreover, previous reports showed that cordycepin production could be increased by ultraviolet, ^{60}Co γ-ray, and blue light LED irradiation. For instance, the cordycepin titer of *Paecilomyces hepiali* ZJB18001strain was increased 2.3-fold *via* ^{60}Co γ-ray and ultraviolet irradiation compared with that from the wild strain (27, 29, 31). Additionally, nutrient stress (distinct carbon, nitrogen, phosphorous sources, and ratios) and environmental stress (lighting time, temperature, pH, and shaking speed) were also effective strategies. It was reported that glucose and casein hydrolysate were the most beneficial carbon and nitrogen sources in cordycepin production (2.3-fold improvement relative to that of the control), and especially, production was greatly affected by casein hydrolysate (29).

Salt stress has negative effects on the growth and survival of organisms, such as leading to water loss and cell shrinking, and several metabolic changes are observed (32, 33). However, to the best of our knowledge, a detailed mechanism of the response of *C. militaris* to salt treatment and its effect on the enrichment of cordycepin remains to be elucidated. The high-salt fermenting environment prolongs the process of substrate catabolism and biosynthesis for the decrease in cell growth and enzyme performance. Thus, the construction of industrial strains with a high cordycepin production and salt tolerance for industrial production is highly desirable. To better comprehend the molecular mechanism of salt-action on cordycepin production, a transcriptome analysis was carried out in the present study. Our study demonstrated the effect of different salt concentrations on cordycepin contents in the CM01 strain, followed by a transcriptome analysis based on RNA sequencing of each salt-treated *C. militaris*, coupled with gene oncology (GO) analysis and Kyoto Encyclopedia of Genes and Genomes (KEGG) pathway enrichment of differentially expressed genes (DEGs). Generally, there is an array of genes that regulates the synthesis of bioactive metabolites, and these genes were upregulated or downregulated during the biosynthesis of cordycepin. Therefore, mRNA expression analysis of several genes involved in the cordycepin biosynthesis pathway was also performed to determine the effect of different salt treatments on potential target genes whose modulation may increase cordycepin production to meet the industrial needs.

MATERIALS AND METHODS

Fungal Strain and Cultivation

In this study, the *C. militaris* strains involved in the experiments was the commonly used strain in our laboratory, CM01strain. This strain is an isolate of *C. militaris* with a mating type of *M4T1-1*. A basal medium, containing (g/L) glucose 20, peptone 5, KH_2PO_4 1, $MgSO_4{\cdot}7H_2O$ 0.5, Vitamin B_1 0.05, and Vitamin B_2 0.05, was used. In total, 200 g potato was milled and boiled with water and filtrated with gauze. The filtrates were mixed with the basal medium, and then water was added to the final volume of 1,000 ml to prepare the liquid medium. After that, the pH of the liquid medium was adjusted to 7.2. The prepared liquid medium was divided into 250 ml flasks (100 ml per flask), coupled with 2 g agar, and one of them was not added agar for strain activating. In total, 0, 3, 5, and 7 g NaCl per 100 ml were added to the medium as treatments, which were equivalent to control, slight stress, moderate stress, and severe salt treatment, respectively. And then all of the media were sterilized in moist heat sterilization autoclave for 20 min at 121°C. When the culture medium was cooled, *C. militaris* strain CM01 was incubated in the prepared liquid medium for activating strain under aseptic conditions. The vibration culture with a speed of 120–140 rpm/min was employed to expand the culture when the white mycelium grows from the seed block (generally 24 h). The activated strain was followed by inoculation on distinct salt-treated potato dextrose agar (PDA) plates and cultured in darkness at a temperature of 22°C. The culture was incubated for 5–7 days. After the media were covered by mycelia, these plates were transferred to the light culture at a temperature of 22°C and lighting intensity of 600 lx for 15 h each day (about 5 days). It was followed by scraping and then drying the *C. militaris* mycelia overnight at 60°C for the biomass determination. All experiments were performed in triplicate to ensure reproducibility.

Extraction of Cordycepin From *C. militaris*

After 5 days of light culture, *C. militaris* mycelium was harvested, and then cordycepin content was determined for the next analysis. Specifically, the mycelia was lyophilized, vacuum freeze-dried to a constant weight, and ground to powder. Two grams of dry powder were weighted from each sample to perform High Performance Liquid Chromatography (HPLC) detection. HPLC assay was conducted on Waters Alliance e2695 HPLC (Milford, MA, USA) using a UV detector set at 260 nm equipped with a ZorbaxSB-C18 column (4.6 × 250 mm, 5 μm). The analysis conditions were as follows: mobile phase, 85% ultra-pure water/methanol (85:15, v/v), and the elution rate was 1.5 ml min^{-1}; injection volume, 20 μl. A standard cordycepin curve was generated using 0.02–0.25 μg/ml cordycepin standard (Sigma-Aldrich, Burlington, MA, USA). The cordycepin yield was calculated using the detected peak area according to the standard curve. The cordycepin concentration of mycelia presented in our study was calculated by normalizing in the equal biomass.

Extraction of Total RNA, Library Establishment, and Transcriptome Sequencing

Total RNA extraction was performed with a fungal RNA kit (Omega Bio-tek, Norcross, GA, USA) by following the operating instructions, coupled with DNA digestion. NanoDrop ND-1000 spectrophotometer (Thermo Scientific, Wilmington, DE, USA) and Bioanalyzer 2100 (Agilent Technologies, Palo Alto, CA, USA) were employed to analyze RNA concentration and integrity. Thereafter, mRNA was enriched by Oligo (dT) beads. The mRNAs were fragmented and used as templates to synthesize cDNA. The cDNA fragments were purified using QiaQuick PCR extraction kit, end-repaired, single-nucleotide adenine addition, and ligated to Illumina sequencing adapters to create the cDNA library. The size of the ligation products was selected by agarose gel electrophoresis, amplified, and sequenced using Illumina HiSeqTM2500 (Biomarker Biotechnology Co., Beijing, China) (34). RNA-Seq data of *C. militaris* under salt treatment were

deposited in the NCBI/SRA database (https://www.ncbi.nlm.nih.gov/sra), under the Bioproject accession number PRJNA770191; BioSample: SAMN22211876-SAMN22211879.

Transcriptome Analysis

The transcriptome datasets are raw reads containing adapters or low-quality bases. Therefore, reads will be further filtered by our previous criterion to get clean reads and thus removed (35). Moreover, Bowtie2 software (http://bowtie-bio.sourceforge.net/bowtie2) was performed to remove reads that mapped to ribosome RNA (rRNA) database to get the final clean reads, which were further employed for assembly and transcriptome analysis (36). For gene expression analysis, the obtained clean-read data sets of the four different cultures were mapped to the reference genome *C. militaris* CM01 (NCBI accession number. AEVU00000000) using Tophats2 (v2.0.3.12) (37). RSEM software was used to quantify gene abundances, and the quantification of gene expression level was normalized using the Fragments Per Kilobase of transcript per Million mapped reads (FPKM) method (38, 39).

DEGs Annotation

Differentially expressed genes across samples were identified using edgeR on the R package (version 3.4.2) according to the RSEM results (40). The absolute value of fold change $\geq$2 and false discovery rate (FDR) within 0.05 were set as the threshold for the detection of significant DEGs among four treatments (CK vs. NaCl-3, -5, and -7) (34). Then the identified DEGs were carried out into hierarchical clustering, with the KEGG pathway enrichment analysis. To further analyze the DEG annotations, GO functional classification and Kyoto Encyclopedia of Genes and Genomes (KEGG) pathway enrichment analysis were carried out based on the GO database (41) and KEGG database (42).

Quantitative Real-Time PCR Validations of DEGs

To validate the transcriptional level results from RNA-Seq data analysis, four genes (encode cordycepin synthetase) *Cns1*, *Cns2*, *Cns3*, and *Cns4* are involved in the cordycepin biosynthesis in *C. militaris* were selected for real-time RT-PCR validation. The qRT-PCR template cDNA was synthesized from 0.5 μg of total RNA by Fungal RNA Kit. Reverse transcription of each RNA sample was performed to get the first-strand cDNA using the PrimeScript RT reagent Kit with gDNA Eraser (Takara, Dalian, China). Each qRT-PCR reaction system had a total volume of 10 μl, containing cDNA, relevant primers, and the SYBR Green Real-time PCR Master Mix (Takara). Real-time RT-PCR was performed using Real-Time PCR System (Bio-Rad, Hercules, CA, USA). GAPDH was served as the internal control (reference gene) for normalization of the target gene expression and to correct for variation between samples. The thermal cycle for RT-PCR was as follows: 95°C for 2 min, followed by 40 cycles of 95°C for 10 sec, 60°C for 15 sec, and 72°C for 20 sec. Melting curve analyses of the amplification products were performed at the end of each PCR reaction to ensure that only specific products were amplified. Primers used for the candidate genes are designed according to Illumina sequencing data by using Primer Premier 5 and listed in **Supplementary Table S1**. The comparative $2^{-\Delta\Delta CT}$ method was employed to calculate relative expression levels between the target genes.

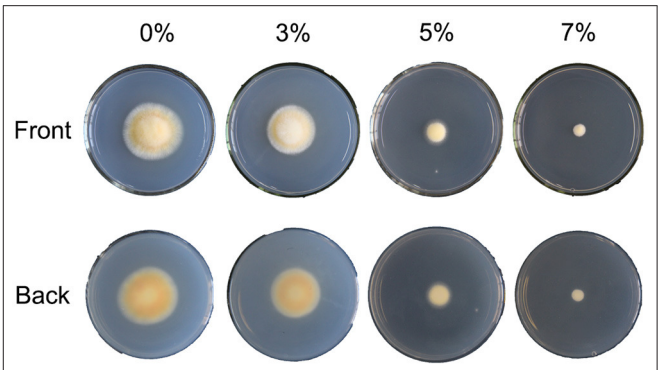

FIGURE 1 | The phenotype of *C. militaris* is affected by different salt treatments. 0, 3, 5, and 7% are equivalent to the control, slight, moderate, and severe salt treatment, respectively.

Data Analysis

Three independent experiments were performed, and all the data in this study are presented as mean ± SE of three replicates. Data from the same period were evaluated by one-way nested ANOVA, followed by the least significant difference test (LSD) for mean comparison. One tail student *t*-test was conducted between the control and salt-treated groups to calculate the *p*-values. All statistical analysis was performed with SAS 9.20 software (SAS Institute Inc., Cary, NC, USA) at the $p < 0.05$.

RESULTS

Growth Characteristics and Cordycepin Production From *C. militaris* After Salt Treatments

To explore the effects of salt treatment on cell growth and cordycepin production of *C. militaris*, a preliminary study of distinct concentrations of salt treatments was conducted. After strain activation, incubation, and dark and light culture, the phenotypes of *C. militaris* mycelioid colonies of the salt-treated group were significantly different from the control (**Figure 1**). As the result showed, the growth of *C. militaris* was significantly restricted by salt treatment and the colony size descends remarkably as the salt concentration increases, especially under the 5 and 7% salt treatments. When the salt concentration is beyond 7%, the mycelia of *C. militaris* cannot even grow at all. It was followed by determining the biomass of the *C. militaris* mycelia. According to the obtained results, the biomass was decreased with the increase of salt concentration (**Supplementary Figure S1**). Analogous to colony diameter, the lowest biomass of the *C. militaris* mycelia was found in the 7% salt-treated group.

High Performance Liquid Chromatography detection assay was performed to determine the production of cordycepin of

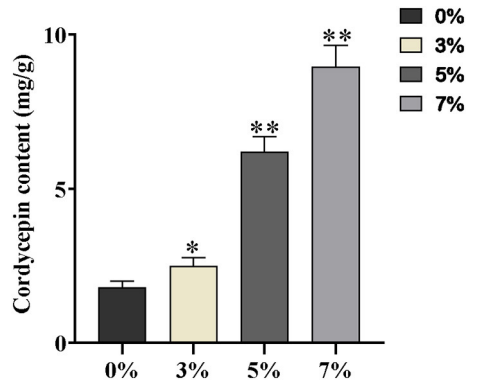

FIGURE 2 | The contents of cordycepin with mg/g dry weight 0, 3, 5, and 7% are equivalent to the control, slight, moderate, and severe salt treatment, respectively. Asterisks indicate statistically significant differences between groups (Student's *t*-test): * and ** indicating significance level was accepted at $P \leq 0.05$ and $P < 0.01$, respectively, as compared to control.

each salt-treated group. Although the growth of *C. militaris* was inhibited by distinct salt treatments, the cordycepin production of per unit volume of mycelium has increased notably, accompanied by the improvement of salt concentration (**Supplementary Figure S2**). Noteworthily, the content of cordycepin treated with 7% salt was five-fold higher than that of the control group, and the remaining cordycepin content with mg/g dry weight is presented in **Figure 2**.

Transcriptome Overview

To investigate the molecular mechanism of salt treatment that increases the per-volume content of cordycepin in *C. militaris*, a transcriptome analysis based on RNA sequencing of each salt-treated *C. militaris* was performed. Four cDNA samples from *C. militaris* mycelia were processed by the Illumina HiSeq platform, and the transcriptome data obtained by sequencing results were listed in **Table 1**. This resulted in the generation of 40.81, 40.50, 45.22, and 55.58 million clean reads per library, respectively. The GC content for all treatments was ∼57%, and the % ≥Q30 (99.9% accuracy of bases) was >94% for all samples, indicating a good quality of the sequencing data which can be used to do the following analysis. After mapping the sequenced reads to the reference genome, more than 92.5% of the reads in all four samples were mapped. Additionally, a total of 134,436, 155,697, 159,689, and 162,615 single nucleotide polymorphism (SNP) numbers were generated, and most of them were synonymous mutations according to the subsequent annotation.

DEGs Analysis

To identify genes with altered expression levels with salt treatment, the overall transcription levels of genes were quantified by Revenue Passenger Kilometers (RPKM) metrics. According to global transcriptional changes from normalizing the DEG data (**Supplementary Table S2**), a total of 3,885 genes showed altered expression levels in the three salinity treatment groups, as compared to the control. There were 2,917 DEGs in the

TABLE 1 | Summary of the sequencing data of *C. militaris* under different salt concentrations.

Samples	Control	NaCl-3	NaCl-5	NaCl-7
Clean reads	40817724	45502268	45225634	55588246
GC Content	57.51%	57.26%	57.30%	57.57%
Q30	94.47%	95.00%	94.28%	94.74%
Mapping rates	92.52%	92.71%	93.01%	93.79%
SNP number	134436	155697	159689	162615
Genic SNP	102703	112702	115509	116064
Intergenic SNP	31733	42995	44180	46551

Control vs. NaCl-7 group, most of all groups, 1,501 upregulated genes (51%) and 1,416 downregulated genes (49%); followed by 2,413 and 2,371 DEGs in the Control vs. NaCl-5 and Control vs. NaCl-3 groups, separately. In addition, there were no significant differences between NaCl-3 vs. NaCl-5 and NaCl-5 vs. NaCl-7 groups (**Figure 3A**). Venn diagram analysis of DEGs between the control and salt treatment treatments revealed that 1,396 DEGs were commonly shared among the distinct salt treatments, the other commonly shared DEGs between every two groups were 180, 281, and 563, respectively (**Figure 3B**). Moreover, a heatmap was drawn to present the hierarchical clustering of the DEGs among samples (**Supplementary Figure S3**). As shown in the heatmap, the expression profiles between the control and three salt-treated groups were different, illustrating that the effect of different salt concentrations on *C. militaris* is distinct GO functional classification of DEGs.

To analyze the function of DEGs and gene annotation on the control and salt treatment strains, GO classification and functional enrichment were performed. Generally, GO annotation consists of three types: biological process, cellular component, and molecular function. Based on GO annotation, a total of 1,096, 1,060, and 866 DEGs were assigned to the ontologies "biological process", "cellular component", and "molecular function", respectively; for the biological process classification, most of DEGs focused on "metabolic process", "cellular process", and "single-organism process" item, etc. In the part of cellular component, "cell", "membrane", and "membrane part" were the most highly represented categories; while for the molecular function classification, "catalytic activity" was the most enriched GO term, followed by "binding", and "transporter activity", and the detailed distribution of GO terms are illustrated in **Figure 4**.

KEGG Pathway Enrichment of DEGs

To obtain a better insight into the interactions of functional genes by pathway-based analysis, all the genes were mapped to the KEGG database to classify the biological functions of the DEGs. Specific gene enrichment was observed in 79 pathways. Nineteen pathways showed DEG enrichment (**Figure 5**). It was observed that the pathway with the lowest *q* value and the largest number of DEGs was the pathway related to amino sugar and nucleotide sugar metabolism, followed by the pathways related to the synthesis of unsaturated fatty acids,

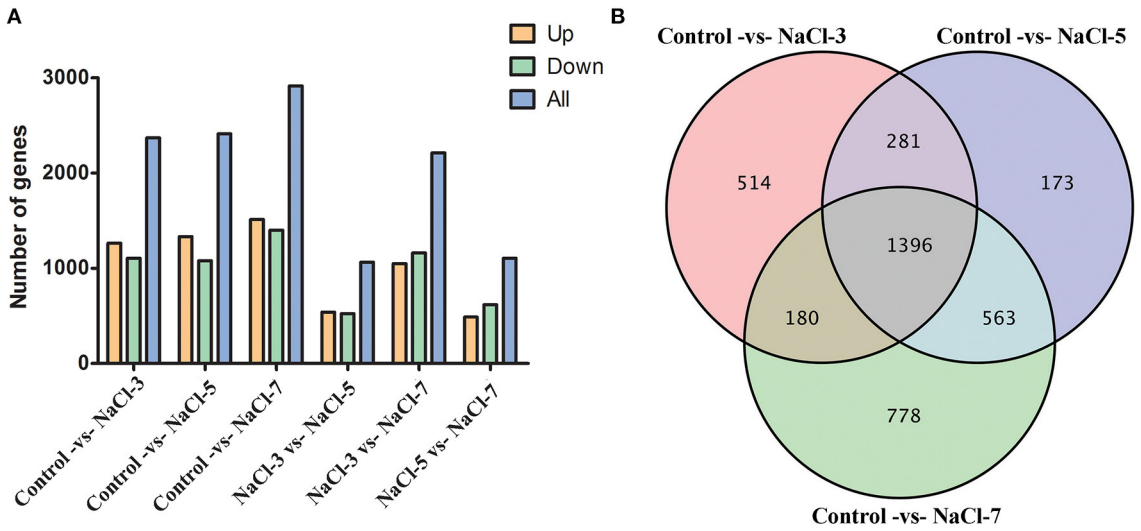

FIGURE 3 | Distribution of differentially expressed genes (DEGs) in the six samples. **(A)** DEGs' distribution between control and three different salt treatments; **(B)** Venn diagram of the commonly expressed genes between samples. NaCl-3, 5, and 7 represent 3, 5, and 7% salt concentrations, respectively.

nitrogen metabolism, and glycerolipid metabolism. Furthermore, there were 9 pathways with a *P*-value <0.05, such as "fatty acid degradation" (**Supplementary Table S3**). "Amino sugar and nucleotide sugar metabolism", "Biosynthesis of unsaturated fatty acids", and "Glycerolipid metabolism" showed an even greater significant enrichment ($P < 0.01$).

Analysis of the Genes Related to Cordycepin Synthesis Pathway

Since the cordycepin content was significantly improved by salt treatment, DEGs related to cordycepin synthesis were carefully identified by KEGG pathway analysis. According to the previously reported and generally accepted cordycepin biosynthesis pathway, this pathway started from adenosine to synthesize cordycepin and PTN (**Figure 6**). Four key genes involved in the cordycepin synthesis pathway, *Cns1*, *Cns2*, *Cns3*, and *Cns4*, were performed qRT-PCR validation. Though the fold changes of these genes in qRT-PCR were slightly different from that of RNA-Seq results, they shared a similar change tendency (**Supplementary Figure S4**). Based on the analysis of the cordycepin synthesis pathway and PCR results, the expression levels of *Cns1* and *Cns2* were decreased with the increase of salt concentration compared with the control, except *Cns1* on NaCl-7 group and *Cns2* on NaCl-3 group. *Cns1* and *Cns2* showed high expression levels on these two groups beyond that of the control. The dynamic changes of *Cns1* and *Cns2* expression levels illustrated that the response of these two genes to distinct salt treatments may differ. On the contrary, the expression level of *Cns3* was upregulated compared to the control, especially in the NaCl-7 group. This result indicated that the pathway of adenosine into 3′AMP might be greatly activated and finally increase the content of cordycepin under the treatment of 7% salt concentration. Additionally, the expression level of *Cns4* was also increased remarkably with the increment of salt concentration, revealing that salt treatment might likely facilitate the out pumping of PTN.

DISCUSSION

Considerable efforts have been put into the improvement of cordycepin production. The previous report showed that cordycepin content could be increased by nutrient stress (distinct carbon, nitrogen, phosphorous sources, and ratios), environmental stress (lighting time, temperature, pH, and shaking speed), and adding supplementation (inorganic salts, porcine liver extracts or vegetable oils, amino acids, or nucleoside analog) (8, 27–29). Though the pathway and related biosynthesis mechanisms of cordycepin have been well documented, the dependency of *C. militaris* activity on different salt concentrations in a medium remains unclear. To obtain more insight on *C. militaris* adaptations to salt stress conditions, precise physiological knowledge is needed. Therefore, a pre-experiment was carried out to evaluate the effect of salinity treatment on cordycepin production in *C. militaris*. In the present study, it was found that distinct salt concentration significantly inhibited the growth of *C. militaris* strains. The colony diameter and biomass of *C. militaris* strains were decreased with the increase of salt concentration (**Figure 1** and **Supplementary Figure S1**). Obviously, *C. militaris* strain encountered osmotic stress due to the high-salt environment, and the salt tolerance of *C. militaris* cells might be essential for the long-term fermentation. High salinity represents a stress-induced high osmotic perturbation to cells since the excess salt disturbs osmotic potential and leads to metabolic toxicity (43). Analogously, clear growth defects under salinity conditions were also observed in *Streptomyces coelicolor*, and major changes occurred in the primary and secondary metabolism (Sugars, polyols, amino acids, nucleotides, and their derivatives) (33).

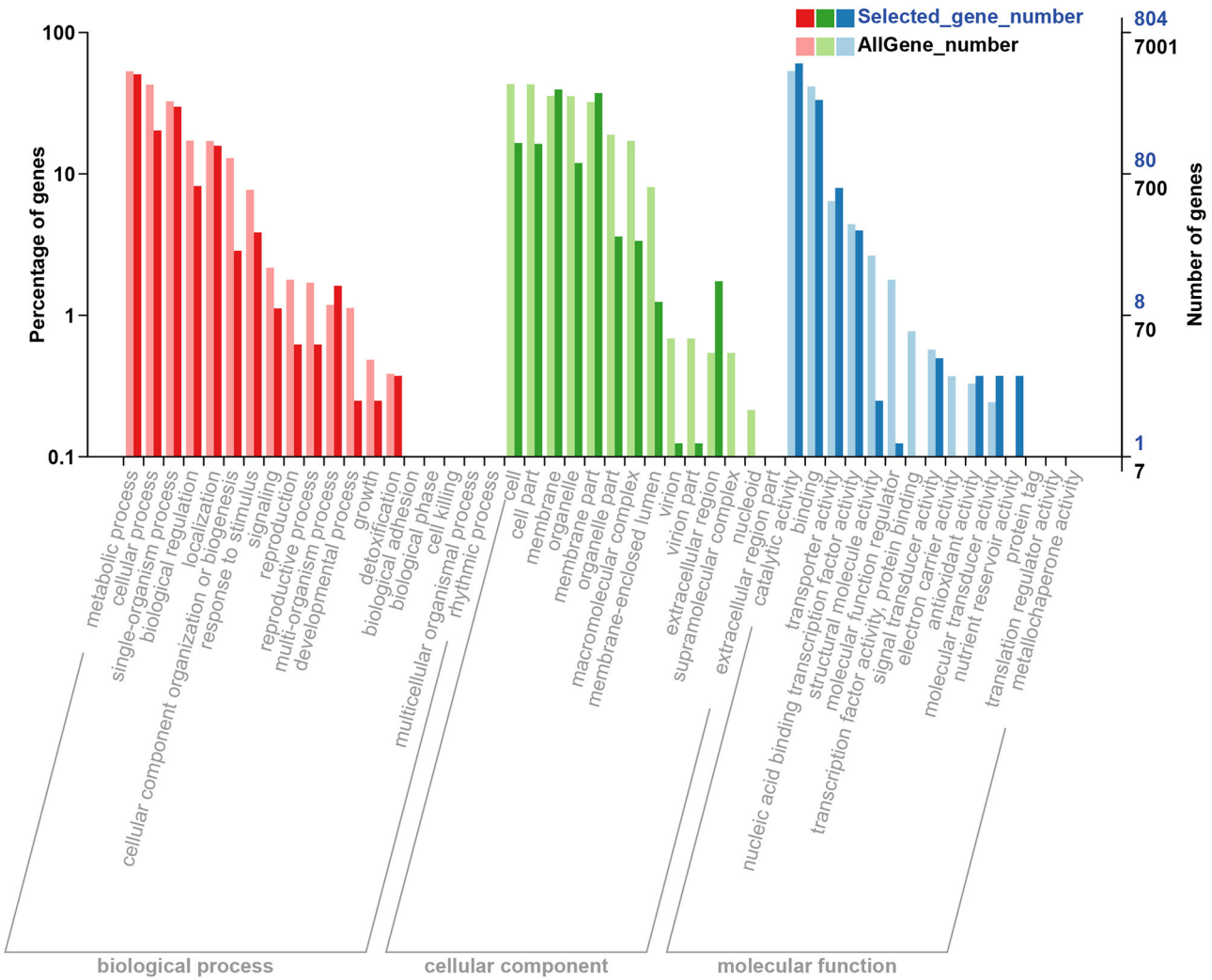

FIGURE 4 | GO classification and enrichment of the DEGs based on the GO database [the *x*-axis represents the GO term and enrichment, and the *y*-axis represents the percentage of genes (left) and the number of DEGs (right)]. Selected_gene_number represents the number of DEGs. GO, gene oncology; DEGs, differentially expressed genes.

The evolutions of varying morphological, physiological, and molecular mechanisms of adaptation are the main strategies of Halophilic fungi in reflection to osmotic stress conditions (44). Exactly, the morphological responses are meristematic growth, pigmentation, and changes in the cell wall and membrane composition (45). Moreover, the physiological responses consist of intracellular potassium and sodium ion content synthesis, accumulation of organic compatible solutes, and extracellular polysaccharide production. As for the molecular responses, it was reflected in the dynamic changes in gene expression related to physiological responses to enhanced salt concentration (44).

Contrary to the inhibited growth of *C. militaris* strain, the accumulation of cordycepin has a positive correlation with salt concentration after culturing in the PDA plates for 5 days (**Figure 2**). The yield of cordycepin on the NaCl-7 group was five-fold higher than that without salt supplementary. It was assumed that a high-salt environment might be optimal for cordycepin accumulation, whereas related molecular responses to an increased extracellular saline condition in *C. militaris* strain have not been identified. To figure out the metabolic pathway from the additive salt to cordycepin, four samples were collected, and transcriptome sequencing was performed based on RPKM metrics. Exposure of *C. militaris* cells to salt treatment results in a substantial transcriptional regulation, and 3,885 genes have altered expressions in three salinity treatment groups relative to the control (**Figure 3**). In the case of the NaCl-7 group, the number of DEGs reached a peak, revealing a greater degree of change in gene expressions in the high salt group than that in the low salt group. In fact, exposure of *C. militaris* cells to the high-salt environment implies threats of specific cation toxicity. So as to adapt to extracellular salinity, there is a transient induction of transcription that activates stress-protective genes (46, 47).

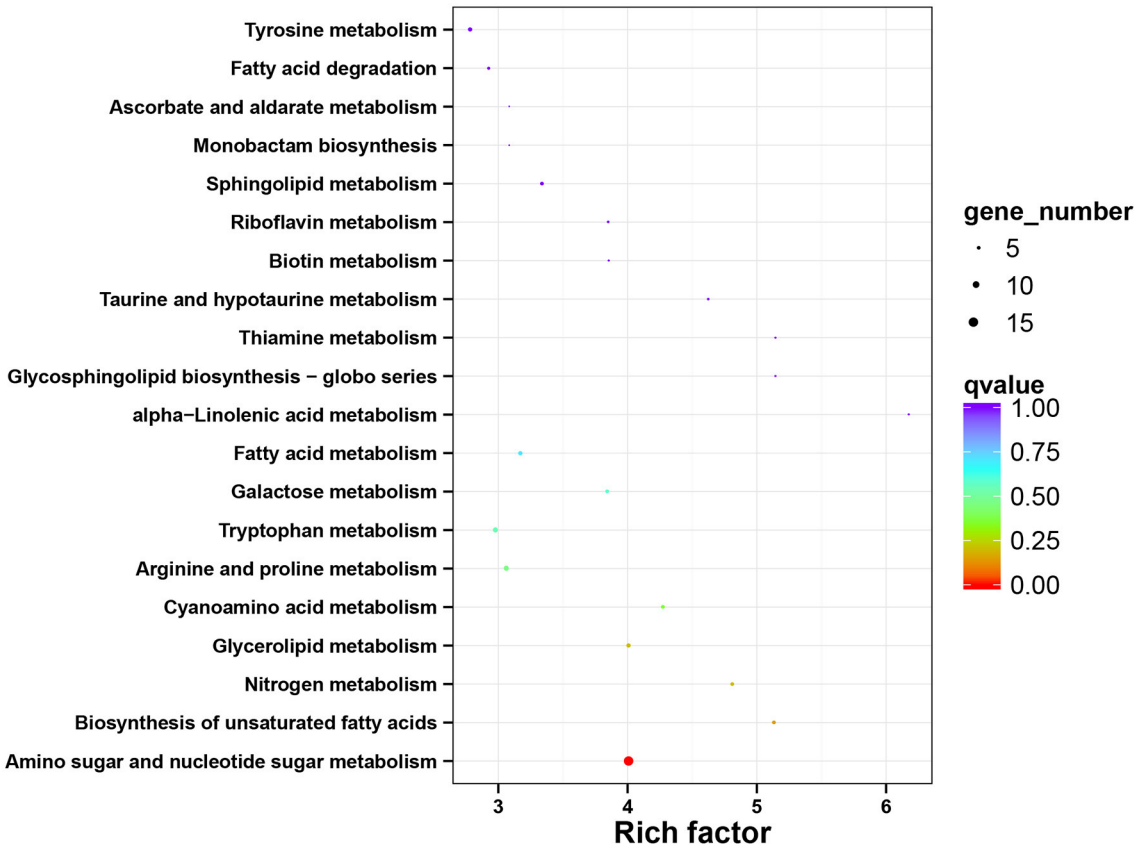

FIGURE 5 | The functional enrichment analysis of DEGs using KEGG annotation. The *x*-axis represents the rich factor, and the y-axis represents the pathway name. DEGs, differentially expressed genes; KEGG, kyoto encyclopedia of genes and genomes.

Furthermore, to analyze and classify the DEGs, the sequencing data were uploaded to the GO and KEGG databases (**Figures 4**, **5**). GO classification results of DEGs showed that the salinity treatment may facilitate the metabolic process to produce more metabolites (cordycepin accumulation) and consequently activate membrane transportation (out-pumping of PTN). The cordycepin metabolism and the purine metabolism pathway have been elucidated in detail by comprehensive transcriptome and proteome analysis of *C. militaris* (21, 48). It was reported that cordycepin production can be increased by adding L-alanine, and a high transcriptional level of several genes encoding enzymes on the pathway of adenosine synthesis was also observed (8). Similarly, the majority of DEGs classified in "metabolic process" and "catalytic activity" items in this study showed different salt treatments may activate adenosine synthesis-related enzymes. And these enzymes catalyze series reactions related to adenosine synthesis and finally lead to the accumulation of cordycepin. Meanwhile, KEGG classification indicated that the most DEGs significantly enriched in the pathway of "Amino sugar and nucleotide sugar metabolism", "Biosynthesis of unsaturated fatty acids", and "Glycerolipid metabolism". It was illustrated that salt treatment affected the specific energy metabolism and membrane composition changes. Most of the DEGs were relevant to the pathway of "Amino sugar and nucleotide sugar metabolism", which revealed that the addition of salt might increase energy molecule production and further promote the cordycepin accumulation. It is generally accepted that cell membranes are one of the first targets to suffer from injurious effects of stress, leading to impaired cell membrane integrity and functions (49, 50). Plenty of studies have documented the modifications of cellular lipid profiles in response to osmotic shock (51, 52). In the present study, there were also a large number of DEGs enriched in the pathway of "Biosynthesis of unsaturated fatty acids" and "Glycerolipid metabolism", which was consistent with the abovementioned Halophilic fungi in reflection to salt treatment condition by changing the membrane composition (morphological responses) (45). Additionally, it was reported that glycerolipid metabolism and high osmotic glycerol (HOG) signaling pathway enable micro-organisms to respond to various extracellular stimuli and also to adjust their cellular machinery to change the environments (53). Two isoenzymes of DL-glycerol-3-phosphatase in the glycerolipid metabolism pathway from *Saccharomyces cerevisiae* facilitate the ability of cells to expose to osmotic stress *via* the HOG pathway (54). Therefore, numbers of DEGs enriched in the pathway of glycerolipid metabolism in *C. militaris* strain indicated

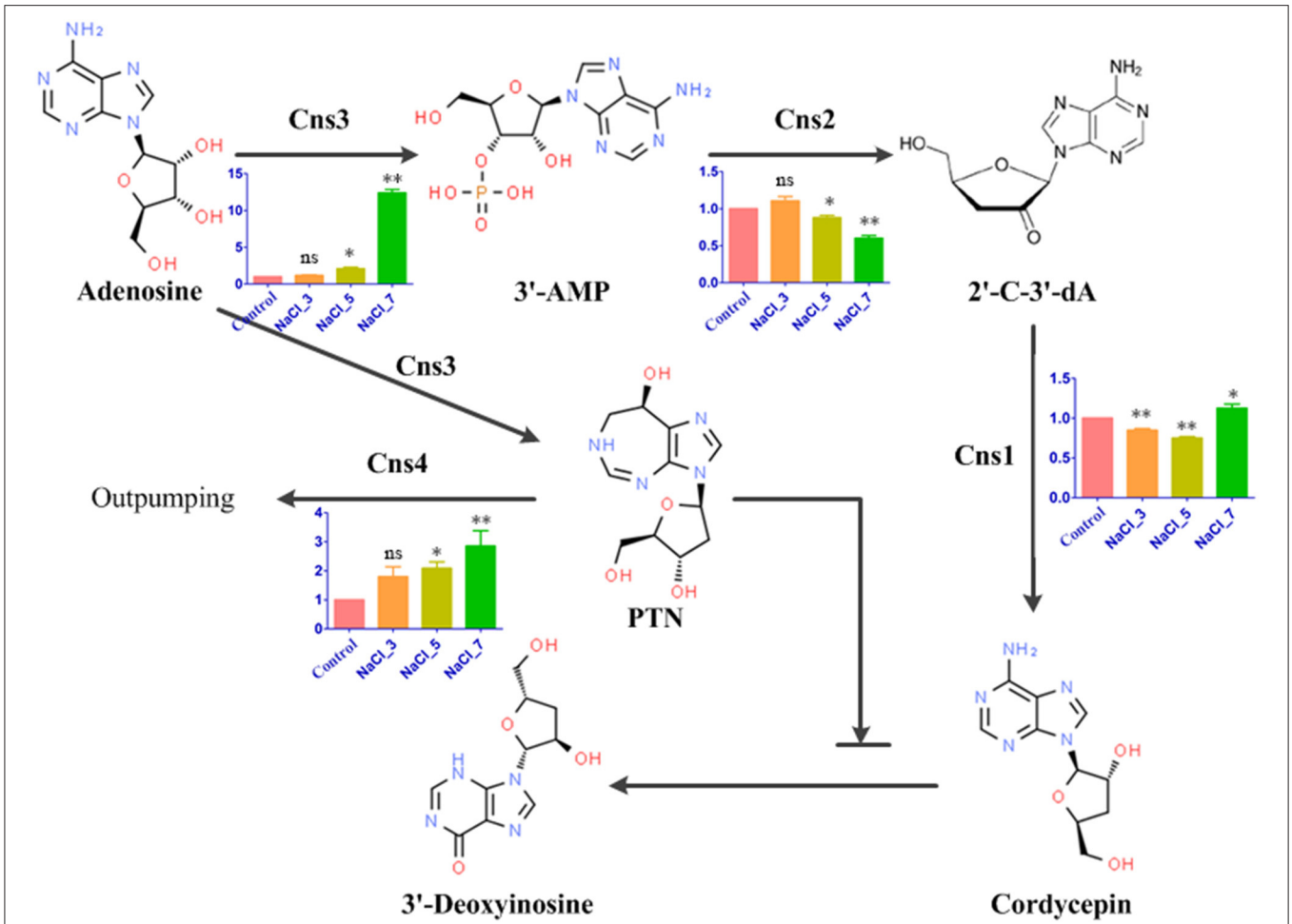

FIGURE 6 | Cordycepin biosynthesis pathway in *C. militaris* and qRT-PCR results. Bar chart with 4 colors represents the relative expression levels of four genes in response to distinct salt treatments. The bars represent the average (±SE) of biological repeats. NaCl-3, 5, and 7 represent 3%, 5%, and 7% salt concentrations, respectively. Asterisks indicate statistically significant differences between groups (Student's *t*-test): * and ** indicating significance level was accepted at $P \leq 0.05$ and $P < 0.01$, respectively, ns: no significant difference, as compared to control.

the addition of salt may achieve the same effect on that of *Saccharomyces cerevisiae*.

In the aforementioned context, cordycepin synthesis was mediated by a biosynthetic gene cluster, which consisted of gene *Cns1*-*Cns4* (21). Additionally, PTN, a purine analog with the activity of anticancer and adenosine deaminase inhibition, was noteworthily produced in coupling with cordycepin by *Cns3* (55). In the present study, dynamic changes of the transcription level of these four vital genes were observed based on the data obtained by transcriptome analysis. To further confirm the reliability and availability of these four DEGs, a real-time RT-PCR experiment was carried out. Overall, these qRT-PCR results showed that the DEGs transcription level was consistent with the result obtained by transcriptome analysis (**Figure 6**). Genes *Cns1*, *Cns3*, and *Cns4* were remarkably upregulated under high salt concentration which showed osmotic stress conditions may have beneficial to accumulating the cordycepin and transporting the PTN to the extracellular environment. *Cns2* was downregulated under distinct salt treatments (except on the Nacl-3 group), implying that the process of 3′AMP dephosphorylated to 2′-C-3′-dA by phosphohydrolase activity of *Cns2* was inhibited by salt treatment, and detailed molecular mechanism still needs further experimental validation. In addition, it has been reported that the yield of cordycepin was increased 2.7-fold by overexpression of the *Cns1*/*Cns2* fusion gene (21). Combined with the results in our study, it is worth trying that overexpression of the *Cns1*/*Cns2* or *Cns1*/*Cns2*/*Cns3* fusion gene *via* individually transformed the control strain of *C. militaris* under salt treatment. Furthermore, it has been reported that several genes can regulate osmoadaptation, such as salt-tolerant gene HOG and fatty acid metabolism gene delta-9 fatty acid desaturases (56, 57). Thus, it can be expected that the obtaining of industrial strains possesses salt tolerance and high cordycepin production *via* overexpression of the cordycepin biosynthetic gene and salt-tolerant gene. Interestingly, a significant upregulation of ribonucleotide reductase (RNR, 70.19-fold), 5′-Nucleotidase (*NT5E*, 63.43-fold), *purA* (Adenylosuccinate synthase, 8.43-fold), and Adenylate kinase (*ADEK*, 17.52-fold) gene expression was

observed upon hypoxanthine treatment, which are downstream genes responsible for cordycepin biosynthesis in *Ophiocordyceps sinensis* (30). Analogous effects have also been achieved on several other potent growth supplements, such as amino acids, plant hormones, and vitamins. These results indicated both salt treatment and the addition of potent growth supplements can activate the cordycepin biosynthesis pathway leading to improved cordycepin content. Moreover, recent research first reported the transcriptome and proteomics of *Cordyceps kyushuensis* Kob, which is close relative to *C. militaris* (58). Similar to *C. militaris,* a single gene cluster containing *ck1-ck4*, which can synthesize both cordycepin and PTN, has been identified in *Cordyceps kyushuensis* Kob using BLAST. Therefore, it is worth exploiting the potential of *Cordyceps kyushuensis* Kob on the increment of cordycepin production in the near future apart from *C. militaris.* With the deep analysis of transcriptome and proteomics, more useful information to do contribution to the cosmetic and pharmaceutical industries can be provided by improving the yield of cordycepin.

CONCLUSIONS

To better unravel the salt response mechanism of *C. militaris* and its effects on cordycepin content, our research performed a transcriptome analysis of *C. militaris* under the distinct salt treatments. The HPLC analysis depicted high salt treatment was beneficial to enhance cordycepin production. Combined with GO analysis and KEGG pathway enrichment, the upregulated transcriptome level of genes responsible for the biosynthetic pathways of energy generation and lipid metabolism might be the major reason for the accumulation of cordycepin. Finally, mRNA expression analysis of four genes involved in the cordycepin biosynthesis pathway was carried out by RT-PCR, and the results showed that the transcription level of these genes was consistent with that of transcriptome analysis. Taken together, our study provides a global transcriptome characterization of the osmotic stress adaptation process in *C. militaris* and paves the way for constructing industrial strains that possess salt tolerance and high cordycepin production.

DATA AVAILABILITY STATEMENT

The datasets presented in this study can be found in online repositories. The names of the repository/repositories and accession number(s) can be found below: https://www.ncbi.nlm.nih.gov/, PRJNA770191.

AUTHOR CONTRIBUTIONS

GL: conceptualization, visualization, and writing-original draft preparation. YZ: conceptualization. XC and YC: project administration. BZ and XL: supervision and funding acquisition. BH: writing review, editing, and funding acquisition. All authors contributed to the article and approved the submitted version.

FUNDING

This research was funded by the Natural Science Foundation of Jiangxi Province (Grant Nos. 20202BABL203043, 20202BAB215003, and 20212BAB215005) and Jiangxi Double Thousand Plan Cultivation Program for Distinguished Talents in Scientific and Technological Innovation (jxsq2019201011).

ACKNOWLEDGMENTS

Thanks to Yayi Tu for the critical review of this manuscript.

SUPPLEMENTARY MATERIAL

The Supplementary Material for this article can be found online at: https://www.frontiersin.org/articles/10.3389/fnut.2021.793795/full#supplementary-material

Figure S1 | Determination of the biomass of the *C. militaris* mycelia under salt treatment. 0, 3, 5, and 7% are equivalent to the control, slight, moderate, and severe salt treatment, respectively.

Figure S2 | HPLC comparison of cordycepin production among the control and three salt treatment groups. 0, 3, 5, and 7% represent the control, slight, moderate, and severe salt-treated groups, respectively.

Figure S3 | Heatmap of the hierarchical clustering of the DEGs. A, B, and C represent Control vs. NaCl-3, -5, and -7, respectively, (the *x*-axis represents each compared sample; the *y*-axis represents the DEGs. The coloring indicates the fold change: high, green; low, red). DEGs, differentially expressed genes.

Figure S4 | A comparison of transcriptional level change of genes (*Cns1-Cns4*) between transcriptome analysis and RT-PCR validation.

Table S1 | qRT-PCR primers used in this study.

Table S2 | The identification of significant DEGs among four treatments (Control vs. NaCl-3, -5, and -7). DEGs, differentially expressed genes.

Table S3 | KEGG pathway enrichment of DEGs. DEGs, differentially expressed genes; KEGG, kyoto encyclopedia of genes and genomes.

REFERENCES

1. Wang L, Zhang WM, Hu B, Chen YQ, Qu LH. Genetic variation of Cordyceps militaris and its allies based on phylogenetic analysis of rDNA ITS sequence data. *Fungal Divers.* (2008) 31:147–55. Available online at: https://www.fungaldiversity.org/fdp/sfdp/31-11.pdf
2. Shrestha B, Tanaka E, Hyun MW, Han J-G, Kim CS, Jo JW, et al. Coleopteran and lepidopteran hosts of the entomopathogenic genus cordyceps sensu lato. *J Mycol.* (2016) 2016:1–14. doi: 10.1155/2016/7648219
3. Das SK, Masuda M, Sakurai A, Sakakibara M. Medicinal uses of the mushroom Cordyceps militaris: current state and prospects. *Fitoterapia.* (2010) 81:961–8. doi: 10.1016/j.fitote.2010.07.010
4. Zhou X, Gong Z, Su Y, Lin J, Tang K. Cordyceps fungi: natural products, pharmacological functions and developmental products. *J Pharm Pharmacol.* (2009) 61:279–91. doi: 10.1211/jpp.61.03.0002
5. Dong JZ, Wang SH, Ai XR, Yao L, Sun ZW, Lei C, et al. Composition and characterization of cordyxanthins from Cordyceps militaris fruit bodies. *J Funct Foods.* (2013) 5:1450–5. doi: 10.1016/j.jff.2013.06.002
6. Cunningham KG, Manson W, Spring FS, Hutchinson SA. Cordycepin. A metabolic product isolated from cultures of cordyceps militaris (Linn) link. *Nature.* (1950) 166:949–949. doi: 10.1038/166949a0
7. Zhang G, Yin Q, Han T, Zhao Y, Su J, Li M, et al. Purification and antioxidant effect of novel fungal polysaccharides from the stroma of Cordyceps kyushuensis. *Ind Crops Prod.* (2015) 69:485–91. doi: 10.1016/j.indcrop.2015.03.006

8. Chen BX, Wei T, Xue LN, Zheng QW, Ye ZW, Zou Y, et al. Transcriptome analysis reveals the flexibility of cordycepin network in cordyceps militaris activated by L-alanine addition. *Front Microbiol.* (2020) 11:577. doi: 10.3389/fmicb.2020.00577
9. Thananusak R, Laoteng K, Raethong N, Zhang Y, Vongsangnak W. Metabolic responses of carotenoid and cordycepin biosynthetic pathways in cordyceps militaris under light-programming exposure through genome-wide transcriptional analysis. *Biology* 9:242. doi: 10.3390/biology9090242
10. Tuli HS, Sandhu SS, Sharma AK. Pharmacological and therapeutic potential of cordyceps with special reference to cordycepin. (2014). 4:1–12. doi: 10.1007/s13205-013-0121-9
11. Holbein S, Wengi A, Decourty L, Freimoser FM, Jacquier A, Dichtl B. Cordycepin interferes with 3' end formation in yeast independently of its potential to terminate RNA chain elongation. *RNA*. (2009) 15:837–49. doi: 10.1261/rna.1458909
12. Noh E-M, Kim J-S, Hur H, Park B-H, Song E-K, Han M-K, et al. Cordycepin inhibits IL-1β-induced MMP-1 and MMP-3 expression in rheumatoid arthritis synovial fibroblasts. *Rheumatology*. (2008) 48:45–8. doi: 10.1093/rheumatology/ken417
13. Pan BS, Lin CY, Huang BM. The effect of cordycepin on steroidogenesis and apoptosis in MA-10 mouse leydig tumor cells. *Evid Based Complement Alternat Med.* (2011) 2011:750468. doi: 10.1155/2011/750468
14. Tian X, Li Y, Shen Y, Li Q, Wang Q, Feng L. Apoptosis and inhibition of proliferation of cancer cells induced by cordycepin (Review). *Oncol Lett*. (2015) 10:595–9. doi: 10.3892/ol.2015.3273
15. Fishman P, Bar-Yehuda S, Liang BT, Jacobson KA. Pharmacological and therapeutic effects of A3 adenosine receptor agonists. *Drug Discov Today*. (2012) 17:359–66. doi: 10.1016/j.drudis.2011.10.007
16. Cho HJ, Cho JY, Rhee MH, Kim HS, Lee HS, Park HJ. Inhibitory effects of cordycepin (3'-deoxyadenosine), a component of Cordyceps militaris, on human platelet aggregation induced by thapsigargin. *J Microbiol Biotechnol.* (2007) 17:1134–8.
17. Zhou X, Cai G, He Y, Tong G. Separation of cordycepin from Cordyceps militaris fermentation supernatant using preparative HPLC and evaluation of its antibacterial activity as an NAD+-dependent DNA ligase inhibitor. *Exp Ther Med.* (2016) 12:1812–6. doi: 10.3892/etm.2016.3536
18. Kaczka EA, Trenner NR, Arison B, Walker RW, Folkers K. Identification of cordycepin, a metabolite of Cordyceps militaris, as 3'-deoxyadenosine. *Biochem Biophys Res Commun.* (1964) 14:456–7. doi: 10.1016/0006-291X(64)90086-5
19. Hanessian S, DeJongh D, McCloskey JA. Further evidence on the structure of cordycepin. *Biochimica et Biophysica Acta (BBA)—General Subjects.* (1966) 117:480–2. doi: 10.1016/0304-4165(66)90101-2
20. Zheng P, Xia Y, Xiao G, Xiong C, Hu X, Zhang S, et al. Genome sequence of the insect pathogenic fungus Cordyceps militaris, a valued traditional chinese medicine. *Genome Biol.* (2011) 12:R116. doi: 10.1186/gb-2011-12-11-r116
21. Xia Y, Luo F, Shang Y, Chen P, Lu Y, Wang C. Fungal cordycepin biosynthesis is coupled with the production of the safeguard molecule pentostatin. *Cell Chem Biol.* (2017) 24:1479–89 e1474. doi: 10.1016/j.chembiol.2017.09.001
22. Tuli HS, Sharma AK, Sandhu SS, Kashyap D. Cordycepin: A bioactive metabolite with therapeutic potential. *Life Sci.* (2013) 93:863–9. doi: 10.1016/j.lfs.2013.09.030
23. Wu P, Wan D, Xu G, Wang G, Ma H, Wang T, et al. An unusual protector-protégé strategy for the biosynthesis of purine nucleoside antibiotics. *Cell Chem Biol.* (2017) 24:171–81. doi: 10.1016/j.chembiol.2016.12.012
24. Kunhorm P, Chaicharoenaudomrung N, Noisa P. Enrichment of cordycepin for cosmeceutical applications: culture systems and strategies. *Appl Microbiol Biotechnol.* (2019) 103:1681–91. doi: 10.1007/s00253-019-09623-3
25. Dong JZ, Lei C, Ai XR, Wang Y. Selenium enrichment on cordyceps militaris link and analysis on its main active components. *Appl Biochem Biotechnol.* (2012) 166:1215–24. doi: 10.1007/s12010-011-9506-6
26. Fan D-d, Wang W, Zhong J-J. Enhancement of cordycepin production in submerged cultures of Cordyceps militaris by addition of ferrous sulfate. *Biochem Eng J.* (2012) 60:30–5. doi: 10.1016/j.bej.2011.09.014
27. Lin L-T, Lai Y-J, Wu S-C, Hsu W-H, Tai C-J. Optimal conditions for cordycepin production in surface liquid-cultured Cordyceps militaris treated with porcine liver extracts for suppression of oral cancer. *J Food Drug Anal.* (2018) 26:135–44. doi: 10.1016/j.jfda.2016.11.021
28. Tang J, Qian Z, Wu H. Enhancing cordycepin production in liquid static cultivation of Cordyceps militaris by adding vegetable oils as the secondary carbon source. *Bioresour Technol.* (2018) 268:60–7. doi: 10.1016/j.biortech.2018.07.128
29. Lee SK, Lee JH, Kim HR, Chun Y, Lee JH, Yoo HY, et al. Improved cordycepin production by cordyceps militaris KYL05 using casein hydrolysate in submerged conditions. *Biomolecules*. (2019) 9:461. doi: 10.3390/biom9090461
30. Kaushik V, Singh A, Arya A, Sindhu SC, Sindhu A, Singh A. Enhanced production of cordycepin in Ophiocordyceps sinensis using growth supplements under submerged conditions. *Biotechnol Rep*. (2020) 28:e00557. doi: 10.1016/j.btre.2020.e00557
31. Cai X, Jin JY, Zhang B, Liu ZQ, Zheng YG. Improvement of cordycepin production by an isolated Paecilomyces hepiali mutant from combinatorial mutation breeding and medium screening. *Bioprocess Biosyst Eng*. (2021) 44:2387–98. doi: 10.1007/s00449-021-02611-w
32. Mishra AK, Singh SS. Protection against salt toxicity in Azolla pinnata-Anabaena azollae symbiotic association by using combined-N sources. *Acta Biol Hung.* (2006) 57:355–65. doi: 10.1556/ABiol.57.2006.3.9
33. Kol S, Merlo ME, Scheltema RA, de Vries M, Vonk RJ, Kikkert NA, et al. Metabolomic characterization of the salt stress response in Streptomyces coelicolor. *Appl Environ Microbiol.* (2010) 76:2574–81. doi: 10.1128/AEM.01992-09
34. He B, Ma L, Hu Z, Li H, Ai M, Long C, et al. Deep sequencing analysis of transcriptomes in Aspergillus oryzae in response to salinity stress. *Appl Microbiol Biotechnol.* (2018) 102:897–906. doi: 10.1007/s00253-017-8603-z
35. He B, Hu Z, Ma L, Li H, Ai M, Han J, et al. Transcriptome analysis of different growth stages of Aspergillus oryzae reveals dynamic changes of distinct classes of genes during growth. *BMC Microbiol.* (2018) 18:12. doi: 10.1186/s12866-018-1158-z
36. Langmead B, Salzberg SL. Fast gapped-read alignment with Bowtie 2. *Nat Methods.* (2012) 9:357–9. doi: 10.1038/nmeth.1923
37. Kim D, Salzberg SL. TopHat-Fusion: an algorithm for discovery of novel fusion transcripts. *Genome Biol.* (2011) 12:R72. doi: 10.1186/gb-2011-12-8-r72
38. Mortazavi A, Williams BA, McCue K, Schaeffer L, Wold B. Mapping and quantifying mammalian transcriptomes by RNA-Seq. *Nat Methods*. (2008) 5:621–8. doi: 10.1038/nmeth.1226
39. Dewey CN, Bo LJBB. RSEM: accurate transcript quantification from RNA-Seq data with or without a reference. *Genome*. (2011) 12:323–3. doi: 10.1186/1471-2105-12-323
40. Love MI, Huber W, Anders S. Moderated estimation of fold change and dispersion for RNA-Seq data with *DESeq*2. *Genome Biol*. (2014) 15:550. doi: 10.1186/s13059-014-0550-8
41. Ashburner M, Ball CA, Blake JA, Botstein D, Butler H, Cherry JM, et al. Gene Ontology: tool for the unification of biology. *Nat Genet.* (2000) 25:25–9. doi: 10.1038/75556
42. Kanehisa M, Araki M, Goto S, Hattori M, Hirakawa M, Itoh M, et al. KEGG for linking genomes to life and the environment. *Nucleic Acids Res.* (2008) 36(Database issue):D480–4. doi: 10.1093/nar/gkm882
43. Taymaz-Nikerel H, Cankorur-Cetinkaya A, Kirdar B. Genome-Wide Transcriptional response of *Saccharomyces cerevisiae* to stress-induced perturbations. *Front Bioeng Biotechnol.* (2016) 4:17. doi: 10.3389/fbioe.2016.00017
44. Musa H, Kasim FH, Nagoor Gunny AA, Gopinath SCB. Salt-adapted moulds and yeasts: Potentials in industrial and environmental biotechnology. *Process Biochem.* (2018) 69:33–44. doi: 10.1016/j.procbio.2018.03.026
45. Zajc J, Zalar P, Plemenitaš A, Gunde-Cimerman N. The mycobiota of the salterns. In: Raghukumar C, editor. Biology *of Marine Fungi*. Berlin, Heidelberg: Springer (2012). p. 133–58. doi: 10.1007/978-3-642-23342-5_7
46. López-Maury L, Marguerat S, Bähler J. Tuning gene expression to changing environments: from rapid responses to evolutionary adaptation. *Nat Rev Genet*. (2008) 9:583–93. doi: 10.1038/nrg2398
47. Martínez-Montañés F, Pascual-Ahuir A, Proft M. Toward a genomic view of the gene expression program regulated by osmostress in yeast. *Omics.* (2010) 14:619–27. doi: 10.1089/omi.2010.0046
48. Yin Y, Yu G, Chen Y, Jiang S, Wang M, Jin Y, et al. Genome-wide transcriptome and proteome analysis on different

developmental stages of Cordyceps militaris. *PLoS ONE.* (2012) 7:e51853. doi: 10.1371/journal.pone.0051853
49. Bajji M, Kinet J-M, Lutts S. The use of the electrolyte leakage method for assessing cell membrane stability as a water stress tolerance test in durum wheat. *Plant Growth Regul.* (2002) 36:61–70. doi: 10.1023/A:1014732714549
50. Izzo V, Bravo-San Pedro JM, Sica V, Kroemer G, Galluzzi L. Mitochondrial Permeability Transition: New Findings and Persisting Uncertainties. *Trends Cell Biol.* (2016) 26:655–67. doi: 10.1016/j.tcb.2016.04.006
51. Mutnuri S, Vasudevan N, Kastner M, Heipieper HJ. Changes in fatty acid composition of Chromohalobacter israelensis with varying salt concentrations. *Curr Microbiol.* (2005) 50:151–4. doi: 10.1007/s00284-004-4396-2
52. Srivastava A, Singh SS, Mishra AK. Modulation in fatty acid composition influences salinity stress tolerance in Frankia strains. *Ann Microbiol.* (2014) 64:1315–23. doi: 10.1007/s13213-013-0775-x
53. Plemenitaš A, Gunde-Cimerman N. Cellular responses in the halophilic black yeast hortaea werneckii to high environmental salinity. In: Gunde-Cimerman N, Oren A, Plemenitaš A, editors. *Adaptation to Life at High Salt Concentrations in Archaea, Bacteria, and Eukarya*. Netherlands:Springer. (2005). p. 453–70. doi: 10.1007/1-4020-3633-7_29
54. Norbeck J, Påhlman A-K, Akhtar N, Blomberg A, Adler L. Purification and Characterization of Two Isoenzymes of DL-Glycerol-3-phosphatase from Saccharomyces cerevisiae: identification of the corresponding GPP1 and GPP2 genes and evidence for osmotic regulation of Gpp2p expression by the osmosensing mitogen-activated protein kinase signal transduction pathway*. *J Biol Chem.* (1996) 271:13875–81. doi: 10.1074/jbc.271.23.13875
55. Kane BJ, Kuhn JG, Roush MK. Pentostatin: an adenosine deaminase inhibitor for the treatment of hairy cell leukemia. *Ann Pharmacother.* (1992) 26:939–47. doi: 10.1177/106002809202600718
56. Li H, Ma L, Hu Z, Tu Y, Jiang C, Wu Q, et al. Heterologous expression of AoD9D enhances salt tolerance with increased accumulation of unsaturated fatty acid in transgenic Saccharomyces cerevisiae. *J Ind Microbiol Biotechnol.* (2019) 46:231–9. doi: 10.1007/s10295-018-02123-9
57. Kuo CY, Chen SA, Hsueh YP. The High Osmolarity Glycerol (HOG) pathway functions in osmosensing, trap morphogenesis and conidiation of the nematode-trapping fungus *Arthrobotrys oligospora*. *J Fungi.* (2020) 6:191. doi: 10.3390/jof6040191
58. Zhao X, Zhang G, Li C, Ling J. Cordycepin and pentostatin biosynthesis gene identified through transcriptome and proteomics analysis of Cordyceps kyushuensis Kob. *Microbiol Res.* (2019) 218:12–21. doi: 10.1016/j.micres.2018.09.005

Conflict of Interest: The authors declare that the research was conducted in the absence of any commercial or financial relationships that could be construed as a potential conflict of interest.

Publisher's Note: All claims expressed in this article are solely those of the authors and do not necessarily represent those of their affiliated organizations, or those of the publisher, the editors and the reviewers. Any product that may be evaluated in this article, or claim that may be made by its manufacturer, is not guaranteed or endorsed by the publisher.

frontiers in Nutrition

ORIGINAL RESEARCH
published: 31 December 2021
doi: 10.3389/fnut.2021.795491

A Two-Stage Adaptive Laboratory Evolution Strategy to Enhance Docosahexaenoic Acid Synthesis in Oleaginous Thraustochytrid

Sen Wang[1,2,3,4,8,9], *Weijian Wan*[1,2,8,9], *Zhuojun Wang*[1,2,5,8,9], *Huidan Zhang*[1,2,3,4,8,9], *Huan Liu*[1,2,3,4,8,9], *K. K. I. U. Arunakumara*[6], *Qiu Cui*[1,2,3,4,5,8,9] *and Xiaojin Song*[1,2,3,4,5,7,8,9]*

[1] Key Laboratory of Biofuels, Qingdao Institute of Bioenergy and Bioprocess Technology, Chinese Academy of Sciences, Qingdao, China, [2] Shandong Provincial Key Laboratory of Energy Genetics, Qingdao Institute of Bioenergy and Bioprocess Technology, Chinese Academy of Sciences, Qingdao, China, [3] Shandong Energy Institute, Qingdao, China, [4] Qingdao New Energy Shandong Laboratory, Qingdao, China, [5] University of Chinese Academy of Sciences, Beijing, China, [6] Department of Crop Science, Faculty of Agriculture, University of Ruhuna, Kamburupitiya, Sri Lanka, [7] Center for Ocean Mega-Science, Chinese Academy of Sciences, Qingdao, China, [8] Shandong Engineering Laboratory of Single Cell Oil, Qingdao Institute of Bioenergy and Bioprocess Technology, Chinese Academy of Sciences, Qingdao, China, [9] Qingdao Engineering Laboratory of Single Cell Oil, Qingdao Institute of Bioenergy and Bioprocess Technology, Chinese Academy of Sciences, Qingdao, China

OPEN ACCESS

Edited by:
Yuanda Song, Shandong University of Technology, China

Reviewed by:
Asha Arumugam Nesamma, International Centre for Genetic Engineering and Biotechnology, India
Xu Zhou, Harbin Institute of Technology, Shenzhen, China

***Correspondence:**
Xiaojin Song
songxj@qibebt.ac.cn

Specialty section:
This article was submitted to Food Chemistry, a section of the journal Frontiers in Nutrition

Received: *15 October 2021*
Accepted: *03 December 2021*
Published: *31 December 2021*

Citation:
Wang S, Wan W, Wang Z, Zhang H, Liu H, Arunakumara KKIU, Cui Q and Song X (2021) A Two-Stage Adaptive Laboratory Evolution Strategy to Enhance Docosahexaenoic Acid Synthesis in Oleaginous Thraustochytrid. Front. Nutr. 8:795491. doi: 10.3389/fnut.2021.795491

Thraustochytrid is a promising algal oil resource with the potential to meet the demand for docosahexaenoic acid (DHA). However, oils with high DHA content produced by genetic modified thraustochytrids are not accepted by the food and pharmaceutical industries in many countries. Therefore, in order to obtain non-transgenic strains with high DHA content, a two-stage adaptive laboratory evolution (ALE) strategy was applied to the thraustochytrid *Aurantiochytrium* sp. Heavy-ion irradiation technique was first used before the ALE to increase the genetic diversity of strains, and then two-step ALE: low temperature based ALE and ACCase inhibitor quizalofop-p-ethyl based ALE were employed in enhancing the DHA production. Using this strategy, the end-point strain E-81 with a DHA content 51% higher than that of the parental strain was obtained. The performance of E-81 strain was further analyzed by component analysis and quantitative real-time PCR. The results showed that the enhanced in lipid content was due to the up-regulated expression of key enzymes in lipid accumulation, while the increase in DHA content was due to the increased transcriptional levels of polyunsaturated fatty acid synthase. This study demonstrated a non-genetic approach to enhance lipid and DHA content in non-model industrial oleaginous strains.

Keywords: adaptive laboratory evolution, thraustochytrid *Aurantiochytrium*, docosahexaenoic acid, heavy-ion irradiation, lipid accumulation

INTRODUCTION

Very long-chain polyunsaturated fatty acids (ω-3) (ω-3 PUFAs), such as eicosapentaenoic acid (EPA, C20:5) and docosahexaenoic acid (DHA, C22:6), are considered as the essential fatty acids in human nutrition and health (1–3). Since human are not able to synthesize EPA and DHA *de novo*, therefore, adequate intakes from external sources are required (4). Currently, deep-sea fish oil is the traditional source of PUFAs, while it is insufficient to meet the global demand for PUFAs (5–7). Thraustochytrid *Aurantiochytrium*, a heterotrophic non-photosynthetic protist, is well-known for its capacity to accumulate DHA (8). Its biomass accumulation could be more than

100 g/L, with the total lipid over 40% of dry cell weight (DCW) and DHA content over 40% of total fatty acids (TFAs) (9–11). Moreover, thraustochytrids can use glucose, glycerol, and molasses, etc., as a carbon source for fermentation, while some species have the xylose utilization capacity (11–13). The broad substrate utilization capacity increases the potential of thraustochytrids as microbial cell factories for lipid biosynthesis. Thus, oil produced from *Aurantiochytrium* appears to be a sustainable resource to fill the gap between the demand and supply of DHA (3, 14). However, its commercial exploitation has been restricted by the substandard productivity and high fermentation costs. Currently, several genetic engineering strategies have been successfully performed to optimize the lipid-accumulating capacity of *Aurantiochytrium* (15–18). However, the use of genetic modified strains is prohibited in food industry in many countries, and consumer acceptance remains a contentious issue (19). Therefore, an adaptive laboratory evolution (ALE) strategy has been developed in order to obtain non-transgenic strains with high DHA content.

Microorganisms are capable of acquiring beneficial phenotypes through random genetic mutations, thus they can rapidly adapt to changing environments. During the ALE process, microorganisms are repeatedly grown under certain stress conditions to induce positive phenotypes. In contrast to genetic modified engineering, ALE enjoys the advantage of regulating many different genes in parallel without the introduction of other genes (20). ALE has been successfully applied in strains improvement, including important model organisms, such as *Saccharomyces cerevisiae* (21), and many microalgae, such as *Crypthecodinium cohnii* (22) and *Dunaliella salina* (23). In recent years, ALE was also applied in thraustochytrids to modify strains. Sun et al. developed a high-oxygen based ALE strategy in thraustochytrid *Schizochytrium* to improve its growth performance (24), a high salinity based ALE method to improve its lipid production (20), and a cooperative two-factor ALE method to enhance both the final biomass and lipid content (25). All these studies demonstrate ALE is a powerful method to enhance the specific properties of thraustochytrids, however, more innovative selective pressures still need to be identified and applied to improve the DHA content.

Although compared with genetic engineering, ALE has some major benefits, it also has some inherent limitations such as the longer running time and the higher operating cost. Mutations are considered as a basis of ALE, and the increase of genotypic diversity can speed up evolution process (21). In a *Escherichia coli* study, a combined ALE with genome shuffling strategy successfully enhanced the desired n-butanol tolerance (26). Similarly, the multiplexed automated genome engineering (MAGE) technology was applied to expedite the design and evolution of organisms with new and improved properties (27). Thus, increasing mutation rate may expedite the evolutionary process. Considering the application area of targeted strains, non-genetic modified methods may be more suitable for the food industry. Heavy-ion irradiation is a novel and powerful mutagenic technique that is capable of inducing a broad range of mutations. Due to the higher linear energy transfer (LET), it possess the ability to break DNA double-strand more effectively than the other mutagenic methods; such as ethyl methane sulfonate (EMS), X-rays or γ-rays (28). Therefore, heavy-ion irradiation was applied before ALE to improve the diversity of starting strains.

Since inhibiting enzyme proteins can perturb or even inhibit metabolism, thus the selective pressure of enzyme inhibitors can also be applied in ALE process to improve the characteristics of organisms. Recently, an ACCase inhibitor based ALE was successfully applied in *C. cohnii* to improve the lipid accumulation (29). However, the enzyme inhibitors usually have a significant negative effect on biomass accumulation. For example, although the tested enzyme inhibitors could improve lipid productivity, they all inhibit the cell growth in *Chlamydomonas reinhardtii* at varying degrees (30). In any case, enhancing lipid biosynthesis by adding the enzyme inhibitors in the ALE process may be a useful strategy.

In this study, a non-genetic modified approach was performed in non-model oleaginous thraustochytrid *Aurantiochytrium* to obtain a mutant with high DHA yield though a two-stage ALE strategy. We first applied heavy-ion irradiation technique to increase the genotypic diversity of strain, and then a two-step ALE was used to enhance the DHA content. Finally, a E-81 strain was got with the DHA production increases by 51% compared with that in starting strain. This study demonstrated a non-genetic approach to efficiently enhance lipid and DHA content in non-model industrial oleaginous strains.

MATERIALS AND METHODS

Strains and Culture

Aurantiochytrium sp. SD116 was isolated from the mangrove and reported in our previous study (8). It was cultured in seed liquid medium containing 30 g/L glucose, 10 g/L yeast extract, and 10 g/L artificial sea salt. The culture was shaken at 200 rpm and grown at 25°C. *Aurantiochytrium* cells were then transferred into fermentation medium containing 60 g/L glucose, 20 g/L yeast extract, and 15 g/L sea salt to determine the lipid profiles.

Heavy-Ion Irradiation Mutagenesis

Aurantiochytrium cells at logarithmic phase were subjected to heavy-ions irradiation mutagenesis. The cells were exposed to an ion beam at the Heavy-Ion Research Facility in Lanzhou, Institute of Modern Physics, Chinese Academy of Sciences where the irradiation was done with different doses (0, 20, 40, 80, 120, 160, and 200 Cy) of carbon ions ($^{12}C^{6+}$). The carbon ion energy was measured as 80 MeV/u, and the average linear energy transfer (LET) value was 31 keV μm^{-1}. After irradiation, the cells were placed on seed medium plates to assess the mortality. Cell

Abbreviations: DHA, docosahexaenoic acid; ALE, adaptive laboratory evolution; PUFA, polyunsaturated fatty acids; EPA, eicosapentaenoic acid; DCW, dry cell weight; TFAs, total fatty acids; qRT-PCR, quantitative real-time PCR; LET, linear energy transfer; EMS, ethyl methane sulfonate; ACCase, acetyl-CoA carboxylase; CS, citrate synthase; ICDH, isocitrate dehydrogenase; ME, malic enzyme; PKS, polyketide synthase; UDPGP, UDP-glucose pyrophosphorylase.

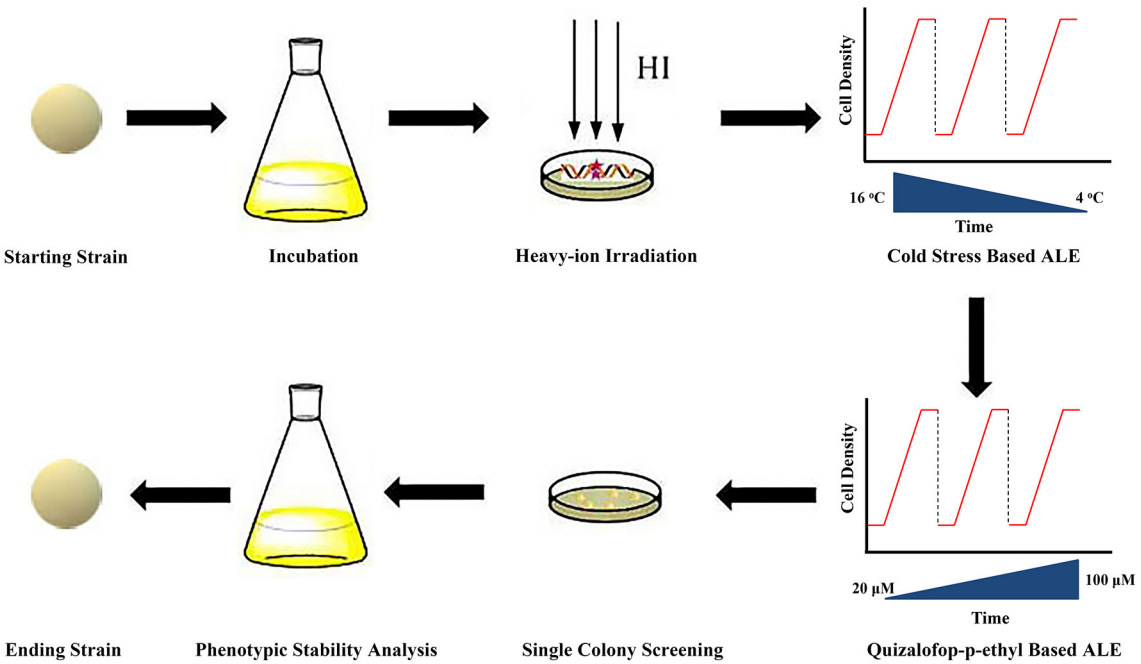

FIGURE 1 | Overview of the modified ALE strategy. HI, heavy-ion irradiation; CS, cold stress; QE, quizalofop-p-ethyl.

survival rate = colony counts of irradiated cells/colony counts of irradiated cells with 0 Gy × 100%. And cell mortality = 100% – cell survival rate.

Adaptive Laboratory Evolution (ALE)

Cells were inoculated into the seed medium where the ALE process commenced. Then the temperature of the medium was gradually decreased from 16 to 4°C with 4°C per change (**Figure 1**). When the cells entered into stationary phase (biomass was almost no changed after 12 h), an aliquot of 2% (v/v) culture was re-inoculated into a fresh medium. During the evolution process, the growth rate of the cells was found to be increased. When the growth rate reached the maximum, the temperature of the medium was gradually decreased. This experimental evolution proceeded for ∼20 cycles for ∼100 days, and the endpoint strains were named as E-C strains.

Before the second-round ALE, the cell mortality was firstly assessed with different concentrations (0, 5, 10, 15, 20, 25, and 30 μM) of quizalofop-p-ethyl in the agar plates containing seed medium. Cell survival rate = colony counts with different doses of quizalofop-p-ethyl/colony counts with 0 μM quizalofop-p-ethyl × 100%. And cell mortality = 100% – cell survival rate. Then the ACCase inhibitor quizalofop-p-ethyl was used for the second-round ALE. The concentration of quizalofop-p-ethyl was gradually increased from 20 to 100 μM with 20 μM per change. After the growth rate reached the maximum at 100 μM quizalofop-p-ethyl, the evolution proceeded for 10 cycles for ∼60 days. Then the endpoint strains were plated on seed medium plates to select the single colonies.

Quantitative Real-Time PCR (qRT-PCR) Analysis

Briefly, cells of *Aurantiochytrium* were harvested and immersed in RNAlock Reagent (TIANGEN, China), and stored at −80°C until use. Total RNA was isolated using TRIzol reagent (Invitrogen, USA) according to the manufacturer's instructions. RNA purity was checked using a Nano-300 spectrophotometer (Aosheng, China), and RNA degradation and contamination was monitored on 1% agarose gels. Synthesis of cDNA was carried out with a Revert Aid First strand cDNA Synthesis Kit (Thermo Scientific), and cDNA was used as the template for qRT-PCR analysis with the primers listed in **Supplementary Table 1**. Actin was used as an internal control to normalize the expression levels. Then, the relative abundance of different mRNA molecules was calculated based on the previous method (29).

Biomass, Glucose Consumption, Lipid, Fatty Acid Composition Analysis, and Component Analysis

Biomass was expressed as dry cell weight (DCW). Five milliliters samples were harvested and freeze-dried to constant weight at −50°C. The glucose concentration was analyzed with a SBA-40E Biosensor (Institute of Biology, Shandong Academy of Sciences, China).

Total lipid was extracted using a combination solvent of chloroform and methanol (2:1, v/v). The extracted lipids were transferred to a pre-weighed glass tube and vacuum evaporated under 50°C, then the total lipid was weighed. To obtain the fatty acid methyl esters (FAMEs), the total lipid was dissolved in 1 mL of chloroform and incubated with 2% (v/v) sulfuric

acid/methanol at 85°C for 2.5 h. FAMEs were determined by gas chromatography (Agilent Technologies, 7890B) (31).

Kjeldahl nitrogen determination method was employed in determining the protein content (32). Lyophilized samples were hydrolyzed with 6 M hydrochloric acid for 20 h, and then amino acids were measured by the amino acid analyzer (A300; membraPure, Germany).

The carbohydrate content was assayed following the Phenol-Sulfuric acid method. Lyophilized samples were ground using a mortar and then hydrolyzed in boiling water with 6 M hydrochloric acid for 0.5 h. After cooling, 10% (w/w) NaOH was used to regulate pH = 7.0. Hydrolysate was then taken for carbohydrate content determination by the Phenol-Sulfuric acid method (33).

Fed-Batch Fermentation

The fed-batch fermentation experiment was performed in a 5 L Biostat® B plus bioreactor as described previously (34). The cultures were grown in 2.5 L of initial fed-batch fermentation medium at 25°C. The aeration and stirring speed are fixed at 2 VVM and 800 rpm, respectively. The glucose concentration was estimated with the SBA-40E Biosensor and maintained at about 20 g/L by continuously feeding of a supplement with a glucose concentration of 800 g/L. Moreover, 100 mL of yeast extract solution with a concentration of 150 g/L was added every 24 h, until 72 h of fermentation. The pH was maintained at 6.5 by adding 2 M NaOH. The initial fed-batch fermentation medium contained 100 g/L glucose, 10 g/L yeast extract, 5 g/L tryptone, 5 g/L KH_2PO_4, 1 g/L $MgSO_4$, and 15 g/L artificial seawater. One milliliter of antifoam, THI®X-298 (Thinking Finechem, Yantai, China), was added at the beginning to control foam formation. Samples (50 mL) for off-line determination of biomass, glucose, lipid, and fatty acid profiles were drawn at 12 h intervals until the end of the fermentation.

Calculation and Statistical Analysis

All data are the means of three replicates and reported as the mean ± SE. The statistical analysis was carried out by Excel, and the significance of differences ($p < 0.05$ and $p < 0.01$) was assessed using a *t*-test.

RESULTS AND DISCUSSION

Enhancement of Diversity of Starting Strains via Heavy-Ion Irradiation

Mutations are the basis underlying ALE, thus increased mutation rate could expedite the evolutionary process (27). Heavy-ion irradiation is a powerful mutagenic technique that is capable of inducing a broad range of mutations. In the present study, heavy-ion irradiation was applied before ALE to increase the genetic diversity of starting strains. A higher mutation rate can be effective to a certain extent only, because it may also lead a genetic burden. Therefore, the effect of the dosage of irradiation on cell mortality was first investigated. When *Aurantiochytrium* cells were exposed to seven heavy-ion irradiation doses (0, 20, 40, 80, 120, 160, and 200 Gy), a dose-dependent mortality was observed (**Supplementary Figure 1**). The mortality rate was found to be increased approximately from 50 to 80%, respectively, for 120 and 160 Gy, which were regarded as the best range for mutation breeding. Therefore, mutants from 120 and 160 Gy irradiation treatments were selected for ALE experiment.

High DHA Production Strain E-81 Obtained From ALE

It is known that PUFAs play an important role in resisting stresses such as low temperature by increasing the fluidity of microbial cell membranes (35, 36). According to previous reports (37, 38), low temperatures can promote the biosynthesis of PUFAs in thraustochytrids while decrease their growth rate. Therefore, the first-round ALE aiming at enhancing the DHA content was conducted under cold stress conditions. Mutant cells generated through the irradiation treatments (120 and 160 Gy) were used as the starting strains, which were subjected to the ALE. The temperature was decreased from 16 to 4°C during the entire ALE process (**Figure 1**). Finally, the strains with the maximum growth rate at 4°C were named as E-C strains. The content of DHA in E-C strains was found to be increased by 15% compared to that of SD116, which is 48% of its total fatty acids (TFA) (**Supplementary Figure 2**). However, in terms of the total lipid content, both E-C and SD116 strains were found to be almost alike (**Supplementary Figure 2**).

Acetyl-CoA carboxylase (ACCase) is capable of catalyzing the first bottleneck step in fatty acid biosynthesis. As reported

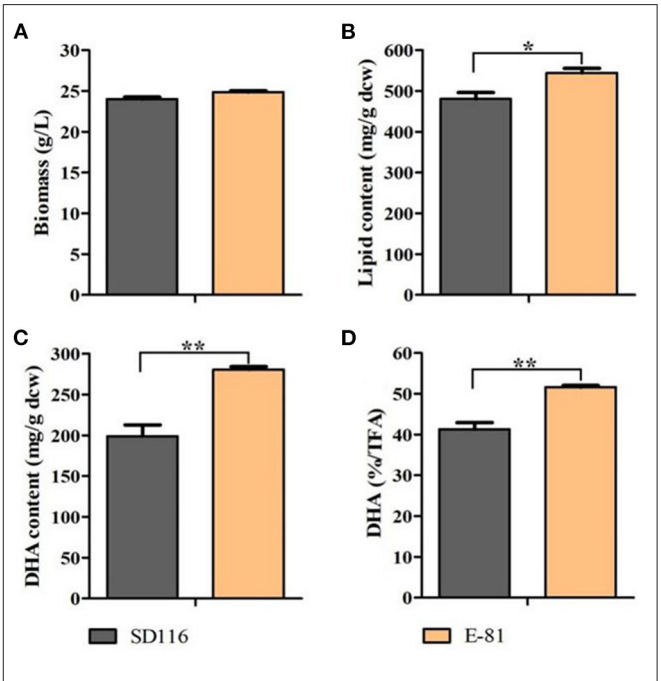

FIGURE 2 | Analysis of the biomass and lipid profiles in SD116 and E-81. **(A)** Biomass, **(B)** lipid content, **(C)** DHA content, and **(D)** DHA purity in total fatty acids (TFA). $^{**}P < 0.01$ and $^{*}P < 0.05$.

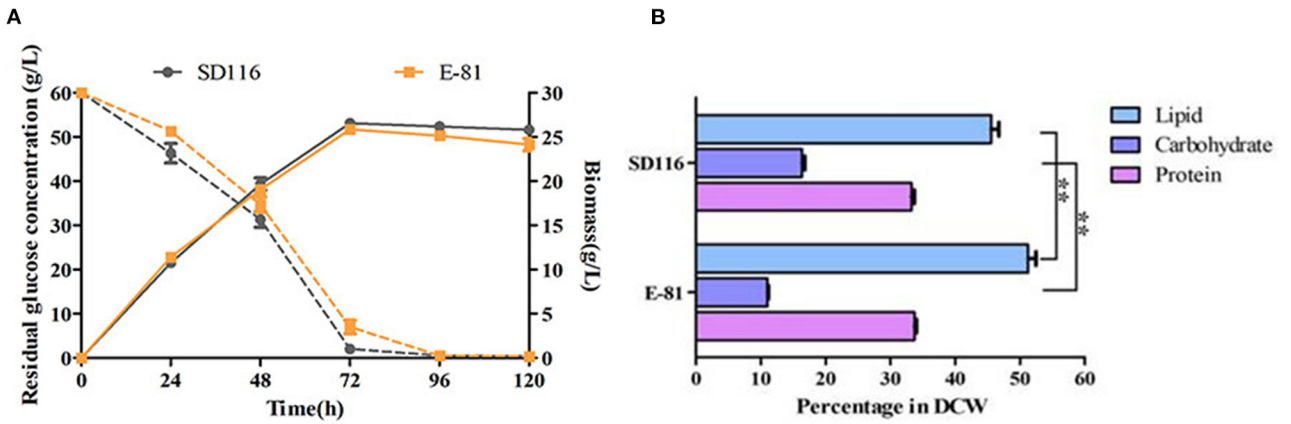

FIGURE 3 | Characterization of cell growth **(A)** and biomass composition **(B)** in strains SD116 and E-81. $^{**}P < 0.01$.

in previous studies, the lipid production in oleaginous microorganisms could be increased by the enhanced activity of ACCase (15, 39). Quizalofop-p-ethyl is an ACCase inhibitor that usually used to enhance lipid accumulation in organisms. Chaturvedi screened *Nannochloropsis oculata* mutants with quizalofop-p-ethyl and found that the ACCase activity of herbicide-resistance microalgae had increased ∼2-fold (40). Another study reported that the lipid content of mutagenized microalgae was 59% higher than wild type, indicating that screening mutants with the herbicide quizalofop-p-ethyl could lead to enhance lipid accumulation (41). Therefore, quizalofop-p-ethyl was selected in the second-round of ALE. As shown in **Supplementary Figure 3**, the cell mortality rate at 30 μM quizalofop-p-ethyl was almost 100%. Therefore, 20 μM quizalofop-p-ethyl was used as the started concentration for ALE process. Unlike the result of cell mortality rate, cells could grow in the lipid medium with 30 μM quizalofop-p-ethyl. The concentration of quizalofop-p-ethyl was thus increased gradually from 20 to 100 μM during the process. Similar to the cold stress-based ALE, the cell growth rate reached the maximum at 100 μM quizalofop-p-ethyl, and then the streak plate method was performed to select the single colonies.

96 single colonies were taken and then cultured in fermentation medium for 96 h. Lipid profiles of these strains were screened (**Supplementary Figure 4**) to select the strain with the highest DHA yield and purity. As shown in **Figure 2**, the biomass yield of E-81 was equivalent to that of SD116. And the total lipid content had reached 544 mg/g DCW, which was 13% higher than SD116 (**Figure 2B**). In addition, the DHA yield and purity in E-81 strain were increased by 41 and 25%, respectively, compared to those of SD116 (**Figures 2C,D**).

All inclusive, a modified ALE strategy was designed for *Aurantiochytrium* sp. SD116 to enhance the DHA purity and yield (**Figure 1**): (1) heavy-ion irradiation strategy was used to increase the diversity of starting strains; (2) cold stress based ALE and quizalofop-p-ethyl based ALE were performed to improve the PUFA content and total lipid production, respectively; and finally, (3) the phenotypic stable ending strain with high DHA yield and purity was obtained by continuously passaging.

Changes of Metabolic Network in Strain E-81

As shown in **Figure 3A**, both the cell growth and glucose consumption rates of E-81 were similar to those of SD116, implying that the biomass productivity in E-81 was almost comparable to that of SD116. Taking the lipid content of E-81, which showed a significant increase (∼55% of DCW) into account, we hypothesized that E-81 has the potential to convert more carbon to lipid by rewiring the intracellular metabolism. As shown in **Figure 3B**, the protein contents of SD116 and E-81 were indistinguishable, though, a noticeable decrease in total carbohydrate content was observed in E-81 compared to that of in SD116 (∼5% of DCW). These results implied that E-81 strain could redirect the carbon allocation from carbohydrate to lipid. To verify this hypothesis, the transcriptional levels of key enzymes in lipid accumulation were analyzed.

The growth cycle of *Aurantiochytrium* sp. is characterized by two distinct physiological stages, namely the growth phase and the oleaginous phase. Therefore, the transcription profiles at 48 and 72 h which represented these two phases, respectively, were monitored. During the growth phase, the oleaginous microorganisms convert the carbon source into cell mass, which is rich in proteins, but poor in quantities of lipids (42). As shown in **Figure 4**, the transcription levels of the genes responsible for fatty acid biosynthesis which include *FAS*, *OrfA*, *OrfB*, and *OrfC* (43) were not significantly varied between E-81 and SD116 in the growth phase, though the transcription levels of citrate synthase (*CS*), isocitrate dehydrogenase (*ICDH*), and malic enzyme (*ME*) were significantly increased in E-81 strain than the other. *CS* and *ICDH* are the key enzymes in TCA cycle, whereas ME is the key enzyme in pyruvate malate shuttle.

Both of these pathways are known to generate biosynthetic precursors which are involved in the production of energy or reducing power that are essential for the biosynthesis of various macromolecules. Therefore, the increased transcription levels of *CS*, *ICDH,* and *ME* in E-81 strain may provide more biosynthetic precursors.

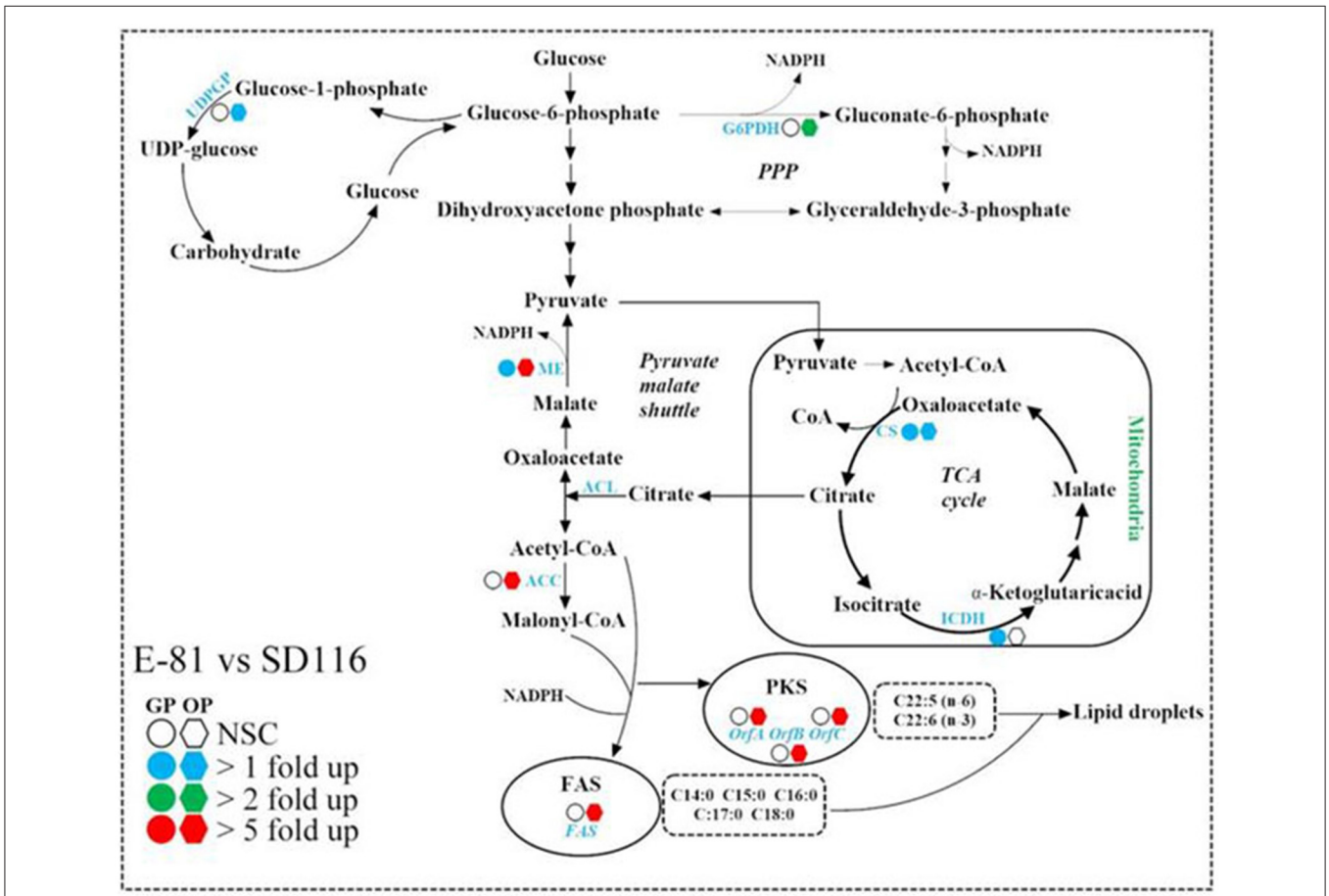

FIGURE 4 | Comparison of the transcription levels of key enzymes in fatty acid synthesis pathways of SD116 and E-81 strain. G6PDH, glucose-6-phosphate dehydrogenase; ME, malic enzyme; CS, citrate synthase; ICDH, isocitrate dehydrogenase; ACL, ATP citrate lyase; ACC, acetyl-CoA carboxylase; FAS, fatty acid synthase; PKS, polyketide-like polyunsaturated fatty acid synthase; OrfA, PKS subunit A; OrfB, PKS subunit B; OrfC, PKS subunit C; UDPGP, UDP-glucose pyrophosphorylase; NSC, no significant change; GP, growth phase; OP, oleaginous phase.

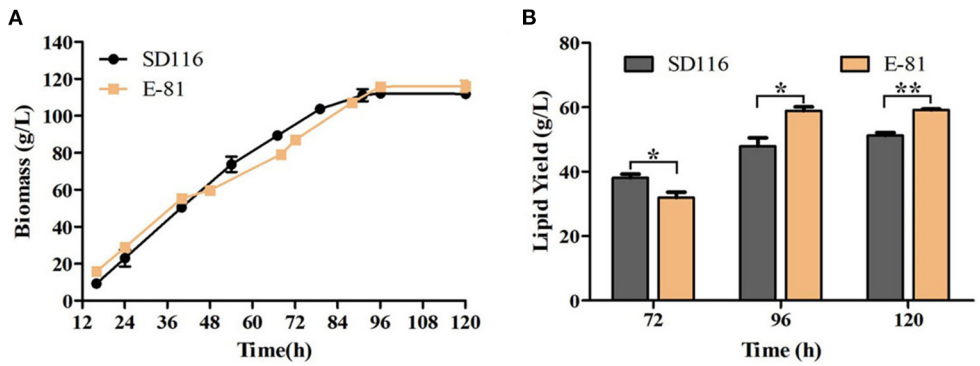

FIGURE 5 | Fed-batch fermentation of SD116 and E-81 strains. **(A)** Growth curve; **(B)** total lipid yield. $^{**}P < 0.01$ and $^{*}P < 0.05$.

Growth phase is followed by the lipid accumulation in the oleaginous phase. ICDH inhibition is critical at the beginning of lipogenesis, because the disturbance of the TCA cycle could induce an intra-mitochondrial accumulation of citric acid which is then excreted to the cytoplasm in exchange with malate (42). At the oleaginous phase of the present study, the transcription levels of *CS* and *ME* were up-regulated while no changes of the transcription level of *ICDH* was observed in E-81 strain, suggesting that more acetyl-CoA could be synthesized in E-81 strain than SD116. The accumulated pool of acetyl-CoA along with reducing power could increase lipid and DHA productivities (44). In the oleaginous phase, the transcription level of *ACC* in E-81 strain increases more than 5-fold compared with that in SD116, indicating ACCase inhibitor based ALE is an effective approach to increase ACCase expression, and more carbon resources can be used for lipid biosynthesis. There are two competing fatty acid synthesis pathways in *Aurantiochytrium* [(17); **Figure 4**]. Fatty acid synthase (FAS) pathway is mainly responsible for synthesis of saturated fatty acids (SFA), and polyketide synthase-like fatty acid (PKS) pathway which contains three genes namely, *OrfA*, *OrfB*, and *OrfC* encoding for PKS proteins synthesizes PUFA. The ratio of the transcription levels of PKS and FAS is closely related to the fatty acid composition. Compared with SD116, all the genes involved in lipid synthesis, including fatty acid biosynthesis genes *FAS*, *OrfA*, *OrfB*, and *OrfC*, and NADPH biosynthesis genes *ME* and *G6PDH*, were significantly up-regulated in strain E-81. This may be attributed to the increased total lipid production in strain E-81. Furthermore, the ratio of the transcription levels of PKS and FAS were more evidently up-regulated in E-81 strain than in SD116 at the oleaginous phase (**Supplementary Figure 5**), which explained the reason for higher PUFA content in E-81 strain.

Previous studies have showed that some microalgae could increase lipid productivity by inhibiting the biosynthesis of protein or starch (29, 45, 46). Taking the complexity of carbohydrate component into account, only the transcription level of UDP-glucose pyrophosphorylase (*UDPGP*), which could produce UDP-glucose as a substrate to synthesize carbohydrate, was detected here (**Figure 4**). As shown in **Figure 4**, the transcription level of *UDPGP* in E-81 strain was up-regulated at 72 h, although no significant difference between the two strains was found at 48 h. However, it was found that the carbohydrate content in E-81 strain was decreased, which was inconsistent with the increase in the transcription level of *UDPGP*. In previous report showed the relative transcription ratios of PKS and FAS genes affect the fatty acid component, and both the enhanced transcripts of PKS and the decreased transcripts of FAS can improve the DHA content (31, 47). Here, the transcription level ratio of *ACC* and *UDPGP* were significantly increased, which may direct more carbon resource into lipid biosynthesis (37). Therefore, it was believed that although the transcription level of *UDPGP* increases, E-81 reduces the carbohydrate synthesis efficiency through other overall regulation. Based on all of these results, it is obvious that the enhancement of fatty acid synthesis pathway could be the main reason attributed to the increased lipid production in strain E-81.

TABLE 1 | The analysis of lipid and fatty acid composition in SD116 and E-81 at the end-point of fed-batch fermentation (5th day).

Fatty acids	SD116	E-81	*P*-value
C14:0 (% TFAs*)	2.90 ± 0.03	1.60 ± 0.60	0.036
C16:0 (% TFAs)	41.2 ± 0.46	33.9 ± 2.00	0.004
C18:0 (% TFAs)	3.01 ± 0.01	1.15 ± 0.32	0.001
ARA (% TFAs)	1.55 ± 0.01	1.17 ± 0.12	0.044
EPA (% TFAs)	1.10 ± 0.01	0.81 ± 0.09	0.030
DPA (% TFAs)	9.80 ± 0.08	8.48 ± 1.50	0.203
DHA (% TFAs)	39.2 ± 0.38	52.6 ± 2.50	0.001
Palmitic acid yield (g/L)	21.0 ± 0.6	20.0 ± 0.8	0.268
DPA yield (g/L)	5.00 ± 0.1	5.00 ± 0.6	0.847
DHA yield (g/L)	20.0 ± 0.5	31.0 ± 1.4	0.001
Total PUFAs yield (g/L)	27.0 ± 0.6	37.0 ± 1.3	0.001
Total SFA yield (g/L)	37.0 ± 0.6	37.0 ± 0.6	0.671
Total lipid yield (g/L)	51.0 ± 1.3	59.0 ± 0.4	0.001

**TFAs, total fatty acids.*

Fed-Batch Fermentation

The fermentation performance of E-81 strain in DHA production was further investigated through a fed-batch fermentation experiment conducted with a 5 L fermentor. The final biomass of E-81 strain was 117 g/L, and no significant difference of biomass was observed between the E-81 and SD116 strains (**Figure 5A**). Moreover, the final glucose consumption concentration of the two strains is almost the same (315 vs. 306 g/L). However, the fatty acid composition and lipid yield had significantly changed. As shown in **Figure 5B** and **Table 1**, the DHA content was reached 52.5% of TFA, which has an increase of 33.9% compared with the original strain SD116. The lipid yields of SD116 and E-81 strain were 51.0 and 59.0 g/L, respectively, after 5 day fermentation. The total DHA yield in E-81 strain was 31.0 g/L and found a 55% increase than that of SD116 (31.0 vs. 20.0 g/L), while no significant variations in the total SFA and DPA yield were recorded.

Thraustochytrids including *Aurantiochytrium*, could use a variety of substrates as carbon sources. Generally, when glucose is used as the carbon source, the DHA content of thraustochytrids is higher, while higher lipid content can be obtained when glycerol and acetic acid are used as the carbon source, which the DHA content is slightly lower (48–50). Therefore, comprehensive considerations such as substrate cost, sustainable availability, etc. need to be considered when selecting the carbon sources. At present, fed-batch fermentation is the main method for algal based DHA production. Researchers try to improve the efficiency of the fermentation process by optimizing various parameters such as pH (49), osmotic pressure (51), and aeration methods (9). Currently, computer simulation and computer-aided have also been used to improve the fermentation process (52). Through the computer-aided design, improvements to the industrial processes could be determined without performing excessive experiments.

CONCLUSIONS

In order to obtain non-transgenic strains with high DHA content, heavy-ion irradiation was first used to increase the genetic diversity of the original strains, and then two-step ALE: low temperature based ALE and quizalofop-p-ethyl based ALE were performed to enhance the DHA and lipid accumulation. Using this strategy, the DHA content of the end-point strain E-81 was 51% higher than that of the parent strain. This study demonstrated a non-genetic approach to enhance lipid and DHA content in non-model industrial oleaginous strains.

DATA AVAILABILITY STATEMENT

The original contributions presented in the study are included in the article/**Supplementary Material**, further inquiries can be directed to the corresponding author/s.

AUTHOR CONTRIBUTIONS

QC and XS conceived the study. SW and WW were responsible for the ALE. HZ, HL, and ZW carried out the test of fatty acids. WW and XS carried out the fermentation experiments. KA and XS performed data analysis. SW, KA, and XS wrote the paper. All the authors reviewed and approved the final manuscript.

FUNDING

This work was supported by the National Key Research and Development Program (2019YFD0901904), National Natural Science Foundation of China (Nos. 42006114, 42106108, and 32001053), the Shandong Province Natural Science Foundation (ZR2020QD099), the Key Deployment Project of Centre for Ocean Mega-Research of Science, Chinese Academy of Sciences (COMS2019J07), Qingdao independent innovation major project (Grant No. 21-1-2-23-hz), and supported by QIBEBT (Grant: QIBEBT I201933). This study was also supported by Dalian National Laboratory for Clean Energy (DNL), CAS.

ACKNOWLEDGMENTS

We would like to thank the colleagues at HIRFL for providing high-quality carbon ion beam irradiation.

SUPPLEMENTARY MATERIAL

The Supplementary Material for this article can be found online at: https://www.frontiersin.org/articles/10.3389/fnut.2021.795491/full#supplementary-material

REFERENCES

1. Swanson D, Block R, Mousa SA. Omega-3 fatty acids EPA and DHA: health benefits throughout life. *Adv Nutr*. (2012) 3:1–7. doi: 10.3945/an.111.000893
2. Watanabe Y, Tatsuno I. Omega-3 polyunsaturated fatty acids focusing on eicosapentaenoic acid and docosahexaenoic acid in the prevention of cardiovascular diseases: a review of the state-of-the-art. *Expert Rev Clin Pharmacol*. (2021) 14:79–93. doi: 10.1080/17512433.2021.1863784
3. Du F, Wang YZ, Xu YS, Shi TQ, Liu WZ, Sun XM, et al. Biotechnological production of lipid and terpenoid from thraustochytrids. *Biotechnol Adv*. (2021) 48:107725. doi: 10.1016/j.biotechadv.2021.107725
4. Xin Y, Lu Y, Lee YY, Wei L, Jia J, Wang Q, et al. Producing designer oils in industrial microalgae by rational modulation of co-evolving type-2 diacylglycerol acyltransferases. *Mol Plant*. (2017) 10:1523–39. doi: 10.1016/j.molp.2017.10.011
5. Salem N Jr., Eggersdorfer M. Is the world supply of omega-3 fatty acids adequate for optimal human nutrition? *Curr Opin Clin Nutr Metab Care*. (2015) 18:147–54. doi: 10.1097/MCO.0000000000000145
6. Tocher DR, Betancor MB, Sprague M, Olsen RE, Napier JA. Omega-3 long-chain polyunsaturated fatty acids, EPA and DHA: bridging the gap between supply and demand. *Nutrients*. (2019) 11:89. doi: 10.3390/nu11010089
7. Finco AMO, Mamani LDG, Carvalho JC, de Melo Pereira GV, Thomaz-Soccol V, Soccol CR. Technological trends and market perspectives for production of microbial oils rich in omega-3. *Crit Rev Biotechnol*. (2017) 37:656–71. doi: 10.1080/07388551.2016.1213221
8. Gao M, Song X, Feng Y, Li W, Cui Q. Isolation and characterization of *Aurantiochytrium* species: high docosahexaenoic acid (DHA) production by the newly isolated microalga, *Aurantiochytrium* sp. SD116. *J Oleo Sci*. (2013) 62:143–51. doi: 10.5650/jos.62.143
9. Ju JH, Oh BR, Ko DJ, Heo SY, Lee JJ, Kim YM, et al. Boosting productivity of heterotrophic microalgae by efficient control of the oxygen transfer coefficient using a microbubble sparger. *Algal Res*. (2019) 41:101474. doi: 10.1016/j.algal.2019.101474
10. Alarcon C, Shene C. Fermentation 4.0, a case study on computer vision, soft sensor, connectivity, and control applied to the fermentation of a thraustochytrid. *Comput Indust*. (2021) 128:103431. doi: 10.1016/j.compind.2021.103431
11. Pawar PR, Lali AM, Prakash G. Integration of continuous-high cell density-fed-batch fermentation for *Aurantiochytrium limacinum* for simultaneous high biomass, lipids and docosahexaenoic acid production. *Bioresour Technol*. (2021) 325:124636. doi: 10.1016/j.biortech.2020.124636
12. Sun XM, Xu YS, Huang H. Thraustochytrid cell factories for producing lipid compounds. *Trends Biotechnol*. (2020) 39:648–50. doi: 10.1016/j.tibtech.2020.10.008
13. Merkx-Jacques A, Rasmussen H, Muise DM, Benjamin JJR, Kottwitz H, Tanner K, et al. Engineering xylose metabolism in thraustochytrid T18. *Biotechnol Biofuels*. (2018) 11:248. doi: 10.1186/s13068-018-1246-1
14. Ye H, He Y, Xie Y, Sen B, Wang G. Fed-batch fermentation of mixed carbon source significantly enhances the production of docosahexaenoic acid in *Thraustochytriidae* sp. PKU#Mn16 by differentially regulating fatty acids biosynthetic pathways. *Bioresour Technol*. (2020) 297:122402. doi: 10.1016/j.biortech.2019.122402
15. Wang F, Bi Y, Diao J, Lv M, Cui J, Chen L, et al. Metabolic engineering to enhance biosynthesis of both docosahexaenoic acid and odd-chain fatty acids in *Schizochytrium* sp. S31. *Biotechnol Biofuels*. (2019) 12:141. doi: 10.1186/s13068-019-1484-x
16. Li Z, Meng T, Ling X, Li J, Zheng C, Shi Y, et al. Overexpression of malonyl-CoA: ACP transacylase in *Schizochytrium* sp. to improve polyunsaturated fatty acid production. *J Agric Food Chem*. (2018) 66:5382–91. doi: 10.1021/acs.jafc.8b01026
17. Cui GZ, Ma Z, Liu YJ, Feng Y, Sun Z, Cheng Y, et al. Overexpression of glucose-6-phosphate dehydrogenase enhanced the polyunsaturated fatty acid composition of *Aurantiochytrium* sp. SD116. *Algal Res*. (2016) 19:138–45. doi: 10.1016/j.algal.2016.08.005
18. Ren LJ, Zhuang XY, Chen SL, Ji XJ, Huang H. Introduction of omega-3 desaturase obviously changed the fatty acid profile and sterol

content of *Schizochytrium* sp. *J Agric Food Chem*. (2015) 63:9770–6. doi: 10.1021/acs.jafc.5b04238
19. Grossmann M, Kiessling F, Singer J, Schoeman H, Schroder MB, von Wallbrunn C. Genetically modified wine yeasts and risk assessment studies covering different steps within the wine making process. *Ann Microbiol*. (2011) 61:103–15. doi: 10.1007/s13213-010-0088-2
20. Sun XM, Ren LJ, Bi ZQ, Ji XJ, Zhao QY, Huang H. Adaptive evolution of microalgae *Schizochytrium* sp. under high salinity stress to alleviate oxidative damage and improve lipid biosynthesis. *Bioresour Technol*. (2018) 267:438–44. doi: 10.1016/j.biortech.2018.07.079
21. Dragosits M, Mattanovich D. Adaptive laboratory evolution – principles and applications for biotechnology. *Microb Cell Fact*. (2013) 12:64. doi: 10.1186/1475-2859-12-64
22. Li X, Pei G, Liu L, Chen L, Zhang W. Metabolomic analysis and lipid accumulation in a glucose tolerant *Crypthecodinium cohnii* strain obtained by adaptive laboratory evolution. *Bioresour Technol*. (2017) 235:87–95. doi: 10.1016/j.biortech.2017.03.049
23. Fu W, Guethmundsson O, Paglia G, Herjolfsson G, Andresson OS, Palsson BO, et al. Enhancement of carotenoid biosynthesis in the green microalga *Dunaliella salina* with light-emitting diodes and adaptive laboratory evolution. *Appl Microbiol Biotechnol*. (2013) 97:2395–403. doi: 10.1007/s00253-012-4502-5
24. Sun XM, Ren LJ, Ji XJ, Chen SL, Guo DS, Huang H. Adaptive evolution of *Schizochytrium* sp. by continuous high oxygen stimulations to enhance docosahexaenoic acid synthesis. *Bioresour Technol*. (2016) 211:374–81. doi: 10.1016/j.biortech.2016.03.093
25. Sun XM, Ren LJ, Bi ZQ, Ji XJ, Zhao QY, Jiang L, et al. Development of a cooperative two-factor adaptive-evolution method to enhance lipid production and prevent lipid peroxidation in *Schizochytrium* sp. *Biotechnol Biofuels*. (2018) 11:65. doi: 10.1186/s13068-018-1065-4
26. Reyes LH, Almario MP, Winkler J, Orozco MM, Kao KC. Visualizing evolution in real time to determine the molecular mechanisms of n-butanol tolerance in *Escherichia coli*. *Metab Eng*. (2012) 14:579–90. doi: 10.1016/j.ymben.2012.05.002
27. Wang HH, Isaacs FJ, Carr PA, Sun ZZ, Xu G, Forest CR, et al. Programming cells by multiplex genome engineering and accelerated evolution. *Nature*. (2009) 460:894–8. doi: 10.1038/nature08187
28. Murata H, Abe T, Ichida H, Hayashi Y, Yamanaka T, Shimokawa T, et al. Heavy-ion beam mutagenesis of the ectomycorrhizal agaricomycete *Tricholoma matsutake* that produces the prized mushroom "matsutake" in conifer forests. *Mycorrhiza*. (2018) 28:171–7. doi: 10.1007/s00572-017-0810-z
29. Diao J, Song X, Cui J, Liu L, Shi M, Wang F, et al. Rewiring metabolic network by chemical modulator based laboratory evolution doubles lipid production in *Crypthecodinium cohnii*. *Metab Eng*. (2019) 51:88–98. doi: 10.1016/j.ymben.2018.10.004
30. Wase N, Tu B, Allen JW, Black PN, DiRusso CC. Identification and metabolite profiling of chemical activators of lipid accumulation in green algae. *Plant Physiol*. (2017) 174:2146–65. doi: 10.1104/pp.17.00433
31. Wang Z, Wang S, Feng Y, Wan W, Zhang H, Bai X, et al. Obtaining high-purity docosahexaenoic acid oil in thraustochytrid *Aurantiochytrium* through a combined metabolic engineering strategy. *J Agric Food Chem*. (2021) doi: 10.1021/acs.jafc.1c03781
32. Song X, Wang J, Wang Y, Feng Y, Cui Q, Lu Y. Artificial creation of *Chlorella pyrenoidosa* mutants for economic sustainable food production. *Bioresour Technol*. (2018) 268:340–5. doi: 10.1016/j.biortech.2018.08.007
33. Masuko T, Minami A, Iwasaki N, Majima T, Nishimura S, Lee YC. Carbohydrate analysis by a phenol-sulfuric acid method in microplate format. *Anal Biochem*. (2005) 339:69–72. doi: 10.1016/j.ab.2004.12.001
34. Wang S, Lan C, Wang Z, Wan W, Zhang H, Cui Q, et al. Optimizing eicosapentaenoic acid production by grafting a heterologous polyketide synthase pathway in the thraustochytrid *Aurantiochytrium*. *J Agric Food Chem*. (2020) 68:11253–60. doi: 10.1021/acs.jafc.0c04299
35. de Mendoza D. Temperature sensing by membranes. *Annu Rev Microbiol*. (2014) 68:101–16. doi: 10.1146/annurev-micro-091313-103612
36. Ma Z, Tian M, Tan Y, Cui G, Feng Y, Cui Q, et al. Response mechanism of the docosahexaenoic acid producer *Aurantiochytrium* under cold stress. *Algal Res*. (2017) 25:191–9. doi: 10.1016/j.algal.2017.05.021
37. Hu F, Clevenger AL, Zheng P, Huang Q, Wang Z. Low-temperature effects on docosahexaenoic acid biosynthesis in *Schizochytrium* sp. TIO01 and its proposed underlying mechanism. *Biotechnol Biofuels*. (2020) 13:172. doi: 10.1186/s13068-020-01811-y
38. Ma Z, Tan Y, Cui G, Feng Y, Cui Q, Song X. Transcriptome and gene expression analysis of DHA producer *Aurantiochytrium* under low temperature conditions. *Sci Rep*. (2015) 5:14446. doi: 10.1038/srep14446
39. Han X, Zhao Z, Wen Y, Chen Z. Enhancement of docosahexaenoic acid production by overexpression of ATP-citrate lyase and acetyl-CoA carboxylase in *Schizochytrium* sp. *Biotechnol Biofuels*. (2020) 13:131. doi: 10.1186/s13068-020-01767-z
40. Chaturvedi R, Uppalapati SR, Alamsjah MA, Fujita Y. Isolation of quizalofop-resistant mutants of *Nannochloropsis oculata* (Eustigmatophyceae) with high eicosapentaenoic acid following N-methyl-N-nitrosourea-induced random mutagenesis. *J Appl Phycol*. (2004) 16:135–44. doi: 10.1023/B:JAPH.0000044826.70360.8e
41. Tanadul OU, Noochanong W, Jirakranwong P, Chanprame S. EMS-induced mutation followed by quizalofop-screening increased lipid productivity in *Chlorella* sp. *Bioprocess Biosyst Eng*. (2018) 41:613–9. doi: 10.1007/s00449-018-1896-1
42. Dourou M, Aggeli D, Papanikolaou S, Aggelis G. Critical steps in carbon metabolism affecting lipid accumulation and their regulation in oleaginous microorganisms. *Appl Microbiol Biotechnol*. (2018) 102:2509–23. doi: 10.1007/s00253-018-8813-z
43. Yue XH, Chen WC, Wang ZM, Liu PY, Li XY, Lin CB, et al. Lipid distribution pattern and transcriptomic insights revealed the potential mechanism of docosahexaenoic acid traffics in *Schizochytrium* sp. A-2. *J Agric Food Chem*. (2019) 67:9683–93. doi: 10.1021/acs.jafc.9b03536
44. Mariam I, Kareya MS, Nesamma AA, Jutur PP. Delineating metabolomic changes in native isolate *Aurantiochytrium* for production of docosahexaenoic acid in presence of varying carbon substrates. *Algal Res*. (2021) 55:102285. doi: 10.1016/j.algal.2021.102285
45. Ajjawi I, Verruto J, Aqui M, Soriaga LB, Coppersmith J, Kwok K, et al. Lipid production in *Nannochloropsis gaditana* is doubled by decreasing expression of a single transcriptional regulator. *Nat Biotechnol*. (2017) 35:647–52. doi: 10.1038/nbt.3865
46. Li Y, Han D, Hu G, Sommerfeld M, Hu Q. Inhibition of starch synthesis results in overproduction of lipids in *Chlamydomonas reinhardtii*. *Biotechnol Bioeng*. (2010) 107:258–68. doi: 10.1002/bit.22807
47. Wang S, Lan C, Wang Z, Wan W, Cui Q, Song X. PUFA-synthase-specific PPTase enhanced the polyunsaturated fatty acid biosynthesis via the polyketide synthase pathway in *Aurantiochytrium*. *Biotechnol Biofuels*. (2020) 13:152. doi: 10.1186/s13068-020-01793-x
48. Chang G, Gao N, Tian G, Wu Q, Chang M, Wang X. Improvement of docosahexaenoic acid production on glycerol by *Schizochytrium* sp. S31 with constantly high oxygen transfer coefficient. *Bioresour Technol*. (2013) 142:400–6. doi: 10.1016/j.biortech.2013.04.107
49. Shafiq M, Zeb L, Cui G, Jawad M, Chi Z. High-density pH-auxostat fed-batch culture of *Schizochytrium limacinum* SR21 with acetic acid as a carbon source. *Appl Biochem Biotechnol*. (2020) 192:1163–75. doi: 10.1007/s12010-020-03396-6
50. Kujawska N, Talbierz S, Debowski M, Kazimierowicz J, Zielinski M. Optimizing docosahexaenoic acid (DHA) production by *Schizochytrium* sp. grown on waste glycerol. *Energies*. (2021) 14:1685. doi: 10.3390/en14061685
51. Hu XC, Ren LJ, Chen SL, Zhang L, Ji XJ, Huang H. The roles of different salts and a novel osmotic pressure control strategy for improvement of DHA production by *Schizochytrium* sp. *Bioprocess Biosyst Eng*. (2015) 38:2129–36. doi: 10.1007/s00449-015-1452-1
52. Contreras B, Basto D, Gelves G. Modelling of DHA production from *S. limacinum* ouc88: fed-batch perspectives. *J Phys*

Conf Ser. (2021) 2049:012076. doi: 10.1088/1742-6596/2049/1/012076

Conflict of Interest: The authors declare that the research was conducted in the absence of any commercial or financial relationships that could be construed as a potential conflict of interest.

Publisher's Note: All claims expressed in this article are solely those of the authors and do not necessarily represent those of their affiliated organizations, or those of the publisher, the editors and the reviewers. Any product that may be evaluated in this article, or claim that may be made by its manufacturer, is not guaranteed or endorsed by the publisher.

frontiers in Nutrition

REVIEW
published: 23 February 2022
doi: 10.3389/fnut.2022.851402

Key Enzymes in Fatty Acid Synthesis Pathway for Bioactive Lipids Biosynthesis

Xiao-Yan Zhuang[1], *Yong-Hui Zhang*[1], *An-Feng Xiao*[1], *Ai-Hui Zhang*[2*] and *Bai-Shan Fang*[1,2]

[1] College of Food and Biological Engineering, Jimei University, Xiamen, China, [2] Department of Chemical and Biochemical Engineering, College of Chemistry and Chemical Engineering, Xiamen University, Xiamen, China

Dietary bioactive lipids, one of the three primary nutrients, is not only essential for growth and provides nutrients and energy for life's activities but can also help to guard against disease, such as Alzheimer's and cardiovascular diseases, which further strengthen the immune system and maintain many body functions. Many microorganisms, such as yeast, algae, and marine fungi, have been widely developed for dietary bioactive lipids production. These biosynthetic processes were not limited by the climate and ground, which are also responsible for superiority of shorter periods and high conversion rate. However, the production process was also exposed to the challenges of low stability, concentration, and productivity, which was derived from the limited knowledge about the critical enzyme in the metabolic pathway. Fortunately, the development of enzymatic research methods provides powerful tools to understand the catalytic process, including site-specific mutagenesis, protein dynamic simulation, and metabolic engineering technology. Thus, we review the characteristics of critical desaturase and elongase involved in the fatty acids' synthesis metabolic pathway, which aims to not only provide extensive data for enzyme rational design and modification but also provides a more profound and comprehensive understanding of the dietary bioactive lipids' synthetic process.

Keywords: bioactive lipids, desaturase, elongase, fatty acid synthesis pathway, oleogenic microorganisms

OPEN ACCESS

Edited by:
Xiao-Jun Ji,
Nanjing Tech University, China

Reviewed by:
Hu-Hu Liu,
Hunan Agricultural University, China
Xiao-Man Sun,
Nanjing Normal University, China

***Correspondence:**
Ai-Hui Zhang
zhangaihui@xmu.edu.cn

Specialty section:
This article was submitted to Food Chemistry, a section of the journal Frontiers in Nutrition

Received: *09 January 2022*
Accepted: *25 January 2022*
Published: *23 February 2022*

Citation:
Zhuang X-Y, Zhang Y-H, Xiao A-F, Zhang A-H and Fang B-S (2022) Key Enzymes in Fatty Acid Synthesis Pathway for Bioactive Lipids Biosynthesis. Front. Nutr. 9:851402. doi: 10.3389/fnut.2022.851402

INTRODUCTION

Lipid plays a critical role in maintaining the normal function of growth and metabolism, which is not only an essential factor for the fluidity of the plasma membrane but is also a carrier to store material and energy (1). Long chain polyunsaturated fatty acids (LCPUFAs) are the main active and functional components in lipid. With the continuous improvement of people's life quality, more and more attention is paid to the intake and proportion of various kinds of LCPUFAs in the daily diet (2). The fatty acids in the daily diet are mainly consisted of saturated ones and unsaturated ones. According to the different positions of unsaturated double bonds, LCPUFAs can be mainly divided into ω3 and ω6 series, such as docosahexaenoic acid (DHA, C22:6$^{\Delta4,7,10,13,16,19}$ ω3), eicosapentaenoic acid (EPA, C20:4$^{\Delta5,8,11,14,17}$, ω3), and arachidonic acid (AA, C20:4$^{\Delta5,8,11,14}$, ω6) (3). These LCPUFAs also play a crucial role in not only growth and brain development but also in preventing cardiovascular diseases, hypertension, and diabetes (4). Therefore, the Food and Agriculture Organization of the United Nations (FAO) and the World Health Organization (WHO) issued a joint statement that the intake of LCPUFAs fatty acids daily should not be

<1.3 g (5). However, mammals can't *de novo* synthesize these LCPUFAs, which make getting supplements from diet to be particularly important (6).

In daily diet, the intake of LCPUFAs is the primary driver of deep-sea fish and vegetable oil. Adapt to a low-temperature marine environment, deep-sea fish oil is rich in LCPUFAs, enriched from the marine microalgae (7, 8). Some plants such as soybeans, flax, and peanut, can store lipid in their seed, from which humans could extract and harvest linoleic acid (LA, $18{:}2^{\Delta 9,12}$, ω6) and α-linolenic acid (ALA, $C18{:}3^{\Delta 9,12,15}$, ω3) rich oil (9, 10). However, harvesting the LCPUFAs from plants and deep-sea fish is a time-consuming process, which was also limited by climate, land and ecological environment (11, 12). Furthermore, the plant could not provide LCPUFAs of DHA and ARA, while overfishing caused more deadly consequences, including destructive fishing practices, killing off the fish, and breaking the ecological balance (13). Thus, with the explosion of population, the LCPUFAs harvest speed from these two approaches can no longer meet market demand needs. Fortunately, the development of LCPUFAs from oleaginous microorganisms and microalgae provides an alternative source for increasing market demand. At present, many LCPUFAs' production processes have been developed, including *Schizochytrium* sp., *Mortierella alpina*, *Thraustochytrids* and *Yarrowia lipolytica* (14–17). Compared with LCPUFAs from plant and fish oil, the LCPUFAs driver from microorganisms and microalgae own many advantages. On the one hand, it broke the loose of climate and ground; on the other hand, higher proliferation, growth and LCPUFAs rich oil accumulation rate enhance the productivity and low the cost. Thus, the development LCPUFAs rich oil strategies attract more attention from scientists worldwide, promoting the development and research rate significantly.

Based on the previous studies, the synthesis approaches of LCPUFAs mainly consisted of the fatty acid synthesis pathway (FAS) and polyketosynthase (PKS) pathway (18, 19). Compared with PKS, the FAS pathway is more extensive and typical in all oleogenic microorganisms. As shown in **Figure 1**, many kinds of fatty acid desaturases and elongases play an essential role in synthesizing LCPUFAs, which perform the functions of introducing double bonds and extending the carbon chain. Thus, this paper reviews the features of and advances of these critical enzymes in LCPUFAs synthetic pathway. We also discuss the challenge and the most promising breakthrough direction of enzyme in LCPUFAs synthetic pathway, which aims to provide detailed information and novel ideas for the follow-up research in this field.

VITAL DESATURASE IN ω-6 AND ω-3 PATHWAY

Δ9-Desaturase

Δ9-desaturase is a central enzyme to synthesize the long chain monounsaturated fatty acids (LCMUFAs) from long chain saturated fatty acids (LCSFAs), which catalyze stearic acid (SA, 18:0) and palmitic acid (PA; C16:0) to oleic acid (OA, $18{:}1^{\Delta 9}$) and palmitoleic acid (POA, $C16{:}1^{\Delta 9}$) (**Figure 1**). Scientists also have identified and characterized the various Δ9-fatty acid desaturase gene from *Rhodotorula toruloides* (20) and *Pseudomonas sp.* (21) (**Table 1**). These Δ9-desaturases shared three histidine-conserved boxes that would be the catalytic position of Δ9 fatty acid desaturase. The RtΔ9FAD protein was also predicted to have four possible transmembrane domains (54).

As the obstacles in harvest crystal structures of fatty acid desaturases located in the membrane, homology modeling could predict the three-dimensional structures. The docking studies could be employed to predict the active center of the desaturases. Predicted by docking results, His34, His71, and, His206 were the possible residues to contact with the docked palmitic acid, located in the first, second, and third conserved histidine boxes (21). Another study of homology modeling and docking also showed that four α-helices constitute the catalytic site and transmembrane domain in Δ9-desaturase from *Arthrospira platensis* (55). Beyond that, 3D structure modeling studies revealed that three variant amino acids (F160, A223, and L156) in domain Δ9-desaturase encoded by gene *PtAAD* narrow the space of substrate binding center, explaining the reason of substrate preference of this especial Δ9-desaturase for palmitic acid (22, 23) (**Table 2**).

By overexpressing the *Rt*Δ*9FAD* gene into *R. toruloides,* the transformant produces 5-fold more oleic acid content in total amount (54). At the same time, Liu and his colleague (23) reported a Δ9-desaturase from *Phaeodactylum tricornutum* to prefer palmitic acid-ACP as a substrate to promote the palmitoleic acid under average and stress culture conditions. Rau and his colleague also find that the Δ9-desaturase from *Aurantiochytrium sp.* T66 could accept palmitic acid and stearic acid as substrates (59). The reasonable explanation for substrate preference was also given out through homology modeling and docking in the last paragraph.

Δ12-Desaturase

Δ12-desaturase is a vital enzyme in the first step of LCPUFAs synthesized from LCMUFAs, which catalyze oleic acid (OA, $18{:}1^{\Delta 9}$) to linoleic acid (LA, $18{:}2^{\Delta 9,12}$) (**Figure 1**). Scientists also have identified and characterized the various Δ12-fatty acid desaturase gene from *Isochrysis galbana* (24), *Acanthamoeba castellanii* (25), *Chlamydomonas sp*. (26), *Calendula officinalis* (27), *Helianthus annuus* (28), *Chlorella vulgaris* (29), *P. tricornutum* (30), and *Haematococcus pluvialis* (31), whose detailed information is listed in **Table 1**. These Δ12-desaturases also share three conserved histidine boxes, which are considered the catalytic center and are critical for desaturase activity.

Different environment stressors will influence the *FAD2* (coding Δ12-desaturase) transcription of the oleaginous microorganism. In *Y. lipolytica*, the low temperature or substrate (n-alkanes or oleic acid) induce the upregulation of Δ12-desaturase (60). Similarly, low temperature (15°C), high salinity (salinity of 62 and 93%), and nitrogen starvation (220 μmol/L) upregulate the abundance of *IgFAD2* transcript in *I. galbana* as well (24).

Overexpress Δ12-desaturase in oleogenic microorganisms could enhance the product accumulation significantly. After

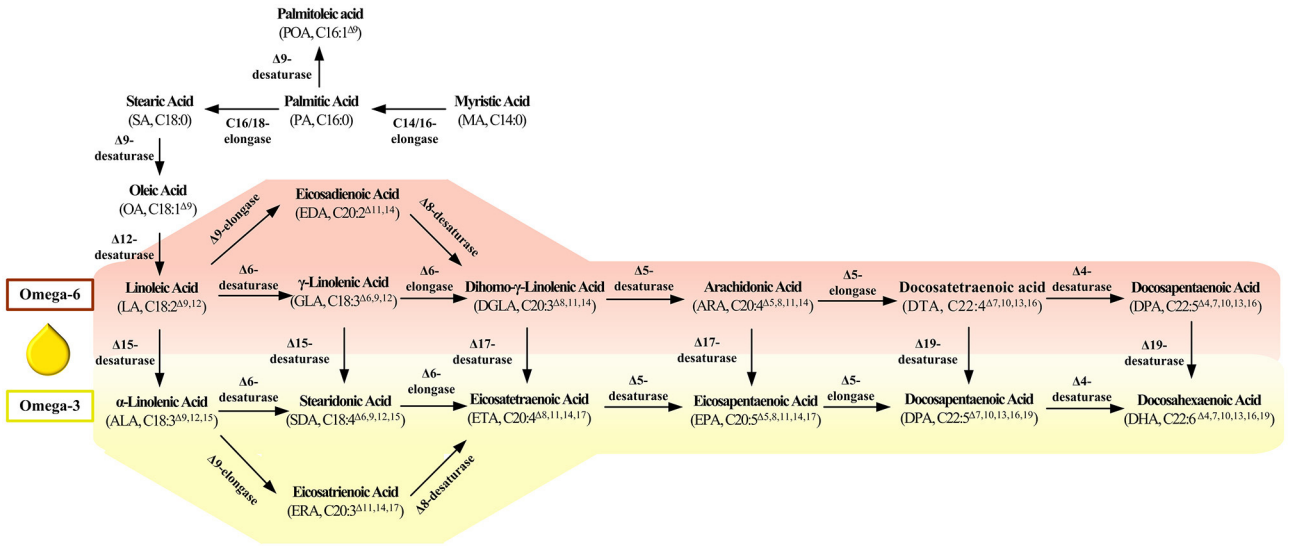

FIGURE 1 | Key enzyme in the fatty acids' synthesis pathway.

heterologous overexpress Δ12-desaturase from *M. alpina* or *Fusarium verticillioides* in the oleaginous yeast *Rhodosporidium toruloides*, linoleic acid concentration increased up to 1.3 g/L, which was 5-fold higher than that in the parent strain (61). Overexpression of endogenous *RtFAD2* in *R. toruloides* also improved lipid and linoleic acid (32). Conversely, the growth rate was slower at 12°C under the deletion of *FAD2* gene (coding Δ12-desaturase) in *Y. lipolytica*, which was recovered by the addition of 18:2, not 18:1.

Δ6-Desaturase

Δ6-desaturase catalyze linoleic acid (LA, C18:$2^{\Delta 9,12}$) and α-linolenic acid (ALA, C18:$3^{\Delta 9,12,15}$) to γ-linolenic acid (GLA, C18:$3^{\Delta 6,9,12}$) and produce stearidonic acid (SDA, C18:$4^{\Delta 6,9,12,15}$). Scientists also have identified and characterized the various Δ6-desaturase from *Glossomastix chrysoplasta* (33), *Pythium sp.* (39), *Isochrysis* sp. (42), and *Mucor sp.* (43). Araki and his colleague identified a novel gene encoding Δ6- desaturase from *Rhodococcus sp.* Different from others, this desaturase preferred saturated fatty acids as substrates and catalyzed hexadecanoic acid to cis-6-hexadecenoic acid (38) (**Table 1**).

By analyzing the sequence of the Δ6-desaturase from *Mucor sp.*, Jiang et al. found that −919 to −784 bp in the promoter region plays a vital role in the high activity of Δ6-desaturase (62). Compared with native Δ6-desaturase in *Pythium sp.*, the codon-optimized strategy could markedly enhance Δ-6 desaturated products, in which the substrate conversion rates of LA and ALA increased from 5.4 and 4.2% to 62.7 and 60.9%, respectively (39). Zhu et al. (63) found that overexpression of endogenous Δ6-desaturase significantly enhances the eicosapentaenoic acid accumulation in *P. tricornutum*, compared with overexpression of heterologous one (64). However, the other scientist reported another result that differed massively in *M. alpina*. First, the Δ-6 desaturase from *M. alpina* (57) and *M. pusilla* (65) has the characteristic of significant substrate preference, in which the *MpFADS6* (from *M. pusilla*) and *MaFADS6-I* (from *M. alpina*) prefer to ALA and LA, respectively. Zhang et al. (34) also isolated and identified a Δ6-desaturase from *Pythium splendens* with a preference to LA. Second, they further introduced the exogenous gene encoding ALA-preferring Δ6-desaturase from *M. pusilla* into the *M. alpina,* EPA yield was increased from 22.99 ± 2.7 mg/L in WT *M. alpina* up to 588.5 ± 29.6 mg/L in engineered one in 5-L fermentation, in which peony seed oil (0.1%) and peony seed meal (50 g/L) were exogenously added as a substitution to ALA (66). Last, they introduced the exogenous gene from *Thalassiosira pseudonana* (41), encoding a higher Δ6-desaturase activity (*TpFADS6*) for ALA, to the high ALA producer of *Dunaliella salina* (40). After performing culture conditions optimization, the EPA concentration increased from 1.6 ± 0.2 to 554.3 ± 95.6 mg/L, 343.8-fold higher than that in the wild-type strain (40). Beyond that, the expression of *IsFAD6* (encoding Δ6-desaturase) was upregulated in high salinity, low temperature, and high nitrogen deficiency culture condition, indicating *IsFAD6* respond to the various abiotic stresses (61). At the same time, heterologous expression Δ6-desaturase in *Nannochloropsis oceanica* enhanced both growth and photosynthetic efficiency (67).

Scientists also focused on studying detailed characteristics to harvest a deeper insight into the mechanism. Song et al. (68) demonstrated that amino acid residues 114–174, 206–257, and 258–276 play a vital role in substrate recognition for Δ6-desaturase. Shi et al. (57) also found that MpFADS6 (from *M. pusilla*) and MaFADS6-I (from *M. alpina*) showed a difference in substrate preference. Further studies based on the domain swapping approach reveal that sequences between the histidine boxes I and II played a pivotal role in which mutation of G194, E222, M227, and V399/I400 cause a significant decrease in the ALA conversion rate of MpFADS6 (57) (**Table 2**).

TABLE 1 | The characteristic of the desaturase in ω-6 and ω-3 pathway.

Desaturase	Source	Conversion rate	Gene (bp)	Amino acid	Molecular mass (kDa)	GeneBank No.	References
Δ9	*Rhodotorula toruloides*	/	1,635	545	60.8	XP_016270987.1	(20)
	Pseudomonas sp.	/	1,182	394	45	AMX81567.1	(21)
	Phaeodactylum tricornutum	11.9%	1,227	408	46.36	/	(22, 23)
Δ12	*Isochrysis galbana*	/	1,158	386	42.8	ABD58898.1	(24)
	Acanthamoeba castellanii	/	1,224	407	/	ABK15557.1	(25)
	Chlamydomonas sp.	/	1,845	433	/	ACX42440.1	(26)
	Calendula officinalis	/	1,411	383	/	AAK26633.1	(27)
	Helianthus annuus	/	1,259	382	/	AAL68983.1	(28)
	Chlorella vulgaris	/	2,032	385	/	ACF98528.1	(29)
	Phaeodactylum tricornutum	/	1,526	436	/	AAO23564.1	(30)
	Haematococcus pluvialis	/	1,137	378	43.29	MH817076.1	(31)
	Rhodotorula toruloides	/	1,356	451	50.6	XM_016420199.1	(20, 32)
Δ6	*Glossomastix chrysoplasta*	7% to ALA, 6% to LA	1,821	465	51.9	AAU11445.1	(33)
	Pythium splendens	/	1,380	459	52.7	JX431892.1	(34)
	Myrmecia incisa	3.14% to LA, 2.21% to ALA	1,443	480	/	JN205756.1	(35)
	Mucor rouxii	/	1,831	467	/	AAR27297.1	(36)
	Micromonas pusilla	60% to ALA, 10% to LA	1,570	463	54.52	XM_003056946.1	(37)
	Rhodococcus sp.	/	1,242	413	45	AB847088.1	(38)
	Pythium sp.	62.7% to LA, 60.9% to ALA	1,401	466	52.8	ALE65995.1	(39)
	Dunaliella salina	/	1,329	422	/	/	(40)
	Thalassiosira pseudonana	/	1,455	484	/	AY817155.1	(41)
	Isochrysis sp.	2.3% to LA, 6.3% to ALA	1,478	482	∼78	KR005946.1	(42)
	Mucor sp.		1,572	523		AB090360.1	(43)
Δ5	*Leishmania major*	5% to DGLA, 6% to ETA	1,254	417	/	HQ678521.1	(44)
	Mortierella alpina	12% to DGLA, 12.5% to ETA	1,341	446	/	GU593328.1	(44)
	Ostreococcus tauri	9% to DGLA, 11% to ETA	1,476	491	/	HQ678520.1	(44)
	Ostreococcus lucimarinus	6% to DGLA, 8% to ETA	1,476	491	/	HQ678519.1	(44)
	Paramecium tetraurelia	13% to DGLA, 14% to ETA	1,542	513	/	HQ678517.1	(44)
	Oblongichytrium sp.	24.8% to DGLA, 36.6% to ETA	1,308	435	50	AB432913.1	(45)
	Thraustochytrium sp.	19.9% to DGLA, 22.9% to ETA	1,320	439	/	EU643618.1	(46, 47)
	Isochrysis sp	/	1,170	382	70	KR062001.1	(48)
Δ4	*Isochrysis galbana*	34 % to DPA	1,302	433	48.1	JQ664598.1	(49)
	Isochrysis sphaerica	79.8 to DPA	1,284	427	47.9	JQ791105.1	(50)
	Ostreococcus lucimarinus	10% to DPA, 4% to DTA	1,409	459	/	XM_001415706.1	(51)
	Pavlova lutheri	∼30% to DPA and DTA	1,619	445	49	AAQ98793.1	(52)
	Pavlova viridis	/	1,440	479	52.7	GU594191.1	(53)

By employing site-directed mutation, the scientist found that mutants Q409R and M242P lost the desaturation function, while mutants F419V and A374Q weakened the catalytic activities. Combined with molecular modeling, they reveal that electronic transfer in the catalytic process correlated with histidine-conserved region III, while desaturation is highly correlated with histidine-conserved regions I and II (37) (**Table 2**). These results from site-specific mutagenesis and molecular modeling bridge the gap between structure and the catalytic mechanism of these desaturases.

Δ5-Desaturase

Δ5-desaturase catalyze dihomo-γ-linolenic acid (DGLA, C20:3$^{\Delta 8,11,14}$) and eicosatetraenoic acid (ETA, C20:4$^{\Delta 8,11,14,17}$) to arachidonic acid (AA, C20:4$^{\Delta 5,8,11,14}$) and eicosapentaenoic acid (EPA, C20:4$^{\Delta 5,8,11,14,17}$). Scientists have also identified and characterized the various Δ5-desaturase genes from *Paramecium tetraurelia* (44), *Ostreococcus tauri* (44), *Ostreococcus lucimarinus* (44), *Thraustochytrium sp.* (46), and *Oblongichytrium sp.* (45). The amino acid sequence from this Δ5-desaturase was significantly homologous, containing three conserved histidine boxes and a cytochrome b5 domain (**Table 1**).

Tavares et al. (44) carried out a research on substrate preferences and desaturation efficiencies of Δ5-desaturase from *P. tetraurelia*, *O. tauri,* and *O. lucimarinus.* Their results also demonstrated that Δ5-desaturase from *O. tauri, O. lucimarinus, M. alpina*, and *P. tetraurelia* prefer the

TABLE 2 | The effect of site directed mutagenesis on the performance of desaturase.

Enzyme	Source	Mutation site	Performance	References
Δ9-desaturase	*Phaeodactylum tricornutum*	F160L, A223T, and L156M	Substrate preference changes from C16:0 to C18:0	(23)
Δ12-desaturase	*Mortierella alpina*	P166L or H116Y	Loss the catalytic activity from 18:1$^{\Delta}$9 to 18:2$^{\Delta 9,12}$	(56)
Δ12-desaturase	*Mortierella alpina*	W131L or S218G or N389D	Activity weakened slightly	(56)
Δ6-desaturase	*Micromonas pusilla*	F419V or A374Q	Activity decreases to the half of wild type	(37)
		Q409R or M242P	Completely inactivated	(37)
		Q236N or A423C	Activity enhanced slightly	(37)
		Q190A, S197Q, and Q209G	No significant change	(37)
		V399I/I400E, E222S, and M227K	Activity decreases to 40.26, 31.42, and 31.61%, respectively (wild type: 71.37%).	(57)
		G194L	Activity decreases to 6.5%, respectively (wild type: 71.37%).	(57)
Δ15-desaturase	*Chlamydomonasreinhardtii*	T286S	No significant change	(1)
		T286Y, T286H, T286C, or T286G	Loss of catalytic activity	(1)
	Mortierella alpina	E111D, T322S, and F353H	No significant change to wild type	(58)
		W106F and V137T	Markedly decreased the conversion rate for AA (40 to 50%)	(58)
		A44S, M156I, and W291M	Markedly increase the conversion rate for AA (30–40%)	(58)

substrates bound in phospholipid to a promiscuous acyl carrier substrate, while Δ5-desaturase from *L. major* was an acyl coenzyme A-dependent.

Heterologous expression Δ5-desaturase from *Thraustochytrium aureum* in *Aurantiochytrium limacinum* triggers increase of AA and EPA by 4.6- and 13.2-fold, which is driven by the thraustochytrid ubiquitin promoter (47). After disrupting the Δ5-desaturase in *M. alpina*, scientists achieve a higher percentage of DGLA (40.1%) accumulation in total lipid (69). At the same time, overexpressing the Δ5-desaturase in *P. tricornutum* exhibited a significant increment of unsaturated fatty acids, EPA (increase by 58%), and neutral lipid content (increase up to 65%) (70). Thus, these results demonstrated the critical role of Δ5-desaturase in catalyzing the DGLA and ETA to AA and EPA, respectively.

Δ4-Desaturase

Δ4-desaturase catalyze docosatetraenoic acid (DTA, C22:4$^{\Delta 7,10,13,16}$) and docosapentaenoic acid (DPA, C22:5$^{\Delta 7,10,13,16,19}$) to docosapentaenoic acid (DPA, C22:5$^{\Delta 4,7,10,13,16}$) and docosahexaenoic acid (DHA, C22:6$^{\Delta 4,7,10,13,16,19}$). As very important LCPUFAs, more researchers focus on another more efficient PKS pathway to synthesize DHA from *Schizochytrium sp*. However, the scientist also identified this desaturase encoding gene from *I. galbana* (49), *Isochrysis sphaerica* (50), *Pavlova lutheri* (52), *and Pavlova viridis* (53). Among them, the one from *P. lutheri* desaturated DTA (C22:4$^{\Delta 7,10,13,16}$) and DPA, (C22:5$^{\Delta 7,10,13,16,19}$) (52), while the others from *I. galbana* and *I. sphaerica* prefer DPA (C22:5$^{\Delta 7,10,13,16,19}$) as substrate (49, 50) (**Table 1**).

CATALYZE PERFORMANCE OF ω3-DESATURASE

Δ15-Desaturase

Some desaturase can convert ω-6 fatty acids to ω-3 fatty acids, which is named ω-3 desaturase. Δ15-desaturase is a kind of ω3-desaturase with C18 fatty acid as substrate, which catalyzes linoleic acid (LA, 18:2$^{\Delta 9,12}$) and γ-linolenic acid (GLA, C18:3$^{\Delta 6,9,12}$) to α-linolenic acid (ALA, C18:3$^{\Delta 9,12,15}$) and stearidonic acid (SDA, C18:4$^{\Delta 6,9,12,15}$), respectively. Scientists found that low temperature and high salinity could motivate the upregulation of *CiFAD3* (coding Δ15-desaturase) expression in *Chlamydomonas reinhardtii* (71).

Substrate preference was an exciting topic determined by the structure and amino acid in the enzyme's binding site. Scientists found that Δ15-desaturase from *Riftia pachyptila* (72) and *M. alpina* (73) show a preference for C18 fatty acids, while Δ17-desaturase from *Pythium aphanidermatum* (74) display a higher catalytic activity for C20 fatty acids (**Table 3**). On combining site directed mutagenesis, homology modeling, and molecular docking, scientists revealed that the W106 and V137 related to substrate recognition (mutations in these amino acids significantly decreased the enzyme activity), and the A44, M156, and W291 residues related to the higher desaturation activity for C20 substrates (mutations in these amino acids markedly increase the conversion rate of AA). Beyond that, the amino acids residues that bind to CoA groups govern substrate preference (58) (**Table 2**). Scientists also found that the threonine residue located in the fourth transmembrane was essential for the typical structure and function of Δ15-desaturase in *C. reinhardtii,* and the mutations in this site resulted in varying degrees of activity weaken (1) (**Table 2**).

TABLE 3 | The characteristic of the ω3-desaturase.

Desaturase	Source	Conversion rate (%)	Gene (bp)	Amino acid	Molecular Mass (kDa)	GeneBank No.	References
Δ15	*Chlamydomonas sp.*	/	1,845	433	49.2	GQ888689.1	(26)
	Mortierella alpina	59.7% to LA, 29.6% to AA	1,212	403		KF433065.1	(73, 75)
	Riftia pachyptila	3.4% to LA, 4.2% to GLA	1,587	403	/	KY399781.1	(72)
Δ17	*Pythium aphanidermatum*	63.8% to AA	1,533	/	/	FW362186.1	(74)
	Phytophthora sojae	60% to AA	1,092	/	/	FW362213.1	(74)
	Phytophthora ramorum	65% to AA	1,086	/	/	FW362214.1	(74)

Δ17-Desaturase

Δ17-desaturase is another kind of ω3-desaturase with C20 fatty acid as a substrate which catalyzes dihomo-γ-linolenic acid (DGLA, C20:3$^{\Delta 8,11,14}$) and arachidonic acid (AA, C20:4$^{\Delta 5,8,11,14}$) to eicosatetraenoic acid (ETA, C20:4$^{\Delta 8,11,14,17}$) and eicosapentaenoic acid (EPA, C20:4$^{\Delta 5,8,11,14,17}$), respectively. Considerable efforts have been focused on identified and characteristic Δ17-desaturase, which could convert 20°C ω-6 fatty acids to ω-3 fatty acids. Scientists have identified the Δ17-desaturase from *P. aphanidermatum* (74), *Phytophthora sojae* (74), *Phytophthora ramorum* (74), *Saprolegnia diclina* (76), and *Phytophthora infestans* (77) (**Table 3**). Among them, Δ17-desaturase from *S. diclina, P. aphanidermatum, P. sojae,* and *Phytophthora ramorum* exhibited a great preference to convert AA to EPA. Thus, Ge and his colleague (78) transformed the Δ17-desaturase encoding gene from *P. aphanidermatum* into *M. alpina* to achieve EPA production with a 49.7% conversion rate of AA. Tang and his colleague identified a new Δ17-desaturase from *Phytophthora parasitica,* exhibiting high activity for C20 substrate (conversion rate was 70% for AA) and week activity for C18 substrate. They further introduce the gene *PPD17* encoding this Δ17-desaturase into the *M. alpina*, resulting in the conversion of AA to EPA (1.9 g/L) (79). In our previous work, a Δ17-desaturase encoding gene from *S. diclina* was also introduced into the genome of the *Schizochytrium* sp. through homologous recombination. Compared with the wild-type strains, the ω-3/ω-6 ratio in fatty acid in genetically modified strains increased from 2.1 to 2.58, and 3% of DPA was converted to DHA (80).

CHARACTERISTIC OF FATTY ACID ELONGASE

Δ6-Elongase

Δ6-elongase is a kind of fatty acid elongase with C20 fatty acid as a substrate which catalyze γ-linolenic acid (GLA, C18:3$^{\Delta 6,9,12}$) and stearidonic acid (SDA, C18:4$^{\Delta 6,9,12,15}$) to dihomo-γ-linolenic acid (DGLA, C20:3$^{\Delta 8,11,14}$) and eicosatetraenoic acid (ETA, C20:4$^{\Delta 8,11,14,17}$), respectively. Yu et al. (81) identified a Δ6-elongase localized to the endoplasmic reticulum, whose expression level was enhanced by nitrogen starvation. Jeennor et al. (82) identified a Δ6-elongase gene from *Pythium* sp., exhibiting a high specificity for C18 PUFAs with a double bond at Δ6-position. Co-overexpression of Δ9-desaturase, Δ12-desaturase, and Δ6-elongase in *Aspergillus oryzae*, scientists achieve success in enhancing free dihomo-γ-linolenic acid production with a yield of 284 mg/L (83). Shi et al. (84) identified a Δ6-elongase *N. oceanica,* which applied its elongated function on C18 PUFAs with a double bond at Δ6-position. This elongase encoding gene not only attenuated DGLA, ARA, and EPA content, but also enhanced GLA content, supporting the vital role of this enzyme in the exclusive ω-6 pathway of EPA biosynthesis (84) (**Table 4**).

Δ5-Elongase

Δ5-elongase is a kind of fatty acid elongase with C20 fatty acid as substrate which catalyze arachidonic acid (AA, C20:4$^{\Delta 5,8,11,14}$) and eicosapentaenoic acid (EPA, C20:4$^{\Delta 5,8,11,14,17}$) to Docosatetraenoic acid (DTA, C22:4$^{\Delta 7,10,13,16}$) and Docosapentaenoic acid (DPA, C22:5$^{\Delta 7,10,13,16,19}$), respectively. Employing fluorescent protein as an indicator, Niu et al. (87) found the Δ5-elongase from *Pavlova viridis* located in the endoplasmic reticulum. Robert and his colleague identified a Δ-5 elongase from *Pavlova salina* and characterized the exclusive elongase function for EPA. Furthermore, the scientist heterologous expressed the gene encoding Δ5-elongase in the moss *Physcomitrella patens* from the algae *Pavlova sp.* and harvested 4.51 mg/l Docosapentaenoic acid (DPA, C22:5$^{\Delta 7,10,13,16,19}$) from endogenous arachidonic acid (89). Jiang et al. identified a Δ5-elongase from *P. tricornutum,* exhibiting a substrate preference for EPA. Co-expressed the Δ5-elongase and Δ4-desaturase in *Pichia pastoris*, they successfully construct a pathway for docosahexaenoic acid biosynthesis (88) (**Table 4**). There also exists another alternative pathway for Δ6-elongase/Δ6-desaturase, which is called Δ9-elongase/Δ8-desaturase pathway originated from euglenoid species (74). Δ9-elongase is a kind of fatty acid elongase with C18 fatty acid as a substrate which catalyze linoleic acid (LA, C18:2$^{\Delta 9,12}$) and α-linolenic acid (ALA, C18:3$^{\Delta 9,12,15}$) to eicosadienoic acid (EDA, 20:2 C18:3$^{\Delta 11,14}$) and eicosatrienoic acid (ERA, C20:4$^{\Delta 11,14,17}$), respectively. Then, Δ8-desaturase further catalyze EDA and ERA to dihomo-γ-linolenic acid (DGLA, C20:3$^{\Delta 8,11,14}$) and eicosatetraenoic acid (ETA, C20:4$^{\Delta 8,11,14,17}$). However, compared with other elongase and desaturase, there is relatively little research about these enzymes.

TABLE 4 | The characteristic of the elongase.

Elongase	Source	Conversion rate (%)	Gene (bp)	Amino acid	Molecular Mass (kDa)	GeneBank No.	References
Δ6	*Myrmecia incisa*	24 to GLA 41 to SDA	1,331	288	29.9	EU846098.1	(81)
	Pythium sp.	29.3 to GLA36.5 to SDA	837	277	32.1	KJ546459.1	(82)
	Nannochloropsis oceanica	70.5 to GLA 34.6 to SDA	831	276	/	KY214452.1	(84, 85)
Δ5	*Pavlova salina*	30.2 to EPA	1,220	302	/	AY926605.1	(86)
	Pavlova viridis	/	1,228	314	34	EF486525.1	(87)
	Phaeodactylum tricornutum	87.9 to EPA	1,110	369	/	XP_002176686.1	(88)

ENZYME STRUCTURE ANALYSIS

Structure Analysis of Front-End Desaturase

The desaturases, introduce a double-bound between the carboxyl (end) and the original double bonds (front) in the substrate, were defined as front-end desaturase, including Δ4, Δ5, Δ6, Δ9, and Δ12 desaturase. Thus, these enzymes share similar characteristics in a structure. First, these enzymes consisted of hydrophobic transmembrane regions and hydrophilic nontransmembrane regions. However, they still exhibit differences in evolution. For example, the number of the transmembrane regions was different in each enzyme, in which the number is 2, 3, and 4 for Δ4, Δ6, and Δ8 desaturase, respectively. Second, these enzymes are fellowed by cytochrome b5-like binding domain with "HPGG" motif in the N-terminus, which is reserved for cytochrome b5 and NAD(P)H as electron donors (31, 51). Third, nontransmembrane regions contain three histidine-rich motifs, which were considered for the binding position of di-iron and are critical for desaturase activity (21, 31). The three histidine-rich motifs that were highly conservative consisted of HXXXH, HXXHH, and (H/Q)XXHH in this enzyme, which demonstrated the similarity and homology of them in origin. Thus, the mutation of the amino acid close to the substrate-binding region (three histidine-rich motifs) will cause a significant impact on desaturase activity and substrate preference. As shown in **Table 2**, the mutations of these functional domains (F160L, A223T, and L156M), located at the bottom of substrate binding position, cause the substrate preference changes from C16:0 to C18:0 (23).

Structure Analysis of ω3-Desaturase

The structure of ω3-desaturase was similar to that of front-end desaturase, which consisted of hydrophobic transmembrane regions and hydrophilic nontransmembrane regions (79). In detail, ω3-desaturase included three highly conservative histidine-rich motifs (HXXXH, HXXHH, and (H/Q)XXHH) and more than four transmembrane domains (1, 26). The three highly conservative histidine-rich motifs were also predicted as the critical position of di-iron for substrate binding. However, cytb5 "HPGG" motif was not located in the N terminal of the enzyme. Beyond that, many amino acids were conservative in this ω3-desaturase. As shown in **Table 2**, T286 in Δ15-desaturase from *Chlamydomonas reinhardtii* was responsible for catalytic activity (1) while A44S, W106, E111, M156, V137, W291M, T322S, and F353H in Δ15-desaturase in Δ15-desaturase from *Mortierella alpina* was responsible for substrate preference (58).

Structure Analysis of Elongase

The characteristic of amino acid sequence exhibit a significant difference with that of desaturase, which may also lead to the difference in structure. In detail, elongase contains seven transmembrane regions and three/five different kinds of conservative motifs. The motifs in Δ5-elongase consisted of a histidine-rich box (SFLHVYHHV), a tyrosine-rich box (YLTQAQLVQF), and a conserved motif (MYXYY) in (87). However, Δ6-elongase contains four motifs (KxxExxDT, QxxFLHxYHH, NxxxHxxMYxYY, and TxxQxxQ) and a histidine-rich catalytic motif (and HVYHH) (82). These conservative motifs were essential for di-iron binding and responsible for enzyme activity.

Structure Analysis Method

Enzyme structure model and information are collected from protein crystals, which is hindered by a lack of time and labor resources. These difficulties are especially marked in transmembrane protein, including fatty acid desaturase and elongase, widely distributed in cytomembrane, endoplasmic reticulum, and chloroplast membrane. Currently, only two kinds of three-dimensional structures of the membrane fatty acid desaturases are available, one is the mouse stearoyl-CoA desaturase (**Figure 2A**, PDB ID: 4YMK), and the other is human integral membrane stearoyl-CoA desaturase (**Figure 2B**, PDB ID: 4ZYO). Thus, homology modeling and docking are the essential methods to analyze the structure of bacterial membrane fatty acid desaturases and elongase in the current state (21). Herein, we summarized the research approach of homology modeling and docking based on the previous work (21–23, 55). First, after homology analyzes the amino acid sequence, the scientist can determine templates with higher homology and resolution in the protein database (e.g., Protein Data Bank, PDB). Second, scientists began to predict the structure based on the crystal structure of templates by employing some structure prediction software (e.g., Swiss Model and Modeler). Third, a scientist will assess the structure from many predictions. After score and energy minimization, some software will select the optimal structural model from the candidate. Fourth, the active site of the structural model was predicted using the software. Last, the docking simulations process was performed by the software of Autodock. The scientist could

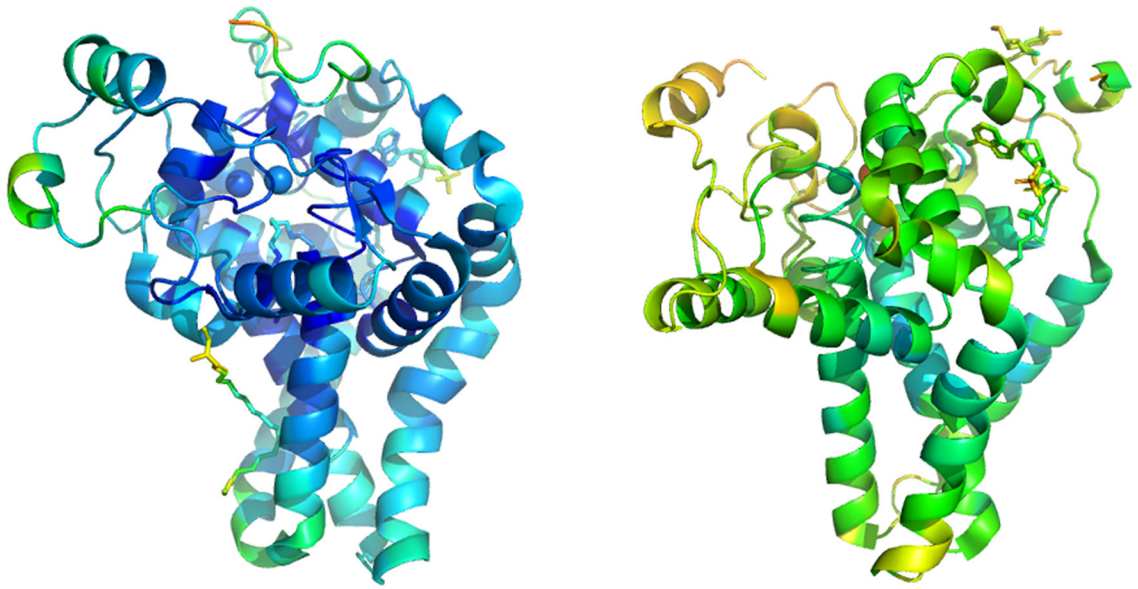

FIGURE 2 | The crystal structure of transmembrane fatty acid desaturases. **(A)**, crystal structure of mouse stearoyl-CoA desaturase (PDB ID: 4YMK). **(B)**, human integral membrane stearoyl-CoA desaturase (PDB ID: 4ZYO).

run the docking result through Gromacs and harvest stable conformation information with a substrate binding in the active site, which was then evaluated using RMSD (Root Mean Squared Deviation). Combined with site-specific mutagenesis, a scientist could match the performance of the mutant with structure variation, which could provide a reasonable explanation for the mutation (22, 58).

CONCLUSIONS AND PERSPECTIVES

Dietary bioactive lipids are important nutriments to maintain the typical metabolic status of the organism. As the practical component in lipid, the crucial role is self-evident of LCPUFAs in boosting the development of the brain and immune system and preventing cardiovascular disease. More importantly, what chip is to the electronic equipment, an enzyme is to the cell factory. These fatty acid synthesis related enzymes play a vital role in the desaturation and elongation of the carbon chain. These enzymes exist widely in plants, fungus, microalgae, and bacteria located in the cell and/or organelle membrane, including endoplasmic reticulum and chloroplast. Thus, the Open Reading Frames and amino acid sequence of these enzymes share a high degree of homology among the genera, which also provide evidence for the origins and evolutionary processes. Employing site-specific mutagenesis, homology modeling, and docking studies, scientists reveal that the structure made by the amino acids at a specific site contributes to substrate preference and catalytic activity. Many enzyme engineering strategies used for high content LCPUFAs rich oil synthesis were also summarized. Thus, the review of these important advances on desaturase and elongase could not only provide extensive data for enzyme rational design and modification but also light up the way for the efficiency LCPUFAs rich oil production.

As shown in **Table 2**, many researchers have created the desaturase mutants with single-site and multisite. Combining the catalytic performance of each mutant with the results from homologous modeling, they can deduce the position of crucial amino acids related to the catalytic activity and substrate preference. However, it is a nonrational and time-consuming process that much work was an indispensable part of harvesting positive mutants. Moreover, most of the time, we do not obtain positive mutants, fortunately. So, it is essential to utilize these hard-earned data, whether positive or negative. Thus, the database could be constructed from positive and negative catalytic performance as listed in **Table 2**, which could serve as a sample of artificial intelligence (AI) learning. After training and learning are repeated, it will obtain the undisclosed objective laws and provide us a better experimental scheme potential. At last, the AI model will guide us in moving in the right direction and approach the enzyme with higher catalytic activity quickly (90, 91).

Scientists have identified many kinds of desaturase and elongase from different organisms and analyzed their amino acid composition and substrate preference. However, the lacke of three-dimensional crystal structure data still restricts the comprehensive and deep analysis of these enzymes, which remain an excellent challenge for researcher. On the one hand, the cryo-electron microscopy technique has been widely applied in analyzing transmembrane protein, which could provide a reliable experimental basis for modeling (92). On the other hand, the rapid-developed AI techniques (such

as AlphaFold and RoseTTAFold) are also a powerful tool for protein structure prediction, which could guide enzyme design and modifications (93, 94). Combined crystal structure analysis with molecular dynamics simulation, we can explore more information from catalytic efficiency, structure change, electron and proton transfer, which could provide a rational strategy to enhance catalytic performance, change substrate preference, improve catalytic stability. Novel technology, including nanopore (95), scanning tunneling microscope-break junction (96), atomic force microscope (97), and optical tweezers (98) will enable scientists to go a step further in enzyme research. Beyond that, metabolic engineering equipped with machine learning techniques (neural network and Bayesian optimization etc.) (99, 100), and omics analysis (101, 102) could also be employed to design, regulate, and optimize the metabolic pathway for high-efficiency LCPUFAs rich oil production. In the future, comprehensive interdisciplinary research will become the theme and contribute to enzymatic research.

AUTHOR CONTRIBUTIONS

X-YZ, Y-HZ, A-FX, and B-SF planned the manuscript, wrote and revised it. They were helped by A-HZ in revision and writing. All authors contributed to the article and approved the submitted version.

FUNDING

The National Postdoctoral Program for Innovative Talents (No. BX20200197) and National Natural Science Foundation of China (No. 21978245).

ACKNOWLEDGMENTS

The authors would like to thank the National Postdoctoral Program for Innovative Talents (No. BX20200197) and National Natural Science Foundation of China (No. 21978245) for their support.

REFERENCES

1. Lim JM, Vikramathithan J, Hwangbo K, Ahn JW, Park YI, Choi DW, et al. Threonine 286 of fatty acid desaturase 7 is essential for omega-3 fatty acid desaturation in the green microalga *Chlamydomonas reinhardtii*. *Front Microbiol.* (2015) 6:1–8. doi: 10.3389/fmicb.2015.00066
2. Zhang Y, Zhang TY, Liang Y, Jiang LZ, Sui XN. Dietary bioactive lipids: a review on absorption, metabolism, and health properties. *J Agr Food Chem.* (2021) 69:8929–43. doi: 10.1021/acs.jafc.1c01369
3. Duan JJ, Song YY, Zhang X, Wang CJ. Effect of omega-3 polyunsaturated fatty acids-derived bioactive lipids on metabolic disorders. *Front Physiol.* (2021) 12:646491. doi: 10.3389/fphys.2021.646491
4. Ji XJ, Ren LJ, Huang H. Omega-3 biotechnology: a green and sustainable process for omega-3 fatty acids production. *Front Bioeng Biotech*. (2015) 3:158. doi: 10.3389/fbioe.2015.00158
5. FAO/WHO (Food and Agriculture Organization of the United Nations/ World Health Organization). Fats and oils in human nutrition. Report of a joint expert consultation. Food and Agriculture Organization of the United Nations, Rome, Italy (1994)s.
6. Leonard AE, Pereira SL, Sprecher H, Huang YS. Elongation of long chain fatty acids. *Prog Lipid Res.* (2004) 43:36–54. doi: 10.1016/S0163-7827(03)00040-7
7. Palmerini CA, Mazzoni M, Giovinazzo G, Arient G. Blood lipids in Antarctic and in temperate-water fish species. *J Membr Biol.* (2009) 230:125–31. doi: 10.1007/s00232-009-9192-2
8. Sahena F, Zaidul ISM, Jinap S, Saari N, Jahurul HA, Abbas KA, et al. PUFAs in fish: extraction, fractionation, importance in health. *Compr Rev Food Sci F.* (2009) 8:59–74. doi: 10.1111/j.1541-4337.2009.00069.x
9. Liu C, Chen FS, Xia YM. Composition and structural characterization of peanut crude oil bodies extracted by aqueous enzymatic method. *J Food Compos Anal.* (2022) 105:104238. doi: 10.1016/j.jfca.2021.104238
10. Belury MA, Raatz SS, Conrad Z. Modeled substitution of traditional oils with high oleic acid oils decreases essential fatty acid intake in children. *Am J Clin Nutr*. (in press). doi: 10.1093/ajcn/nqab407
11. Sun XM, Ren LJ, Bi ZQ, Ji XJ, Zhao QY, Jiang L, et al. Development of a cooperative two-factor adaptive-evolution method to enhance lipid production and prevent lipid peroxidation in *Schizochytrium sp*. *Biotechnol Biofuels.* (2018) 11:65. doi: 10.1186/s13068-018-1065-4
12. Carlson KM, Heilmayr R, Gibbs HK, Noojipady P, Burns DN, Morton DC, et al. Effect of oil palm sustainability certification on deforestation and fire in Indonesia. *P Natl Acad Sci USA*. (2018) 115:121–6. doi: 10.1073/pnas.1704728114
13. Barclay WR, Meager KM, Abril JR. Heterotrophic production of long chain omega-3 fatty acids utilizing algae and algaelike microorganisms. *J Appl Phycol.* (1994) 6:123–9. doi: 10.1007/BF02186066
14. Jiang JY, Zhu SY, Zhang YT, Sun XM, Hu XC, Huang H, et al. Integration of lipidomic and transcriptomic profiles reveals novel genes and regulatory mechanisms of *Schizochytrium sp*. in response to salt stress.s *Bioresource Technol.* (2019) 294:122231. doi: 10.1016/j.biortech.2019.122231
15. Rayaroth A, Tomar RS, Mishra RK. One step selection strategy for optimization of media to enhance arachidonic acid production under solid state fermentation. *LWT-Food Sci Technol.* (2021) 152:112366. doi: 10.1016/j.lwt.2021.112366
16. Ma W, Wang YZ, Nong FT, Du F, Xu YS, Huang PW. An emerging simple and effective approach to increase the productivity of *thraustochytrids microbial* lipids by regulating glycolysis process and triacylglycerols' decomposition. *Biotechnol Biofuels.* (2021) 14:247. doi: 10.1186/s13068-021-02097-4
17. Lu R, Cao LZ, Wang KF, Ledesma-Amaro R, Ji XJ. Engineering *Yarrowia lipolytica* to produce advanced biofuels: Current status and perspectives. *Bioresource Technol.* (2021) 341:125877. doi: 10.1016/j.biortech.2021.125877
18. Wang QT, Feng YB, Lu YD, Xin Y, Shen C, Wei L, et al. Manipulating fatty-acid profile at unit chain-length resolution in the model industrial oleaginous microalgae nannochloropsis. *Metab Eng.* (2021) 66:157–66. doi: 10.1016/j.ymben.2021.03.015
19. Ji XJ, Zhang AH, Nie ZK, Wu WJ, Ren LJ, Huang H. Efficient arachidonic acid-rich oil production by *Mortierella alpina* through a repeated fed-batch fermentation strategy. *Bioresource Technol.* (2014) 170:356–60. doi: 10.1016/j.biortech.2014.07.098
20. Zhu Z, Zhang S, Liu H, Shen H, Lin X, Yang F, et al. A multi-omic map of the lipid-producing yeast *Rhodosporidium toruloides*. *Nat Commun.* (2012) 3:1–11. doi: 10.1038/ncomms2112
21. Garba L, Yussoff MAM, Abd Halimi KB, Ishak SNH, Ali MSM, Oslan SN, et al. Homology modeling and docking studies of a delta 9-fatty acid desaturase from a cold-tolerant *Pseudomonas sp* AMS8. *Peer J.* (2018) 6:e4347. doi: 10.7717/peerj.4347
22. Smith R, Jouhet J, Gandini C, Nekrasov V, Marechal E, Napier JA. Plastidial acyl carrier protein Delta 9-desaturase modulates eicosapentaenoic acid biosynthesis and triacylglycerol accumulation in Phaeodactylum tricornutum. *Plant J.* 106:1247–59. doi: 10.1111/tpj.15231
23. Liu BL, Sun Y, Hang W, Wang XD, Xue JN, Ma RY, et al. Characterization of a novel acyl-ACP Δ^9 desaturase gene responsible for palmitoleic acid accumulation in a diatom *Phaeodactylum tricornutum*. *Front Microbiol.* (2020) 11:584589. doi: 10.3389/fmicb.2020.584589

24. Han XT, Wang S, Zheng L, Liu WS. Identification and characterization of a delta-12 fatty acid desaturase gene from marine microalgae *Isochrysis galbana*. *Acta Oceanol Sin.* (2019) 38:107–13. doi: 10.1007/s13131-019-1354-1
25. Sayanova O, Haslam R, Guschina I, Lloyd D, Christie WW, Harwood JL, et al. A bifunctional delta 12, delta 15-desaturase from *Acanthamoeba castellanii* directs the synthesis of highly unusual n-1 series unsaturated fatty acids. *J Bio Chem.* (2006) 281:36533–41. doi: 10.1074/jbc.M605158200
26. Zhang PY, Liu SH, Cong BL, Wu GT, Liu CL, Lin XZ, et al. A novel omega-3 fatty acid desaturase involved in acclimation processes of polar condition from Antarctic ice algae *Chlamydomonas sp*. ICE-L. *Mar Biotechnol.* (2011) 13:393–401. doi: 10.1007/s10126-010-9309-8
27. Qiu X, Reed DW, Hong H, MacKenzie SL, Covello PS. Identification and analysis of a gene from calendula officinalis encoding a fatty acid conjugase. *Plant Physiol.* (2001) 125:847–55. doi: 10.1104/pp.125.2.847
28. Martinez-Rivas JM, Sperling P, Luehs W, Heinz E. Spatial and temporal regulation of three different microsomal oleate desaturase genes (FAD2) from normal-type and high-oleic varieties of sunflower (*Helianthus annuus L*). *Mol Breed.* (2001) 8:159–68. doi: 10.1023/A:1013324329322
29. Lu YD, Chi XY, Yang QL, Li ZX, Liu SF, Gan QH, et al. Molecular cloning and stress-dependent expression of a gene encoding Δ12-fatty acid desaturase in the *Antarctic microalga* Chlorella vulgaris NJ-7. *Extremophiles*. (2009) 13:875–84. doi: 10.1007/s00792-009-0275-x
30. Domergue F, Spiekermann P, Lerchl J, Beckmann C, Kilian O, Kroth PG, et al. New insight into *Phaeodactylum tricornutum* fatty acid metabolism cloning and functional characterization of plastidial and microsomal delta12-fatty acid desaturases. *Plant Physiol.* (2003) 131:1648–60. doi: 10.1104/pp.102.018317
31. Zhang L, Chen WB, Yang SP, Zhang YB, Xu JL, Yang DJ, et al. Identification and functional characterization of a novel delta 12 fatty acid desaturase gene from *Haematococcus pluvialis*. *J Ocean U China.* (2020) 19:1362–70. doi: 10.1007/s11802-020-4418-0
32. Wu CC, Ohashi T, Kajiura H, Sato Y, Misaki R, Honda K, et al. Functional characterization and overexpression of delta 12-desaturase in the oleaginous yeast *Rhodotorula toruloides* for production of linoleic acid-rich lipids. *J Biosci Bioeng.* (2021) 131:631–9. doi: 10.1016/j.jbiosc.2021.02.002
33. Hsiao TY, Holmes B, Blanch HW. Identification and functional analysis of a delta-6 desaturase from the marine microalga *Glossomastix chrysoplasta*. *Mar Biotechnol.* (2007) 9:154–65. doi: 10.1007/s10126-006-6075-8
34. Zhang R, Zhu Y, Ren L, Zhou P, Hu J, Yu L. Identification of a fatty acid Δ6-desaturase gene from the eicosapentaenoic acid-producing fungus *Pythium splendens* RBB-5. *Biotechnol Lett.* (2013) 35:431–8. doi: 10.1007/s10529-012-1101-6
35. Zhang L, Cao HS, Ning P, Zhou ZG. Functional characterization of a Δ6 fatty acid desaturase gene and its 5′-upstream region cloned from the arachidonic acidrich microalga *Myrmecia incisa* Reisigl (Chlorophyta). *J Oceanol Limnol.* (2018) 36:2308–21. doi: 10.1007/s00343-019-7305-z
36. Laoteng K, Ruenwai R, Tanticharoen M, Cheevadhanarak S. Genetic modification of essential fatty acids biosynthesis in *Hansenula polymorpha*. *FEMS Microbiol Lett.* (2005) 245:169–78. doi: 10.1016/j.femsle.2005.03.006
37. Cui J, Chen H, Tang X, Zhang H, Chen YQ, Chen W. Consensus mutagenesis and computational simulation provide insight into the desaturation catalytic mechanism for delta 6 fatty acid desaturase. *Biochem Bioph Res Co.* (2022) 586:74–80. doi: 10.1016/j.bbrc.2021.11.050
38. Araki H, Hagihara H, Takigawa H, Tsujino Y, Ozaki K. Novel genes encoding hexadecanoic acid delta 6-desaturase activity in a *Rhodococcus sp*. *Curr Microbiol.* (2016) 73:646–51. doi: 10.1007/s00284-016-1106-9
39. Jeennor S, Cheawchanlertfa P, Suttiwattanakul S, Panchanawaporn S, Chutrakul C, Laoteng K. The codon-optimized Δ6-desaturase gene of *Pythium sp*. as an empowering tool for engineering n3/n6 polyunsaturated fatty acid biosynthesis. *BMC Biotechnol.* (2015) 15:82. doi: 10.1186/s12896-015-0200-6
40. Shi HS, Luo X, Wu RN, Yue XQ. Production of eicosapentaenoic acid by application of a delta-6 desaturase with the highest ALA catalytic activity in algae. *Microb Cell Fact.* (2018) 17:2–15. doi: 10.1186/s12934-018-0857-3
41. Tonon T, Sayanova O, Michaelson LV, Qing R, Harvey D, Larson TR, et al. Fatty acid desaturases from the microalga *Thalassiosira pseudonana*. *FEBS J.* (2005) 272:3401–12. doi: 10.1111/j.1742-4658.2005.04755.x
42. Thiyagarajan S, Arumugam M, Senthil N, Vellaikumar S, Kathiresan S. Functional characterization and substrate specificity analysis of delta6-desaturase from marine microalga *Isochrysis sp*. *Biotechnol Lett.* (2018) 40:577–84. doi: 10.1007/s10529-017-2501-4
43. Michinaka Y, Aki T, Shimauchi T, Nakajima T, Kawamoto S, Shigeta S, et al. Differential response to low temperature of two delta 6 fatty acid desaturases from *Mucor circinelloides*. *Appl Microbiol Biot.* (2003) 62:362–8. doi: 10.1007/s00253-003-1326-3
44. Tavares S, Grotkjaer T, Obsen T, Haslam RP, Napier JA, Gunnarsson N. Metabolic engineering of *Saccharomyces cerevisiae* for production of eicosapentaenoic acid, using a novel detal 5-desaturase from *Paramecium tetraurelia*. *Appl Environ Microb.* (2011) 77:1854–61. doi: 10.1128/AEM.01935-10
45. Kumon Y, Kamisaka Y, Tomita N, Kimura K, Uemura H, Yokochi T, et al. Isolation and characterization of a delta 5-desaturase from *Oblongichytrium sp*. *Biosci Biotech Bioch.* (2008) 72:2224–7. doi: 10.1271/bbb.80235
46. Huang JZ, Jiang XZ, Xia XF, Yu AQ, Mao RY, Chen XF, et al. Cloning and functional identification of delta5 fatty acid desaturase gene and its 5 ’-upstream region from marine fungus *Thraustochytrium sp*. FJN-10. *Mar Biotechnol*. 13:12–21. doi: 10.1007/s10126-010-9262-6
47. Kobayashi T, Sakaguchi K, Matsuda T, Abe E, Hama Y, Hayashi M, et al. Increase of eicosapentaenoic acid in *Thraustochytrids* through *Thraustochytrid Ubiquitin* promoter-driven expression of a fatty acid delta 5 desaturase gene. *Appl Environ Microb.* (2011) 77:3870–6. doi: 10.1128/AEM.02664-10
48. Thiyagarajan S, Khandelwal P, Senthil N, Vellaikumar S, Arumugam M, Dubey AA, et al. Heterologous production of polyunsaturated fatty acids in *E. coli* using delta 5-desaturase gene from microalga *Isochrysis sp*. *Appl Biochem Biotech.* (2021) 193:869–83. doi: 10.1007/s12010-020-03460-1
49. Shi TL, Yu AQ, Li M, Ou XY, Xing LJ, Li MC. Identification of a novel C22-D4-producing docosahexaenoic acid (DHA) specific polyunsaturated fatty acid desaturase gene from *Isochrysis galbana* and its expression in *Saccharomyces cerevisiae*. *Biotechnol Lett.* (2012) 34:2265–74. doi: 10.1007/s10529-012-1028-y
50. Guo B, Jiang ML, Wan X, Gong YM, Liang Z, Hu CJ. Identification and heterologous expression of a δ4-fatty acid desaturase gene from *Isochrysis sphaerica*. *J Microbiol Biotechnol.* (2013) 23:1413–21. doi: 10.4014/jmb.1301.01065
51. Ahmann K, Heilmann M, Feussner I. Identification of a delta 4-desaturase from the microalga *Ostreococcus lucimarinus*. *Eur J Lipid Sci Tech.* (2011) 113:832–40. doi: 10.1002/ejlt.201100069
52. Tonon T, Harvey D, Larson TR, Graham IA. Identification of a very long chain polyunsaturated fatty acid delta4-desaturase from the microalga *Pavlova lutheri*. *FEBS Lett.* (2003) 553:440–4. doi: 10.1016/S0014-5793(03)01078-0
53. Xu Y, Niu Y, Kong J. Heterologous overexpression of a novel delta-4 desaturase gene from the marine microalga *Pavlova viridis* in *Escherichia coli* as a Mistic fusion. *World J Microbiol Biotechnol.* (2011) 27:2931–7. doi: 10.1007/s11274-011-0776-5
54. Tsai YY, Ohashi T, Wu CC, Bataa D, Misaki R, Limtong S, et al. Delta-9 fatty acid desaturase overexpression enhanced lipid production and oleic acid content in *Rhodosporidium toruloides* for preferable yeast lipid production. *J Biosci Bioeng.* (2019) 127:430–40. doi: 10.1016/j.jbiosc.2018.09.005
55. Ben Amor F. Ben, Hlima H, Abdelkafi S, Fendri I. Insight into Arthrospira platensis delta 9 desaturase: a key enzyme in poly-unsaturated fatty acid synthesis. *Mol Biol Rep.* (2018) 45:1873–9. doi: 10.1007/s11033-018-4333-2
56. Sakuradani E, Abe T, Matsumura K, Tomi A, Shimizu S. Identification of mutation sites on delta 12 desaturase genes from *Mortierella alpina* 1S-4 mutants. *J Biosci Bioeng.* (2009) 107:99–101. doi: 10.1016/j.jbiosc.2008.10.011
57. Shi HS, Chen HQ, Gu ZN, Song Y, Zhang H, Chen W, et al. Molecular mechanism of substrate specificity for delta 6 desaturase from *Mortierella alpina* and *Micromonas pusilla*. *J Lipid Res.* (2015) 56:2309–21. doi: 10.1194/jlr.M062158
58. Rong CC, Chen HQ, Wang MX, Gu ZN, Zhao JX, Zhang H, et al. Molecular mechanism of substrate preference for ω-3 fatty acid desaturase from *Mortierella alpina* by mutational analysis and molecular docking. *Appl Microbiol Biotechnol.* (2018) 102:9679–89. doi: 10.1007/s00253-018-9321-x

59. Rau EM, Aasen IM, Ertesvåg H. A non-canonical delta 9-desaturase synthesizing palmitoleic acid identified in the thraustochytrid *Aurantiochytrium sp*. T66.*s Appl Microbiol Biot.* (2021) 105:75. doi: 10.1007/s00253-021-11562-x
60. Tezaki S, Iwama R, Kobayashi S, Shiwa Y, Yoshikawa H, Ohta A, et al. Detal 12-fatty acid desaturase is involved in growth at low temperature in yeast *Yarrowia lipolytica*. *Biochem Biophy Res Co.* (2017) 488:165–70. doi: 10.1016/j.bbrc.2017.05.028
61. Wang YN, Zhang SF, Pötter M, Sun WY, Li L, Yang XB, et al. Overexpression of Δ12-fatty acid desaturase in the oleaginous yeast *Rhodosporidium toruloides* for production of linoleic acid-rich lipids. *Appl Biochem Biotechnol.* (2016) 180:1497–507. doi: 10.1007/s12010-016-2182-9
62. Jiang XZ, Liu HJ, Niu YC, Qi F, Zhang ML, Huang JZ. Functional identification and regulatory analysis of detal 6-fatty acid desaturase from the oleaginous fungus *Mucor sp*. EIM-10. *Biotechnol Lett.* (2017) 39:453–61. doi: 10.1007/s10529-016-2268-z
63. Zhu BH, Tu CC, Shi HP, Yang GP, Pan KH. Overexpression of endogenous delta-6 fatty acid desaturase gene enhances eicosapentaenoic acid accumulation in *Phaeodactylum tricornutum*. *Process Biochem.* (2017) 57:43–9. doi: 10.1016/j.procbio.2017.03.013
64. Chen G, Qu SJ, Wang Q, Bian F, Peng ZY, Zhang Y, et al. Transgenic expression of delta-6 and delta-15 fatty acid desaturases enhances omega-3 polyunsaturated fatty acid accumulation in *Synechocystis sp*. PCC6803. *Biotechnol Biofuels.* (2014) 7:2–10. doi: 10.1186/1754-6834-7-32
65. Petrie JR, Shrestha P, Mansour MP, Nichols PD, Liu Q, Singh SP. Metabolic engineering of omega-3 long-chain polyunsaturated fatty acids in plants using an acyl-CoA Δ6-desaturase with ω3-preference from the marine microalga *Micromonas pusilla*. *Metab Eng.* (2010) 12:233–40. doi: 10.1016/j.ymben.2009.12.001
66. Shi HS, Chen HQ, Gu ZN, Zhang H, Chen W, Chen YQ. Application of a delta-6 desaturase with α-linolenic acid preference on eicosapentaenoic acid production in *Mortierella alpina*. *Microb Cell Fact.* (2016) 15:2–14. doi: 10.1186/s12934-016-0516-5
67. Yang F, Yuan W, Ma Y, Balamurugan S, Li HY, Fu S, et al. Harnessing the lipogenic potential of detal 16-desaturase for simultaneous hyperaccumulation of lipids and polyunsaturated fatty acids in *Nannochloropsis oceanica*. *Front Mar Sci.* (2019) 6:682. doi: 10.3389/fmars.2019.00682
68. Song LY, Zhang Y, Li SF, Hu J, Yin WB, Chen YH, et al. Identification of the substrate recognition region in the Δ6-fatty acid and Δ8-sphingolipid desaturase by fusion mutagenesis. *Planta.* (2014) 239:753–63. doi: 10.1007/s00425-013-2006-x
69. Kikukawa H, Sakuradani E, Ando A, Okuda T, Shimizu S, Ogawa J. Microbial production of dihomo-gamma-linolenic acid by delta 5-desaturase gene-disruptants of *Mortierella alpina* 1S-4. *J Biosci Bioeng.* (2016) 122:22–6. doi: 10.1016/j.jbiosc.2015.12.007
70. Peng KT, Zheng CN, Xue J, Chen XY, Yang WD, Liu JS, et al. Delta 5 fatty acid desaturase upregulates the synthesis of polyunsaturated fatty acids in the marine diatom *Phaeodactylum tricornutum*. *J Arg Food Chem.* (2014) 62:8773–6. doi: 10.1021/jf5031086
71. Nguyen HM, Cuine S, Beyly-Adriano A, Legeret B, Billon E, Auroy P, et al. The green microalga Chlamydomonas reinhardtii has a single omega-3 fatty acid desaturase that localizes to the chloroplast and impacts both plastidic and extraplastidic membrane lipids. *Plant Physiol.* (2013) 163:914–28. doi: 10.1104/pp.113.223941
72. Liu HL, Wang H, Cai SY, Zhang HB. A Novel ω3-desaturase in the deep sea giant tubeworm *Riftia pachyptila*. *Mar Biotechnol.* (2017) 19:345–50. doi: 10.1007/s10126-017-9753-9
73. Wang M, Chen H, Ailati A, Chen W, Chilton FH, Lowther WT, et al. Substrate specificity and membrane topologies of the iron-containing ω3 and ω6 desaturases from *Mortierella alpina*. *Appl Microbiol Biotechnol.* (2017) 102:211–23. doi: 10.1007/s00253-017-8585-x
74. Xue Z, He H, Hollerbach D, Macool DJ, Yadav NS, Zhang H, et al. Identification and characterization of new detal-17 fatty acid desaturases. *Appl Microbiol Biotechnol.* (2013) 97:1973–85. doi: 10.1007/s00253-012-4068-2
75. Wang L, Chen W, Feng Y, Ren Y, Gu Z, Chen H, et al. Genome characterization of the oleaginous fungus *Mortierella alpina*. *PLoS ONE.* (2011) 6:e28319. doi: 10.1371/journal.pone.0028319
76. Okuda T, Ando A, Negoro H, Muratsubaki T, Kikukawa H, Sakamoto T, et al. Eicosapentaenoic acid (EPA) production by an oleaginous fungus *Mortierella alpina* expressing heterologous the detal 7-desaturase gene under ordinary temperature. *Eur J Lipid Sci Technol.* (2015) 117:1919–27. doi: 10.1002/ejlt.201400657
77. Fu Y, Fan XZ, Li XZ, Wang H, Chen HJ. The desaturase opin17 from phytophthora infestans converts arachidonic acid to eicosapentaenoic acid in CHO cells. *Appl Biochem Biotech.* (2013) 171:975–88. doi: 10.1007/s12010-013-0332-x
78. Ge CF, Chen HQ, Mei TT, Tang X, Chang LL, Gu ZN, et al. Application of a ω-3 desaturase with an arachidonic acid preference to eicosapentaenoic acid production in *Mortierella alpina*. *Front Bioeng Biotechnol.* (2018) 5:1–10. doi: 10.3389/fbioe.2017.00089
79. Tang X, Chen HQ, Mei TT, Ge CF, Gu ZN, Zhang H, et al. Characterization of an omega-3 desaturase from phytophthora parasitica and application for eicosapentaenoic acid production in *Mortierella alpina*. *Front Microbiol.* (2018) 9:1878. doi: 10.3389/fmicb.2018.01878
80. Ren LJ, Zhuang XY, Chen SL, Ji XJ, Huang H. Introduction of ω-3 desaturase obviously changed the fatty acid profile and sterol content of *Schizochytrium sp*. *J Agric Food Chem.* (2015) 63:9770–6. doi: 10.1021/acs.jafc.5b04238
81. Yu SY, Li H, Tong M, Ouyang LL, Zhou ZG. Identification of a Δ6 fatty acid elongase gene for arachidonic acid biosynthesis localized to the endoplasmic reticulum in the green microalga *Myrmecia incisa* Reisigl. *Gene.* (2012) 493:219–27. doi: 10.1016/j.gene.2011.11.053
82. Jeennor S, Cheawchanlertfa P, Suttiwattanakul S, Panchanawaporn S, Chutrakul C, Laoteng K. Novel elongase of *Pythium sp* with high specificity on delta (6)-18C desaturated fatty acids. *Biochem Bioph Res Co.* (2014) 450:507–12. doi: 10.1016/j.bbrc.2014.06.004
83. Tamano K, Yasunaka Y, Kamishima M, Itoh A, Miura A, Kan E, et al. Enhancement of the productivity of free dihomo-gamma-linolenic acid via co-overexpression of elongase and two desaturase genes in *Aspergillus oryzae*. *J Biosci Bioeng.* (2020) 130:480–8. doi: 10.1016/j.jbiosc.2020.07.004
84. Shi Y, Liu MJ, Pan YF, Hu HH, Liu J. Δ6 Fatty acid elongase is involved in eicosapentaenoic acid biosynthesis *via* the ω6 pathway in the marine alga *Nannochloropsis oceanica*. *J Agric Food Chem.* (2021) 69:9837–48. doi: 10.1021/acs.jafc.1c04192
85. Poliner E, Pulman JA, Zienkiewicz K, Childs K, Benning C, Farre EM, et al. A toolkit for *Nannochloropsis oceanica* CCMP1779 enables gene stacking and genetic engineering of the eicosapentaenoic acid pathway for enhanced long-chain polyunsaturated fatty acid production. *Plant Biotechnol J.* (2018) 16:298–309. doi: 10.1111/pbi.12772
86. Robert SS, Petrie JR, Zhou XR, Mansour MP, Blackburn SI, Green AG, et al. Isolation and characterisation of a delta 5-fatty acid elongase from the marine microalga *Pavlova salina*. *Mar Biotechnol.* (2009) 11:410–8. doi: 10.1007/s10126-008-9157-y
87. Niu Y, Kong J, Fu LY, Yang J, Xu Y. Identification of a novel C20-elongase gene from the marine microalgae *Pavlova viridis* and its expression in *Escherichia coli*. *Mar Biotechnol.* (2009) 11:17–23. doi: 10.1007/s10126-008-9116-7
88. Jiang ML, Guo B, Wan X, Gong YM, Zhang YB, Hu CJ. Isolation and characterization of the Diatom *Phaeodactylum* Δ5-Elongase gene for transgenic LC-PUFA production in *Pichia pastoris*. *Mar Drugs.* (2014) 12:1317–34. doi: 10.3390/md12031317
89. Kaewsuwan S, Bunyapraphatsara N, Cove DJ, Quatrano RS, Chodok P. High level production of adrenic acid in *Physcomitrella patens* using the algae *Pavlova sp* delta (5)-elongase gene. *Bioresource Technol.* (2010) 101:4081–8. doi: 10.1016/j.biortech.2009.12.138
90. Hie Brian L, Yang Kevin K. Adaptive machine learning for protein engineering. *Curr Opin Struc Biol.* (2021) 72:145–52. doi: 10.1016/j.sbi.2021.11.002
91. Pertusi DA, Moura ME, Jeffryes JG, Prabhu S, Biggs BW, Tyo KEJ. Predicting novel substrates for enzymes with minimal experimental effort with active learning. *Metab Eng.* (2017) 44:171–81. doi: 10.1016/j.ymben.2017.09.016
92. Gauto DF, Estrozi LF, Schwieters CD, Effantin G, Macek P, Sounier R, et al. Integrated NMR and cryo-EM atomic-resolution structure

determination of a half-megadalton enzyme complex. *Nature Commun.* (2019) 10:2697. doi: 10.1038/s41467-019-10490-9
93. Tunyasuvunakool K, Adler J, Wu Z, Green T, Zielinski M, Zidek A, et al. Highly accurate protein structure prediction for the human proteome. *Nature*. (2021) 596:590–6. doi: 10.1038/s41586-021-03828-1S
94. Baek M, DiMaio F, Anishchenko I, Dauparas J, Ovchinnikov S, Lee GR, et al. Accurate prediction of protein structures and interactions using a three-track neural network. *Science.* (2021) 373:871–6. doi: 10.1126/science.abj8754
95. Cao MY, Wang H, Tang HR, Zhao DD, Li YX. Enzyme-encapsulated zeolitic imidazolate frameworks formed inside the single glass nanopore: catalytic performance and sensing application. *Anal Chem.* (2021) 93:12257–64. doi: 10.1021/acs.analchem.1c01790
96. Zhuang XY, Zhang AH, Qiu SY, Tang C, Zhao SQ, Li HC, et al. Coenzyme coupling boosts charge transport through single bioactive enzyme junctions. *IScience.* (2020) 23:101001. doi: 10.1016/j.isci.2020.101001
97. Liu JY, Ghanizadeh H, Li XM, Han ZY, Qiu YW, Zhang Y, et al. study of the interaction, morphology, and structure in trypsin-epigallocatechin-3-gallate complexes. *Molecule.* (2021) 26:4567. doi: 10.3390/molecules26154567
98. Zhuang XY, Wu Q, Zhang AH, Liao LX, Fan BS. Single-molecule biotechnology for protein researches. *Chinese J Chem Eng.* (2021) 30:212–24. doi: 10.1016/j.cjche.2020.10.031
99. Kumar P, Adamczyk PA, Zhang XL, Andrade RB, Romero PA, Ramanathan P, et al. Active and machine learning-based approaches to rapidly enhance microbial chemical production. *Metab Eng.* (2021) 67:216–26. doi: 10.1016/j.ymben.2021.06.009
100. Czajka JJ, Oyetunde T, Tang YJ. Integrated knowledge mining, genome-scale modeling, and machine learning for predicting *Yarrowia lipolytica* bioproduction. *Metab Eng.* (2021) 67:227–36. doi: 10.1016/j.ymben.2021.07.003
101. Kennes-Veiga DM, Gonzalez-Gil L, Carballa M, Lema JM. Enzymatic cometabolic biotransformation of organic micropollutants in wastewater treatment plants: a review. *Bioresource Technol.* (2022) 344:126291. doi: 10.1016/j.biortech.2021.126291
102. Zhang AH, Ji XJ, Wu WJ, Ren LJ, Yu YD, Huang H. Lipid fraction and intracellular metabolite analysis reveal the mechanism of arachidonic acid-rich oil accumulation in the aging process of *Mortierella alpina*. *J Agr Food Chem.* (2015) 63:9812–9. doi: 10.1021/acs.jafc.5b04521

Conflict of Interest: The authors declare that the research was conducted in the absence of any commercial or financial relationships that could be construed as a potential conflict of interest.

Publisher's Note: All claims expressed in this article are solely those of the authors and do not necessarily represent those of their affiliated organizations, or those of the publisher, the editors and the reviewers. Any product that may be evaluated in this article, or claim that may be made by its manufacturer, is not guaranteed or endorsed by the publisher.

frontiers | Frontiers in Nutrition

ORIGINAL RESEARCH
published: 26 April 2022
doi: 10.3389/fnut.2022.876649

Strategic Development of *Aurantiochytrium* sp. Mutants With Superior Oxidative Stress Tolerance and Glucose-6-Phosphate Dehydrogenase Activity for Enhanced DHA Production Through Plasma Mutagenesis Coupled With Chemical Screening

Yusuf Nazir[1,2,3], Pranesha Phabakaran[1], Hafiy Halim[1], Hassan Mohamed[1,4], Tahira Naz[1], Aidil Abdul Hamid[5]* and Yuanda Song[1]**

[1] Colin Ratledge Center for Microbial Lipids, School of Agricultural Engineering and Food Science, Shandong University of Technology, Zibo, China, [2] Department of Food Sciences, Faculty of Science and Technology, Universiti Kebangsaan Malaysia, Bangi, Malaysia, [3] Innovation Centre for Confectionery Technology (MANIS), Faculty of Science and Technology, Universiti Kebangsaan Malaysia, Bangi, Malaysia, [4] Department of Botany and Microbiology, Faculty of Science, Al-Azhar University, Assiut, Egypt, [5] Department of Bioscience and Biotechnology, Universiti Kebangsaan Malaysia, Bangi, Malaysia

Thraustochytrids, such as *Aurantiochytrium* and *Schizochytrium*, have been shown as a promising sustainable alternative to fish oil due to its ability to accumulate a high level of docosahexaenoic acid (DHA) from its total fatty acids. However, the low DHA volumetric yield by most of the wild type (WT) strain of thraustochytrids which probably be caused by the low oxidative stress tolerance as well as a limited supply of key precursors for DHA biosynthesis has restricted its application for industrial application. Thus, to enhance the DHA production, we aimed to generate *Aurantiochytrium* SW1 mutant with high tolerance toward oxidative stress and high glucose-6 phosphate dehydrogenase (G6PDH) activities through strategic plasma mutagenesis coupled with chemical screening. The WT strain (*Aurantiochytrium* sp. SW1) was initially exposed to plasma radiation and was further challenged with zeocin and polydatin, generating a mutant (YHPM1) with a 30, 65, and 80% higher overall biomass, lipid, and DHA production in comparison with the parental strains, respectively. Further analysis showed that the superior growth, lipid, and DHA biosynthesis of the YHMP1 were attributed not only to the higher G6PDH and enzymes involved in the oxidative defense such as superoxide dismutase (SOD) and catalase (CAT) but also to other key metabolic enzymes involved in lipid biosynthesis. This study provides an effective approach in developing the *Aurantiochytrium* sp. mutant with superior DHA production capacity that has the potential for industrial applications.

Keywords: thraustochytrids, plasma mutagenesis, chemical screening, DHA production, zeocin, polydatin, *Aurantiochytrium*

OPEN ACCESS

Edited by:
Jinsong Bao,
Zhejiang University, China

Reviewed by:
Sachin Vyas,
Luleå University of Technology, Sweden
Xu Zhou,
Harbin Institute of Technology, China

****Correspondence:***
Yusuf Nazir
yusufnazir@ukm.edu.my
Aidil Abdul Hamid
aidilmikrob@gmail.com
Yuanda Song
ysong@sdut.edu.cn

Specialty section:
This article was submitted to Food Chemistry, a section of the journal Frontiers in Nutrition

Received: *15 February 2022*
Accepted: *11 March 2022*
Published: *26 April 2022*

Citation:
Nazir Y, Phabakaran P, Halim H, Mohamed H, Naz T, Abdul Hamid A and Song Y (2022) Strategic Development of Aurantiochytrium sp. Mutants With Superior Oxidative Stress Tolerance and Glucose-6-Phosphate Dehydrogenase Activity for Enhanced DHA Production Through Plasma Mutagenesis Coupled With Chemical Screening. Front. Nutr. 9:876649. doi: 10.3389/fnut.2022.876649

INTRODUCTION

The global demand for docosahexaenoic acid (DHA, 22:6, n-3), an essential omega-3 polyunsaturated fatty acid, has increased tremendously over the past few years and is expected to keep on growing in the future (1). DHA is commonly marketed as dietary supplements, pharmaceuticals, infant formulas, and functional foods and has been extensively applied in aqua and animal feed to generate healthier, increased growth, and survival rate for farmed fish and animals (1). DHA has been reported to be vital for human health and well-being especially in supporting the development of the brain and eye of infants as well as curing or preventing several chronic diseases including hypertension, Alzheimer, arthritis, and adult-onset diabetes mellitus (2). In addition, a recent report showed that omega-3, particularly DHA, is able to decrease severity among patients with COVID-19 by lowering the production of proinflammatory cytokines that resulted in decreased viral entry and promoted better immune function (3). Yet, despite the importance, a recent study showed that more than 90% of the global population consumed less than the recommended optimal dose of DHA (0.25 g/day) in the diet (4). Oil extracted from marine fatty fish (often referred to as fish oil), such as Salmon and Tuna, is at present the major source of DHA (4). The expanding demands for DHA worldwide are now placing pressure on both fisheries and the fish oil supply, and it is expected to be unable to meet the market demand soon. This is due to declining of the fatty fish sources due to overfishing as well as other environmental factors. There are also possible health risks associated with the consumption of fish oils, such as food poisoning and allergies, particularly when there are issues of seawater contamination or toxicity and outbreaks of fish diseases (4). Considering the disadvantages of fish-oil-based DHA and for better commercial gains, efforts have been made to find alternative sustainable sources for omega-3 fatty acid production.

Microbial oil, being produced in a controlled environment, is one of the current topics of massive research due to its sustainability and advantages compared with fish oil (5). Thraustochytrids such as *Aurantiochytrium*, *Schizochytrium*, and *Thraustochytrium* are marine heterotopic protists, commonly known as marine microalgae, which are excellent DHA producers as they are capable of producing up to 35–55% DHA from the total fatty acids (TFAs) (6). Furthermore, DHA from thraustochytrids has also been proven to be safe for human consumption as it is free from the common algal toxins such as domoic acid and prymnesin produced by some members of its kingdom Chromista (7). Therefore, its applications as a novel food supplement and infant formula have been recommended in many countries throughout the world. However, the low DHA production yield remains to be the key limiting factor for large-scale DHA production from thraustochytrids.

Although various strategies have been developed, stress-based strategies coupled with oxygen-rich culture conditions have been shown to be the most effective approaches in enhancing the lipids well as DHA biosynthesis in thraustochytrids (8–10). However, this strategy often resulted in the inevitable formation of a high level of reactive oxygen species (ROS) causing severe oxidative damage that resulted in the loss of protein function as well as peroxidation of lipid (11, 12). Lipids, particularly PUFA, are highly susceptible to oxygen radical attack, and the resulting oxidative species are detrimental to cell metabolism and limit lipid productivity (13). Several studies have found that mitigation of oxidative stress through the addition of antioxidants, strain improvement through adaptive laboratory evolution (ALE), and overexpression of the genes involved in oxidative defense has significantly improved the DHA and PUFA content in thraustochytrids (12, 14–16). Furthermore, enforcing the pool of precursors for lipid biosynthesis, particularly the Acetyl-CoA and NADPH, has also been another promising strategy to enhance lipid and DHA production in thraustochytrids (17–20). In thraustochytrids, the supply of Acetyl-CoA pool is achieved by the action of ATP-citrate lyase (ACL) that cleaves citrate to generate acetyl CoA and oxaloacetate. The subsequent conversion of acetyl CoA into fatty acids requires a high level of NADPH as the principal reductant which is predominantly supplied by malic enzymes (ME) and glucose 6-phosphate dehydrogenase (G6PDH) (21). However, studies by Cui et al. (19, 22) found that the NADPH supply for the FAS pathway (which is responsible for saturated fatty acid production in thraustochytrids) and polyketide pathways (responsible for PUFA production) might be specific where overexpression of ME, as well as the G6PDH, has been found to enhance the production of saturated fatty acids and PUFA content in *Aurantiochytrium* sp. YLH70, respectively. Thus, the generation of mutants that possess both high oxidative tolerance and G6PDH activity is hypothesized to be able to enhance the DHA production in thraustochytrids.

In this study, we aimed to generate *Aurantiochytrium* SW1 mutant with high tolerance toward oxidative stress and high G6PDH activities through plasma mutagenesis coupled with chemical screening strategies. Plasma mutagenesis is one of the most efficient techniques in generating extensive mutation in microbes as it has been proven to poses high bioavailability, high energy density, poor repair effects, and good spatial resolution of energy deposition compared with traditional radiation sources (e.g., UV, γ-, and χ-rays) (23). It has already been successfully employed for mutation breeding of different microorganisms including bacteria (24), fungi (25), and microalgae (26, 27). For increased efficiency in generating mutant with the desired traits, the mutant generated after the plasma mutagenesis will be then challenged with zeocin and polydatin, generating mutant with superior oxidative stress G6PDH activity. Zeocin is a bleomycin-family glycopeptide antibiotic (28), a potent antibiotic that significantly inhibits the growth of thraustochytrids by generating a pseudo enzyme that interacts with oxygen and creates radicals free of superoxide and hydroxide which instigate lipid peroxidation and other cellular molecule oxidations, resulting in cellular damage. In contrast, polydatin (3,4,5-trihydroxystilbene-3-β-d-glucoside; transresveratrol 3-β-mono-D-glucoside; and piceid) is a chemical compound present in polygonum cuspidate and other plants that have been reported to inhibit G6PDH, the key enzyme for pentose phosphate pathway (29). This study provides the first report that integrates plasma mutagenesis coupled with zeocin and polydatin-based screening

strategy, to generate mutants with superior tolerance to oxidative stress as well as high G6PDH activity for enhanced DHA production by thraustochytrids.

MATERIALS AND METHODS

Organism and Culture Conditions

The starting microorganism used in this study is *Aurantiochytrium* sp. SW1 (GenBank: KF500513), provided by Microbial Physiology Lab, School of Biosciences and Biotechnology, Universiti Kebangsaan Malaysia as well as Colin Ratledge Centre for Microbial Lipid, Shandong University of Technology and has been deposited in UNiCC UPM under the accession number of [UPMC 963]. This organism was maintained on seawater nutrient agar (SNA) as slant culture which contained 28 g/L nutrient agar and 17.5 g/L artificial seawater accounting for 50% (w/w) salinity. Seed cultures were prepared by inoculating 100 ml of a seeding broth with a strip of SNA slant agar containing ∼10 colonies of 48 h-old SW1 cells in 500 ml Erlenmeyer flasks. Seed cultures were then incubated at 28°C for 48 h with an agitation rate of 200 rpm. The medium used in seed cultures contained 60 g/L glucose, 2 g/L yeast extract, 10 g/L monosodium glutamate (MSG), and 6 g/L artificial sea salt. The composition of sea salt used in this study was described by Manikan et al. (6). Seed culture with an inoculum size of 10% (v/v) was then inoculated into the production medium for further study. There were two different media used as the production medium; (1) Burja which contained similar composition of the seed media and (2) glucose, peptone, and tryptone (GPT) that is also contained similar composition of glucose and sea salt as the seed media but the nitrogen sources (MSG and yeast extract) were replaced to peptone and tryptone (8+4 g/L, respectively).

Determination of SW1 Sensitivity Toward Zeocin and Polydatin

Fifty microliters of SW1 culture in the exponential phase (36 h) was spread on SNA plates containing 0, 5, 10, 15, 20, 25, or 30 μM/ml of zeocin as well as 0, 50, 100, 200, 300, 400, 500, and 600 μM/ml of polydatin and incubated at 28°C for up to 7 days. However, for SNA plates with zeocin, only 2 g/L pf artificial sea salt was added as zeocin was sensitive toward high salt concentration. A graph of the lethal rate vs. concentration of the chemicals was plotted. A minimal three replicate plates were used for each condition.

Plasma Mutagenesis and Screening of the Potential Mutant

Before mutagenesis, the SW1 cells were cultivated in a 500 ml shake flask containing 100 ml production medium at 28°C, 200 rpm for 36 h and then diluted to OD600 value between 0.6 and 0.8 with 0.2 mol/L sterile phosphate-buffered saline (PBS) buffer (pH 7.4). To protect cells from lysis caused by water evaporation, glycerol (10% v/v) was added to the cell suspension. A 20-μl aliquot of the above suspension was applied to a sterilized sample plate. The sample plate was later exposed to plasma radiation for a given time under the operating parameters of; radio frequency power input of 100 W, helium flow rate of 10 L/min, and plasma action distance of 2 mm. After mutagenesis, the cells were directly eluted with 1 ml sterile PBS buffer. After the appropriate dilution, 100 μl of the cell suspension was spread onto agar plates and incubated at 28°C for up to 7 days. The lethal rate was determined and optimized for optimal exposure time with the plasma radiation. Then, using the optimal lethal rate, the radiated SW1 cells were then spread on the agar containing zeocin (incubated in dark) and incubated at 28°C for up to 7 days. The colony that survived was then streaked on the agar containing polydatin, and the colonies that grew on the plate were selected for further analysis.

Comparative Analysis of the Wild Type (SW1) and the Mutant Strains (YHPM1)

Comparative analysis on the growth, lipid, fatty acids, antioxidant enzymes, stress marker, and other key metabolic enzymes of the wild type (SW1) and the mutant strains (YHPM1) was carried out in a 500-ml shake flask, containing 100 ml cultivation media for 48 and 96 h of cultivation. The two different production media used during the screening process are as mentioned in the "Organism and Culture Conditions" section. The dry cell weight, lipid, and fatty acid compositions were determined according to the "Determination of dry cell weight, lipid extraction, and fatty acid analysis" section.

Cell-Free Extract Preparations and Enzyme Assays

The mutant and the WT cells were harvested using centrifugation and were then suspended in an extraction buffer. Then, the cells were subsequently disrupted by ultrasonication (Scientz-II D sonifier, Ningbo Scientz Biotechnology Co., Ltd. CHN) at 400 W × 5 s with cooling in between on ice for 10 min (30). The cells were then centrifuged at 12,000 × *g* for 10 min at 4°C using Eppendorf centrifuge 5810R, and the supernatant was filtered through the Whatman No. 1 filter paper to recover the cell-free extract. The supernatant containing cytoplasmic and mitochondrial enzymes was subjected to enzyme activity analysis. The activities of four enzymes, namely, malic enzyme (ME), ATP: citrate lyase (ACL), glucose-6-phosphate dehydrogenase (G-6-PDH), and $NADP^+$-isocitrate dehydrogenase (ICDH) were determined using continuous assays following the oxidation and reduction of NAD(P)(H) at 340 nm and 30°C. The change in absorbance was followed continuously for 10 min using software (UVPROBE2.31). Specific activity is expressed as nmol/min·mg protein. Superoxide dismutase (SOD) and catalase (CAT) activities were determined using an assay kit (Beyotime Institute of Biotechnology, Shanghai, China) according to the manufacturer's instructions. The specific activity (U/mg protein) was defined as the activity unit/mg protein. Protein concentration was determined using the Bradford method with bovine serum albumin (BSA) as a standard (31).

ROS Determination

The intracellular ROS levels were determined using the Reactive Oxygen Species Assay Kit (Beyotime Institute of Biotechnology, Shanghai, China) according to the manufacturer's instructions.

In brief, 1 ml of SW1 cultures were harvested and washed with PBS buffer. A diluted dichlorodihydrofluorescein diacetate (DCFH-DA) probe was then added into the cell suspension and incubated at 37°C for 30 min. The excess probe was washed twice with PBS buffer to ensure only the intracellular fluorescence was measured. Fluorescence intensity was detected using a fluorescence spectrophotometer with the excitation and emission wavelengths at 485 and 535 nm, respectively.

Lipid Peroxidation Assay (Malondialdehyde Assay)

The lipid peroxidation level was determined by measuring the malondialdehyde (MDA) equivalent according to the method proposed by Heath and Packer (32). In brief, the harvested cells of 1 ml were disrupted, homogenized in 5% (w/v) trichloroacetic acid (TCA), and then centrifuged at 10,000 × *g* for 10 min at 4°C. The supernatant was then mixed with 0.67% (w/v) thiobarbituric acid (TBA) solution and boiled for 20 min. The absorbance of the reaction mixture was recorded at 532 and 600 nm. The absorbance value recorded at 532 nm was subtracted by the non-specific absorbance value recorded at 600 nm, and the MDA equivalent content was measured using the 155 mM/cm extinction coefficient.

Cultivation of YHPM1 and SW1 in 5L Bioreactor

The YHPM1 and SW1 growth, lipid, and DHA production capacity were compared using carried 5-L bench-top bioreactors (Minifors-Infors HT) with 3 L working volume with the utilizing GPT media as described in the "Comparative analysis of the wild type (SW1) and the mutant strains (YHPM1)" section. The temperature of the culture was controlled at 28°C, and the impeller speed was fixed at 500 rpm with the aeration of 1 vvm. Samples were then collected every 12 h for 120 h to determine the biomass, lipid, DHA, and residual sugar concentration.

Analytical Methods

Analysis of Glucose

The supernatant obtained from the centrifugation of the biomass was utilized to measure the residual glucose content, using the glucose oxidase kit according to a previous study (33, 34).

Determination of Dry Cell Weight, Lipid Extraction, and Fatty Acid Analysis

The dry cell weight of SW1 was determined according to the previous method (30). Lipid extraction was performed using chloroform–methanol (2:1, v/v), as described by Folch et al. (35). The extract was vaporized at room temperature and dried in a vacuum desiccator until a constant weight was attained. Fatty acid compositions of the samples were determined as fatty acid methyl esters (FAMEs) by gas chromatography (HP 5890) equipped with a capillary column (BPX 70, 30 cm, 0.32 μm). FAME was prepared by dissolving 0.05 g of the sample in 0.95 ml hexane, and the mixture was added to 0.05 ml of 1 M sodium methoxide. The injector was maintained at 200°C. Then, 1 μl of the sample was injected using helium as a carrier gas with a flow rate of 40 $cm^3 min^{-1}$. The temperature of the GC column was gradually increased at 7°C min^{-1} from 50 (5 min hold) to 200°C (10 min hold). Fatty acid peaks were identified using Chrome Leon Chromatography software (Dionex, Sunnyvale, California, USA). FAMEs were identified and quantified by comparison with the retention time and peak areas of SUPELCO FAME standard (Bellefonte, PA, USA).

Statistical Analysis

SPSS 16.0 (SPSS Inc. Chicago, IL, USA) software was used to perform the statistical analysis with three independent replicates ($n = 3$), and the data obtained from the experiments were used to calculate the mean values and the standard errors. The differences between means of the test were calculated using the Student's *t*-test, and $p < 0.05$ was considered significantly different.

RESULTS

Mutagenesis With Plasma Radiation

To determine the optimal exposure time of the plasma radiation, the SW1 cells were treated with plasma radiation for varying durations (i.e., 0, 10, 20, 30, 40, 60, 80, or 100 s), and the cell was then incubated at 28°C for up to 7 days. The result showed that the optimal treatment time was at the 80 s with the lethal rate of 98.0–99.0%. A high lethal rate was used in this study to generate mutants with extensive mutation as well as avoid the lengthy screening process. According to previous studies, an extensive mutation level was typically achieved when the lethal rate was above 90% (36). Besides, a superior strain of *Bacillus subtilis* was generated after plasma mutagenesis treatment with a 95% lethal rate (24).

Screening of Mutant High Oxidative Tolerance and G6PDH Activity

The agar plates containing 0, 5, 10, 15, 20, 25, or 30 μM/ml of zeocin as well as 0, 50, 100, 200, 300, 400, 500, and 600 μM/ml polydatin were prepared to determine the inhibition levels of both chemicals toward SW1 (**Figures 1A,B**). The result showed that the inhibition levels of SW1 increased with the increase of zeocin and polydatin concentration, reaching ∼95–98% with 20 μM/ml zeocin and 500 μM/ml polydatin, respectively. Thus, agar plates containing 20 μM/ml zeocin and 500 μM/ml polydatin were used to screen and isolate SW1 mutants with superior oxidative defense as well and G6PDH activity. After exposing SW1 to the plasma radiation, the SW1 cells were immediately spread on the agar plates containing 20 μM/ml of zeocin and incubated for 4–7 days. Only approximately 5 ± 1.25 colonies were observed on the zeocin plates, and then, all the five colonies were transferred to the polydatin plates and were further incubated for another 4–7 days. Interestingly, only one colony (named YHPM1) was able to survive on the agar plate containing 500 μM/ml polydatin. Thus, to evaluate and compare the cellular physiology of the mutant with the WT strain, a comparative study was conducted.

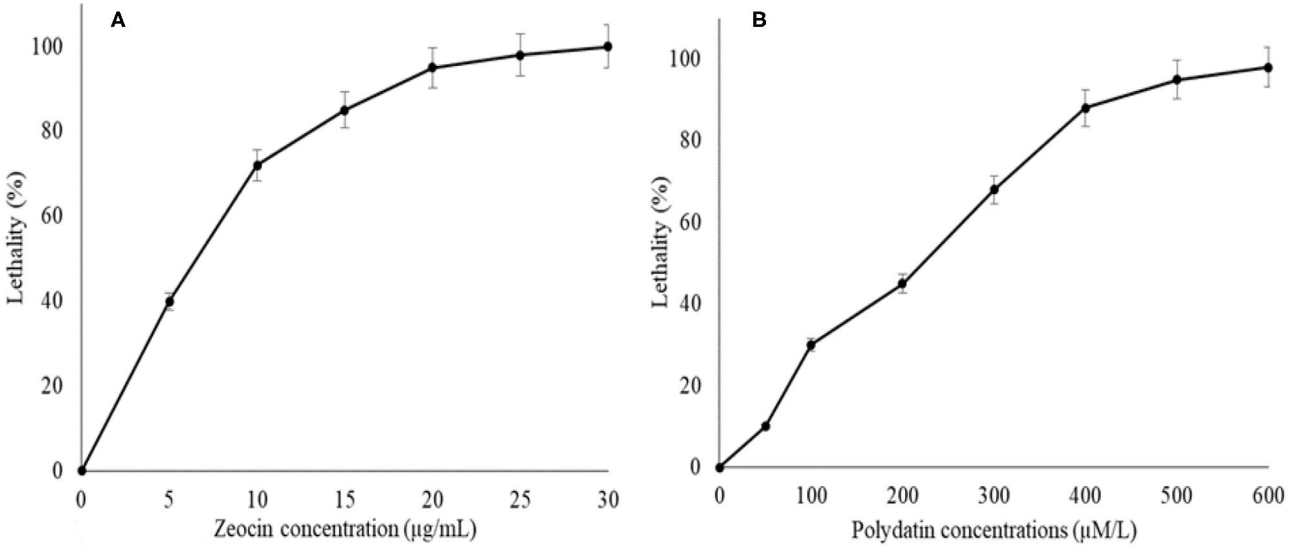

FIGURE 1 | The lethal rates curves of SW1 cultured in agar plates containing; **(A)** 0, 5, 10, 15, 20, 25, and 30 μg/mL zeocin as well as **(B)** 0, 50, 100, 200, 300, 400, 500, and 600 μM/L of polydatin, respectively. Values and error bars represent the means and the standard deviations of triplicate experiments ($n = 3$).

Comparative Analysis on Cellular Morphology, Cell Growth, and Fatty Acid Biosynthesis as Well as Oxidative and Key Metabolic Enzymes of YHPM1 and SW1

To evaluate the changes in the cellular morphology of YHPM1 over the wild type (SW1), both the cultures were cultivated in a 500-ml shake flask for 96 h of cultivation, and the differences in the cellular morphology were compared (**Figure 2**). The result showed that both strains exhibited significant differences in the cellular size where most of the YHM1 poses a relatively bigger in diameter (approximately between 5 and 20 μM) colonies in comparison to the WT (2–10 μM). Besides, the YHM1 cell was shown to be more intact with a compact and large lipid droplet within the cell in comparison to SW1, confirming the mutation effect at the morphological level (**Figure 2**).

In addition, to further evaluate the mutation effect of YHPM1 over SW1, a comparative study on cellular growth, total lipid, and fatty acid biosynthesis capabilities was performed with two different media, namely Burja and GPT at 48 and 96 h of cultivations, respectively. As shown in **Figure 3**, YHPM1 exhibited superior growth in comparison with SW1 in both media and cultivation hours. The most pronounced impact was observed in GPT media where YHPM1 poses 18 and 43% greater biomass production at 48 and 96 h of cultivation, in comparison with SW1, respectively. Furthermore, the lipid content of YHPM1 reached 64.18% in GPT media at 96 h of cultivation where it is 22.27% higher than that of the WT. Furthermore, the total lipid production (g/L) of YHPMI was 67.42 and 47.19% higher than that of SW1 in GPT and Burja media, respectively.

Furthermore, a pronounced change in the fatty acid compositions was also observed in both strains. The YHPM1 strain was shown to poses a 15–27% higher PKS product which is mainly composed of the DPA and DHA in both media and cultivation hours in comparison to SW1 (**Table 1**). In addition, a much significant difference was observed in the total DHA production (g/L) where YHPM1 produced ∼8.0 g/L DHA when grown with GPT media at 96 h of cultivation, 60% higher than that of SW1 (**Figure 3D**). These results indicated that the mutant strain exhibited not only a superior growth and lipid content but also PUFAs and DHA production.

Comparative Analysis on Oxidative Defense and Key Metabolic Enzymes of YHPM1 and SW1

To confirm the effects of polydatin- and zeocin-based screening, the activity of G6PDH, 6PGDH, as well as the antioxidant enzymes of the mutant (YHPM1) and wild type (SW1), was compared. The results showed that G6PDH and 6PGDH activities in YHPM1 were, in fact, higher than SW1 with the most significant increase found at 48 h of cultivation, achieving a nearly 2.2- and 1.8-fold higher than that of SW1, respectively (**Figure 4**). In addition, both the SOD and CAT activities inYHPM1 was also exhibited a 3–4-fold higher than that of SW1 especially in GPT media after 96 h of cultivation, consistent with its ability to grow at a high concentration of zeocin during the screening process.

In addition, the impact on the other key enzymes involved in lipogenesis was also elucidated. A pronounce impact was also observed in ACL activities where YHPM1 exhibited a 68.12% higher activity compared with SW1 at 96 h of cultivation in the GPT media. Nevertheless, the activity of ME in YHPM1, although higher at 48 h, but not significant at 96 h of cultivation in comparison with SW1, indicating the significant elevation in

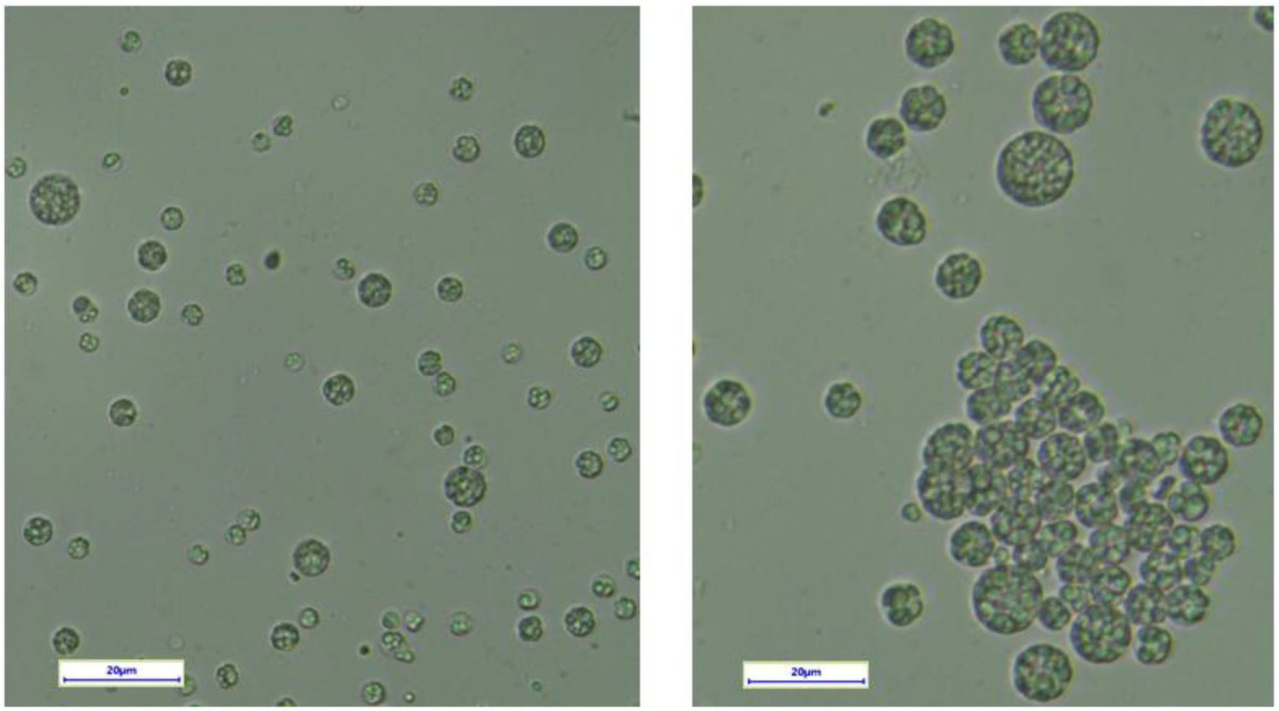

FIGURE 2 | The cellular morphology of **(A)** SW1 and **(B)** YHPM1 under the light microscope. The scale bar represents 20 μm.

the total lipid content, was attributed to the higher NADPH supply from G6PDH and 6PGDH, which explains the significant improvement in the PUFA content of YHPM1. Furthermore, the oxidative stress indicators of YHPM1, ROS, and MDA were also shown to be 25–53% lower than that of SW1 especially at the 96 h of cultivation, mainly attributed to the stronger antioxidant aptitudes poses by YHPM1 in comparison with SW1 (**Figure 5**).

Based on this result, it is indicated that YHPM1 has higher overall growth, lipid, and DHA production capacity as compared with SW1 in the shake flask level. To evaluate its potential for industrial-scale application, an upscaling experiment at a 5 L bioreactor scale was conducted.

Cultivation of YHPM1 and SW1 in 5 L Bioreactor

A comparative study of SW1 vs. YHPM1 was conducted to evaluate the growth, lipid, and DHA production capacity in a larger fermentation scale, by utilizing GPT media as described in the "Cultivation of YHPM1 and SW1 in 5L bioreactor" section (**Figure 6**). The result showed that YHPM1 exhibited a 30, 65, and 80% higher overall biomass, lipid, and DHA production in comparison with SW1, respectively (**Figures 6A–C**). Besides, YHPM1 also exhibits a faster substrate utilization rate (**Figure 6D**) as compared with that of the WT, a characteristic that is comparable with the other high DHA producing strains of thraustochytrids such as *Schizochytrium* sp. HX308 (37), *Schizochytrium* sp.31 (38), and *Aurantiochytrium* sp. SR21 (39). Thus, a mutant strain of *Aurantiochytrium* sp. that has a promising potential for industrial-scale DHA production has been successfully developed in this study.

DISCUSSION

Thraustochytrids are unique due to its ability to produce high lipid and DHA content from its DCW, but the low volumetric DHA production limits its application at the industrial scale. Thus, many studies have been conducted to enhance the DHA production yields from thraustochytrids (8–10). One of the factors attributed to the high oleaginousity of thraustochytrids is due to the fact that there are two distinct pathways involved in the biosynthesis of fatty acids in this organism: the type I fatty acid synthase (FAS) pathway and a polyketide synthase (PKS) pathways (40). It was later found that only the PKS pathway is responsible for the DHA biosynthesis in thraustochytrids (41). Thus, efforts have been made to enhance DHA production by overexpressing the genes involved in PKS pathways as well as elucidating the specific NADPH supplier for the PKS pathways (17, 19). Studies by Cui et al. (19) showed that the overexpression of G6PDH activity significantly enhanced PUFA production in thraustochytrids, thus, indicating that the NADPH for the PKS pathway is specifically channeled by the G6PDH. Aside from the NADPH, it is also important to develop strategies to mitigate the oxidative stress in the thraustochytrids, since

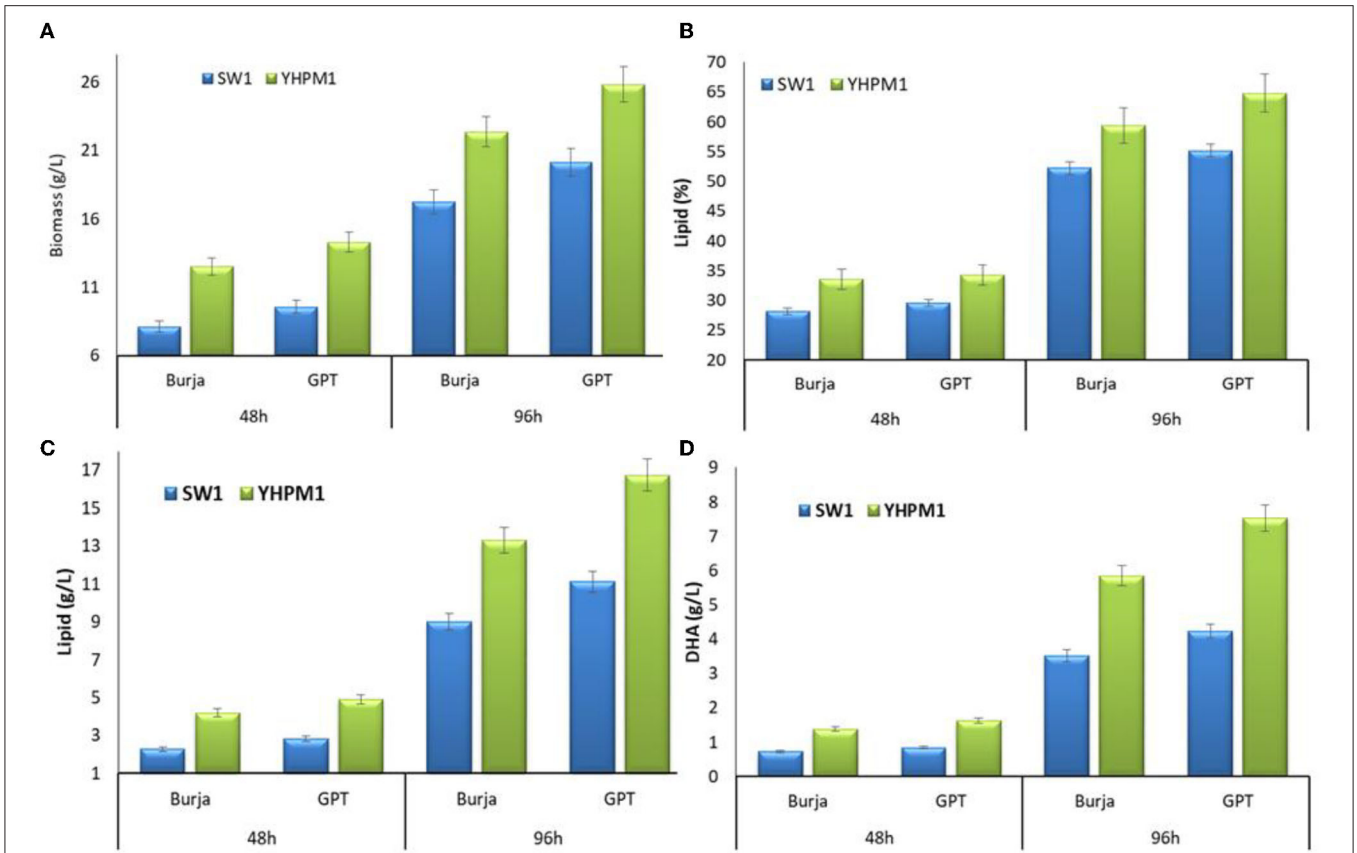

FIGURE 3 | The **(A)** biomass, **(B)** lipid content (%), **(C)** lipid production (g/L) as well as **(D)** DHA production (g/L) of SW1 and YHPM1 cultured in 500 mL shake flask for 48 and 96 h of cultivation in Burja and GPT media. Values and error bars represent the means and the standard deviations of triplicate experiments ($n = 3$).

TABLE 1 | The fatty acid compositions of SW1 and YHPM1 cultured in 500 ml shake flask for 48 and 96 h of cultivation in Burja and GPT media.

Fatty acids	Burja				GPT			
	48 h		96 h		48 h		96 h	
	SW1	YHPM1	SW1	YHPM1	SW1	YHPM1	SW1	YHPM1
14:0	3.62 ± 0.17	3.94 ± 0.20	3.01 ± 0.11	3.36 ± 0.19	4.71 ± 0.26	3.48 ± 0.22	3.10 ± 0.17	2.25 ± 0.17
14:1	0.24 ± 0.01	0.21 ± 0.01	0.30 ± 0.01	0.19 ± 0.03	0.56 ± 0.03	0.49 ± 0.05	0.41 ± 0.03	0.33 ± 0.02
15:0	3.23 ± 0.16	2.24 ± 0.11	2.41 ± 0.09	1.91 ± 0.27	4.88 ± 0.27	4.64 ± 0.26	1.20 ± 0.07	1.23 ± 0.07
16:0	45.12 ± 2.17	43.56 ± 2.23	38.13 ± 1.45	33.83 ± 2.40	43.59 ± 2.40	42.97 ± 2.36	41.70 ± 2.91	36.12 ± 1.99
17:0	1.33 ± 0.06	0.95 ± 0.05	1.53 ± 0.06	0.74 ± 0.04	0.76 ± 0.03	0.51 ± 0.03	1.30 ± 0.07	1.02 ± 0.06
18:0	1.40 ± 0.07	1.34 ± 0.07	1.02 ± 0.04	1.08 ± 0.07	1.23 ± 0.09	1.06 ± 0.06	1.42 ± 0.08	1.34 ± 0.07
20:5n3 (EPA)	0.25 ± 0.01	0.31 ± 0.02	0.83 ± 0.03	0.75 ± 0.02	0.45 ± 0.03	0.41 ± 0.02	0.75 ± 0.04	0.79 ± 0.04
22:5n3 (DPA)	6.14 ± 0.29	7.10 ± 0.36	9.31 ± 0.35	11.35 ± 0.38	6.86 ± 0.40	7.78 ± 0.43	8.40 ± 0.46	10.24 ± 0.56
22:6n3 (DHA)	34.56 ± 1.66	38.79 ± 1.99	41.89 ± 1.59	45.92 ± 1.91	34.77 ± 1.74	36.60 ± 2.01	40.56 ± 2.88	44.81 ± 2.46
Other minor fatty acids	2.03 ± 0.10	1.52 ± 0.08	1.65 ± 0.06	0.87 ± 0.12	2.19 ± 0.10	1.71 ± 0.09	1.35 ± 0.13	1.85 ± 0.10
FAS products	59.05 ± 2.83	53.80 ± 2.76	47.97 ± 1.82	41.90 ± 3.19	57.92 ± 1.59	55.21 ± 3.04	50.29 ± 2.77	44.16 ± 2.43
PKS products	40.95 ± 1.97	46.20 ± 2.37	52.03 ± 1.98	58.10 ± 2.21	42.08 ± 2.33	44.79 ± 2.46	49.71 ± 2.15	55.84 ± 3.07

Values represent the means of triplicate experiments (n = 3).

lipids, particularly PUFA, are highly susceptible to oxygen radical attacks that limit the DHA productivity (13). Thus, the generation of mutants with high oxidative tolerance and G6PDH activity would be one of the most efficient ways to increase the DHA production by thraustochytrids, including the *Aurantiochytrium* sp.

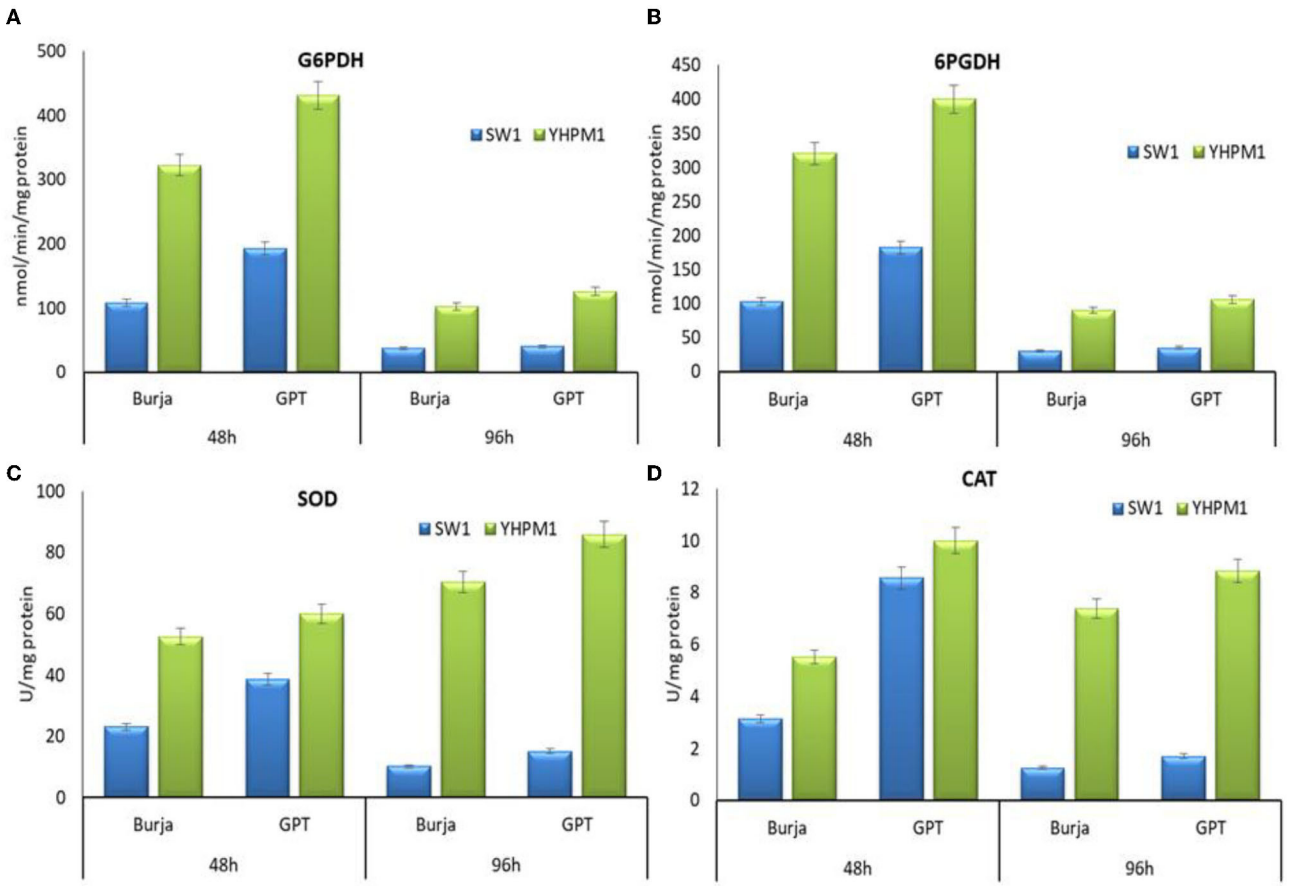

FIGURE 4 | The activity of **(A)** G6PDH, **(B)** 6PGDH, **(C)** SOD as well as **(D)** CAT of SW1 and YHPM1 cultured in 500 mL shake flask for 48 and 96 h of cultivation in Burja and GPT media. Values and error bars represent the means and the standard deviations of triplicate experiments ($n = 3$).

At present, the advancement in microbial genetic engineering and synthetic biology has led to a significant increase in super strain development for the production of important metabolites of interest, including PUFAs from the microalgae (17, 42, 43). Nevertheless, genetic engineering technology in *thraustochytrids* including the *Aurantiochytrium* sp. is still in its infancy as the development of a transformation system was only realized by Sakaguchi et al. (44). Furthermore, due to the uncertain and complex metabolic regulation network of *Aurantiochytrium* sp., it was found that changes in one or two genes do not warrant producing transformants with the desired trait. For example, although the overexpression of G6PDH gave a promising impact on the PUFA and DHA content of *Aurantiochytrium* sp. SD116, the growth was significantly compromised, thus reducing the overall DHA production (g/L) compared with the WT strain (19). Therefore, the selection of suitable mutagenesis approaches remains the major challenge in producing the thraustochytrid mutant with desirable traits.

Plasma mutagenesis can directly mutate the *Aurantiochytrium* sp. strains by penetrating the cell wall with high transfer values of linear energy, thus, creating a stronger mutation effect (45). ROS produced by plasma can alter the structure and permeability of the cell membrane and interact with DNA and other macromolecules to change the cell metabolic activity and genetic characteristics, triggering the SOS repair mechanism, which can produce different kinds of mismatch sites (45). Furthermore, this technique has been proven to create more mutation sites than other techniques. Therefore, in this study, plasma radiation was deployed to generate mutants with superior growth and DHA biosynthetic capacity. Nevertheless, this technique is not without flaw as the process of obtaining mutants with the desired traits is difficult to realize due to random mutation impact. Thus, to obtain mutants with the desired traits, it is still crucial to develop proper and efficient screening methods after the mutagenesis process. Most conventional screening methods, such as phenotypic screening, are time and labor-consuming (36). Since certain chemicals are known to inhibit certain pathways which may result in impaired cellular metabolism of cells, it can be used to be the selective pressure to screen thraustochytrid mutant with desired traits (27).

In this study, zeocin and polydatin are the chemicals that were selected to be used as a selective pressure for the mutant generated through plasma mutagenesis. Zeocin is an antibiotic that is highly noxious to thraustochytrids where it instigates

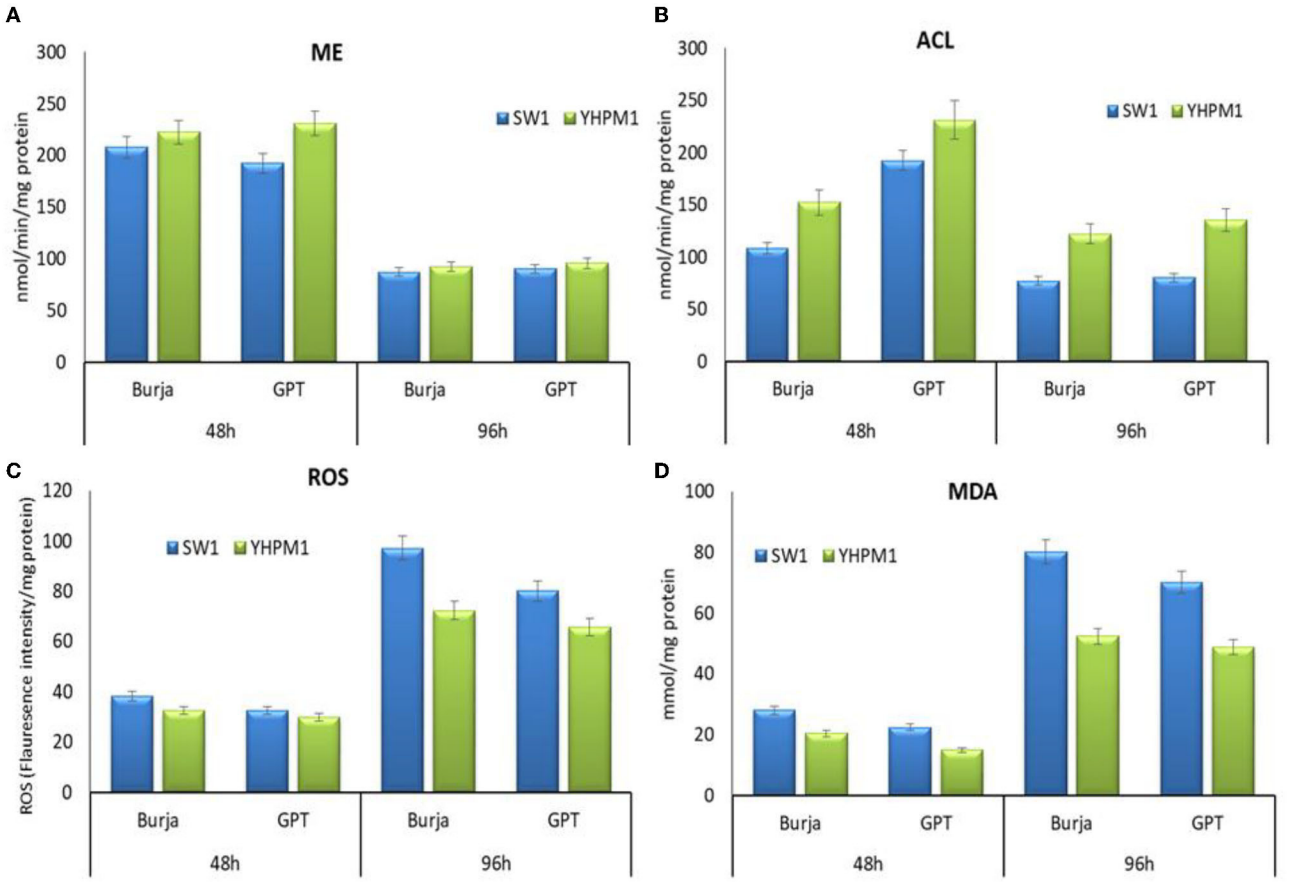

FIGURE 5 | The activity of **(A)** ME, **(B)** ACL, **(C)** ROS as well as **(D)** MDA of SW1 and YHPM1 cultured in 250 mL shake flask for 48 and 96 h of cultivation in Burja and GPT media. Values and error bars represent the means and the standard deviations of triplicate experiments ($n = 3$).

high ROS production in the cell, resulting in cell death (36). Zeocin with a concentration of 20 μg/ml that resulted in a 98% lethal rate on the WT strain was selected as the selective pressure for the mutant generated through plasma mutagenesis, obtaining mutant with high oxidative tolerance. In contrast, 500 μg/ml polydatin, which showed a 95% inhibition rate to the WT strain, was selected as the elective pressure to generate mutant with high G6PDH activity. This led to the identification of the YHPM1 strain, where this mutant is able to withstand the toxic effect of both chemicals used during the screening process.

The mutation effect was initially confirmed by cellular morphology, where YHPM1 poses significantly bigger cells, ranging from 5 to 20 μM, differing from the common size of *Aurantiochytrium* sp. which ranges from 2 to 10 μM in diameter (6). This observation was also in line with what was reported by Geng et al. (46) who found that the higher biomass and fatty acid content of the engineered strain *Schizochytrium* sp. HX-308 was followed by a much intact cellular morphology in comparison with the WT. Furthermore, analysis from the fatty acid content also reveals some insight into the mutation effect as YHPM1 and SW1 pose altered composition of major fatty acids, especially C14:0, C15:0, C16:0, C22:n5 (DPA), and C22:n6 (DHA). YHPM1 was found to poses higher content of DPA and DHA, as well as the overall PUFA content, as compared with SW1 probably due to more active PKS machineries than the FAS.

In addition, the mutation effect was further confirmed by determining the changes in the key metabolic enzymes compared with the WT. There was a clear change in the activity of the antioxidant enzymes in both of the strains. The SOD and CAT activities of the mutant (YHPM1) were ∼3–4-fold higher than that of the WT, confirming the effect of zeocin screening. Zeocin works on cells by chelating metal ions (primarily iron) to generate radicals free of superoxide and hydroxide, which instigate lipid peroxidation and other cellular molecule oxidations, resulting in cellular damage (28). YHPM1 was capable to survive the lethal concentration of zeocin during the screening process as it poses a higher antioxidant capacity compared to the others. *Aurantiochytrium* sp. strain with a good antioxidant capacity is one of the important criteria as it correlates to its higher capacities to produce DHA and circumvent lipid peroxidation, which is one of the major causes of PUFA and DHA degradations

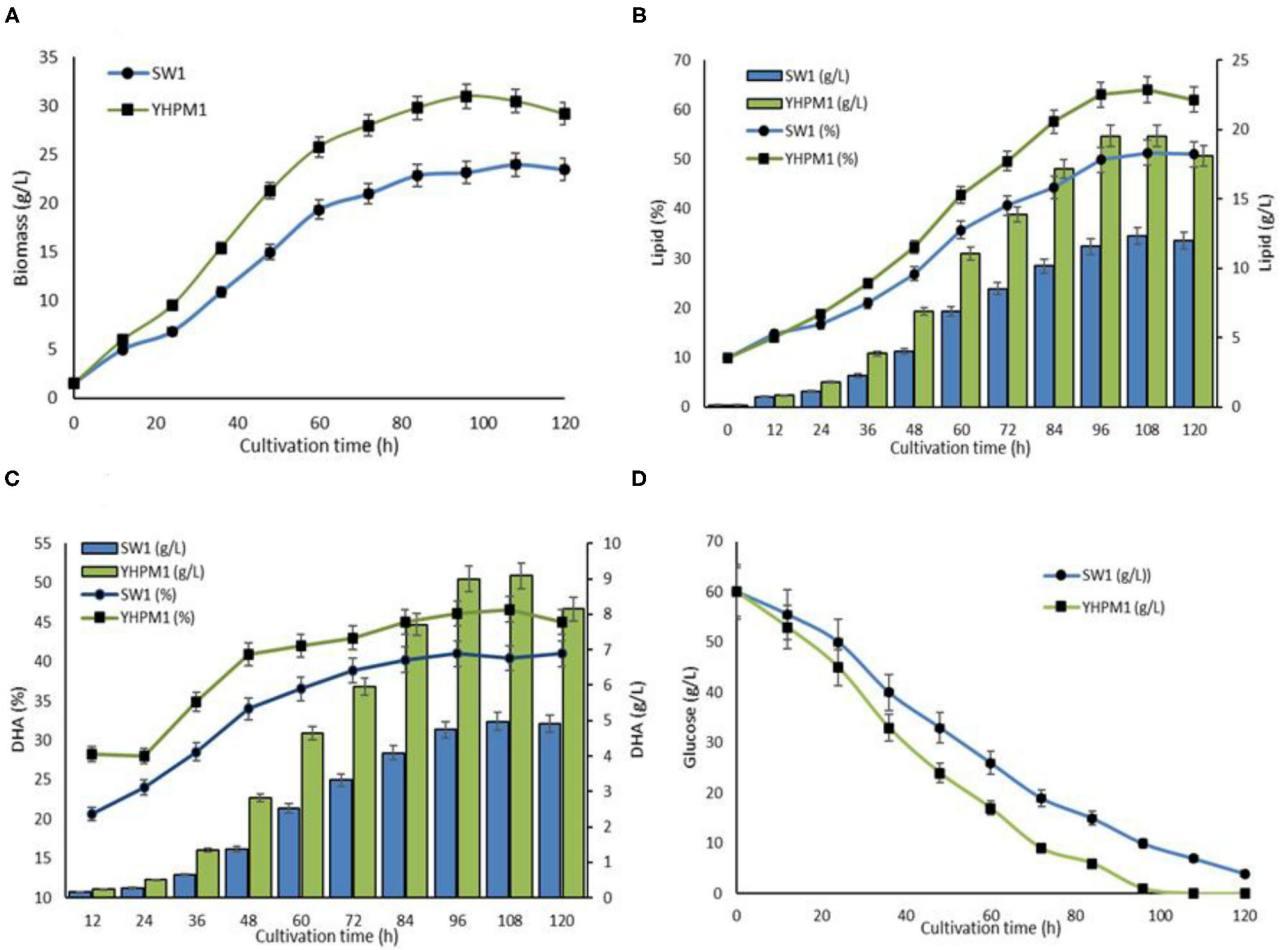

FIGURE 6 | (A) Biomass, **(B)** lipid, **(C)** DHA, and **(D)** glucose consumption rate of YHPM1 and SW1 cultivated in 5L bioreactor for 120 h.

TABLE 2 | Different metabolic engineering strategies to enhance docosahexaenoic acid (DHA) production from thraustochytrid strains.

Thraustochytrids strains	Strategy	Lipid content (%, g/g biomass)	DHA content (% of total fatty acids)	DHA biosynthetic capacity (g DHA/g Biomass)	References
Schizochytrium sp. ATCC 20888	Overexpression of ACL and ACC genes from *Schizochytrium* sp.	73.0%	38%	0.28	(47)
Schizochytrium sp. PKU#Mn4	Overexpression of the antioxidative gene superoxide dismutase from *Schizochytrium* sp.	35.6%	41%	0.15	(16)
Aurantiochytrium sp. SD116	Heavy-ion irradiation technique coupled with then two-step ALE: low temperature-based ALE and ACCase inhibitor quizalofop-p-ethyl based ALE	60%	52.6%	0.31	(48)
Schizochytrium sp. PKU#Mn4	ARTP mutagenesis coupled with the acetyl-CoA carboxylase (ACCase) inhibitor (clethodim)-based screening	45%	42%	0.18	(27)
Aurantiochytrium sp. YHPM1	Plasma mutagenesis coupled with zeocin and polydatin screening	61%	45%	0.30	This study.

(16). Several studies have shown that enhancement of the oxidative defense has a positive correlation with the increase of PUFA content in microalgae, particularly the thraustochytrids (11, 12). For example, the addition of antioxidants such as ascorbic acid (14) and sesamol, as well as overexpression of SOD in *Schizochytrium* sp. (16), have successfully alleviated the oxidative stress and increased the DHA content in the microalgae by elevating the total antioxidant capacity as well as lowering the ROS and lipid peroxidation in the cells. Lipids, particularly PUFA, are highly susceptible to oxygen radical attack, and the resulting oxidative species are detrimental to cell metabolism and limit lipid productivity (13).

Aside from posing a higher antioxidant capacity, YHPM1 was also shown to have significantly higher activity of the G6PDH and 6PGDH activities (**Figure 3**). Higher G6PDH activity has been implicated with more active PKS machineries as it has been proposed to be responsible for the NADPH supply in the PKS pathway of *Aurantiochytrium* sp. (19). Nevertheless, no inhibition of growth was observed in this mutant strain, differing from the previous study which reported that the overexpression of G6PDH resulted in compromised growth, despite the positive effect on the PUFA and DHA contents (19). Furthermore, the activity of other key enzymes especially the ACL was also significantly higher in YHPM1 in comparison to the wild type (SW1). From the activity of the key enzymes, it was demonstrated that YMPM1 generates a higher provision of NADPH as well as acetyl-CoA compared with SW1, explaining its higher lipid and DHA biosynthesis capacity.

In the effort to enhance the DHA production by thraustochytrids, numerous metabolic engineering strategies have been developed (**Table 2**). It was found that the lipid and DHA contents, as well as the DHA biosynthetic capacity of YHPM1 generated in this study were comparable with the other high DHA yielding thraustochytrids, indicating that YHPM1 has a promising potential for lab and large-scale DHA production.

CONCLUSION

A mutant strain of *Aurantiochytrium* sp. (YHPM1) has been successfully developed through plasma mutagenesis coupled with zeocin and polydatin screening strategies, which possess a significantly higher DHA biosynthetic capacity in comparison with the parental strain. In addition, the potential mechanism for the superior growth, lipid, and DHA biosynthetic capacity of the mutant strain, compared with the parent strain, was also elucidated. This study provides the first report that integrates plasma mutagenesis coupled with zeocin- and polydatin-based screening strategies, to generate mutants with superior tolerance to oxidative stress as well as high G6PDH activity for enhanced DHA production by thraustochytrids.

DATA AVAILABILITY STATEMENT

The raw data supporting the conclusions of this article will be made available by the authors, without undue reservation.

AUTHOR CONTRIBUTIONS

YN conceived the study, designed and performed the experiments, interpreted the data, and drafted the manuscript. HH and PP participated in the experimentation. HM and TN data analysis. AA and YS participated in study design, supervised all experimental procedures, and finalized the manuscript. All authors contributed to the article and approved the submitted version.

ACKNOWLEDGMENTS

The authors thank the Geran Galakan Penyelidik Muda (GGPM-2021-026), the National Natural Science Foundation of China (Grants no. 31972851 and 31670064), and the TaiShan Industrial for funding this research.

REFERENCES

1. Oliver L, Dietrich T, Marañón I, Villarán MC, Barrio RJ. Producing omega-3 polyunsaturated fatty acids: a review of sustainable sources and future trends for the EPA and DHA market. *Resources.* (2020) 9:148. doi: 10.3390/resources9120148
2. Ghasemi Fard S, Wang F, Sinclair AJ, Elliott G, Turchini GM. How does high DHA fish oil affect health? A systematic review of evidence. *Crit Rev Food Sci Nutr.* (2019) 59:1684–727. doi: 10.1080/10408398.2018.1425978
3. Hathaway III D, Pandav K, Patel M, Riva-Moscoso A, Singh BM, Patel A, et al. Omega 3 fatty acids and COVID-19: a comprehensive review. *Infect Chemother.* (2020) 52:478. doi: 10.3947/ic.2020.52.4.478
4. Colombo SM, Rodgers TF, Diamond ML, Bazinet RP, Arts MT. Projected declines in global DHA availability for human consumption as a result of global warming. *Ambio.* (2020) 49:865–80. doi: 10.1007/s13280-019-01234-6
5. Xin Y, Lu Y, Lee YY, Wei L, Jia J, Wang Q, et al. Producing designer oils in industrial microalgae by rational modulation of co-evolving type-2 diacylglycerol acyltransferases. *Mol Plant.* (2017) 10:1523–39. doi: 10.1016/j.molp.2017.10.011
6. Manikan V, Nazir MYM, Kalil MS, Isa MHM, Kader AJA, Yusoff WMW, et al. A new strain of docosahexaenoic acid producing microalga from Malaysian coastal waters. *Algal Res.* (2015) 9:40–7. doi: 10.1016/j.algal.2015.02.023
7. Ratledge C. An opinion on the safety data for the DHA-rich oil from *Schizochytrium* sp., also known as DHASCO-S. GRAS Notification for DHA Algal Oil Derived from *Schizochytrium* sp. (2003) 5.
8. Ling X, Guo J, Liu X, Zhang X, Wang N, Lu Y, et al. Impact of carbon and nitrogen feeding strategy on high production of biomass and Docosahexaenoic Acid (DHA) by *Schizochytrium* sp. LU310. *Bioresour Technol.* (2015) 184:139–47. doi: 10.1016/j.biortech.2014.09.130
9. Chang G, Gao N, Tian G, Wu Q, Chang M, Wang X. Improvement of docosahexaenoic acid production on glycerol by *Schizochytrium* sp. S31 with constantly high oxygen transfer coefficient. *Bioresour Technol.* (2013) 142:400–6. doi: 10.1016/j.biortech.2013.04.107
10. Ganuza E, Anderson AJ, Ratledge C. High-cell-density cultivation of *Schizochytrium* sp. in an ammonium/pH-auxostat fed-batch system. *Biotechnol Lett.* (2008) 30:1559–64. doi: 10.1007/s10529-008-9723-4
11. Sun XM, Ren LJ, Bi ZQ, Ji XJ, Zhao QY, Jiang L, et al. Development of a cooperative two-factor adaptive-evolution method to enhance lipid production and prevent lipid peroxidation in *Schizochytrium* sp. *Biotechnol Biofuels.* (2018) 11:1–16. doi: 10.1186/s13068-018-1065-4

12. Sun XM, Ren LJ, Bi ZQ, Ji XJ, Zhao QY, Huang, et al. Adaptive evolution of microalgae *Schizochytrium* sp. under high salinity stress to alleviate oxidative damage and improve lipid biosynthesis. *Bioresour Technol.* (2018) 267:438–44. doi: 10.1016/j.biortech.2018.07.079
13. Ayala A, Muñoz MF, Argüelles S. Lipid peroxidation: production, metabolism, and signaling mechanisms of malondialdehyde and 4-hydroxy-2-nonenal. *Oxid Med Cell Longev*. (2014) 2014:360438. doi: 10.1155/2014/360438
14. Ren LJ, Sun XM, Ji XJ, Chen SL, Guo DS, Huang H. Enhancement of docosahexaenoic acid synthesis by manipulation of antioxidant capacity and prevention of oxidative damage in *Schizochytrium* sp. *Bioresour Technol.* (2016) 223:141–8. doi: 10.1016/j.biortech.2016.10.040
15. Liu B, Liu J, Sun P, Ma X, Jiang Y, Chen F. Sesamol enhances cell growth and the biosynthesis and accumulation of docosahexaenoic acid in the microalga *Crypthecodinium cohnii*. *J Agric Food Chem.* (2015) 63:5640–5. doi: 10.1021/acs.jafc.5b01441
16. Zhang S, He Y, Sen B, Chen X, Xie Y, Keasling JD, et al. Alleviation of reactive oxygen species enhances PUFA accumulation in *Schizochytrium* sp. through regulating genes involved in lipid metabolism. *Metab Eng Commun.* (2018) 6:39–48. doi: 10.1016/j.meteno.2018.03.002
17. Li Z, Meng T, Ling X, Li J, Zheng C, Shi Y. Overexpression of malonyl-CoA: ACP transacylase in *Schizochytrium* sp. to improve polyunsaturated fatty acid production. *J Agric Food Chem.* (2018) 66:5382–91. doi: 10.1021/acs.jafc.8b01026
18. Zeng L, Bi Y, Guo P, Bi Y, Wang T, Dong L, et al. Metabolic analysis of schizochytrium mutants with high DHA content achieved with ARTP mutagenesis combined with iodoacetic acid and dehydroepiandrosterone screening. *Front Bioeng Biotechnol.* (2021) 9:738052. doi: 10.3389/fbioe.2021.738052
19. Cui GZ, Ma Z, Liu YJ, Feng Y, Sun Z, Cheng Y, et al. Overexpression of glucose-6-phosphate dehydrogenase enhanced the polyunsaturated fatty acid composition of *Aurantiochytrium* sp. SD116. *Algal Res.* (2016) 19:138–45. doi: 10.1016/j.algal.2016.08.005
20. Diao J, Song X, Cui J, Liu L, Shi M, Wang F, et al. Rewiring metabolic network by chemical modulator based laboratory evolution doubles lipid production in *Crypthecodinium cohnii*. *Metab Eng.* (2019) 51:88–98. doi: 10.1016/j.ymben.2018.10.004
21. Hayashi S, Satoh Y, Ogasawara Y, Maruyama C, Hamano Y, Ujihara T, et al. Control mechanism for cis double-bond formation by polyunsaturated fatty-acid synthases. *Angew Chem Int Ed.* (2019) 58:2326–30. doi: 10.1002/anie.201812623
22. Cui G, Wang Z, Hong W, Liu YJ, Chen Z, Cui Q, et al. Enhancing tricarboxylate transportation-related NADPH generation to improve biodiesel production by *Aurantiochytrium*. *Algal Res.* (2019) 40:101505. doi: 10.1016/j.algal.2019.101505
23. Wang L, Chen X, Wu G, Zeng X, Ren X, Li S, et al. Genome shuffling and gentamicin-resistance to improve ε-poly-l-lysine productivity of *Streptomyces albulus* W-156. *Appl Biochem Biotechnol.* (2016) 180:1601–17. doi: 10.1007/s12010-016-2190-9
24. Ma Y, Yang H, Chen X, Sun B, Du G, Zhou Z, et al. Significantly improving the yield of recombinant proteins in *Bacillus subtilis* by a novel powerful mutagenesis tool (ARTP): alkaline α-amylase as a case study. *Protein Expr Purif.* (2015) 114:82–8. doi: 10.1016/j.pep.2015.06.016
25. Li X, Liu R, Li J, Chang M, Liu Y, Jin Q, et al. Enhanced arachidonic acid production from *Mortierella alpina* combining atmospheric and room temperature plasma (ARTP) and diethyl sulfate treatments. *Bioresour Technol.* (2015) 177:134–40. doi: 10.1016/j.biortech.2014.11.051
26. Cao S, Zhou X, Jin W, Wang F, Tu R, Han S, et al. Improving of lipid productivity of the oleaginous microalgae *Chlorella pyrenoidosa* via atmospheric and room temperature plasma (ARTP). *Bioresour Technol.* (2017) 244:1400–6. doi: 10.1016/j.biortech.2017.05.039
27. Liu L, Bai M, Zhang S, Li J, Liu X, Sen, et al. ARTP Mutagenesis of *Schizochytrium* sp. PKU# Mn4 and clethodim-based mutant screening for enhanced docosahexaenoic acid accumulation. *Mar Drugs.* (2021) 19:564. doi: 10.3390/md19100564
28. Takimoto CH, Calvo E. Principles of oncologic pharmacotherapy. *Cancer Manag.* (2008) 11:1–9.
29. Mele L, Paino F, Papaccio F, Regad T, Boocock D, Stiuso, et al. A new inhibitor of glucose-6-phosphate dehydrogenase blocks pentose phosphate pathway and suppresses malignant proliferation and metastasis *in vivo*. *Cell Death Dis.* (2018) 9:1–12. doi: 10.1038/s41419-018-0635-5
30. Nazir Y, Halim H, Al-Shorgani NKN, Manikan V, Hamid AA, Song Y. Efficient conversion of extracts from low-cost, rejected fruits for high-valued Docosahexaenoic acid production by *Aurantiochytrium* sp. SW1. *Algal Res.* (2020) 50:101977. doi: 10.1016/j.algal.2020.101977
31. Wynn JP, bin Abdul Hamid, A, Ratledge C. The role of malic enzyme in the regulation of lipid accumulation in filamentous fungi. *Microbiology.* (1999) 145:1911–17. doi: 10.1099/13500872-145-8-1911
32. Heath RL, Packer L. Photoperoxidation in isolated chloroplasts: I. Kinetics and stoichiometry of fatty acid peroxidation. *Arch Biochem Biophys.* (1968) 125:189–98. doi: 10.1016/0003-9861(68)90654-1
33. Nazir Y, Halim H, Prabhakaran, Ren X, Naz T, Mohamed H, et al. Different classes of phytohormones act synergistically to enhance the growth, lipid and DHA biosynthetic capacity of *Aurantiochytrium* sp. SW1. *Biomolecules.* (2020) 10:755. doi: 10.3390/biom10050755
34. Nazir Y, Shuib S, Kalil MS, Song Y, Hamid AA. Optimization of culture conditions for enhanced growth, lipid and docosahexaenoic acid (DHA) production of Aurantiochytrium SW1 by response surface methodology. *Sci Rep.* (2018) 8:1–12. doi: 10.1038/s41598-018-27309-0
35. Folch J, Lees M, Sloane Stanley GH. A simple method for the isolation and purification of total lipids from animal tissues. *J biol Chem.* (1957) 226:497–509. doi: 10.1016/S0021-9258(18)64849-5
36. Zhao B, Li Y, Li C, Yang H, Wang W. Enhancement of Schizochytrium DHA synthesis by plasma mutagenesis aided with malonic acid and zeocin screening. *Appl Microbiol Biotechnol.* (2018) 102:2351–61. doi: 10.1007/s00253-018-8756-4
37. Guo DS, Ji XJ, Ren LJ, Li GL, Yin FW, Huang H. Development of a real-time bioprocess monitoring method for docosahexaenoic acid production by *Schizochytrium* sp. *Bioresour Technol.* (2016) 216:422–7. doi: 10.1016/j.biortech.2016.05.044
38. Wang F, Bi Y, Diao J, Lv M, Cui J, Chen, et al. Metabolic engineering to enhance biosynthesis of both docosahexaenoic acid and odd-chain fatty acids in *Schizochytrium* sp. S31. *Biotechnol Biofuels.* (2019) 12:1–14. doi: 10.1186/s13068-019-1484-x
39. Li J, Liu R, Chang G, Li X, Chang M, Liu Y, et al. A strategy for the highly efficient production of docosahexaenoic acid by *Aurantiochytrium limacinum* SR21 using glucose and glycerol as the mixed carbon sources. *Bioresour Technol.* (2015) 177:51–7. doi: 10.1016/j.biortech.2014.11.046
40. Metz JG, Roessler, Facciotti D, Levering C, Dittrich F, Lassner M, et al. Production of polyunsaturated fatty acids by polyketide synthases in both prokaryotes and eukaryotes. *Science.* (2001) 293:290–3. doi: 10.1126/science.1059593
41. Ratledge C. Fatty acid biosynthesis in microorganisms being used for single cell oil production. *Biochimie.* (2004) 86:807–15. doi: 10.1016/j.biochi.2004.09.017
42. Muñoz CF, Südfeld C, Naduthodi MI, Weusthuis RA, Barbosa MJ, Wijffels RH, et al. Genetic engineering of microalgae for enhanced lipid production. *Biotechnol Adv.* (2021) 52:107836. doi: 10.1016/j.biotechadv.2021.107836
43. Sproles AE, Fields FJ, Smalley TN, Le CH, Badary A, Mayfield SP. Recent advancements in the genetic engineering of microalgae. *Algal Res.* (2021) 53:102158. doi: 10.1016/j.algal.2020.102158
44. Sakaguchi K, Matsuda T, Kobayashi T, Ohara JI, Hamaguchi R, Abe E, et al. Versatile transformation system that is applicable to both multiple transgene expression and gene targeting for Thraustochytrids. *Appl Environ Microbiol.* (2012) 78:3193–202. doi: 10.1128/AEM.07129-11
45. Ma Y, Wang Z, Zhu M, Yu C, Cao Y, Zhang D, et al. Increased lipid productivity and TAG content in Nannochloropsis by heavy-ion irradiation mutagenesis. *Bioresour Technol.* (2013) 136:360–7. doi: 10.1016/j.biortech.2013.03.020
46. Geng L, Chen S, Sun X, Hu X, Ji X, Huang H, et al. Fermentation performance and metabolomic analysis of an engineered high-yield PUFA-producing strain of *Schizochytrium* sp. *Bioprocess Biosyst Eng.* (2019) 42:71–81. doi: 10.1007/s00449-018-2015-z

47. Han X, Zhao Z, Wen Y, Chen, Z. Enhancement of docosahexaenoic acid production by overexpression of ATP-citrate lyase and acetyl-CoA carboxylase in *Schizochytrium* sp. *Biotechnol Biofuels*. (2020) 13:131. doi: 10.1186/s13068-020-01767-z
48. Wang S, Wan W, Wang Z, Zhang H, Liu H, Arunakumara, et al. A two-stage adaptive laboratory evolution strategy to enhance docosahexaenoic acid synthesis in oleaginous thraustochytrid. *Front Nutr*. (2021) 8:795491. doi: 10.3389/fnut.2021.795491

Conflict of Interest: The authors declare that the research was conducted in the absence of any commercial or financial relationships that could be construed as a potential conflict of interest.

Publisher's Note: All claims expressed in this article are solely those of the authors and do not necessarily represent those of their affiliated organizations, or those of the publisher, the editors and the reviewers. Any product that may be evaluated in this article, or claim that may be made by its manufacturer, is not guaranteed or endorsed by the publisher.

frontiers | Frontiers in Nutrition

ORIGINAL RESEARCH
published: 03 May 2022
doi: 10.3389/fnut.2022.876817

Evaluation of Different Standard Amino Acids to Enhance the Biomass, Lipid, Fatty Acid, and γ-Linolenic Acid Production in *Rhizomucor pusillus* and *Mucor circinelloides*

Hassan Mohamed[1,2], Mohamed F. Awad[2,3], Aabid Manzoor Shah[1], Yusuf Nazir[1,4], Tahira Naz[1], Abdallah Hassane[2], Shaista Nosheen[1] and Yuanda Song[1]**

[1] Colin Ratledge Center for Microbial Lipids, School of Agricultural Engineering and Food Science, Shandong University of Technology, Zibo, China, [2] Department of Botany and Microbiology, Faculty of Science, Al-Azhar University, Assiut, Egypt, [3] Department of Biology, College of Science, Taif University, Taif, Saudi Arabia, [4] Department of Food Sciences, Faculty of Science and Technology, Universiti Kebangsaan Malaysia, Bangi, Malaysia

OPEN ACCESS

Edited by:
Fernando M. Nunes, University of Trás-os-Montes and Alto Douro, Portugal

Reviewed by:
Fuguo Xing, Institute of Food Science and Technology (CAAS), China
Weaam Ebrahim, Mansoura University, Egypt

***Correspondence:**
Hassan Mohamed
hassanmohamed85@azhar.edu.eg
Yuanda Song
ysong@sdut.edu.cn

Specialty section:
This article was submitted to Food Chemistry, a section of the journal Frontiers in Nutrition

Received: 15 February 2022
Accepted: 31 March 2022
Published: 03 May 2022

Citation:
Mohamed H, Awad MF, Shah AM, Nazir Y, Naz T, Hassane A, Nosheen S and Song Y (2022) Evaluation of Different Standard Amino Acids to Enhance the Biomass, Lipid, Fatty Acid, and γ-Linolenic Acid Production in Rhizomucor pusillus and Mucor circinelloides. Front. Nutr. 9:876817. doi: 10.3389/fnut.2022.876817

In this study, 18 standard amino acids were tested as a single nitrogen source on biomass, total lipid, total fatty acid (TFA) production, and yield of γ-linolenic acid (GLA) in *Rhizomucor pusillus* AUMC 11616.A and *Mucor circinelloides* AUMC 6696.A isolated from unusual habitats. Grown for 4 days at 28°C, shaking at 150 rpm, the maximum fungal biomass for AUMC 6696.A was 14.6 ± 0.2 g/L with arginine and 13.68 ± 0.1 g/L with asparagine, when these amino acids were used as single nitrogen sources, while AUMC 11616.A maximum biomass was 10.73 ± 0.8 g/L with glycine and 9.44 ± 0.6 g/L with valine. These were significantly higher than the ammonium nitrate control ($p < 0.05$). The highest levels of TFA were achieved with glycine for AUMC 11616.A, 26.2 ± 0.8% w/w of cell dry weight, and glutamic acid for AUMC 6696.A, 23.1 ± 1.3%. The highest GLA yield was seen with proline for AUMC 11616.A, 13.4 ± 0.6% w/w of TFA, and tryptophan for AUMC 6696.A, 12.8 ± 0.3%, which were 38% and 25% higher than the ammonium tartrate control. The effects of environmental factors such as temperature, pH, fermentation time, and agitation speed on biomass, total lipids, TFA, and GLA concentration of the target strains have also been investigated. Our results demonstrated that nitrogen assimilation through amino acid metabolism, as well as the use of glucose as a carbon source and abiotic factors, are integral to increasing the oleaginicity of tested strains. Few studies have addressed the role of amino acids in fermentation media, and this study sheds light on *R. pusillus* and *M. circinelloides* as promising candidates for the potential applications of amino acids as nitrogen sources in the production of lipids.

Keywords: lipid accumulation, fatty acids, GLA, nitrogen source, abiotic factors, *Rhizomucor pusillus*, *Mucor circinelloides*

INTRODUCTION

Microorganisms known for naturally synthesizing lipids for more than 20% of their cell dry weight (CDW) are termed oleaginous microorganisms (1, 2). They have frequently been found to produce oils with compositional similarities to plants and fish (3). Nutritionally important polyunsaturated fatty acids (PUFAs), such as γ-linolenic acid (GLA), have been shown in various studies to be beneficial in the avoidance and treatment of multiple diseases (4, 5). Microorganisms have several advantages over traditional plants for producing GLA-rich oils, including simple cultural conditions, a high growth rate, and high yields that are not affected by changes in climatic conditions (6). Thus, GLA production by oleaginous microorganisms is a promising alternative to plant-based production. *Mucor circinelloides*, an oleaginous fungus, has been broadly employed to study GLA production, and it has been chosen as a model oleaginous microbe to produce GLA in various studies (7–11).

Nitrogen sources are essential components for microbial growth media, and several studies have demonstrated that nitrogen sources play important roles in growth conditions and bioactive compound production (12–14). The influences of nitrogen sources on lipid accumulation and unsaturated fatty acid production in oleaginous microorganisms, mainly fungi, have been extensively studied. Sodium nitrate stimulated cell growth, while also increasing lipid accumulation in *Neochloris oleoabundans* (15). Due to their effects on mycelial morphology, *Mortierella alpina* accumulated two times as much arachidonic acid when soybean meal was employed as a nitrogen source in the medium in the presence of yeast extract (16, 17). Organic nitrogen compounds are more favorable for cell growth and lipid production in oleaginous fungus *M. alpina* than inorganic nitrogen sources (18), and it has been observed that different amino acids, used as nitrogen supplementation, can differentially regulate gene expression, which in turn affects lipid production in *Saccharomyces cerevisiae* (19). However, few studies have been carried out to investigate the individual effects of each of the 18 amino acids on lipid biosynthesis in various oleaginous microorganisms.

Different strategies have been suggested for the development of lipid production in microorganisms. Among them, nitrogen restriction has been widely stated as an effective approach for the overproduction of storage lipids in oleaginous microbes (20). Recently, some reports have indicated that nitrogen limitation could also enhance lipid accumulation in oleaginous yeasts (21, 22). However, the impact of different nitrogen deficiency strategies on lipid production in oleaginous microbes, including yeast and filamentous fungi, is thus far unreported. In fermentation media, the carbon/nitrogen (C/N) ratio controls the switch between protein and lipid synthesis; therefore, the C/N ratio of culture media is one of the most critical nutritional factors affecting the total amount of produced lipids. Moreover, it has been observed that the initial C/N ratio should be higher than 20 for maximum lipid accumulation by oleaginous organisms (23, 24).

In our recent work, we have investigated multiple Mucoromycota fungi for GLA, lipid, and carotenoids content, and two strains, *Rhizomucor pusillus* AUMC 11616.A and *Mucor circinelloides* AUMC 6696.A, were chosen for this study, based on their high lipid content, as promising strains for lipid production (25). A literature survey on the oleaginous fungus *R. pusillus* did not reveal any studies on its nitrogen assimilation and lipid production. Therefore, the effects of 18 standard amino acids as single nitrogen sources on fungal growth, glucose consumption, lipid accumulation, and GLA content in *R. pusillus*, as well as in *M. circinelloides*, were investigated in this study. In this study, we explore the significance of using amino acids as nitrogen sources for improving the biotechnological application of oleaginous fungi for lipid accumulation.

MATERIALS AND METHODS

Microorganisms

The strains *R. pusillus* AUMC 11616.A and *M. circinelloides* AUMC 6696.A were obtained from our previous work (25) as pure stock cultures of the laboratory of Microbial Lipids and Fermentation, School of Agriculture Engineering and Food Science, Shandong University of Technology. These strains were initially isolated from unusual niches (animal manure and textile [100%] polyester) and are characterized by the production of high lipid contents. The cultures were stored at 4–6°C on potato dextrose agar (PDA) slants (Hopebio Laboratories, China) and subcultured every 2–3 months.

Microbiological Media and Culture Conditions

The Kendrick and Ratledge medium (K&R), which is rich in carbon and limited in nitrogen, was used in this study during all fermentation stages (26). In total, 100 μl spore suspensions of approximately 1×10^7 spores/ml of *R. pusillus* or *M. circinelloides* were obtained from 5-day-old PDA cultures and inoculated separately into 500 ml baffled flasks containing 150 ml of K&R medium, which contained 30.0 g/L glucose, 3.30 g/L ammonium tartrate, 2.0 g/L Na_2HPO_4, 7.0 g/L KH_2PO_4, 1.50 g/L yeast extract, 1.50 g/L $gSO_4{\cdot}7H_2O$, 0.1 g/L $CaCl_2{\cdot}2H_2O$, 1.0 mg/L $ZnSO_4{\cdot}7H_2O$, 8.0 mg/L $FeCl_3{\cdot}6H_2O$, 0.1 mg/L $Co(NO_3)_2{\cdot}6H_2O$, 0.1 mg/L $LMnSO_4{\cdot}5H_2O$, and 0.1 mg/L $CuSO_4{\cdot}5H_2O$ in 1,000 ml deionized H_2O. All components were sterilized at 121°C for 20 min, except for glucose, which was added after sterilization. The cultures were incubated at 28°C with an agitation speed of 150 rpm and then used as a seed culture at 10% (v/v) to inoculate 500 ml baffled flasks with 150 ml modified K&R (N-limited medium), containing 80.0 g/L glucose and 0.5 g/L nitrogen, without yeast extract. Ammonium tartrate (control) and 18 amino acids were used as single nitrogen sources, and each medium contained 0.5 g nitrogen/L (e.g., 3.29 g/L ammonium tartrate, or 3.19 g/L alanine, or 2.68 g/L glycine, equivalent to 0.5 g/L nitrogen). The cultures were incubated for 96 h at 28°C with agitation at 150 rpm.

Determination of Biomass Concentration

The fungal dry cell mass was harvested by filtration through a Buchner funnel under reduced pressure. The resulting fungal

biomass was rinsed thrice with sterile deionized water to eliminate possible medium residues. After filtration, all samples were frozen overnight in a freeze-dryer at -80°C, lyophilized for a further 48 h, and then the fungal cell dry weight (CDW) was measured by the weighing method. This measurement was carried out in triplicate.

Determination of Glucose Concentrations

Glucose concentration in the culture was measured using a biosensor analyzer (SBA-40E, Shandong University of Technology, China) according to the manufacturer's instructions.

Extraction of Total Lipids

Total lipids were extracted from the dried biomass according to the Folch method with some minor modifications (10). In brief, approximately 20 mg of fungal biomass was vigorously homogenized with 2 ml of 5 M HCl in lipid tubes. Then, these were placed in a water bath at 80°C for 4–5 h (vortexed every 1 h). The mixture was cooled down to room temperature and then added with 2 ml chloroform, 1 ml methanol, and 100 μl pentadecanoic acid as an internal standard (15:0 from Millipore, Sigma-Aldrich, United States), and the resulting mixture was vortexed for 30 s. For proper mixing, tubes were placed in a vertical 360 tube rotator for 1 h and then centrifuged at 3,000 rpm for 5 min to separate the two phases. The lower phase of 2 ml chloroform with extracted lipids was removed and transferred to a new tube. The solvent phase was evaporated under a stream of N_2 and the total lipids were determined as% wt/wt of biomass.

Analysis of Fatty Acid Profile

Fatty acid methyl esters (FAME) were extracted by initially adding 1 ml of 10% methanol in HCl at 60°C for 3 h, followed by 2 ml *n*-Hexane and 1 ml saturated NaCl. All tubes were vortexed for 30–60 s, placed in a vertical 360 tube rotator for 1 h, and then centrifuged at 3,000 rpm for 5 min. The resultant FAMEs were subsequently analyzed by gas chromatography (GC). The GC machine was equipped with a flame ionization detector (FID) and the capillary column DB-FFAP (30 m × 320 μm × 0.25 μm film thickness: Agilent Scientific Instruments), with the temperature program increasing from 160 to 230°C at 8°C min. Following the analysis, a ballistic increase to 300°C allows cleaning of the column during a hold of 2 min. The detector gases were air and hydrogen; their flow rates were regulated at 400 and 30 ml/min, respectively. Nitrogen was used as a make-up gas at 25 ml/min. The injection volume was 1 μl with a total run time of 25 min. Identification and quantification of individual chromatographic peaks were carried out by comparison to the external fatty acid methyl ester standard mixture (Supelco® 37 Component FAME Mix).

Effect of Various Environmental Factors on Tested Strains

Based on the results showing high lipid content, asparagine and glutamine amino acids were chosen as nitrogen sources to investigate the maximum biomass, lipid, fatty acids, and GLA content of *R. pusillus* AUMC 11616.A and *M. circinelloides* AUMC 6696.A, respectively, under selected various abiotic factors. Notably, 150 ml of K&R fermentation medium in 500 ml flasks with asparagine or glutamine was used in this experiment. Four different abiotic factors were used to test their effect on fungal biomass, total lipids, TFA, and GLA yields of the tested strains. To investigate the effects of pH, it was adjusted for values of 4–8. The temperature varied in the range of 15 ± 2°C–40 ± 2°C, and agitation speed ranged from 100 to 250 rpm, while different incubation periods of 1–6 days were also studied.

Statistical Analysis

All data of the experiments were statistically analyzed with three replicates, and the results were presented as mean ± SD (n = 3). Student's t-test was performed in SPSS 16.0 for statistical analysis of the data, and $p < 0.05$ was considered significantly different.

RESULTS

Cultural Characteristics and Phylogenetic Tree Construction

The selected strains *R. pusillus* AUMC 11616.A and *M. circinelloides* AUMC 6696.A were pre-identified based on their morphology and confirmed by the ITS-5.8S ribosomal gene sequences method. The target strains were characterized as fast-growing Mucorales, producing white to gray colonies on PDA agar plates. The ITS ribosomal gene sequence results of AUMC 11616.A and AUMC 6696.A were correlated with the phylogenetic position as shown in **Figure 1**. The microscopic examinations of these strains are shown in **Supplementary Figure 1**.

Effects of 18 Amino Acids on the Growth and Glucose Utilization of Tested Strains

The selected fungal strains AUMC 11616.A and AUMC 6696.A were cultivated in the K&R fermentation media for 4 days. Fungal biomass concentration with different nitrogen sources was determined (**Figure 2**). When compared to ammonium tartrate as control, alanine, proline, glycine, especially arginine and asparagine, stimulated the growth of AUMC 6696.A, and glutamic acid, serine, leucine, especially valine and glycine, stimulated the growth of AUMC 11616.A. When arginine and asparagine were used as single nitrogen sources by AUMC 6696.A, the CDW reached up to 14.5 and 13.6 g/L, respectively, which were 35% and 30% higher than that of ammonium tartrate. In the case of AUMC 11616.A with valine and glycine as nitrogen sources, the CDW reached up to 9.4 and 10.8 g/L, respectively, which were 36% and 42% higher than the control. Contrastingly, the fungal biomass production of the selected strains grown on cysteine, tryptophan, valine, and histidine for AUMC 6696.A, or cysteine and tyrosine for AUMC 11616.A, were markedly lower than that of the ammonium tartrate control. Our findings suggested that

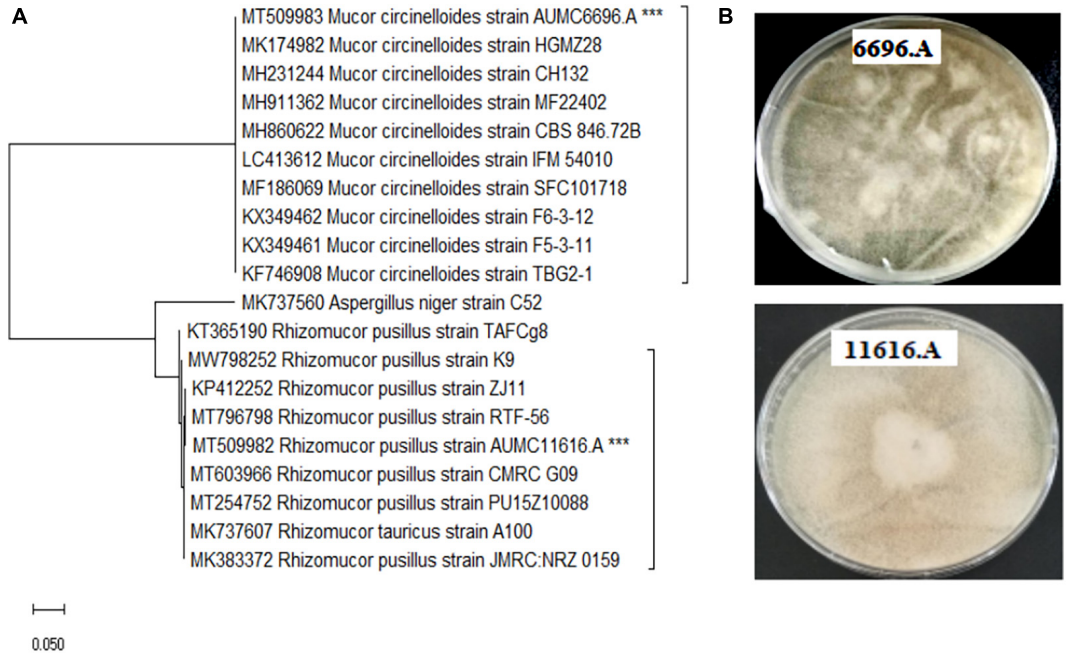

FIGURE 1 | (A) The neighbor-joining (NJ) phylogenetic tree based on ITS gene sequences of AUMC 6696.A and AUMC 11616.A, with closely related strains accessed from the GenBank using BLASTN (http://www.ncbi.nlm.nih.gov/blast/). These sequences were aligned using ClustalW. Bootstrap values included 500 replicates for the NJ method using MEGA software (version 11.0.6). ***indicates tested strain. **(B)** Morphological characteristics of tested strains on agar plates.

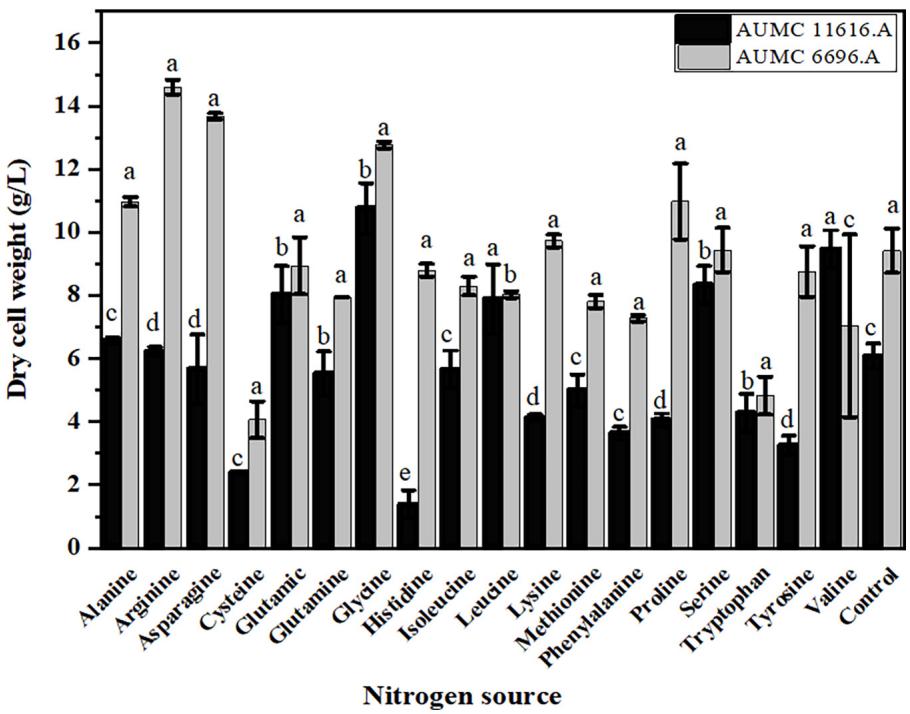

FIGURE 2 | Biomass concentration (g/L) of *R. pusillus* AUMC 11616.A and *M. circinelloides* AUMC 6696.A strains grown at 30°C for 4 days, on different nitrogen sources. Ammonium tartrate was employed as the control. Error bars represent the average standard deviation from three biological replicates. Values that show different superscripts were significantly different from each other using *t*-test ($p < 0.05$).

these amino acids were not good nitrogen sources for the optimal growth of these fungi. These results showed varied significant impacts on biomass dry weight when compared with their control, which may affect lipid metabolism and further impact fatty acid biosynthesis and GLA in AUMC 6696.A and AUMC 11616.A.

Since glucose is utilized as a carbon source during fungal growth, the residual glucose concentration was determined after 4 days of fermentation, showing that the rate of glucose consumption was different in these two strains, dependent on the amino acid source. As shown in **Figure 3**, the residual glucose concentrations of AUMC 11616.A grown on glutamic acid, glycine, methionine, or cysteine and AUMC 6696.A grown on tryptophan, tyrosine, leucine or histidine were significantly higher than that of ammonium tartrate (initial value 80 g/L), and the fungal biomass production was correspondingly lower than that of the control, as shown in **Figure 2**. While the residual glucose concentrations of AUMC 6696.A grown on cysteine, glutamic acid, and glutamine were markedly lower than that of the control, AUMC 11616.A grown on glutamine, proline, and valine were determined to have the lowest concentrations of residual glucose.

Influence of Amino Acids on Total Lipids, Fatty Acids, and Their Composition, and GLA Content in Selected Strains

To investigate the effect of different amino acids on lipid accumulation in AUMC 6696.A and AUMC 11616.A, lipid analysis of these fungi was performed. The resulting CDWs of the tested strains after fermentation were evaluated for their total lipid content and fatty acid composition. Based on our results, the AUMC 6696.A produced higher lipid content than AUMC 11616.A during the cultivation of all tested amino acids. Data in **Figure 4** show the lipid content of the AUMC 11616.A grown on asparagine (31 ± 1.1) and leucine (30.5 ± 09) and AUMC 6696.A grown on glutamine (44.5 ± 1.3) and glutamic acid (43.5 ± 0.2%) had the greatest lipid production. Most amino acid sources, including arginine, glycine, lysine, valine, serine, and cysteine, decreased lipid production in both tested strains compared with the control, while proline and alanine, for AUMC 11616.A, and tryptophan and methionine, for AUMC 6696.A, had no significant effect ($p < 0.001$) on lipid production. These results suggest that asparagine and leucine for AUMC 11616.A and glutamine and glutamic acid for AUMC6696.A were the optimal nitrogen sources for total lipid accumulation. Among tested amino acids, the tested strain AUMC6696.A exhibited not much significant difference in lipid content when compared to control, while asparagine and leucine in AUMC 11616.A strain showed significantly higher in their lipid content when compared with ammonium tartrate as a control.

Total fatty acid production of AUMC 11616.A grown on glycine and AUMC 6696.A grown on glutamic acid were 26.2 ± 0.8 and 23.1 ± 1.3% (w/w) of CDW, respectively, which were the highest among tested nitrogen sources and 1.19 and 1.11 times that of ammonium tartrate controls (**Figure 5**). Notably, tryptophan in AUMC 11616.A (8.9 ± 0.3) and arginine in AUMC 6696.A (8.7 ± 0.2%)

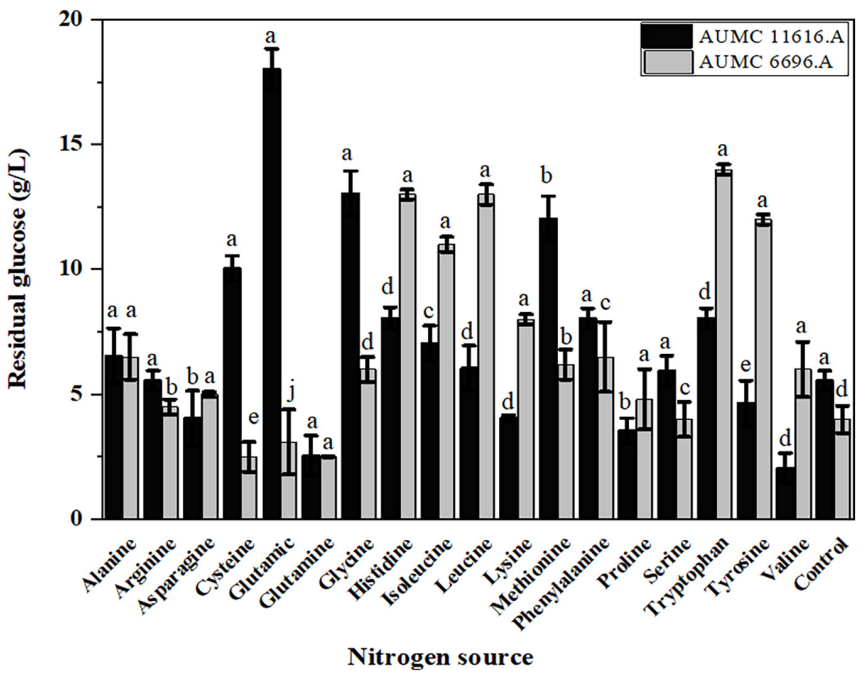

FIGURE 3 | The residual glucose concentration (g/L) of *R. pusillus* AUMC 11616.A and *M. circinelloides* AUMC 6696.A strains grown at 30°C for 4 days, on different nitrogen sources. Ammonium tartrate was employed as the control. Error bars represent the average standard deviation from three biological replicates. Values that show different superscripts were significantly different from each other using *t*-test ($p < 0.05$).

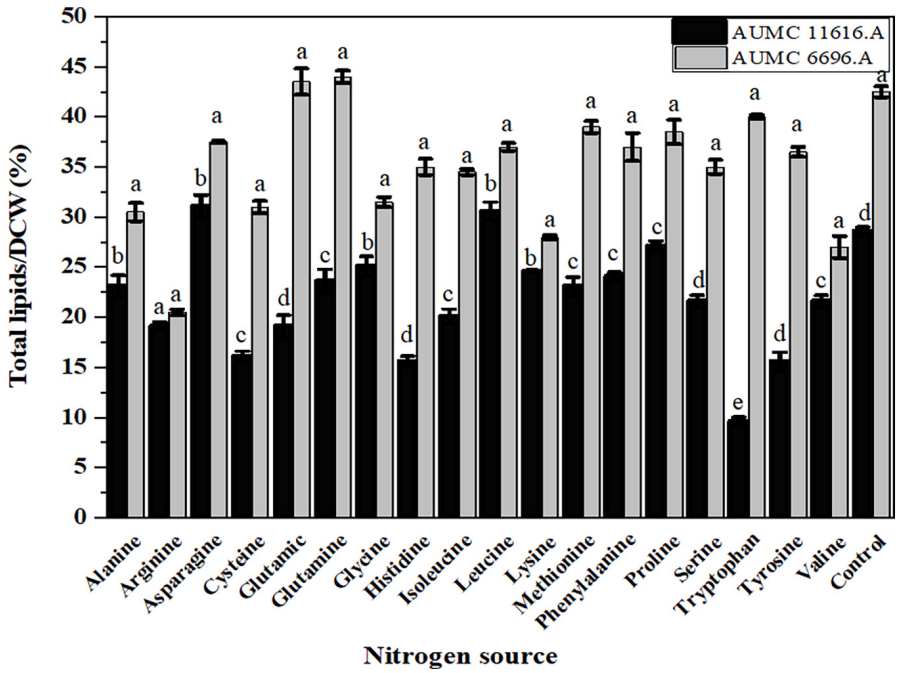

FIGURE 4 | Total lipids production of *R. pusillus* AUMC 11616.A and *M. circinelloides* AUMC 6696.A strains grown at 30°C for 4 days, on different nitrogen sources. Ammonium tartrate was employed as the control. Error bars represent the average standard deviation from three biological replicates. Values that show different superscripts were significantly different from each other using *t*-test ($p < 0.05$).

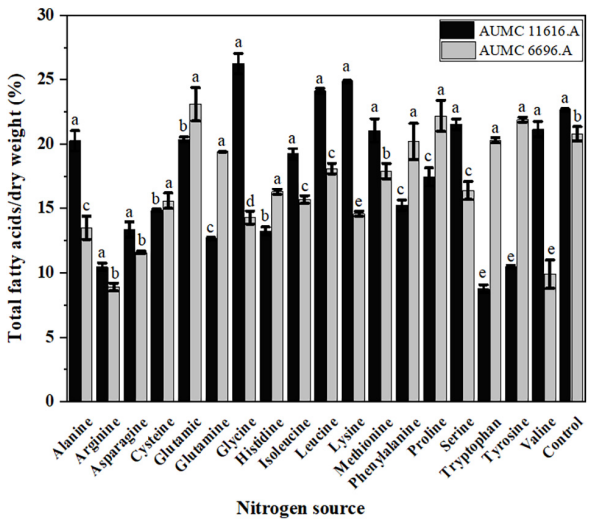

FIGURE 5 | Total fatty acids (TFAs) production of *R. pusillus* AUMC 11616.A and *M. circinelloides* AUMC 6696.A strains grown at 30°C for 4 days, on different nitrogen sources. Ammonium tartrate was employed as the control. Error bars represent the average standard deviation from three biological replicates. Values that show different superscripts were significantly different from each other using *t*-test ($p < 0.05$).

produced the lowest TFAs. These findings indicated no significant impact ($p < 0.061$) on TFAs in both tested strains compared to control.

To investigate the effects of 18 amino acids on the TFA composition of AUMC 11616.A and AUMC 6696.A, strains were grown on glucose as carbon source and with one of the 18 amino acids as nitrogen source, with the same C/N ratio and with the same culture conditions. Oleic acid (C18:1) was the predominant fatty acid grown with each amino acid in both tested strains. Of the 18 amino acids, glutamic acid for AUMC 11616.A and serine for AUMC 6696.A prominently enhanced the stearic acid (18:0) concentration within TFAs 2.17- and 3.9-fold, respectively, compared to ammonium tartrate controls. Additionally, tyrosine for AUMC 11616.A and valine for AUMC 6696.A also greatly improved the palmitoleic acid (C16:1) concentration of TFAs 3.2- and 2.3-fold compared to controls, respectively. A significant decrease in GLA concentration was seen for AUMC 11616.A grown on phenylalanine (74% of control), tryptophan (57%), and histidine (49%), as well as for AUMC 6696.A grown on asparagine (16.5%), leucine (15.1%), and cysteine (13.9%), compared to controls. A potential explanation for this could be due to the relevant desaturases (i.e., Delta-6-desaturase) for the synthesis of GLA being suppressed when these fungi were grown on certain amino acids. Although proline and tryptophan strongly increased the GLA concentration of the TFAs by 25% and 38% in their respective strains, overall fungal biomass and lipid production were not produced in sufficient quantities, therefore showing these are not suitable nitrogen sources for GLA production. Detailed FAs chromatographic analyses based on GC results are listed in **Supplementary Figure 2**, and FAs profile of these fungi are shown in **Table 1**. Through comprehensive analysis, the

TABLE 1 | Fatty acid composition of *R. pusillus* AUMC 11616.A and *M. circinelloides* AUMC 6696.A fungi grown on different amino acids at 28°C for 4 days.

Amino acids (N-source)	Composition of fatty acid (% TFA)													
	C14:0		C16:0		C16:1		C18:0		C18:1		C18:2		C18:3	
	11616.A	6696.A	11616.A	6696.A	11616.A	6696.A	11616.A	6696.A	11616.A	6696.A	11616.A	6696.A	11616.A	6696.A
Alanine	2.2 ± 0.1	3.5 ± 0.1	27.3 ± 0.2	21.1 ± 0.4	1.4 ± 0.1	5.2 ± 0.1	12.6 ± 0.1	3.5 ± 0.1	35.7 ± 1.3	48.7 ± 2.1	12.7 ± 0.2	10.5 ± 0.2	8.1 ± 0.1	7.5 ± 0.1
Arginine	4.3 ± 0.1	3.7 ± 0.1	22.5 ± 0.3	16.8 ± 0.1	8.1 ± 0.1	6.2 ± 0.1	2.3 ± 0.1	3.1 ± 0.13	43.2 ± 1.2	42.5 ± 1.3	13.5 ± 0.2	15.1 ± 0.2	5.9 ± 0.1	12.6 ± 0.1
Asparagine	4.5 ± 0.1	3.0 ± 0.0	20.0 ± 1.2	19.3 ± 1.1	5.1 ± 0.2	4.0 ± 0.1	4.7 ± 0.3	3.0 ± 0.1	37.6 ± 0.6	52.8 ± 1.3	17.6 ± 0.8	10.8 ± 0.1	10.7 ± 0.1	6.6 ± 0.2
Cysteine	4.5 ± 0.1	3.5 ± 0.1	26.3 ± 0.8	23.7 ± 0.5	3.3 ± 0.1	3.1 ± 0.1	9.0 ± 0.2	4.1 ± 0.1	32.5 ± 1.4	50.5 ± 1.9	13.0 ± 0.2	8.7 ± 0.2	11.5 ± 0.2	6.8 ± 0.1
Glutamic acid	0.8 ± 0.0	2.5 ± 0.1	27.5 ± 0.6	21.7 ± 0.4	0.9 ± 0.1	3.4 ± 0.1	18.4 ± 0.4	4.1 ± 0.1	33.4 ± 0.9	45.4 ± 1.8	12.7 ± 0.2	10.9 ± 0.1	6.6 ± 0.1	12.1 ± 0.2
Glutamine	3.5 ± 0.1	2.5 ± 0.1	17.6 ± 0.2	21.7 ± 0.3	6.1 ± 0.1	2.8 ± 0.1	2.1 ± 0.1	4.1 ± 0.1	37.5 ± 03	46.4 ± 0.5	21.2 ± 0.2	11.8 ± 0.1	12.1 ± 0.1	10.5 ± 0.1
Glycine	0.7 ± 0.0	3.1 ± 0.1	27.2 ± 0.8	16.6 ± 0.7	1.2 ± 0.0	4.1 ± 0.1	16.6 ± 0.2	3.8 ± 0.1	33.8 ± 1.4	47.9 ± 1.1	14.0 ± 0.3	12.6 ± 0.1	6.9 ± 0.1	12.0 ± 0.1
Histidine	4.7 ± 0.1	2.1 ± 0.1	30.2 ± 0.8	24.9 ± 1.3	2.7 ± 0.1	1.8 ± 0.1	17.4 ± 0.6	6.2 ± 0.1	29.3 ± 1.5	48.4 ± 1.8	10.8 ± 0.2	8.6 ± 0.1	5.1 ± 0.1	8.2 ± 0.1
Isoleucine	2.1 ± 0.0	3.2 ± 0.1	29.3 ± 0.5	19.6 ± 0.4	1.6 ± 0.0	3.7 ± 0.1	11.5 ± 0.1	3.0 ± 0.1	34.5 ± 0.6	46.7 ± 1.2	15.2 ± 0.8	12.9 ± 0.6	7.5 ± 0.1	11.0 ± 0.2
Leucine	1.8 ± 0.1	3.0 ± 0.1	28.3 ± 0.4	24.7 ± 0.6	1.4 ± 0.0	3.7 ± 0.1	14.7 ± 0.1	4.5 ± 0.1	36.3 ± 1.2	47.0 ± 1.4	12.2 ± 0.3	10.4 ± 0.2	5.5 ± 0.1	6.7 ± 0.1
Lysine	2.2 ± 0.0	3.0 ± 0.0	31.0 ± 0.8	25.7 ± 0.4	2.4 ± 0.0	2.0 ± 0.0	8.2 ± 0.4	9.2 ± 0.3	34.9 ± 0.9	36.7 ± 0.6	12.3 ± 0.2	11.7 ± 0.1	9.0 ± 0.1	11.9 ± 0.1
Methionine	3.0 ± 0.0	2.7 ± 0.1	22.0 ± 0.3	21.6 ± 0.4	3.8 ± 0.1	2.9 ± 0.1	4.6 ± 0.1	4.0 ± 0.1	44.7 ± 1.2	48.7 ± 1.3	12.9 ± 0.2	11.2 ± 0.1	9.1 ± 0.1	8.9 ± 0.1
Phenylalanine	0.2 ± 0.1	2.2 ± 0.1	25.1 ± 0.4	20.1 ± 0.1	1.8 ± 0.1	3.3 ± 0.1	9.3 ± 0.2	4.1 ± 0.13	47.8 ± 1.4	48.1 ± 1.2	11.8 ± 0.2	11.9 ± 0.1	2.3 ± 0.1	10.6 ± 0.1
Proline	4.3 ± 0.1	2.3 ± 0.1	19.5 ± 1.1	21.3 ± 0.8	4.8 ± 0.1	3.7 ± 0.2	2.9 ± 0.0	4.2 ± 0.1	39.0 ± 0.6	44.7 ± 1.1	16.4 ± 0.3	11.2 ± 0.2	13.4 ± 0.2	12.3 ± 0.1
Serine	2.4 ± 0.1	2.6 ± 0.1	24.7 ± 0.4	18.8 ± 0.2	1.1 ± 0.1	1.8 ± 0.1	14.2 ± 0.3	3.2 ± 0.2	31.3 ± 1.2	45.4 ± 1.7	12.7 ± 0.3	13.5 ± 0.2	6.1 ± 0.1	13.4 ± 0.1
Tryptophan	0.3 ± 0.0	1.7 ± 0.1	23.6 ± 0.3	18.3 ± 0.2	1.3 ± 0.0	2.6 ± 0.1	12.7 ± 0.1	3.7 ± 0.1	40.1 ± 1.2	48.6 ± 1.6	15.9 ± 0.5	12.5 ± 0.4	4.3 ± 0.1	12.8 ± 0.4
Tyrosine	6.8 ± 0.3	2.1 ± 0.1	22.8 ± 0.5	24.8 ± 0.6	8.8 ± 0.3	2.6 ± 0.1	8.1 ± 0.1	5.5 ± 0.1	33.6 ± 1.1	44.3 ± 1.2	11.9 ± 0.4	10.2 ± 0.2	8.2 ± 0.1	10.9 ± 0.5
Valine	0.2 ± 0.0	4.3 ± 0.1	28.5 ± 1.3	16.6 ± 0.8	0.9 ± 0.1	6.9 ± 0.1	15.1 ± 0.8	1.9 ± 0.8	34.2 ± 1.2	47.2 ± 1.3	15.3 ± 0.6	14.4 ± 1.1	5.2 ± 0.1	8.3 ± 0.1
Control	2.5 ± 0.0	2.8 ± 0.1	26.3 ± 0.4	23.0 ± 0.2	2.7 ± 0.1	3.0 ± 0.1	8.5 ± 0.1	4.1 ± 0.1	38.9 ± 0.9	48.1 ± 0.7	11.2 ± 0.2	11.1 ± 0.2	10.0 ± 0.1	7.9 ± 0.1

Ammonium tartrate was employed as a control.

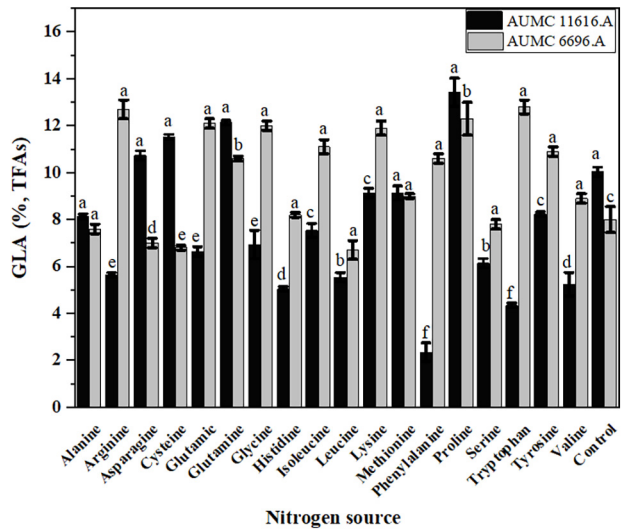

FIGURE 6 | Effect of different amino acids on the GLA content of TFAs in *R. pusillus* AUMC 11616.A and *M. circinelloides* AUMC 6696.A strains grown at 30°C for 4 days, on different nitrogen sources. Ammonium tartrate was employed as the control. Error bars represent the average standard deviation from three biological replicates. Values that show different superscripts were significantly different from each other using *t*-test ($p < 0.05$).

FAs composition of the tested strains was significantly increased compared to the control.

The effect of each amino acid as a nitrogen source on the GLA content of TFAs in these strains is shown in **Figure 6**. Most amino acids markedly decreased the GLA content of TFAs when compared to control, particularly in AUMC 11616.A. Some amino acids, such as lysine and methionine for AUMC 11616.A and alanine and histidine for AUMC 6696.A, had no prominent effect on the GLA content of TFAs, and only proline and tryptophan, as above, significantly increased the GLA content of TFAs in their respective strain. Peaks of different FAs in the tested samples were identified and confirmed by comparing with the retention time stability and peak area repeatability of the standard mixtures. Target FAs in all tested samples appeared relatively clear in GC chromatography as shown in **Figure 7** (as an example).

Effect of Abiotic Factors on AUMC11616.A and AUMC6696.A

K&R media containing asparagine for AUMC 11616.A and glutamine for AUMC 6696.A as nitrogen sources were employed to investigate the effects of abiotic factors, including fermentation time, pH, temperature, and agitation speed, on producing the greatest fungal biomass, total lipids, TFA, and GLA content with these strains. In this investigation, the tested strains were grown for 1, 2, 3, 4, 5, and 6 days. The highest GLA percentage of total fatty acids was 16 ± 0.6% for AUMC 11616.A and 15 ± 0.2% for AUMC 6696.A at the end of the 3rd day, and 19 ± 0.7 and 23 ± 0.9%, respectively, at the end of the 2nd day of incubation, while total lipids, as a percentage of CDW (46 ± 1.5% for AUMC 11616.A and 43 ± 1.2% for AUMC 6696.A) and biomass (12 ± 1.1 g/L for AUMC 11616.A and 11 ± 0.6 g/L for AUMC 6696.A) were seen to be highest at the end of the 4th, 5th, and 6th days of fermentation. Fermentation media with pH ranging from 4 to 8 were also tested. Cultures were grown with various pH levels at 28°C for 4 days. The greatest total lipids (45 ± 1.4% of CDW for AUMC 11616.A and 44 ± 0.8% for AUMC 6696.A) and biomass (10 ± 0.3 g/L for AUMC 11616.A and 10.5 ± 0.6 g/L for AUMC 6696.A) were seen at pH 6. Notably, total biomass and lipid production significantly dropped under suboptimal pH conditions. At this pH, AUMC 6696.A achieved the maximum

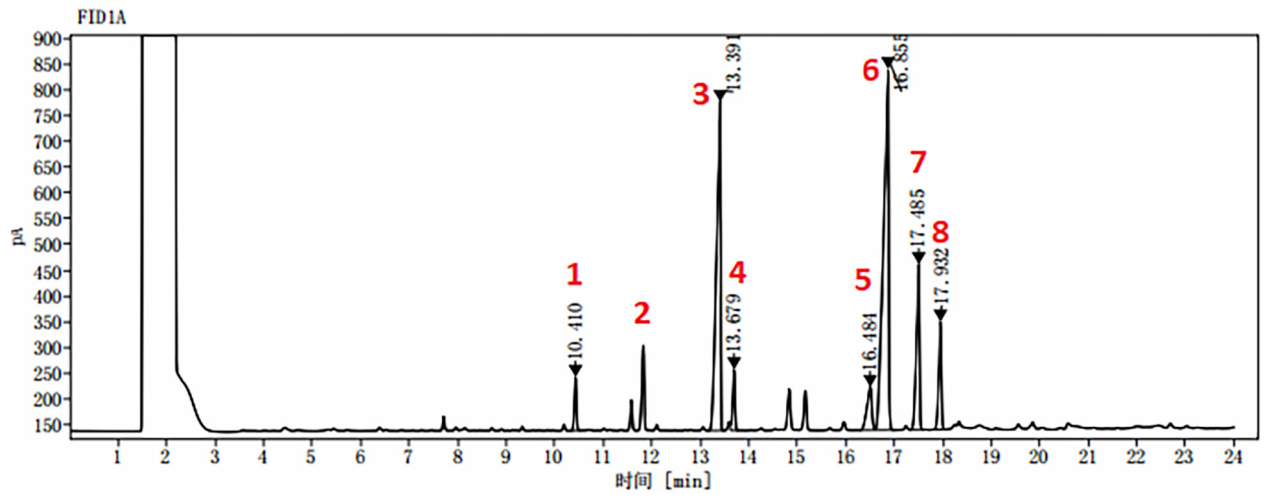

FIGURE 7 | A typical GC chromatogram of target FAs identified from all tested samples. **1**. myristic acid "C14:0" at retention time: 10.410 min; **2**. pentadecanoic acid as standard "C15:0" at retention time: 11.910 min; **3**. palmitic acid "C16:0" at retention time: 13.391 min; **4**. palmitoleic acid "C16:1" at retention time: 13.679 min; **5**. stearic acid "C18:0" at retention time: 16.484 min; **6**. oleic acid "C18:1" at retention time: 16.855 min; **7**. linoleic acid "C18:2" at retention time: 17.485 min; and **8**. γ-linolenic acid "C18:3" at retention time: 17.932 min.

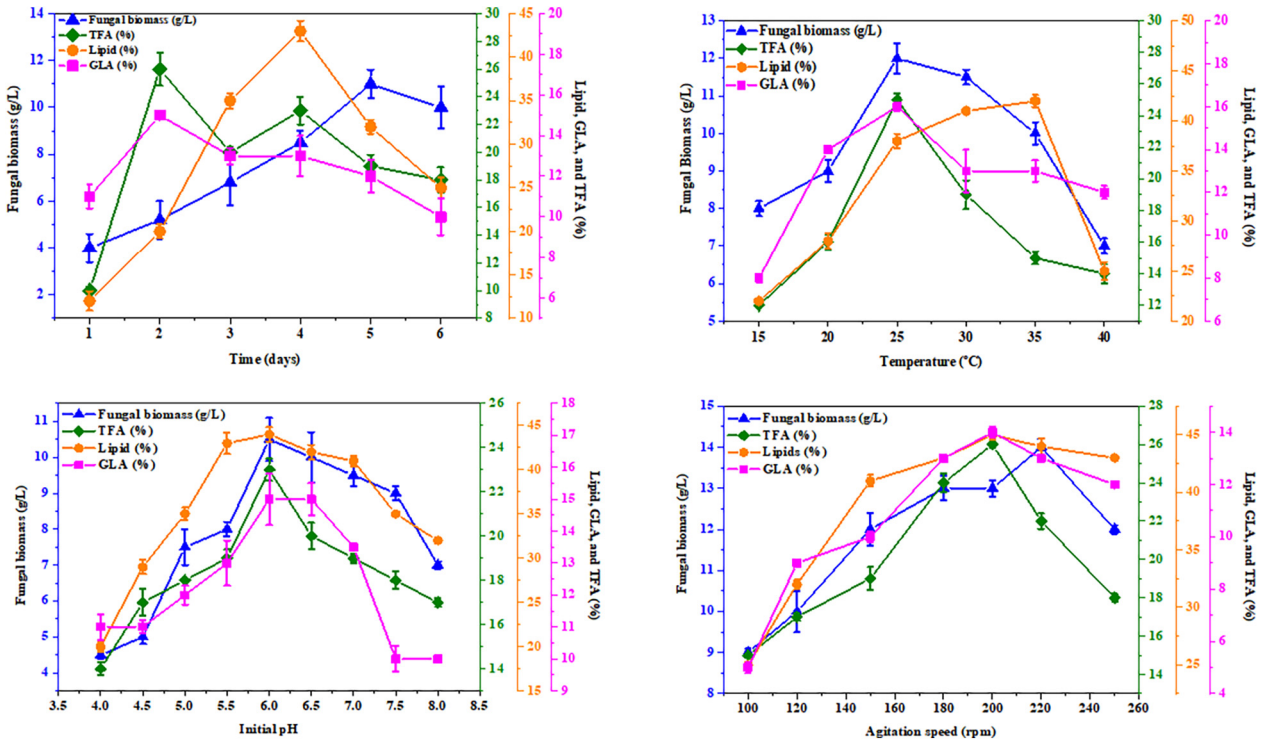

FIGURE 8 | Effect of fermentation time, temperature, initial pH, and agitation speed on the biomass, total lipids, GLA content, and TFAs in *M. circinelloides* AUMC 6696.A. Glutamine was employed as the nitrogen source. Error bars represent the average standard deviation from three biological replicates.

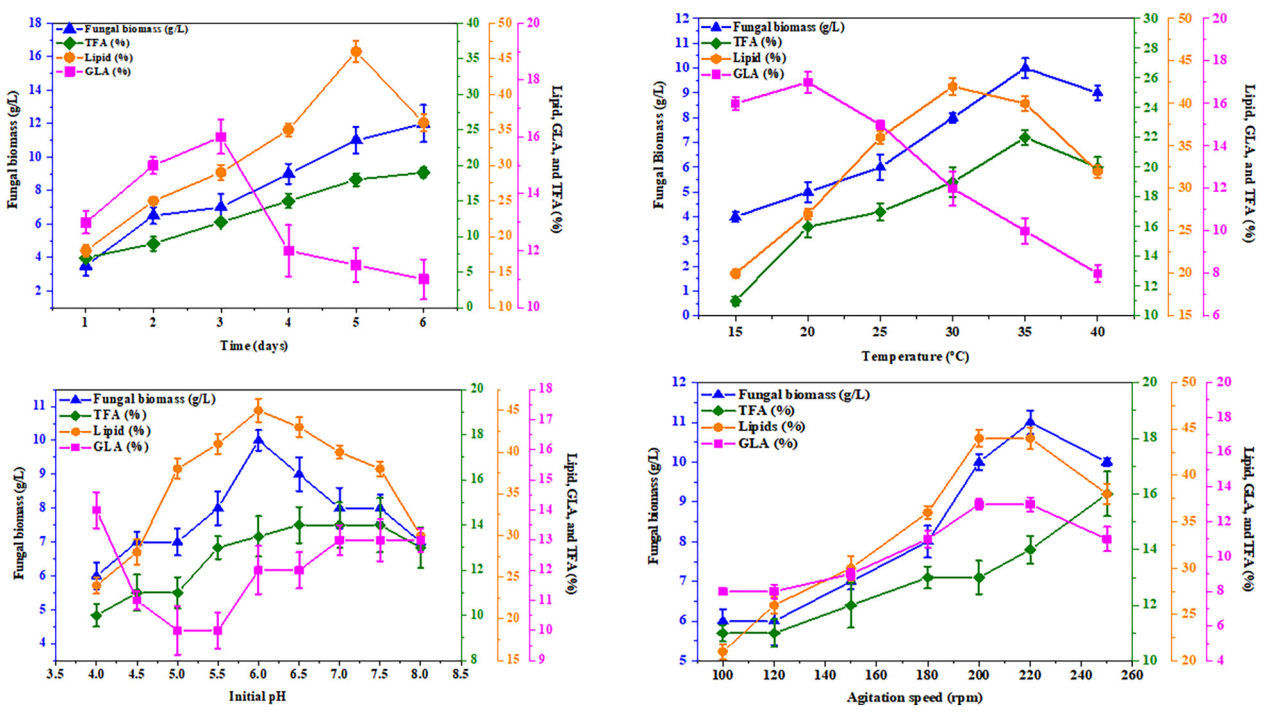

FIGURE 9 | Effect of fermentation time, temperature, initial pH, and agitation speed on the biomass, total lipids, GLA content, and TFAs in *R. pusillus* AUMC 11616.A. Asparagine amino acid was employed as the nitrogen source. Error bars represent the average standard deviations of three biological replicates.

TABLE 2 | GLA comparative analysis among various studies by selected *Mucromycota*.

Organism	C source	N source	GLA (%)	Reference
Mucor fragilis UBOCC-A-109196	Glucose	Yeast extract	24.5	(42)
M. circinelloides AUMC6027	Glucose	$C_4H_9NO_6$ and yeast extract	10.65	(26)
M. circinelloides CBS 277.49	Glucose	Diammonium tartrate	27	(43)
M. circinelloides WJ11	Glucose	Diammonium tartrate	14.5	
M. circinelloides CBS 108.16	Glucose	Tyrosine	8	(33)
M. hiemalis AUMC6031	Glucose	$C_4H_9NO_6$ and yeast extract	10.34	(26)
Cunninghamella blakesleeana JSK2	Glucose	KNO3	21	(44)
C. echinulata ATHUM 4411	Starch and xylose	NH_4^+ and yeast extract	5–11.2	(45, 46)
Gilbertella persicaria DSR1	Glucose	Proline and peptone	12.71	(34)
Mort. isabellina ATHUM 2935	Xylose, whey, and cheese lactose	NH_4^+, yeast extract, and cheese whey,	2.5–3	(46, 47)
Rhizopus stolonifer VKM F-400	Glucose	Yeast extract	20.3	(42)
R. pusillus AUMC 11616.A	Glucose	Proline	13.36	This study
M. circinelloides AUMC 6696.A	Glucose	Tryptophan	12.77	This study

TFA and GLA content of 23 ± 0.5% and 15 ± 0.8%, respectively. However, the maximum production of TFA and GLA for AUMC 11616.A was observed at pH 7 to 8 with 11 ± 0.7% and 13 ± 0.4%, respectively.

To determine the effect of temperature, tested strains were inoculated in fermentation media incubated at temperatures from 15°C to 40°C for 4 days. At 35°C, *R. pusillus* AUMC 11616.A produced maximum biomass (10 ± 0.4 g/L) and TFA content (22 ± 0.4%), while maximum total lipids (42 ± 1.0%) and GLA concentration (17 ± 1.5%) were seen at 30 and 20°C, respectively. *M. circinelloides* AUMC 6696.A produced the highest biomass (12 ± 0.4 g/L), TFA (25 ± 0.3%), and GLA contents (16 ± 0.2%) at 25°C and the highest total lipid content (42 ± 0.6%) at 35°C.

Finally, the agitation speed required for maximum total lipids (44 ± 0.1%) and GLA content (13 ± 0.3%) in AUMC 11616.A was observed at 200–240 rpm, with the highest biomass (11 ± 0.3 g/L) seen at 200 rpm and the highest TFA (16 ± 0.8%) seen at 240 rpm. The results for AUMC 6696.A showed the highest levels of total lipids (45 ± 0.4%), TFA (26 ± 0.2%), and GLA content (14 ± 0.2%) at 200 rpm, while biomass (14 ± 0.2 g/L) was greatest at 220 rpm. The results for all abiotic factors are illustrated in **Figures 8**, **9**.

DISCUSSION

In this study, K&R medium supplemented with certain amino acids as single nitrogen sources was used to obtain higher biomass with a shorter fermentation period for cultures of *R. pusillus* AUMC 11616.A and *M. circinelloides* AUMC 6696.A, and this bioprocess revealed that some amino acids had obvious growth-promoting effects on these oleaginous strains. In previous studies, the ratio of C/N played an essential role in biomass growth and lipid accumulation (24, 27), and the accumulation of lipids by oleaginous fungi is triggered by the exhaustion of exogenous nitrogen in the culture medium (28, 29). These studies have shown that a low ratio of C/N in the early stage of fermentation was beneficial to the microorganism growth; however, a high C/N ratio could enhance the lipid accumulation of oleaginous microorganisms in the subsequent fermentation stage (1, 30). Additionally, amino acids were found to be ideal nitrogen sources as they are used to synthesize proteins, enzymes, and deoxyribonucleic acid, thus promoting growth.

When investigating the effects of different amino acids, under the same culture conditions, on the biomass of *M. circinelloides* AUMC 6696.A and *R. pusillus* AUMC 11616.A, we found significant enhancements in growth with certain amino acids, reaching up to 10.5 ± 0.1 g/L for AUMC 6696.A and 12.6 ± 0.1 g/L for AUMC 11616.A. In an earlier study by Lu et al. (18), multiple organic nitrogen molecules were more suitable for fungal cell growth and lipid production than inorganic nitrogen sources in *Mortierella alpina* (19). Oleaginous yeast *Rhodotorula glutinis* cultivated in a medium containing amino acids had significantly enhanced cell biomass at 13.63 g/L after 3 days compared with the basic medium as a control (31). In another fungus *Cunninghamella echinulata*, it was also found that glutamine and lysine as nitrogen sources produced poor cell growth compared with the ammonium salt (32), and tyrosine appeared to be the most favorable nitrogen source for the cell growth and TFA production in the oleaginous fungus *Mucor circinelloides* CBS108.16 (33). Furthermore, in a recent study by Shah et al. (34), they found that glycine and proline produced the highest biomass and total lipid content, compared to the ammonium tartrate control, in the endophytic oleaginous fungus *Gilbertella persicaria* DSR1 (34). In our work, the 18 standard amino acids differentially affected the growth of *M. circinelloides* AUMC 6696.A and *R. pusillus* AUMC 11616.A, with glycine appearing to be a more favorable nitrogen source for growth.

Several carbon substrates are important to microbial cell growth, and the process of lipid formation in the cell involves the metabolic conversion of external carbon sources into carbohydrates or hydrocarbons, subsequently resulting in lipid accumulation (3, 35). In this study, glucose was employed as the sole carbon substrate. Lipid accumulation in oleaginous microorganisms, particularly fungi, grown on the glucose was

regulated by fatty acid *de novo* synthesis, which was not seen when grown on fatty substrates (36). Since fungal growth might be associated with the utilization of a simple carbon source such as glucose, the concentration of residual glucose was determined after 96 h of fermentation in our selected strains. As with our findings, oleaginous fungus *R. glutinis* showed higher utilization, and rapid consumption of glucose in the cultivation medium, when supplied with different amino acids, increased biomass by 0.32 g/L after 5 days (31).

Lipids are stored as droplets within the fungal cells, mainly in the form of triacylglycerol, and have been considered a valuable and renewable alternative source of high-value byproducts including PUFAs, and GLA in particular (37). Therefore, the studied strains were selected for their high lipid production. Based on our results, these strains produced higher total lipid content during cultivation with certain amino acids: asparagine and leucine for AUMC 11616.A and glutamine and glutamic acid for AUMC 6696.A. Glycine and glutamic also increased TFA content. Previous studies have shown that the type and composition of nitrogen sources and the initial C/N molar ratio in the medium influence lipid accumulation and fatty acid composition in oleaginous fungi, primarily reported in *Mucoromycota* (26, 34, 38). Total lipids, in the presence of ammonium bicarbonate, urea, tyrosine, tryptophan, phenylalanine, glutamine, glutamic acid, isoleucine, and histidine, ranged between 33 and 37% in oleaginous fungus *G. persicaria* DSR1, indicating that these nitrogen sources are suitable for lipid production (30). Our findings are almost consistent with those of Evans and Ratledge, where they showed that when glutamate, arginine, urea, or NH_4Cl were used as nitrogen sources, lipid accumulation in *R. toruloides* CBS14 increased (39). Early reports on oleaginous fungi, such as *M. alpina*, have also shown that organic sources of nitrogen are more suitable for lipid production than inorganic sources (19). Moreover, research on *M. circinelloides* has shown that various amino acids used as nitrogen sources can influence cell biomass, fatty acids, and GLA yields (33). Among such microorganisms, oleaginous Zygomycetes are documented for their high oil production and for producing special fatty acids such as γ-linolenic acid (GLA), which other oleaginous microbes cannot synthesize in large quantities (26, 35, 40).

In this study, the GLA content of TFAs was significantly increased with certain amino acids, particularly with proline for AUMC 11616.A and tryptophan for AUMC 6696.A. In other studies, GLA has been shown to play an important role in humans, improving the health of patients suffering from diabetes, aging, cancer, and immune diseases (26, 41). The highest yield of GLA in this study was significantly more than that obtained from other species of Mucorales and some other Zygomycotina, which are considered potential candidates for the application in the industrial production of PUFAs and other valuable compounds (34). The recent advancement of GLA production in some selected oleaginous *Mucoromycota* is summarized in **Table 2**.

There is a continuing interest in modifying the biochemical composition of fungal species by influencing abiotic or environmental factors. It is well studied that the chemical composition of microorganisms is affected by varied environmental conditions (48). Temperature plays a vital role in growth and lipid accumulation and can alter the composition of cellular fatty acids (34). It was observed that the GLA content of *Mucor rouxii* strain CFR-G15 increased significantly from 14.2% to 21.97% when the incubation temperature was lowered to 14°C (49). Our results demonstrate that the total lipid content, TFA, and GLA concentration decrease at 25 and 30°C as compared to the standard culturing temperature of 28°C. It is a well-known phenomenon that lower temperatures have a stimulatory effect on the biosynthesis of unsaturated fatty acids, which is considered as an adaptive mechanism in microbial cells to retain membrane fluidity (50, 51). It has also been reported that the interactions between pH values and components of cultivation media affect the ability of microorganisms to utilize the available nutrients in the medium (52). Moreover, earlier studies on oleaginous filamentous fungi reported an optimum incubation time of 4–5 days for high GLA and lipid yields (53). Therefore, all further fermentation experiments with the tested strains were incubated for 6 days. Depending on the microbe cultivated and the bio-product studied, increasing agitation speed has also been reported to reduce or promote productivity (54, 55). In another study by Saad et al., their experimental results revealed that lipid and GLA content were increased in samples agitated at 600 and 440 rpm, with values as high as 38.71% and 0.058 (g/g), respectively, in oleaginous fungus *Cunninghamella bainieri* 2A1 (53).

CONCLUSION

This study showed that different amino acid nitrogen sources can affect the cell biomass, fatty acid profile, and yield of GLA in *Rhizomucor pusillus* AUMC 11616.A and *Mucor circinelloides* AUMC 6696.A, which are promising strains for the high production of total lipids and GLA. When cultivated for 4 days at 28°C, shaking at 150 rpm, arginine and asparagine, for AUMC 11616.A, and glycine and valine, for AUMC 6696.A, were the most favorable amino acid nitrogen sources for cell growth, while glycine (AUMC 11616.A) and glutamic acid (AUMC 6696.A) showed the highest TFA production. Additionally, the highest yield of GLA was seen when proline (AUMC 11616.A) and tryptophan (AUMC 6696.A) were employed as sole nitrogen sources. The influence of environmental factors such as temperature, pH, fermentation time, agitation speed on the biomass, total lipids, fatty acid, and GLA concentration of the target strains has been investigated, and the optimal conditions were identified. Based on the significant enhancement in their lipid production and PUFAs, the pentose phosphate pathway could be induced by certain studied amino acids, which increases the activity of lipogenic enzymes. This study serves as a basis for future bioprocess developments of therapeutically important high value-added products, such as GLA, as well as for using amino acids as nitrogen sources. Concerning research on amino acid assimilation, further work is needed

to study the genes involved during fermentation and their biochemical pathways.

DATA AVAILABILITY STATEMENT

The original contributions presented in the study are included in the article/**Supplementary Material**, further inquiries can be directed to the corresponding authors.

AUTHOR CONTRIBUTIONS

HM and YS: conceptualization. HM and MA: methodology. HM and YN: software. HM, AH, and YN: validation. HM, MA, and TN: formal analysis. AS and AH: investigation. HM and SN: data curation. HM and AH: writing – original draft preparation. YS: writing – review and editing and supervision, project administration, and funding acquisition. TN and MA: visualization. All authors have read and agreed to the published version of the manuscript.

FUNDING

This study was supported by the National Natural Science Foundation of China (Grant Nos. 31972851 and 31670064) and TaiShan Industrial Experts Programme (Grant No. tscy20160101).

SUPPLEMENTARY MATERIAL

The Supplementary Material for this article can be found online at: https://www.frontiersin.org/articles/10.3389/fnut.2022.876817/full#supplementary-material

Supplementary Figure 1 | Microscopic Images of lactophenol cotton blue-stained mycelia of *Rhizomucor pusillus* AUMC 11616.A **(A)** branched *sporangiophores* and **(B)** primitive *rhizoides*; and *M. circinelloides* AUMC 6696.A **(C)** *sporangiophores* and **(D)** *sporangiophores* carrying sporangium and spores.

Supplementary Figure 2 | The GC results of the detailed FAs chromatographic analyses.

REFERENCES

1. Ratledge C, Wynn JP. The biochemistry and molecular biology of lipid accumulation in ole-aginous microorganisms. *Adv Appl Microbiol.* (2002) 51:1–52. doi: 10.1016/s0065-2164(02)51000-5
2. Patel A, Karageorgou D, Rova E, Katapodis P, Rova U, Christakopoulos P, et al. An overview of potential Oleaginous microorganisms and their role in biodiesel and omega-3 fatty acid-based industries. *Microorganisms.* (2020) 8:434. doi: 10.3390/microorganisms8030434
3. Papanikolaou S, Muniglia L, Chevalot I, Aggelis G, Marc I. Accumulation of a co-coa-butter-like lipid by *Yarrowia lipolytica* cultivated on agro-industrial residues. *Curr Microbiol.* (2003) 46:124–30. doi: 10.1007/s00284-002-3833-3
4. Monnard CR, Dulloo AG. Polyunsaturated fatty acids as modulators of fat mass and lean mass in human body composition regulation and cardiometabolic health. *Obes Rev.* (2021) 22(Suppl. 2):e13197. doi: 10.1111/obr.13197
5. Shah AM, Yang W, Mohamed H, Zhang Y, Song Y. Microbes: a hidden treasure of polyunsaturated fatty acids. *Front Nutr.* (2022) 9:827837. doi: 10.3389/fnut.2022.827837
6. Somashekar D, Venkateshwaran G, Sambaiah K, Lokesh B. Effect of culture conditions on lipid and gamma-linolenic acid production by mucoraceous fungi. *Process Biochem.* (2003) 38:1719–24. doi: 10.1016/s0032-9592(02)00258-3
7. Aggelis G. Two alternative pathways for substrate assimilation by *Mucor circinelloides*. *Folia Microbiol.* (1996) 41:254–6. doi: 10.1007/bf02814626
8. Ratledge C, Akoh C. *Microbial Production of γ-Linolenic Acid. Handbook of Functional Lipids*. Baco Raton, FL: Taylor & Francis (2006). p. 19–45.
9. Zhang Y, Luan X, Zhang H, Garre V, Song Y, Ratledge C. Improved γ-linolenic acid production in Mucor circinelloides by homologous overexpressing of delta-12 and delta-6 desatu-rases. *Microb Cell Fact.* (2017) 16:113. doi: 10.1186/s12934-017-0723-8
10. Khan MAK, Yang J, Hussain SA, Zhang H, Liang L, Garre V, et al. Construction of DGLA producing cell factory by genetic modification of *Mucor circinelloides*. *Microb Cell Fact.* (2019) 3:64. doi: 10.1186/s12934-019-1110-4
11. Fazili ABA, Shah AM, Zan X, Tahira N, Shaista N, Yusuf N, et al. *Mucor circinelloides*: a model organism for oleaginous fungi and its potential applications in bioactive lipid production. *Microb Cell Fact.* (2022) 21:29. doi: 10.1186/s12934-022-01758-9
12. Nancib N, Nancib A, Boudjelal A, Benslimane C, Blanchard F, Boudrant J. The effect of supplementation by different nitrogen sources on the production of lactic acid from date juice by *Lactobacillus casei* subsp. *rhamnosus*. *Bioresour Technol.* (2001) 78:149–53. doi: 10.1016/s0960-8524(01)00009-8
13. Petridis M, Benjak A, Cook GM. Defining the nitrogen regulated transcriptome of Mycobacterium smegmatis using continuous culture. *BMC Genomics.* (2015) 16:821. doi: 10.1186/s12864-015-2051-x
14. Matos ÂP. The impact of microalgae in food science and technology. *J Am Oil Chem Soc.* (2017) 94:1333–50. doi: 10.1007/s11746-017-3050-7
15. Li Y, Horsman M, Wang B, Wu N, Lan CQ. Effects of nitrogen sources on cell growth and lipid accumulation of green alga *Neochloris oleoabundans*. *Appl Microbiol Biotechnol.* (2008) 81:629–36. doi: 10.1007/s00253-008-1681-1
16. Park EY, Koike Y, Higashiyama K, Fujikawa S, Okabe M. Effect of nitrogen source on mycelial morphology and arachidonic acid production in cultures of *Mortierella* alpina. *J Biosci Bioeng.* (1999) 88:61–7. doi: 10.1016/s1389-1723(99)80177-7
17. Rayaroth A, Tomar RS, Mishra RK. Arachidonic acid synthesis in *Mortierella* alpina: origin, evolution and advancements. *Proc Natl Acad Sci India Sect B Biol Sci.* (2017) 87:1053–66. doi: 10.1007/s40011-016-0714-2
18. Lu J, Peng C, Ji X-J, You J, Cong L, Ouyang P, et al. Fermentation characteristics of *Mortierella* alpina in response to different nitrogen sources. *Appl Biochem Biotechnol.* (2011) 164:979–90. doi: 10.1007/s12010-011-9189-z
19. Godard P, Urrestarazu A, Vissers S, Kontos K, Bontempi G, van Helden J, et al. Effect of 21 different nitrogen sources on global gene expression in the yeast *Saccharomyces cere-visiae*. *Mol Cell Biol.* (2007) 27:3065–86. doi: 10.1128/MCB.01084-06
20. Shihui Y, Wei W, Hui W, Stefanie VW, Philip T, Pienkos MZ, et al. Comparison of nitrogen depletion and repletion on lipid production in yeast and fungal species. *Energies.* (2016) 9:685. doi: 10.3390/en9090685
21. Tsigie YA, Wang CY, Truong CT, Ju YH. Lipid production from *Yarrowia lipolytica* Po1g grown in sugarcane bagasse hydrolysate. *Bioresour Technol.* (2011) 102:9216–22. doi: 10.1016/j.biortech.2011.06.047
22. Seip J, Jackson R, He H, Zhu Q, Hong SP. Snf1 is a regulator of lipid accumulation in *Yarrowia lipolytica*. *Appl Environ Microbiol.* (2013) 79:7360–70. doi: 10.1128/AEM.02079-13
23. Liu J, Sun Z, Chen F. Heterotrophic production of algal oils. In: Pandey A, Lee DJ, Chisti Y, Soccol CR editors. *Biofuels from Algae*. San Diego, CA: Elsevier (2014). p. 111–42. doi: 10.1016/b978-0-444-59558-4.00006-1
24. Gao B, Wang F, Huang L, Hui L, Yuming Z, Chengwu Z. Biomass, lipid accumulation kinetics, and the transcriptome of heterotrophic oleaginous microalga *Tetradesmus* bernardii under different carbon and nitrogen sources. *Biotechnol Biofuels.* (2021) 14:1–116. doi: 10.1186/s13068-020-01868-9

25. Mohamed H, El-Shanawany AR, Shah AM, Nazir Y, Naz T, Ullah S, et al. Comparative analysis of different isolated Oleaginous Mucoromycota fungi for their γ-linolenic acid and carotenoid production. *Biomed Res Int.* (2020) 5:3621543. doi: 10.1155/2020/3621543
26. Nosheen S, Naz T, Yang J, Hussain SA, Fazili ABA, Nazir Y, et al. Role of Snf-β in lipid accumulation in the high li-pid-producing fungus *Mucor circinelloides* WJ11. *Microb Cell Fact.* (2021) 20:52. doi: 10.1186/s12934-021-01545-y
27. Ratledge C. Fatty acid biosynthesis in microorganisms being used for single cell oil production. *Biochimie.* (2004) 86:807–15. doi: 10.1016/j.biochi.2004.09.017
28. Chatzifragkou A, Fakas S, Galiotou-Panayotou M, Michael K, George A, Seraphim P. Commercial sugars as substrates for lipid accumulation in *Cunninghamella echinulata* and *Mor-tierella* isabellina fungi. *Eur J Lipid Sci Technol.* (2010) 112:1048–57. doi: 10.1002/ejlt.201000027
29. Xia C, Zhang J, Zhang W, Hu B. A new cultivation method for microbial oil production: cell pelletization and lipid accumulation by *Mucor circinelloides*. *Biotechnol Biofuels.* (2011) 4:1–15. doi: 10.1186/1754-6834-4-15
30. Liu M, Zhang X, Tan T. The effect of amino acids on lipid production and nutrient removal by *Rhodotorula glutinis* cultivation in starch wastewater. *Biores Technol.* (2016) 218:712–7. doi: 10.1016/j.biortech.2016.07.027
31. Meng L, Xu Z, Tianwei T. The effect of amino acids on lipid production and nutrient removal by *Rhodotorula glutinis* cultivation in starch wastewater. *Biores Technol.* (2016) 218:712–7. doi: 10.1016/j.biortech.2016.07.027
32. Certik M, Megova J, Horenitzky R. Effect of nitrogen sources on the activities of lipogenic enzymes in oleaginous fungus *Cunninghamella echinulata*. *J Gen Appl Microbiol.* (1999) 45:289–93. doi: 10.2323/jgam.45.289
33. Tang X, Zhang H, Chen H, Yong C, Wei C, Yuanda S. Effects of 20 standard amino acids on the growth, total fatty acids Production, and γ-linolenic acid yield in *Mucor circinel-loides*. *Curr Microbiol.* (2014) 69:899–908. doi: 10.1007/s00284-014-0671-z
34. Shah AM, Mohamed H, Zichen Z, Yuanda S. Isolation, characterization and fatty acid analysis of *Gilbertella persicaria* DSR1: a potential new source of high value single-cell oil. *Biomass Bioenergy.* (2021) 151:106156. doi: 10.1016/j.biombioe.2021.106156
35. Subhash GV, Mohan SV. Biodiesel production from isolated oleaginous fungi *Aspergillus* sp. using corncob waste liquor as a substrate. *Biores Technol.* (2011) 102:9286–90. doi: 10.1016/j.biortech.2011.06.084
36. Papanikolaou S, Galiotou-Panayotou M, Chevalot I, Komaitis M, Marc I, Aggelis G. Influence of glucose and saturated free fatty acid mixtures on citric acid and lipid production by *Yarrowia lipolytica*. *Curr Microbiol.* (2006) 52:134–42. doi: 10.1007/s00284-005-0223-7
37. Mhlongo SI, Ezeokoli OT, Roopnarain A, Ndaba B, Sekoai PT, Habimana O, et al. The potential of single-cell oils derived from filamentous fungi as alternative feedstock sources for biodiesel production. *Front Microbiol.* (2021) 28:637381. doi: 10.3389/fmicb.2021.63738
38. Zikou E, Chatzifragkou A, Koutinas A, Papanikolaou S. Evaluating glucose and xylose as cosubstrates for lipid accumulation and γ-linolenic acid biosynthesis of *Thamnidium elegans*. *J Appl Microbiol.* (2013) 114:1020–32. doi: 10.1111/jam.12116
39. Evans CT, Ratledge C. Effect of nitrogen source on lipid accumulation in oleaginous yeasts. *Microbiology.* (1984) 130:1693–704. doi: 10.1099/00221287-130-7-1693
40. Subramaniam R, Dufreche S, Zappi M, Bajpai R. Microbial lipids from renewable re-sources: production and characterization. *J Ind Microbiol Biotechnol.* (2010) 37:1271–87. doi: 10.1007/s10295-010-0884-5
41. Ahmed SU, Singh SK, Pandey A, Kanjilal S, Prasad RB. Application of response surface method for studying the role of dissolved oxygen and agitation speed on gamma-linolenic acid production. *Appl Biochem Biotechnol.* (2009) 152:108–16. doi: 10.1007/s12010-008-8256-6
42. Kosa G, Zimmermann B, Kohler A, Ekeberg D, Afseth NK, Mounier J, et al. High-throughput screening of mucoromycota fungi for production of low- and high-value lipids. *Biotechnol Biofuels.* (2018) 14:66. doi: 10.1186/s13068-018-1070-7
43. Tang X, Chen H, Chen YQ, Chen W, Garre V, Song Y. Comparison of biochemical activities between high and low lipid-producing strains of *Mucor circinelloides*: an explanation for the high oleaginicity of strain WJ11. *PLoS One.* (2015) 10:e0128396. doi: 10.1371/journal.pone.0128396
44. Sukrutha K, Zuzana A, Kunder R, Janakiraman S, Milan C. Optimization of physiologi-cal growth conditions for maximal gamma-linolenic acid production by *Cunninghamella blakesleeana*-JSK2. *J Am Oil Chem Soc.* (2014) 91:1507–13. doi: 10.1007/s11746-014-2507-1
45. Papanikolaou S, Galiotou-Panayotou M, Fakas S, Komaitis M, Aggelis G. Lipid produc-tion by oleaginous Mucorales cultivated on renewable carbon sources. *Eur J Lipid Sci Technol.* (2007) 109:1060–70. doi: 10.1002/ejlt.200700169
46. Fakas S, Papanikolaou S, Batsos A, Galiotou-Panayotou M, Mallouchos A, Aggelis G. Evaluating renewable carbon sources as substrates for single cell oil production by *Cunninghamella echinulata* and *Mortierella* isabellina. *Biomass Bioenergy.* (2009) 33:573–80. doi: 10.1016/j.biombioe.2008.09.006
47. Vamvakaki AN, Kandarakis I, Kaminarides S, Komaitis M, Papanikolaou S. Cheese whey as a renewable substrate for microbial lipid and biomass production by Zygomycetes. *Eng Life Sci.* (2010) 10:348–60. doi: 10.1002/elsc.201000063
48. Ortega LM, Romero L, Moure C, Garmendia G, Albuquerque DR, Pinto VF, et al. Effect of moisture on wheat grains lipid patterns and infection with *Fusarium* graminearum. *Int J Food Microbiol.* (2019) 306:108264. doi: 10.1016/j.ijfoodmicro.2019.108264
49. Mamatha SS, Venkateswaran G. Differential temperature effect on the production of en-hanced gamma linolenic acid in *Mucor* rouxii CFR-G15. *Indian J Microbiol.* (2010) 50:52–6. doi: 10.1007/s12088-010-0053-6
50. Dyal SD, Narine SS. Implications for the use of *Mortierella* fungi in the industrial produc-tion of essential fatty acids. *Food Res Int.* (2005) 38:445–67. doi: 10.1016/j.foodres.2004.11.002
51. Kendrick A, Ratledge C. Desaturation of polyunsaturated fatty acids in *Mucor circinelloides* and the involvement of a novel membrane-bound malic enzyme. *FEBS J.* (1992) 209:667–73. doi: 10.1111/j.1432-1033.1992.tb17334.x
52. Nisha A, Venkateswaran G. Effect of culture variables on mycelial arachidonic acid produc-tion by *Mortierella* alpina. *Food Bioprocess Technol.* (2011) 4:232–40. doi: 10.1007/s11947-008-0146-y
53. Saad N, Abdeshahian P, Kalil MS, Yusoff WMW, Hamid AA. Optimization of aera-tion and agitation rate for lipid and gamma linolenic acid production by *Cunninghamella* bainieri 2A1 in submerged fermentation using response surface methodology. *Sci World J.* (2014) 2014:280146. doi: 10.1155/2014/280146
54. Grimm LH, Kelly S, Krull R, Hempel DC. Morphology and productivity of filamentous fungi. *Appl Microbiol Biotechnol.* (2005) 69:375–84. doi: 10.1007/s00253-005-0213-5
55. Maiorano AE, da Silva ES, Perna RF, Ottoni CA, Moniz Piccoli RA, Fernandez RC, et al. Effect of agitation speed and aeration rate on fructosyltransferase production of *Aspergillus oryzae* IPT-301 in stirred tank bioreactor. *Biotechnol Lett.* (2020) 42:2619–29. doi: 10.1007/s10529-020-03006-9

Conflict of Interest: The authors declare that the research was conducted in the absence of any commercial or financial relationships that could be construed as a potential conflict of interest.

Publisher's Note: All claims expressed in this article are solely those of the authors and do not necessarily represent those of their affiliated organizations, or those of the publisher, the editors and the reviewers. Any product that may be evaluated in this article, or claim that may be made by its manufacturer, is not guaranteed or endorsed by the publisher.

frontiers | Frontiers in Nutrition

REVIEW
published: 19 May 2022
doi: 10.3389/fnut.2022.873657

Production, Biosynthesis, and Commercial Applications of Fatty Acids From Oleaginous Fungi

Xin-Yue Zhang[1], Bing Li[1], Bei-Chen Huang[1], Feng-Biao Wang[1], Yue-Qi Zhang[1], Shao-Geng Zhao[1], Min Li[1], Hai-Ying Wang[2], Xin-Jun Yu[3], Xiao-Yan Liu[4], Jing Jiang[5]* and Zhi-Peng Wang[1]**

[1] School of Marine Science and Engineering, Qingdao Agricultural University, Qingdao, China, [2] Key Laboratory of Sustainable Development of Polar Fishery, Ministry of Agriculture and Rural Affairs, Yellow Sea Fisheries Research Institute, Chinese Academy of Fishery Sciences, Qingdao, China, [3] Key Laboratory of Bioorganic Synthesis of Zhejiang Province, College of Biotechnology and Bioengineering, Zhejiang University of Technology, Hangzhou, China, [4] Jiangsu Key Laboratory for Biomass-Based Energy and Enzyme Technology, Huaiyin Normal University, Huaian, China, [5] School of Environmental Science and Engineering, Suzhou University of Science and Technology, Suzhou, China

OPEN ACCESS

Edited by:
Yuanda Song, Shandong University of Technology, China

Reviewed by:
Heitor Bento, São Paulo State University, Brazil
Alok Patel, Luleå University of Technology, Sweden

***Correspondence:**
Xin-Jun Yu
xjyu@zjut.edu.cn
Zhi-Peng Wang
wangzpmbio@163.com
Jing Jiang
jiangjing@usts.edu.cn

Specialty section:
This article was submitted to Food Chemistry, a section of the journal Frontiers in Nutrition

Received: *11 February 2022*
Accepted: *31 March 2022*
Published: *19 May 2022*

Citation:
Zhang X-Y, Li B, Huang B-C, Wang F-B, Zhang Y-Q, Zhao S-G, Li M, Wang H-Y, Yu X-J, Liu X-Y, Jiang J and Wang Z-P (2022) Production, Biosynthesis, and Commercial Applications of Fatty Acids From Oleaginous Fungi. Front. Nutr. 9:873657. doi: 10.3389/fnut.2022.873657

Oleaginous fungi (including fungus-like protists) are attractive in lipid production due to their short growth cycle, large biomass and high yield of lipids. Some typical oleaginous fungi including *Galactomyces geotrichum*, *Thraustochytrids*, *Mortierella isabellina*, and *Mucor circinelloides*, have been well studied for the ability to accumulate fatty acids with commercial application. Here, we review recent progress toward fermentation, extraction, of fungal fatty acids. To reduce cost of the fatty acids, fatty acid productions from raw materials were also summarized. Then, the synthesis mechanism of fatty acids was introduced. We also review recent studies of the metabolic engineering strategies have been developed as efficient tools in oleaginous fungi to overcome the biochemical limit and to improve production efficiency of the special fatty acids. It also can be predictable that metabolic engineering can further enhance biosynthesis of fatty acids and change the storage mode of fatty acids.

Keywords: oleaginous fungi, triacylglycerols, regulation strategy, fatty acids, Commercial application

INTRODUCTION

Similar to vegetable lipids, microbial lipids mainly include neutral fatty acids (FAs), free FAs and phospholipids (1, 2). Moreover, they share the same existence form with animal and plant lipids, i.e., existing in the cell structure such as membrane with constant content or forming lipid droplets or fat particles in the cytoplasm (3). The bright spheres in **Figure 1** are lipid droplets in cells of different types of strains. Specifically, the outer layer of lipid droplets is a monolayer composed of phospholipids and specific proteins, and the inner core is mainly neutral lipids such as triacylglycerol (TAG) and sterol ester (SE) (4–7).

Microbial lipids are also widely used in the production of biodiesel. Excessive consumption and environmental damage caused by fossil fuels have hindered economic sustainable development (8, 9). Therefore, finding renewable and clean energy that can replace fossil energy is an important prerequisite for the development of green economy, energy conservation, emission reduction, and environmental protection (2). Methyl or ethyl fatty acid ester is obtained from methyl or ethyl esterification of FAs. The cellular lipids are mainly produced in the form of free FAs and acylglycerols (mostly as triglycerides) and are stored in the globular organelles called lipid bodies. Transesterification of microbial lipids is an essential step in microbial lipid production at both laboratory and commercial scale. Direct transesterification can considerably reduce costs,

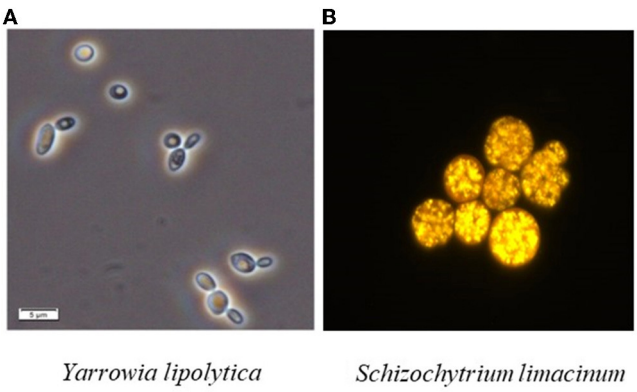

FIGURE 1 | Lipid bodies from different oleaginous fungi. **(A)** Wang et al. (4); **(B)** Fillet et al. (5).

increase sample throughput and improve lipid yields (in particular fatty acid methyl esters, FAMEs). Fatty acid ethyl esters (FAEEs) are typically produced via the chemical transesterification of plant lipids and animal fats. Biosynthesis of FAEEs is limited by the supply of precursor lipids and acetyl-CoA (10–13).

Oleaginous fungi, as lipid-producing microorganisms, are attractive in lipid production due to their short growth cycle, large amount of biomass and high yield of lipids (14, 15). Some filamentous fungi species have been reported able to accumulate polyunsaturated fatty acids (PUFAs), such as *Mortierella isabellina*, *Mucor circinelloides*, *Pythium ultimum* (2, 9). PUFAs play a vital role in human body; (PUFAs) belonging to the ω-3 and ω-6 classes are also substantial as precursors of eicosanoids or being structural components of various membrane phospholipids (9, 16, 17). **Table 1** summarizes some high-yield fungi species and their lipid content.

As fungus-like protists, *Thraustochytrids* are progressively studied for his or her quicker growth rates and high lipid content (28). *Thraustochytrids* were first reported in 1936 and have attracted much attention since 1990 due to their high yield of FAs (29). The accumulated lipids account for more than 50% of dry cell weight (DCW), of which more than 25% is docosahexaenoic acid (DHA) with extremely high economic value. *Aurantiochytrium* sp. is a kind of *thraustochytrids*, which has a high yield of PUFAs, especially DHA (9). At present, the research on FA synthesis from *Aurantiochytrium* sp. is mainly focused on the optimization of culture conditions to increase the yield of unsaturated FAs, especially DHA (7).

Different from oleaginous yeasts, accumulation of fatty acids with important functions is the most attractive point of oleaginous fungi. However, unlike oleaginous yeasts, the recent developments of production, biosynthesis, and commercial applications of fatty acids from oleaginous fungi, have not been reviewed. In this article, we tried to summarize the studies of fatty acids from oleaginous fungi, and provided a point of reference.

TABLE 1 | Lipid contents of some fungi.

Species	Carbon source	Lipid content (%)	PUFAs (%)	References
Aurantiochytrium sp.	Glucose	72.4	+25 (DHA)	(18)
Umbelopsis vinacea	Glucose	63.55	+	(19)
Aurantiochytrium SW1	Fructose	44	52.3 (DHA)	(14)
Aurantiochytrium sp. T66	Glycerol	55	40 (DHA)	(20)
Mortierella alpina	Potato industry wastes	40	35 (ARA)	(21)
Aurantiochytrium sp. SY25	Glucose	/	59.98	(22)
Mucor wosnessenskii CCF 2606	Soybean	6.7 ± 0.3	8.5 ± 0.2 (GLA)	(15)
Mortierella isabelline ATHUM 2935	Glucose (commercial)	83.3	/	(23)
Thraustochytrium sp. T18	Glucose	46.9	35.2 (DHA)	(24)
Galactomyces geotrichum TS61	molasses	69.6	23.67 (LA)	(25)
Mortierella alpina	Glycerol (crude)	33.3	49.2 (LA)	(26)
Mortierella alpina CCFM698	Glucose	31.5	26.7 (EPA)	(27)

REGULATION OF FUNGAL FATTY ACID FERMENTATION

Fungal lipid fermentation can be divided into two stages, i.e., the cell proliferation and the lipid accumulation (30). During the cell proliferation stage, cells proliferate and metabolize vigorously, with the nutrients in the medium consumed rapidly. During the fatty acid accumulation stage, the nitrogen source is exhausted but the carbon source is sufficient in the medium, which makes cells stop proliferating for the most part, with the lipid synthesis becoming the dominated metabolic activity (31–33).

According to the characteristics of fungal lipid fermentation production, controlling the nutrient composition of medium and regulating environmental conditions are a common strategy to promote lipid biosynthesis in lipid fermentation engineering. At present, three regulation strategies are widely adopted for lipid fermentation. The carbon-to-nitrogen (C/N) ratio, carbon and nitrogen sources, pH, incubation temperature and dissolved oxygen are the main factors influencing fatty acid production (18, 34). Nevertheless, other factors also play a crucial role in microbial activity, such as minerals (e.g., sulfur, zinc and phosphorus) and vitamins (e.g., thiamine and biotin) (35). Moreover, secondary metabolites (like citrate) are also an influencing factor for lipid production (34).

Promoting Lipid Accumulation by Nutrients Restriction

As for the de novo lipid accumulation, concentrations of nitrogen and carbon sources respectively determine the biomass content and the quantity of lipids in general (36). Accordingly, the C/N ratio is significant for the accumulated lipid content and the oleaginous microbial biomass (36–39). Previous studies demonstrate that the lipid accumulation is boosted at a C/N molar ratio of greater than 20. It is worth noting that the lipid production declines instead at the C/N ratio higher than 70 in some cases (40). Therefore, to achieve a high-level lipid accumulation, the initial C/N molar ratio should be optimized (41–43). For the lipid fermentation of the *Thraustochytridae* sp. PKU#Sw8, the increase in DHA production coincided with the up-regulation of gene expression under nitrogen-deficient culture conditions (44). Chen et al. (45) optimized the culture of *Thraustochytrid* sp. PKU#SW8 under optimal culture conditions (glycerol, 20 g/L; peptone, 2.5 g/L; 80% seawater; pH 4.0; 28°C), the cell mass, DHA concentration and yield of PKU#SW8 were increased to 7.5 ± 0.05 g/L, 2.14 ± 0.03 g/L and 282.9 ± 3.0 mg/g, respectively, on a 5-L scale fermentation.

Cellular lipid content and lipid yield were 62.2% and 0.205 g/g glucose, respectively, using a medium with a carbon to nitrogen (C/N) molar ratio of 6.1 and a C/P molar ratio of 9,552 (46), which means that the accumulation of lipid can also be regulated by limiting phosphorus in the medium. As a consequence, the regulation of phosphorus and sulfur limitation is of great significance for the production of lipids from nitrogen-rich crude materials (41, 45, 47, 48).

Promoting Lipid Accumulation by Small Molecules

Some small molecules can also regulate the accumulation of lipids (37, 48, 49). Li et al. (50) cultured *Thraustochytriidae* sp., a kind of marine oleaginous protists, by addition of different levels of sodium nitrate (1-50 mM) or urea (1-50 mM) in fermentation culture has a significant effect on fatty acid synthesis. They found that urine (50 mM) culture the cells accumulated 1.16 times the ω-3 PUFAs, of which DHA accounted for 49.49% and docosapentaenoic acid (DPA) was 5.28% compared with the original culture conditions. To sum up, it is easy to control lipid accumulation by small molecules, which is of great significance for the optimization of lipid production conditions (48, 51).

The accumulation of biomass and lipid-synthesizing fungi in any oily substance is highly affected by factors such as pH, temperature, light, and ventilation. Temperature change is also one of the factors affecting lipid accumulation (52, 53). They found that the low temperature has a significant impact on the formation of DHA, which can increase the DHA content from 43 to 65% of the total fatty acids. Low temperature may increase DHA content by facilitating a relatively large amount of substrates to enter the polyketide synthase (PKS) pathway (52).

Promoting Lipid Accumulation by Using Different Fermentation Modes

Generally speaking, there are three ways of microbial fermentation: batch culture, fed-batch culture and continuous culture (38, 54–57). The batch culture is the most widely used for lipid fermentation. Wang et al. (58) studied *Schizochytrium* sp. PKU#Mn4 and *Thraustochytrid* sp. PKU#Mn16, found that the largest DHA yields were 21% and 18.9%, and the yields were 27.6 mg/L-h and 31.9 mg/L-h, respectively in in 5-L bioreactor fermentation operated with optimal conditions and dual oxygen control strategy. The production of DHA increased by 3.4 times and 2.8 times (g/L) respectively. *Rhizopus* sp. using solid-state fermentation and submerged fermentation can produce valuable alternative feed ingredient due to their high protein and the well-balanced lipid content and amino acid profile (59).

In addition, electro-fermentation is a promising technology that can improve the performance of biological processes. When lipids are produced yeast *R. toruloides* under electro-fermentation conditions, the proportion of saturated FAs increases significantly from 37 to 50% (60).

EXTRACTION OF FUNGAL FATTY ACID

The conventional methods of wall breaking mainly include the following: grinding method, acid treatment, cell autolysis method, repeated freezing and thawing, ultrasonication and enzyme treatment (61–65). Among them, the autolysis method has simple steps and low cost, but has poor crushing result and low lipid yield; the enzymatic treatment method has mild conditions and no damage to intracellular substances, but is expensive and cannot be used for large-scale treatment. Ultrasonication is one in every of the additional normally used strategies. Using ultrasound to reinforce the synthesis of designer lipids, researchers have discovered an eco-friendly technique for enhancing the synthesis of designer lipids with numerous nutritional values (66).

The extraction of lipids is mostly done with low-boiling organic solvents. Commonly used solvents are ether, petroleum ether and chloroform. At present, the commonly used extraction methods of microbial lipids are as follows: acid heat method, Soxhlet extraction method, and supercritical CO_2 extraction method (67–71). Among them, the Soxhlet extraction method is relatively accurate, but it is time-consuming and consumes too much organic solvent; the acid-heat method, although the yield is low, is fast and simple, and is suitable for the operation of multiple samples; the supercritical CO_2 extraction method has high instrument requirements and requires Strictly control parameters (67, 71). The process of extracting lipid from fungi using acid-catalyzed predicament, microwave, and rapid ultrasonic-microwave treatment can create it have a high extraction rate, up to 70% (w/w) content (71). It is a novel green extraction method (63).

Cost Estimation of Fungal Fatty Acids

Take DHA as an example for cost estimation (72). If all the carbon sources needed to produce DHA were glucose, the amount of

glucose required to produce 1 ton of biomass would be 2.78 tons. At the 2021 glucose price of us $903.9 per ton, it would cost US $2,512.84 to produce one ton of biomass. If there is only 50% lipid content in 1 ton of biomass, 40% of the lipid content is DHA (73). That's 0.2 tons of DHA. If one ton of DHA is produced, the calculated cost of glucose is $12,564.2. All this takes into account only glucose substrates, but if you add in other cost factors, including water and electricity, publicity, equipment, and so on, the cost of DHA increases further (72).

Recovery processes downstream of the fermenter typically contribute 60–80% to the cost of production of a fermentation product, therefore the fermentation step contributes only around 20–40% to the total production cost. The above analysis leads to the conclusion that the *Schizochytrium limacinum* grown on glucose cannot provide DHA cheaper than fish oil at present. If the biomass was used simply as an aquaculture feed additive, the downstream processing requirements would mostly disappear, although on the basis of equal DHA content, the biomass would still be more expensive than fish oil. Hence the need for cheaper nutrients for growing thraustochytrids (72).

In the future development, it is very important to improve production efficiency and reduce cost. First of all, in terms of carbon sources, the focus should be on replacing glucose while maintaining high biomass and lipid yields. In addition, lignocellulose hydrolysate may prove to be an inexpensive source of carbon for biomass production, which can efficiently metabolize xylose, and xylose metabolic engineering may help reduce fermentation costs (74). Metabolic engineering is also very important (75, 76). Therefore, strains should be improved, complete metabolic flux analysis should be carried out, and the protein engineering field should be evaluated with the goal of metabolic engineering, etc., in order to maximize the fatty acid production in the biomass.

Taking into consideration from another angle, developing new valuable products such as enzymes, and cell wall polysaccharides, during fungal fermentation besides fatty acids, would effectively reduce the cost. This "fungal-based biorefinery" strategy has not been applied in the studies, it may be the another choice to make the production of fatty acids more feasible (77).

FATTY ACID PRODUCTION FROM RAW MATERIALS

Glucose is the most basic carbon source of microorganisms. Many studies explore the glucose-based lipid accumulation of fungi, and the lipid content can reach higher than 70% (w/w) (41, 78–80). However, the large-scale production of microbial fatty acids with glucose as a raw material will face the problems of "competing with people for food" and "competing with food for land", which necessitates the search for other suitable raw materials to reduce the costs (9, 81, 82). Recently, some cheap and available "raw materials" have been widely concerned, such as lignocellulose, non-grain sugar raw materials and commercial wastes (9, 79, 83). **Table 2** summarizes some high-yielding fungal species that use non-glucose as substrates for lipid accumulation.

TABLE 2 | Non-glucose substrates for lipid production.

Species	Carbon source	Lipid content (%)	References
M. circinelloides	Xylose	17.2-17.7	(84)
Ashbya gossypii	Xylose	55	(85)
M. circinelloides Q531	Mulberry branches	28.8±2.85	(86)
M. circinelloides ZSKP	Kitchen vegetable waste	21.4	(87)
M. alpina CBS 528.72	Potato waste	40	(21)
Aurantiochytrium sp. YLH70	Jerusalem artichoke	46.9% (DHA)	(88)
Aurantiochytrium sp. T66	Glycerol	55	(65)
Aspergillus caespitosus ASEF14	Sago processing wastewater (SWW)	37.2	(89)
Cutaneotrichosporon curvatus	Lignocellulose	63	(90)

Lignocellulose

Lignocellulose is constituted by hemicellulose, cellulose and lignin (91). In recent years, lignocellulosic biomass has been recognized as a potential alternative feedstock to produce biofuels (9). The fatty acid production with lignocellulosic biomass includes the following two steps: (1) the degradation of biomass to corresponding monosaccharides by heat-acid treatment or enzyme hydrolysis, and (2) the biodegradable sugar fermentation by promising oleaginous microorganisms (92–95). Lignocellulose cannot be directly utilized, but must be hydrolyzed, which produces compounds that inhibit the growth of fungi, such as furan aldehydes, weak acids, and aromatic compounds, during the pretreatment process (96). The cumulative deleterious effects of some inhibitors (such as furfural, formic acid, acetic acid, and vanillin) on fatty acid accumulation in oleaginous fungi have been investigated (96, 97). Intasit et al. (98) used an integrated biotechnology, fungi and yeast to bioconvert lignocellulosic biomass into biodiesel, first pretreatment of the fungus, the fungus *Aspergillus tubingensis* TSIP 9 lipid yield 121.4 ± 2.7 mg/g-EFB (empty fruit bunch), the integrated biotechnology can greatly facilitate the conversion of lignocellulosic biomass to biodiesel feedstock is a cost-effective and sustainable biotransformation. Zhang et al. (84) deeply analyzed the effects of corn stover hydrolyzate on lipid accumulation by using xylose metabolism engineering strains of *M. circinelloides* strains. The results showed that the fatty acid contents of the engineered *M. circinelloides* strains were increased by 19.8% (in Mc-XI) and 22.3% (in Mc-XK), respectively, compared with the control strain.

Glucose and xylose coexist in lignocellulose hydrolysate. Lipid-producing yeasts consume glucose first and then xylose, and even some lipid-producing yeasts are unable to utilize xylose. Therefore, lignocellulose hydrolysate suffers from long fermentation cycle and low substrate utilization.

High-Carbonhydrate Plant Materials

Jerusalem artichoke is a kind of perennial plant resistant to barren, cold and drought. The planting of Jerusalem artichoke should not occupy cultivated land and other agricultural lands (99). The storage form of sugar in Jerusalem artichoke is inulin, which is a polyfructose linked by β-2,1 glycosidic bond with a glucose residue at the end (100). Yeast or molds can accumulate large amounts of lipids from inulin hydrolysates (101–103). In the medium containing inulin, fatty acids can be produced and the lipid content and biomass of cells can be changed. By converting the inulinase gene, the gene accumulates higher fatty acids (100). *Aurantiochytrium* sp. YLH70 can produce lipid in a medium with 695 mL/L hydrolysate of Jerusalem artichoke. The biomass higher biomass (32.71 g/L) and DHA content (46.9% of the total fatty acid) (88).

Commercial Organic Wastes

The combination of low-cost organic compounds contained in agro-commercial waste and the cultivation of lipid-producing microorganisms can effectively achieve the effect of accumulating lipids (104, 105). Lipid-producing microorganisms use some forms of carbon sources and nutrients for growth and fatty acid accumulation. Organic waste usually contains organic particles, which may be an ideal and inexpensive substrate for microbial fatty acid production, but the chemical composition of organic waste affects the lipid production of different species (104, 106). Lipid-producing yeasts can also transform commercial organic wastes into lipid (105, 107). Crude glycerol is a by-product of biodiesel industry, which is usually treated as commercial waste (64). The engineered strain of the filamentous fungus *Ashbya gossypii* can produce microbial lipids, whose efficiency is improved by three genomic manipulation methods. Using organic commercial waste as a raw material, the strain can accumulate lipid at about 40% of DCW (85). The use of commercial waste to produce lipid is also of great significance to environmental governance.

SYNTHESIS MECHANISM OF FATTY ACIDS IN FUNGI

Essentially, the synthesis of microbial lipids is similar to that of animal and plant lipids. After the carboxylation of acetyl-CoA, saturated or unsaturated FAs are generated through chain extension and desaturation, and then triacylglycerols (TAGs) are formed.

General FA Biosynthesis

The synthesis of FAs in microbial cells requires acetyl-CoA acting as the precursor of FAs and a sufficient supply of NADPH to provide reducibility for the synthesis. It is generally believed that when nitrogen is depleted, the activity of AMP-deaminase increases. This can supplement NH_4^+ for various metabolisms, decrease intracellular AMP level and the activity of isocitrate dehydrogenase (IDH) activated and cause the accumulation of isocitrate in mitochondria (108). Aconitase (AT) in mitochondria is able to catalyze the conversion of over-accumulated isocitrate to citric acid. The citric acid is then transported to the cytoplasm, where the ATP-citrate lyase (ACL) helps its cracking catalysis to acetyl-CoA and oxaloacetic acid (OAA). As a result, abundant acetyl-CoA is produced as the precursor of FAs (109). Acetyl-CoA directly participates in the FA synthesis, while oxaloacetate is first reduced to malate dehydrogenase (MD) and then undergoes oxidative decarboxylation in the presence of malic enzyme (ME) to release NADPH (110). Studies have shown that ME can regulate lipid accumulation in oleaginous microorganisms (111). Accordingly, if the activity of ME is inhibited, the lipid accumulation will decrease. This is because although many reactions in the cellular metabolic network can produce NADPH, the NADPH required by FA synthesis comes almost entirely from ME-catalyzed reactions (111). Catalyzed by acetyl-CoA carboxylase (ACC), acetyl-CoA and CO_2 were transformed into monoyl-CoA. Multiple reactions can be continued in the presence of FAS. Acetyl-CoA combines with ACP to form acetyl-ACP, and malonyl-CoA and acetyl-CoA yield acyl-CoA via a condensation reaction. The three steps of reduction, dehydration and re-reduction are continued, and the FA chain extends by two carbon atoms. NADPH is taken as the reducing cofactor by FAS, and two NADPH molecules are required in each step of the acyl-CoA chain elongation. The chain is repeatedly extended to the desired length of the synthetic organism, and then some FAs are desaturated to form unsaturated FAs (112–114). The related reactions and enzymes are shown in **Figure 2**.

PKS Pathway

The synthesis of some special FAs in microorganisms may be related to PKS. PKS is a sophisticated molecular machine responsible for synthesizing polyketides, which are natural products from the secondary metabolism with similarities to FA (115–117).

The DHA synthesis in *Thraustochytrium*, *Schizochytrium limacinum*, *Aurantiochytrium* sp. is considered to involve the PKS pathway. The successive condensation reactions of precursors catalyzed by PKS can form a variety of polyketides, and then numerous complex compounds are generated through modification reactions such as methylation, redox, glycosylation and hydroxylation (116, 118). In terms of structure and properties, PKS can be divided into three types: modular type (type I), repetition type (type II) and chalcone type (type III). The PKS found in fungi is mostly type I, which is large multifunctional proteins encoded by a single gene. It has multiple similar modules, and some domains are reused in the compound synthesis (117). The type I has a multidomain architecture whose active sites were distributed on large modules, while the type II is composed of monofunctional enzymes, with catalytic sites separated on different proteins (119). Type III polyketide synthases (PKSs) produce secondary metabolites with diverse biological activities, including antimicrobials (120, 121). In contrast to types I and II, type III PKSs are dimers of ketone synthases that undergo a series of reactions such as initiation of primer substrates, decarboxylation condensation of extended substrates,

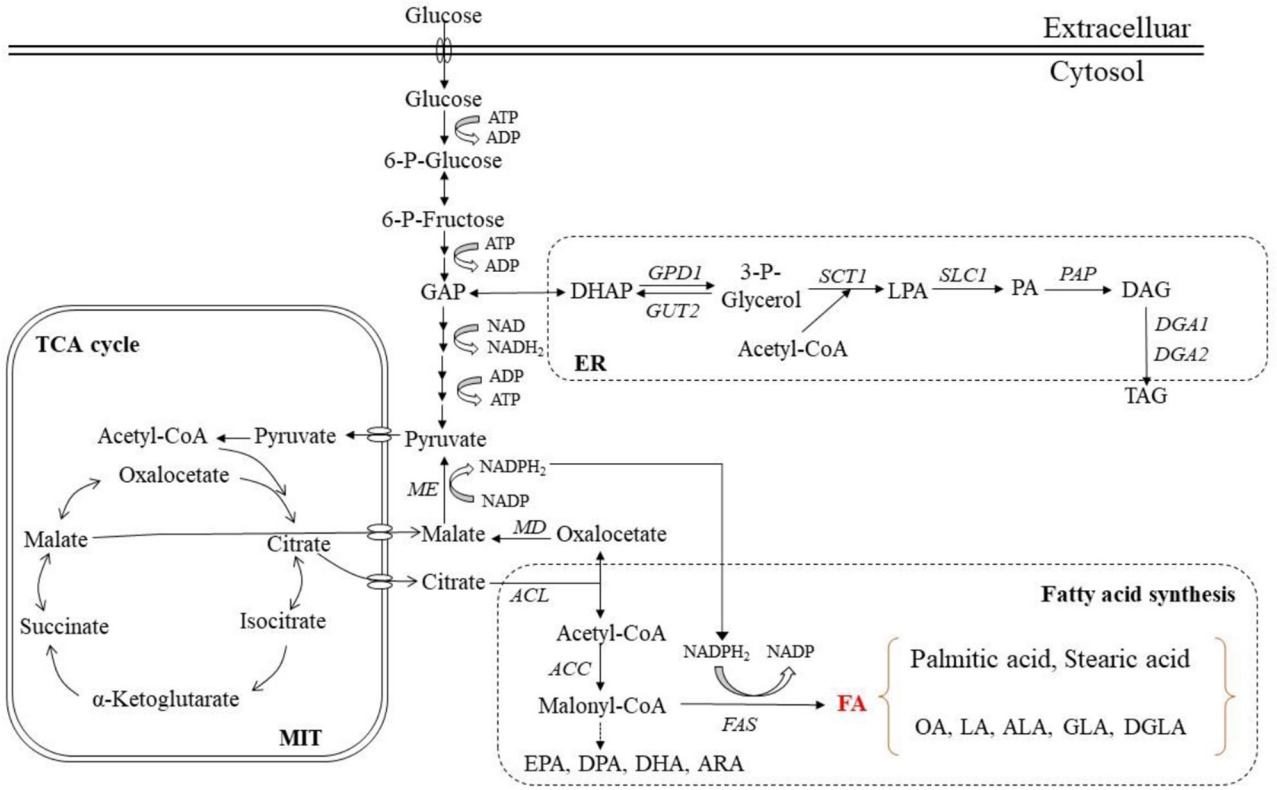

FIGURE 2 | TAGs and fatty acid synthesis in microbial cells. MIT, Mitochondria; ER, Endoplasmic reticulum; ACL, ATP-citrate lyase; FAS, Fatty acid synthase; MD, Malic dehydrogenase; ME, Malic enzyme; ACC, Acetyl-CoA carboxylase; TCA, Tricarboxylic acid cycle; DAG, Diacylglycerol; PA, Phosphatidic acid; TAG, Triacylglycerol; FA, Fatty acid; OA, Oleic acid; LA, Linoleic acid; ALA, α-Linolenic acid; GLA, γ-Linolenic acid; DGLA, Dohomo-γ-linolenic acid; ARA, Arachidonic acid; EPA, Eicosapentaenoic acid; DPA, Docosapentaenoic acid; DHA, Docosahexaenoic acid.

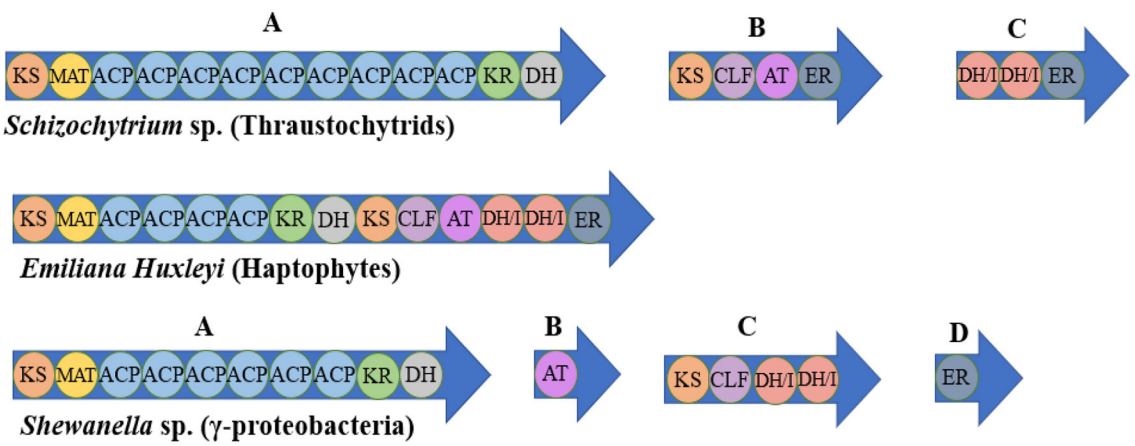

FIGURE 3 | Examples of PUFA synthase organization in various representative organisms. KS, β-ketoacyl synthase; MAT, malonyl-CoA: ACP transacylase; ACP, acyl-carrier protein; KR, β-ketoreductase; DH, dehydratase; CLF, chain length factor; AT, acyl transferase; ER, enoyl-reductase; DH/I, dehydratase/isomerase.

ring closure of growing polyketide chains and aromatization, and produce a variety of biologically active aromatic compounds (122). The PKS pathway of some species is shown in **Figure 3** (119).

TAG Synthesis

At present, TAGs are viewed as an important form of carbon source and energy storage unit in microorganisms. The TAG synthesis pathway is triggered at the point when carbon is

abundant but nitrogen is depleted in the medium. The FA biosynthesis in cytosol involves several reactions which convert the precursor, acetyl-CoA, into long-chain FAs (123). The synthesized acyl-CoA has a typical chain length of 18 or 16 carbon atoms. These C18:0 and C16:0 molecules are then delivered to the endoplasmic reticulum (ER) to be further elongated and desaturated (124–126). The TAG synthesis requires a variety of enzymes, and phosphatidic acid (PA) and diglyceride are two key intermediates in anabolic metabolism.

Generally, the TAG synthesis involves the Kennedy pathway, with glycerol-3-phosphate (G3P) and acyl-CoA serving as the direct substrates in the process (126, 127). The first step of TAG assembly is the conversion of G3P into lysophosphatidic acid (LPA) with G3P acyltransferase (*SCT1*) as the catalyst (128). Subsequently, the LPA acylation occurs to generate PA in the presence of LPA acyltransferase (*SLC1*). Further, under the action of phosphatidic acid phosphatase (PAP), PA is dephosphorylated to produce diacylglycerol (DAG) (129). Finally, TAG is formed after the DAG acylation at the sn-3 position by an acyl-CoA-independent or acyl-CoA-dependent reaction (130, 131). Regarding the acyl-CoA-independent reaction, glycerophospholipid is the acyl group donor and phospholipid DAG acyl-transferase (*LRO1*) catalyzes the process. With respect to the acyl-CoA-dependent reaction, acyl-CoA acts as the final donor of acyl group and DAG acyltransferases, i.e., *DGA1* or *DGA2*, are responsible for the catalysis. Furthermore, acting as the acyl-transferase of an acyl-CoA-dependent reaction, the steryl ester synthetase, which is encoded by *ARE1*, is proved able to promote the DAG acylation (123). The related enzymes and specific reactions are displayed in **Figure 2**.

TAG Degradation

The TAGs accumulated in cells store energy for them. Once carbon becomes insufficient, TAGs would be degraded with acetyl-CoA release so that the cellular metabolism can be maintained. Initially, free fatty acids (FFAs) can be produced from TAGs in the presence of intracellular lipases (TGL3 and TGL4) (132). These FFAs are activated by FAA1 to generate acyl-CoAs, which are then transported by specific transporters (Pxa1 and Pxa2) into the peroxisome (133). Alternatively, the transportation of the produced FFAs into the peroxisome takes place first, followed by the activation to acyl-CoAs therein by acyl/aryl-CoA ligase (AAL) (134). Afterward, acyl-CoAs are degraded in the peroxisome via the β-oxidation pathway to generate acetyl-CoA.

METABOLIC ENGINEERING OF OLEAGINOUS FUNGI

Researchers have modified a variety of lipid-producing fungi to improve production efficiency of fatty acids. On the whole, these modifications can be divided into four categories: (1) enhancement of FA synthesis pathway, (2) enhancement of TAG synthesis pathway, (3) overexpression of key enzymes for providing cofactors, and (4) the blocking competitive pathway (32, 135, 136). **Table 3** summarizes some studies on genetic modification of genes related to lipid synthesis.

TABLE 3 | Researches about lipid synthesis by overexpressing genes or knocking-out genes.

Genes	Species	Lipid content (%)	References
sodit	*M. lusitanicus*	+24.6	(111)
mt	*M. lusitanicus*	+33.8	(111)
Δ*Snf-β*	*M. circinelloides*	+32	(137)
g6pdh1	*M. circinelloides*	+23-38	(138)
g6pdh2	*M. circinelloides*	+41-47	(138)
leuB	*M. circinelloides*	+67-73	(138)
CT	*M. circinelloides*	+51% efflux rate of [14C] citrate	(139)
Δ*CT*	*M. circinelloides*	−18% efflux rate of [14C] citrate	(139)
Δ*-15D*, *MFE1*, *PEX10*	*Y. lipolytica*	77.8	(140)
DGA1, *MFE1*, *PEX10*	*Y. lipolytica*	71	(141)
ACC1	*M. rouxii*	40	(142)
MA-GAPDH1	*M. alpina*	+13	(143)
YlGSY1	*Y. lipolytica*	+60% TAG	(144)
IDH	*M. alpina*	+8.2	(145)
ER	*S. limacinum* SR21	+47.63	(146)
Overexpression of ACL and ACC	*Schizochytrium* sp. ATCC 20888	73	(147)
ELO3	*Schizochytrium* sp. S31	+1.39 times DHA	(148)
sodit-a or/and *sodit-b*	*M. circinelloides*	+10-40	(149)

Enhancement of FA Synthesis Pathway

Previous studies have shown that the expression of acetyl-CoA carboxylase (encoded by *accA*, *accB*, *accC* and *accD*) and thioesterase I (encoded by *tesA*) in *Escherichia coli* can speed up the FA synthesis by six times. This suggests that the catalytic reaction of acetyl-CoA carbohydrase is a rate-limiting step for FA synthesis (150–153). Overexpression of both heterologous Δ-15 desaturase (Δ*-15D*) sourced from flax and endogenous genes (*SCD*, *ACC1*, *DGA1* and Δ*-12D*) along with the deletion of endogenous *MFE1* and *PEX10* can yield a superior lipid producer (140). It is able to produce lipid with content of 77.8% and titer of 50 g/L using glucose as the substrate in a 5 L stirred-tank bioreactor (140).

Han et al. (147) overexpressed in *Schizochytrium* sp. ATCC 20888 using the strong constitutive promoter ccg1, *Schizochytrium* ATP-citrate lyase (ACL) and acetyl-CoA carboxylase (ACC). The lipid content of overexpressed strains obtained by fermentation culture can reach a maximum of 73.0%, an increase of 38.3%. However, the *ACC1* gene from

mold *M. rouxii* is expressed in the *Hansenula polymorpha*, and the fat content is only 40% higher than the original (142), possibly because the fungus has a more powerful metabolic regulation system.

Enhancement of TAG Synthesis Pathway

Diacylglycerol acyltransferase (DGAT) catalyzes the conversion of DAG and acetyl-CoA to TAG, which is the last step in the TAG synthesis (32, 154, 155). When grown in batch conditions and minimal medium, the resulting strain consumes 12 g/L cellulose and accumulates 14% (DCW) lipids (156). Blazeck et al. (141) synergistically regulated multiple key genes related to the degradation and biosynthesis of lipids in *Y. lipolytica* with a combinatorial strategy, including *MFE1*, *AMPD*, *PEX10*, *MAE*, *DGA1*, *ACL1*, *ACL2* and *DGA2*, with 57 distinct genotypes generated. The double deletion of *MFE1* and *PEX10* and the overexpression of *DGA1* were most effective for modification. After the optimization of bioreaction conditions, the engineered strain had a lipid content of 71% (DCW) and a lipid titer of 25 g/L. Markedly, a 60-fold improvement was realized over the original strain.

Overexpression of Key Enzymes for Providing Cofactors

IDH and ME probably play a crucial role in the accumulation of lipids. When glucose-6-phosphate dehydrogenase (G6PD), 6-phosphogluconate dehydrogenase (PGD), IDH and ME are overexpressed in *M. alpina*, total FAs can be increased by 1.7 times; while ME2 is more effective in desaturation, and the content of arachidonic acid (AA) is increased by 1.5 times compared to the control (157). Glyceraldehyde 3-phosphate dehydrogenase (GAPDH) is an enzyme highly conserved in the glycolytic pathway. The lipid-producing filamentous fungus *M. alpina* was used to characterize two copies of the gene encoding GAPDH, and the overexpression strain MA-GAPDH1 increases the lipid content by about 13% (143). First, the total lipid accumulation was increased by overexpressing a malic enzyme from *Crypthecodinium cohnii* to elevate NADPH supply. Then, the inhibition effect on acetyl-CoA carboxylase was relieved by overexpressing a codon-optimized *ELO3* gene from *M. alpina*. After the above two-step engineering, contents of DHA was increased by 1.39-fold, reaching a level of 26.70% of dry cell weight, respectively (148).

The PKS cluster genes are supposed to synthesize PUFAs in *S. limacinum*. Ling et al. (146) improved lipid production domain expression by homologous recombination knocking out two enolate reductase (ER) genes located on the PKS cluster. The addition of triclosan as a modulator of the ER domain resulted in a 51.74% increase in PUFA production and a 47.63% increase in lipid production.

Blocking Competitive Pathways

The main competitive pathways blocking the lipid accumulation in microbial cells include β-oxidation of FAs, synthesis of phospholipids and conversion of phospho-enol-pyruvic acid (PEP) to oxalacetic acid. The β-oxidation occurs in peroxisomes, and peroxisome biogenesis is generally downregulated by the deletion of *PEX3*, *PEX10* and *PEX11* so that the degradation of TAGs can be prevented in commercial strains (158, 159). As an important intermediate metabolite, malate, its subcellular location and concentration have significant effects on fungal lipid metabolism. Yang et al. (149) deleted the two plasma membrane malate transporters "2-oxoglutarate:malate antiporter" (named SoDIT-a and SoDIT-b) of *M. circinelloides* WJ11 and analyzed their effects on growth ability, lipid accumulation and metabolism. Their results showed that the lipid content of the mutant was increased by ∼10–40% compared to the control strain, indicating that defects in plasma membrane malate transport lead to an increase in malate for lipid synthesis.

Additionally, the genes involved in the β-oxidation pathway are often the deletion targets to increase lipid accumulation (160). After the characterization and deletion of the *YlGSY1* gene

TABLE 4 | Sources and uses of various unsaturated fatty acids.

Category	Species	Functions
DHA	*Thraustochytrium*, *Schizochytrium limacinum*, *Aurantiochytrium* sp.	Conducive to retinal development, promote brain development, prevent cardiovascular disease
EPA	*Diasporangium* sp , *Mucor*, *Mortierella alpine Cunninghamell*	Lowers cholesterol levels, resists arteriosclerosis, prevents Alzheimer's disease and vision loss, improves brain function, is added to healthy food and baby food
ARA	*Mortierella*, *Mortierella alpina*, *Mortierella isabellina*	Promoting brain and nervous system development
ALA	*Saccharomyces cerevisiae*	Inhibiting thrombotic diseases, reducing blood pressure and blood lipids
GLA	*Mucor hiemalis*, *Mucor circinelloides*, *Rhizopus*, *Zygomycetes*	Plays an important physiological role in cardiovascular, immune, reproductive and endocrine systems, lowers blood sugar and blood lipids
Palmitic acid	*Schizochytrium*	Treatment of inflammation in cells and organs caused by excessive consumption
LA	*Galactomyces geotrichum*, *Mortierella alpina*, *Mucor circinelloides*	Reducing blood lipid, soften blood vessels, reducing blood pressure, promoting microcirculation
DGLA	*Mortierella alpina*, *Pythium*, *Entomophyhora*	Treating atherosclerosis

encoding glycogen synthase, Bhutada et al. (144) increased the TAG accumulation of the engineered strain by 60% as compared with the wild-type strains. This proves that glycogen synthesis is a competing pathway, and its elimination is beneficial for the production of neutral lipids.

COMMERCIAL APPLICATIONS OF FUNGAL FAs

Recently, many researchers make efforts to explore the applications of microbial lipids in various fields from the food and health industry to the production of plasticizers, lubricants, spices and pesticides. Additionally, they are also promising intermediates in fine chemicals and other industries. This part mainly introduces the applications of polyunsaturated fatty acids from fungi. Polyunsaturated fatty acids (PUFAs) have received increasing attention for their beneficial effects on human health. PUFAs refer to long-chain FAs containing two or more double bonds, mainly including linoleic acid (LA), conjugated linoleic acid (CLA), γ-linolenic acid (GLA), AA, eicosapentaenoic acid (EPA), DHA, which are mostly the precursors of bioactive substances. They have the capabilities of anti-aging, anti-oxidation and anti-inflammation and are able to inhibit the formation, proliferation and metastasis of tumor cells and treat heart disease, hypertension, etc. **Table 4** summarizes the production of unsaturated fatty acids by some fungi and their application functions.

DHA

DHA is an important member of the ω-3 PUFA family and has a wide distribution. Among marine organisms such as fish, shrimps, crabs, and seaweeds, DHA is particularly abundant in lipids of deep-sea fish (161). It can be produced in the *Thraustochytrium*, *Schizochytrium limacinum*, *Aurantiochytrium* sp. and so on. Although DHA can be produced from α-linolenic acid, the reaction rate is low, which thus necessitates its intake from diet (7). It accumulates in retinal tissue and gray matter in general and plays a key role in early visual and neural development (162). Besides, it is conducive to the development of the retinal, neuronal and immune systems at embryonic and post-natal stages (163, 164) and is effective to prevent cardiovascular disease, maintain brain and learning functions and protect inflammation response systems in adulthood (165). As a nutrient, DHA can be used in maternal and infant products. DHA and other unsaturated FAs in microalgae can be fully digested and absorbed by some aquatic organisms to meet the growth and development of juvenile fish and improve their survival rate (166).

EPA

EPA belongs to the ω-3 series of PUFAs. Natural phospholipids containing EPA are mainly found in the eggs and muscle tissues of marine animals. EPA can be produced in Mucorales, *M. alpina* and so on. Studies have revealed that EPA is able to protect the heart against the deleterious effects of sepsis in female rats. The following two reasons account for this beneficial action: (1) The anti-inflammatory activity of EPA which reduces the oxidative stress and preserves the energy metabolism through an increase in UCP3; (2) the incorporation of EPA in membrane phospholipids that increases the vasodilator reserve of the coronary microvessels (167, 168). EPA and DHA have various physiological functions such as reducing cholesterol content, resisting arteriosclerosis, preventing Alzheimer's disease and vision loss and improving brain function (164, 169). EPA and DHA are usually added to health foods and baby foods. High levels of EPA and DHA can be used as drugs to treat cardiovascular and cerebrovascular diseases, e.g., hyperlipidemia and arteriosclerosis. The preparation of high-purity EPA and DHA is the current deep processing target of fish lipids (27, 170). EPA is also an important functional component of breast milk, which is essential for the development of the baby's brain and vision. Therefore, more and more researchers are committed to applying EPA to infant milk powder in hope of improving its nutritional value through simulating the nutrients in breast milk (171).

ARA

ARA is an important member of the ω-6 PUFA family and has a wide distribution. Like DHA, which plays an important role in the development of infants' brains and retinas, it is one of the important factors affecting the quality of infant milk powder (21, 172). *Mortierella*, a fungus of the order *Mucor*, is a good producer of ARA. Research shows that ARA and DHA together constitute 20% of the weight of the human brainstem and are mainly concentrated in the outer neuron membrane and iliac sheath (173, 174). Bieren et al. (175) discovered that ARA metabolites can promote the occurrence of acute inflammation and produced pro-inflammatory mediators, such as PGE2 and PGfc. Lipoxin A_4 derived from ARA can promote the degradation of lipid mediators. ARA accounts for 15–17% of the total FAs in skeletal muscle, which benefits the growth and repair of skeletal muscle tissue (176). Studies have shown that ARA supplementation can stimulate prostaglandin release and induce skeletal muscle hypertrophy through COX-2 dependent pathways (177).

GLA

GLA, one of the essential FAs, is an important component of biofilm (15). The microbial sources of GLA are mainly fungi and microalgae. For example, the microbial sources of GLA mainly include *Spirulina* (*S. maxima*, *S. arthrospirulina*), *Mucor* (*M. rucus* and *M. microflora*), *Rhizopus*, and *Crucifera* (15, 178, 179). GLA plays a significant physiological role in cardiovascular, immune, reproductive and endocrine systems. It is important because of its nutritional value and medicinal applications (180). GLA can act on lipoprotein enzyme and lipase to affect the formation and expression of TAGs, total cholesterol and very-low-density and low-density lipoproteins, thus having the capacity to lower blood lipid (181).

High-Value Chemicals Production From Oleaginous Fungi

In addition to the above-mentioned polyunsaturated fatty acids, some of these strains can also produce high levels of squalene and carotenoids, two other compounds of commercial value with rapidly growing market potential (182). Squalene has antioxidant and anticancer activities with broad applications in food and cosmetics industries. Besides, squalene has been used as vaccine adjuvant in vaccine formulations (43, 183). Since, the demand for squalene has increased during the last decade, microbial production of squalene has been investigated as a promising alternative source for traditional extraction methods from shark liver or plant lipids (184). Microbial strains are capable of producing non-polluting, low-cost, high-quality and sustainable sources of squalene, which is the main direction of the lipid-based biofuel industry.

Aurantiochytrium strains have the potential to produce large amounts of squalene, and *Aurantiochytrium* is known for its potential to produce large amounts of polyunsaturated DHA on a large scale (185). Furthermore, *Thraustochytrid* reported the co-production of squalene and DHA from inexpensive feedstocks such as organic solvent pretreatment spruce hydrolysis (186).

CONCLUSION

Accumulation of fatty acids with important functions is the most attractive point of oleaginous fungi. However, the cost limits application of the functional fatty acids. It is very important to improve production efficiency and reduce cost of the fatty acids. Replacing glucose with raw materials, while maintaining high biomass and lipid yields, was considered a feasible strategy. More fundamentally, many metabolic engineering strategies have been developed as efficient tools in oleaginous fungi to overcome the biochemical limit and to improve production efficiency of fatty acids. Particularly, the special kind of functional fatty acid can be enhanced by modifying the biosynthetic pathway with much higher yield. It also can be predictable that metabolic engineering can change the storage mode of fatty acids, even simplify the extraction. Thus, oleaginous fungi can be developed as hosts for high-value fatty acids and fatty acid-derived chemicals.

AUTHOR CONTRIBUTIONS

Z-PW and X-JY made important contributions to the study conception and design. X-YZ participated in the drafting and revision of the manuscript. BL and B-CH conducted data analysis and interpretation. F-BW, Y-QZ, S-GZ, and ML performed literature research and organization. X-YL, JJ, and H-YW revised the manuscript. All authors read and approved this manuscript and agreed to be responsible for all aspects of the research to ensure the data accuracy and integrity of this work.

FUNDING

This research was supported by the Natural Science Foundation of Shandong Province (ZR2020MC003), the First Class Fishery Discipline Programme in Shandong Province, a special talent programme One Thing One Decision (YishiYiyi) Programme in Shandong Province, China, the Zhejiang Provincial Natural Science Foundation of China (No. LY18C010004), and the Talent Research Foundation of Qingdao Agricultural University (663/1117023, 663/1120036, and 663/1120058).

REFERENCES

1. Darvishi F, Fathi Z, Ariana M, Moradi H. *Yarrowia lipolytica* as a workhorse for biofuel production. *Biochem Eng J*. (2017) 127:87–96. doi: 10.1016/j.bej.2017.08.013
2. Jones AD, Boundy-Mills KL, Barla GF, Kumar S, Ubanwa B, Balan V. Microbial Lipid Alternatives to Plant Lipids. *Methods Mol Biol.* (2019) 1995:1–32. doi: 10.1007/978-1-4939-9484-7_1
3. Zeng SY, Liu HH, Shi TQ, Song P, Ren LJ, Huang H, et al. Recent Advances in Metabolic Engineering of *Yarrowia lipolytica* for Lipid Overproduction. *Eur J Lipid Sci Technol.* (2018) 120:1700352. doi: 10.1002/ejlt.201700352
4. Wang ZP, Xu HM, Wang GY, Chi Z, Chi ZM. Disruption of the MIG1 gene enhances lipid biosynthesis in the oleaginous yeast Yarrowia lipolytica ACA-DC 50109. *Biochim Biophys Acta.* (2013) 1831:675–82. doi: 10.1016/j.bbalip.2012.12.010
5. Fillet S, Adrio JL. Microbial production of fatty alcohols. *World J Microbiol Biotechnol.* (2016) 32:152. doi: 10.1007/s11274-016-2099-z
6. Kikukawa H, Sakuradani E, Ando A, Shimizu S, Ogawa J. Arachidonic acid production by the oleaginous fungus *Mortierella alpina* 1S-4: a review. *J Adv Res.* (2018) 11:15–22. doi: 10.1016/j.jare.2018.02.003
7. Patel A, Rova U, Christakopoulos P, Matsakas L. Mining of squalene as a value-added byproduct from DHA producing marine thraustochytrid cultivated on food waste hydrolysate. Science of The Total Environment. (2020) 139691. doi: 10.1016/j.scitotenv.2020.139691
8. Hu L, Xu J, Zhou S, He A, Tang X, Lin L, et al. Catalytic Advances in the Production and Application of Biomass-Derived 2,5-Dihydroxymethylfuran. *ACS Catal.* (2018) 8:2959–80. doi: 10.1021/acscatal.7b03530
9. Yang Y, Heidari F, Hu B. Fungi (Mold)-based lipid production. *Methods Mol Biol.* (2019) 1995:51–89. doi: 10.1007/978-1-4939-9484-7_3
10. Gao Q, Cao X, Huang YY, Yang JL, Chen J, Wei LJ, et al. Overproduction of fatty acid ethyl esters by the oleaginous yeast *Yarrowia lipolytica* through metabolic engineering and process optimization. *ACS Synth Biol.* (2018) 7:1371–80. doi: 10.1021/acssynbio.7b00453
11. Thangavelu K, Sundararaju P, Srinivasan N. Uthandi S. Bioconversion of sago processing wastewater into biodiesel: Optimization of lipid production by an oleaginous yeast, Candida tropicalis ASY2 and its transesterification process using response surface methodology. *Microb Cell Fact.* (2021) 20:167. doi: 10.1186/s12934-021-01655-7
12. Langseter AM, Dzurendova S, Shapaval V, Kohler A, Ekeberg D, Zimmermann B. Evaluation and optimisation of direct transesterification methods for the assessment of lipid accumulation in oleaginous filamentous fungi. *Microb Cell Fact.* (2021) 20:59. doi: 10.1186/s12934-021-01542-1
13. Zhang Y, Guo X, Yang H, Shi S. The studies in constructing yeast cell factories for the production of fatty acid alkyl esters. *Front Bioeng Biotechnol.* (2022) 9:799032. doi: 10.3389/fbioe.2021.799032
14. Nazir Y, Shuib S, Kalil MS, Song Y, Hamid AA. Optimization of culture conditions for enhanced growth, lipid and docosahexaenoic acid (DHA) production of aurantiochytrium SW1 by response surface methodology. *Sci Rep.* (2018) 8:8909. doi: 10.1038/s41598-018-27309-0
15. Klempová T, Slaný O, Šišmiš M, Marcinčák S, Certík M. Dual production of polyunsaturated fatty acids and beta-carotene with Mucor wosnessenskii by the process of solid-state fermentation using agro-commercial waste. *J Biotechnol.* (2020) 311:1–11. doi: 10.1016/j.jbiotec.2020.02.006

16. Patel A, Matsakas L, Hruzová K, Rova U, Christakopoulos P. Biosynthesis of Nutraceutical Fatty Acids by the Oleaginous Marine Microalgae *Phaeodactylum tricornutum* Utilizing Hydrolysates from Organosolv-Pretreated Birch and Spruce Biomass. *Mar Drugs.* (2019) 17:119. doi: 10.3390/md17020119
17. Poliner E, Farré EM, Benning C. Advanced genetic tools enable synthetic biology in the oleaginous microalgae *Nannochloropsis* sp. *Plant Cell Rep.* (2018) 37:1383–99. doi: 10.1007/s00299-018-2270-0
18. Yu XJ, Huang CY, Chen H, Wang DS, Chen JL Li HJ, Liu XY, et al. High-Throughput Biochemical Fingerprinting of Oleaginous Aurantiochytrium sp. *Strains by Fourier Transform Infrared Spectroscopy (FT-IR) for Lipid and Carbohydrate Productions Molecules.* (2019) 24:1593. doi: 10.3390/molecules24081593
19. Dzurendova S, Zimmermann B, Tafintseva V, Kohler A, Ekeberg D, Shapaval V. The influence of phosphorus source and the nature of nitrogen substrate on the biomass production and lipid accumulation in oleaginous *Mucoromycota* fungi. *Appl Microbiol Biotechnol.* (2020) 104:8065–76. doi: 10.1007/s00253-020-10821-7
20. Heggeset TMB, Ertesvåg H, Liu B, Ellingsen TE, Vadstein O, Aasen IM. Lipid and DHA-production in *Aurantiochytrium* sp. —Responses to nitrogen starvation and oxygen limitation revealed by analyses of production kinetics and global transcriptomes. *Sci Rep.* (2019) 9:19470. doi: 10.1038/s41598-019-55902-4
21. Goyzueta-Mamani LD, de Carvalho JC, Magalhães AI Jr, Soccol CR. Production of arachidonic acid by Mortierella alpina using wastes from potato chips industry. *J Appl Microbiol.* (2021) 130:1592–601. doi: 10.1111/jam.14864
22. Abdel-Wahab MA, El-Samawaty AEMA, Elgorban AM, Bahkali AH. Fatty acid production of *thraustochytrids* from Saudi Arabian mangroves. *Saudi J Biol Sci.* (2021) 28:855–64. doi: 10.1016/j.sjbs.2020.11.024
23. Papanikolaou S, Rontou M, Belka A, Athenaki M, Gardeli C, Mallouchos A, et al. Conversion of biodiesel-derived glycerol into biotechnological products of commercial significance by yeast and fungal strains. *Eng Life Sci.* (2017) 17:262–81. doi: 10.1002/elsc.201500191
24. Lowrey J, Armenta RE, Brooks MS. Recycling of lipid-extracted hydrolysate as nitrogen supplementation for production of biomass. *J Ind Microbiol Biotechnol.* (2016) 43:1105–15. doi: 10.1007/s10295-016-1779-x
25. Altu R, Esim, N, Aykutoglu G, Baltaci MO, Adiguzel A, and Taskin M. Production of linoleic acid-rich lipids in molasses-based medium by oleaginous fungus *Galactomyces geotrichum* TS61. *J Food Process Preserv.* (2020) 44:e14518. doi: 10.1111/jfpp.14518
26. Dedyukhina EG, Chistyakova TI, Mironov AA, Kamzolova SV, Morgunov IG, Vainshtein MB. Arachidonic acid synthesis from biodiesel-derived waste by Mortierella alpina. *Eur J Lipid Sci Technol.* (2014) 116:429–37. doi: 10.1002/ejlt.201300358
27. Huang M, Chen H, Tang X, Lu H, Zhao J, Zhang H, et al. Two-stage pH control combined with oxygen-enriched air strategies for the highly efficient production of EPA by *Mortierella alpina* CCFM698 with fed-batch fermentation. *Bioprocess Biosyst Eng.* (2020) 43:1725–33. doi: 10.1007/s00449-020-02367-9
28. Du F, Wang YZ, Xu YS, Shi TQ, Liu WZ, Sun XM, et al. Biotechnological production of lipid and terpenoid from *thraustochytrids*. *Biotechnol Adv.* (2021) 48:107725. doi: 10.1016/j.biotechadv.2021.107725
29. Fossier Marchan L, Lee Chang KJ, Nichols PD, Mitchell WJ, Polglase JL, Gutierrez T. Taxonomy, ecology and biotechnological applications of thraustochytrids: a review. *Biotechnol Adv.* (2018) 36:26–46. doi: 10.1016/j.biotechadv.2017.09.003
30. Tang M, Zhou W, Liu Y, Yan J, Gong Z, A. two-stage process facilitating microbial lipid production from N-acetylglucosamine by *Cryptococcus curvatus* cultured under non-sterile conditions. *Bioresour Technol.* (2018) 258:255–62. doi: 10.1016/j.biortech.2018.03.015
31. Dias KB, Oliveira NML, Brasil BSAF, Vieira-Almeida EC, Paula-Elias FC, Almeida AF. Simultaneous high nutritional single cell oil and lipase production by *Candida viswanathii*. *Acta Sci Pol Technol Aliment.* (2021) 20:93–102. doi: 10.17306/J.AFS.0856
32. Dourou M, Aggeli D, Papanikolaou S, Aggelis G. Critical steps in carbon metabolism affecting lipid accumulation and their regulation in oleaginous microorganisms. *Appl Microbiol Biotechnol.* (2018) 102:2509–23. doi: 10.1007/s00253-018-8813-z
33. Dourou M, Mizerakis P, Papanikolaou S, Aggelis G. Storage lipid and polysaccharide metabolism in *Yarrowia lipolytica* and *Umbelopsis isabellina*. *Appl Microbiol Biotechnol.* (2017) 101:7213–26. doi: 10.1007/s00253-017-8455-6
34. Carsanba E, Papanikolaou S, Erten H. Production of oils and fats by oleaginous microorganisms with an emphasis given to the potential of the nonconventional yeast *Yarrowia lipolytica*. *Crit Rev Biotechnol.* (2018) 38:1230–43. doi: 10.1080/07388551.2018.1472065
35. Dzurendova S, Zimmermann B, Tafintseva V, Kohler A, Horn SJ, Shapaval V. Metal and Phosphate Ions Show Remarkable Influence on the Biomass Production and Lipid Accumulation in Oleaginous Mucor circinelloides. *J Fungi (Basel).* (2020) 6:260. doi: 10.3390/jof6040260
36. Shafiq M, Zeb L, Cui G, Jawad M, Chi Z. High-Density pH-Auxostat Fed-Batch Culture of *Schizochytrium limacinum* SR21 with Acetic Acid as a Carbon Source. *Appl Biochem Biotechnol.* (2020) 192:1163–75. doi: 10.1007/s12010-020-03396-6
37. Zhang H, Cui Q, Song X. Research advances on arachidonic acid production by fermentation and genetic modification of *Mortierella alpina*. *World J Microbiol Biotechnol.* (2021) 37:4. doi: 10.1007/s11274-020-02984-2
38. Subramanian AM, Nanjan SE, Prakash H, Santharam L, Ramachandran A, Sathyaseelan V, et al. Biokinetics of fed-batch production of poly (3-hydroxybutyrate) using microbial co-culture. *Appl Microbiol Biotechnol.* (2020) 104:1077–95. doi: 10.1007/s00253-019-10274-7
39. Pomraning KR, Kim YM, Nicora CD, Chu RK, Bredeweg EL, Purvine SO, et al. Multi-omics analysis reveals regulators of the response to nitrogen limitation in Yarrowia lipolytica. *BMC Genomics.* (2016) 17:138. doi: 10.1186/s12864-016-2471-2
40. Papanikolaou S, Aggelis G. Lipids of oleaginous yeasts. Part II: Technology and potential applications. *Eur J Lipid Sci Technol.* (2011) 113:1052–73. doi: 10.1002/ejlt.201100015
41. Li YH, Liu B, Zhao ZB. Optimization of culture conditions for lipid production by Rhodosporidium toruloides. *Chin J Biotech.* (2006) 22: 650–6. doi: 10.1016/S1872-2075(06)60050-2
42. Bellou S, Triantaphyllidou IE, Mizerakis P, Aggelis G. High lipid accumulation in *Yarrowia lipolytica* cultivated under double limitation of nitrogen and magnesium. *J Biotechnol.* (2016) 234:116–26. doi: 10.1016/j.jbiotec.2016.08.001
43. Shakeri S, Khoshbasirat F, Maleki M. *Rhodosporidium* sp. DR37: a novel strain for production of squalene in optimized cultivation conditions. *Biotechnol Biofuels.* (2021) 14:95. doi: 10.1186/s13068-021-01947-5
44. Chen X, He Y, Ye H, Xie Y, Sen B, Jiao N, et al. Different carbon and nitrogen sources regulated docosahexaenoic acid (DHA) production of Thraustochytriidae sp. PKU#SW8 through a fully functional polyunsaturated fatty acid (PUFA) synthase gene (pfaB). *Bioresour Technol.* (2020) 318:124273. doi: 10.1016/j.biortech.2020.124273
45. Chen X, Sen B, Zhang S, Bai M, He Y, Wang G. Chemical and physical culture conditions significantly influence the cell mass and docosahexaenoic acid content of *Aurantiochytrium limacinum* strain PKU#SW8. *Mar Drugs.* (2021) 19:671. doi: 10.3390/md19120671
46. Wu S, Hu C, Jin G, Zhao X, Zhao ZK. Phosphate-limitation mediated lipid production by *Rhodosporidium toruloides*. *Bioresour Technol.* (2010) 101: 6124-6129. doi: 10.1016/j.biortech.2010.02.111
47. Wang Y, Zhang S, Zhu Z, Shen H, Lin X, Jin X, et al. Systems analysis of phosphate-limitation-induced lipid accumulation by the oleaginous yeast *Rhodosporidium toruloides*. *Biotechnol Biofuels.* (2018) 11:148. doi: 10.1186/s13068-018-1134-8
48. Kamal R, Shen H, Li Q, Wang Q, Yu X, Zhao ZK. Utilization of amino acid-rich wastes for microbial lipid production. *Appl Biochem Biotechnol.* (2020) 191:1594–604. doi: 10.1007/s12010-020-03296-9
49. Tchakouteu SS, Kopsahelis N, Chatzifragkou A, Kalantzi O, Stoforos NG, Koutinas AA, et al. *Rhodosporidium toruloides* cultivated in NaCl-enriched glucose-based media: adaptation dynamics and lipid production. *Eng Life Sci.* (2016) 17:237–48. doi: 10.1002/elsc.201500125

50. Li S, Hu Z, Yang X, Li Y. Effect of nitrogen sources on omega-3 polyunsaturated fatty acid biosynthesis and gene expression in *Thraustochytriidae* sp. *Mar Drugs.* (2020) 18:612. doi: 10.3390/md18120612
51. Wu SG, Zhao X, Hu CM, Zhang SF, Hua YY, Zhao ZB. Screening of fungi for microbial oil production using N-acetyl-D-glucosamine. China Biotechnol. (2008) 28: 58-62.
52. Hu F, Clevenger AL, Zheng P, Huang Q, Wang Z. Low-temperature effects on docosahexaenoic acid biosynthesis in *Schizochytrium* sp. TIO01 and its proposed underlying mechanism. *Biotechnol Biofuels.* (2020) 13:172. doi: 10.1186/s13068-020-01811-y
53. Aussant J, Guihéneuf F, Stengel DB. Impact of temperature on fatty acid composition and nutritional value in eight species of microalgae. *Appl Microbiol Biotechnol.* (2018) 102:5279–97. doi: 10.1007/s00253-018-9001-x
54. Huang XF, Shen Y, Luo HJ, Liu JN, Liu J. Enhancement of extracellular lipid production by oleaginous yeast through preculture and sequencing batch culture strategy with acetic acid. *Bioresour Technol.* (2018) 247:395–401. doi: 10.1016/j.biortech.2017.09.096
55. Abeln F, Hicks RH, Auta H, Moreno-Beltrán M, Longanesi L, Henk DA, et al. Semi-continuous pilot-scale microbial oil production with *Metschnikowia pulcherrima* on starch hydrolysate. *Biotechnol Biofuels.* (2020) 13:127. doi: 10.1186/s13068-020-01756-2
56. Martínez-Avila O, Sánchez A, Font X, Barrena R. Fed-batch and sequential-batch approaches to enhance the bioproduction of 2-phenylethanol and 2-phenethyl acetate in solid-state fermentation residue-based systems. *J Agric Food Chem.* (2019) 67:3389–99. doi: 10.1021/acs.jafc.9b00524
57. Abeln F, Chuck CJ. Achieving a high-density oleaginous yeast culture: comparison of four processing strategies using *Metschnikowia pulcherrima*. *Biotechnol Bioeng.* (2019) 116:3200–14. doi: 10.1002/bit.27141
58. Wang Q, Ye H, Sen B, Xie Y, He Y, Park S, et al. Improved production of docosahexaenoic acid in batch fermentation by newly-isolated strains of *Schizochytrium* sp. and *Thraustochytriidae* sp through bioprocess optimization. *Synth Syst Biotechnol.* (2018) 3:121–9. doi: 10.1016/j.synbio.2018.04.001
59. Ibarruri J, Cebrián M, Hernández I. Valorisation of fruit and vegetable discards by fungal submerged and solid-state fermentation for alternative feed ingredients production. *J Environ Manage.* (2021) 281:111901. doi: 10.1016/j.jenvman.2020.111901
60. Arbter P, Sinha A, Troesch J, Utesch T, Zeng AP. Redox governed electro-fermentation improves lipid production by the oleaginous yeast *Rhodosporidium toruloides*. *Bioresour Technol.* (2019) 294:122122. doi: 10.1016/j.biortech.2019.122122
61. Kot AM, Gientka I, Bzducha-Wróbel A, Błazejak S, Kurcz A. Comparison of simple and rapid cell wall disruption methods for improving lipid extraction from yeast cells. *J Microbiol Methods.* (2020) 176:105999. doi: 10.1016/j.mimet.2020.105999
62. Garay LA, Boundy-Mills KL, German JB. Accumulation of high-value lipids in single-cell microorganisms: a mechanistic approach and future perspectives. *J Agricult Food Chem*. (2014) 62: 2709–27. doi: 10.1021/jf4042134
63. Martínez JM, Delso C, Aguilar DE, Álvarez I, Raso J. Organic-solvent-free extraction of carotenoids from yeast *Rhodotorula glutinis* by application of ultrasound under pressure. *Ultrason Sonochem.* (2019) 61:104833. doi: 10.1016/j.ultsonch.2019.104833
64. Kumar LR, Yellapu SK, Tyagi RD, Zhang X, A. review on variation in crude glycerol composition, bio-valorization of crude and purified glycerol as carbon source for lipid production. *Bioresour Technol.* (2019) 293:122155. doi: 10.1016/j.biortech.2019.122155
65. Jeevan Kumar SP, Banerjee R. Enhanced lipid extraction from oleaginous yeast biomass using ultrasound assisted extraction: a greener and scalable process. *Ultrason Sonochem.* (2019) 52:25–32. doi: 10.1016/j.ultsonch.2018.08.003
66. Jadhav HB, Gogate PR, Waghmare JT, Annapure US. Intensified synthesis of palm olein designer lipids using sonication. *Ultrason Sonochem.* (2021) 73:105478. doi: 10.1016/j.ultsonch.2021.105478
67. Ong CC, Chen YH. Investigation on cell disruption techniques and supercritical carbon dioxide extraction of *Mortierella alpina* Lipid. *Foods.* (2022) 11:582. doi: 10.3390/foods11040582
68. Breil C, Abert Vian M, Zemb T, Kunz W, and Chemat F. "Bligh and Dyer" and folch methods for solid-liquid-liquid extraction of lipids from microorganisms. comprehension of solvatation mechanisms and towards substitution with alternative solvents. *Int J Mol Sci.* (2017) 18:708. doi: 10.3390/ijms18040708
69. Meullemiestre A, Breil C, Abert-Vian M, and Chemat F. Microwave, ultrasound, thermal treatments, and bead milling as intensification techniques for extraction of lipids from oleaginous *Yarrowia lipolytica* yeast for a biojetfuel application. *Biores Technol.* (2016) 211: 190–199. doi: 10.1016/j.biortech.2016.03.040
70. Svenning JB, Dalheim L, Vasskog T, Matricon L, Vang B, Olsen RL. Lipid yield from the diatom *Porosira glacialis* is determined by solvent choice and number of extractions, independent of cell disruption. *Sci Rep.* (2020) 10:22229. doi: 10.1038/s41598-020-79269-z
71. Patel A, Arora N, Pruthi V, Pruthi PA, A. novel rapid ultrasonication-microwave treatment for total lipid extraction from wet oleaginous yeast biomass for sustainable biodiesel production. *Ultrason Sonochem.* (2019) 51:504–16. doi: 10.1016/j.ultsonch.2018.05.002
72. Chi G, Xu Y, Cao X, Li Z, Cao M, Chisti Y, et al. Production of polyunsaturated fatty acids by Schizochytrium (Aurantiochytrium) spp. *Biotechnol Adv.* (2022) 55:107897. doi: 10.1016/j.biotechadv.2021.107897
73. Metz JG, Roessler P, Facciotti D, Levering C, Dittrich F, Lassner M, et al. Production of polyunsaturated fatty acids by polyketide synthases in both prokaryotes and eukaryotes. *Science.* (2001) 293:290–3. doi: 10.1126/science.1059593
74. Merkx-Jacques A, Rasmussen H, Muise DM, Benjamin JJR, Kottwitz H, Tanner K, et al. Engineering xylose metabolism in *thraustochytrid* T18. *Biotechnol Biofuels.* (2018) 11:248. doi: 10.1186/s13068-018-1246-1
75. Shene C, Paredes P, Flores L, Leyton A, Asenjo JA, Chisti Y. Dynamic flux balance analysis of biomass and lipid production by Antarctic thraustochytrid *Oblongichytrium* sp. RT2316-13. Biotechnol Bioeng. (2020) 117:3006-3017. doi: 10.1002/bit.27463
76. Simensen V, Voigt A, Almaas E. High-quality genome-scale metabolic model of *Aurantiochytrium* sp. *T66 Biotechnol Bioeng.* (2021) 118:2105–17. doi: 10.1002/bit.27726
77. Hu L, He A, Liu X, Xia J, Xu J, Zhou S, et al. Biocatalytic transformation of 5-hydroxymethylfurfural into high-value derivatives: recent advances and future aspects. *ACS Sustain Chem Eng.* (2018) 6:15915–35. doi: 10.1021/acssuschemeng.8b04356
78. Chatterjee S. Venkata Mohan S. Fungal biorefinery for sustainable resource recovery from waste. *Bioresour Technol.* (2022) 345:126443. doi: 10.1016/j.biortech.2021.126443
79. Spagnuolo M, Shabbir Hussain M, Gambill L, Blenner M. Alternative substrate metabolism in *Yarrowia lipolytica*. *Front Microbiol.* (2018) 9:1077. doi: 10.3389/fmicb.2018.01077
80. Zhu LY, Zong MH, Wu H. Efficient lipid production with *Trichosporon fermentans* and its use for biodiesel preparation. Bioresour Technol. (2008) 99: 7881-7885. doi: 10.1016/j.biortech.2008.02.033
81. Zhang Y, He Y, Yang W, Tan F, Li W. Wang Q. *Sheng Wu Gong Cheng Xue Bao.* (2022) 38:565–77. doi: 10.13345/j.cjb.210218
82. Ruan Z, Zanotti M, Zhong Y, Liao W, Ducey C, Liu Y. Co-hydrolysis of lignocellulosic biomass for microbial lipid accumulation. *Biotechnol Bioeng.* (2013) 110:1039–49. doi: 10.1002/bit.24773
83. Celińska E, Nicaud JM, Białas W. Hydrolytic secretome engineering in *Yarrowia lipolytica* for consolidated bioprocessing on polysaccharide resources: review on starch, cellulose, xylan, and inulin. *Appl Microbiol Biotechnol.* (2021) 105:975–89. doi: 10.1007/s00253-021-11097-1
84. Zhang Y, Song Y. Lipid Accumulation by Xylose Metabolism Engineered *Mucor circinelloides* Strains on Corn Straw Hydrolysate. *Appl Biochem Biotechnol.* (2021) 193:856–68. doi: 10.1007/s12010-020-03427-2
85. Díaz-Fernández D, Aguiar TQ, Martín VI, Romaní A, Silva R, Domingues L, et al. Microbial lipids from commercial wastes using xylose-utilizing *Ashbya gossypii* strains. *Bioresour Technol.* (2019) 293:122054. doi: 10.1016/j.biortech.2019.122054
86. Qiao W, Tao J, Luo Y, Tang T, Miao J, Yang Q. Microbial oil production from solid-state fermentation by a newly isolated oleaginous fungus, *Mucor circinelloides* Q531 from mulberry branches. *R Soc Open Sci.* (2018) 5:180551. doi: 10.1098/rsos.180551

87. Zininga JT, Puri AK, Govender A, Singh S, Permaul K. Concomitant production of chitosan and lipids from a newly isolated Mucor circinelloides ZSKP for biodiesel production. *Bioresour Technol.* (2019) 272: 545–51. doi: 10.1016/j.biortech.2018.10.035
88. Yu XJ, Liu JH, Sun J, Zheng JY, Zhang YJ, and Wang ZX. Docosahexaenoic acid production from the acidic hydrolysate of Jerusalem artichoke by an efficient sugar-utilizing *Aurantiochytrium* sp. YLH70. Commercial Crops and Products. (2016) 83: 372-378. doi: 10.1016/j.indcrop.2016.01.013
89. Srinivasan N, Thangavelu K, Sekar A, Sanjeev B, Uthandi S. Aspergillus caespitosus ASEF14, an oleaginous fungus as a potential candidate for biodiesel production using sago processing wastewater (SWW). *Microb Cell Fact.* (2021) 20:179. doi: 10.1186/s12934-021-01667-3
90. Di Fidio N, Liuzzi F, Mastrolitti S, Albergo R, De Bari I. Single Cell Oil Production from Undetoxified Arundo donax L. hydrolysate by Cutaneotrichosporon curvatus. *J Microbiol Biotechnol.* (2019) 29:256–67. doi: 10.4014/jmb.1808.08015
91. Kim JY, Lee HW, Lee SM, Jae J, Park YK. Overview of the recent advances in lignocellulose liquefaction for producing biofuels, bio-based materials and chemicals. *Bioresour Technol.* (2019) 279:373–84. doi: 10.1016/j.biortech.2019.01.055
92. Huang C, Chen XF, Xiong L, Chen XD, Ma LL, Chen Y. Single cell oil production from low-cost substrates: the possibility and potential of its commercialization. *Biotechnol Adv.* (2013) 31:129–39. doi: 10.1016/j.biotechadv.2012.08.010
93. Kothri M, Mavrommati M, Elazzazy AM, Baeshen MN, Moussa TAA, Aggelis G. Microbial sources of polyunsaturated fatty acids (PUFAs) and the prospect of organic residues and wastes as growth media for PUFA-producing microorganisms. FEMS Microbiol Lett. (2020) 367:fnaa 028. doi: 10.1093/femsle/fnaa028
94. Xu J, Liu X, He J, Hu L, Dai B, Wu B. Enzymatic in situ saccharification of rice straw in aqueous-ionic liquid media using encapsulated Trichoderma aureoviride cellulase. *J Chem Technol Biotechnol.* (2014) 90:57–63. doi: 10.1002/jctb.4458
95. Zhao CH, Liu X, Zhan T, He J. Production of cellulase by *Trichoderma reesei* from pretreated straw and furfural residues. *RSC Adv.* (2018) 8:36233–8. doi: 10.1039/C8RA05936E
96. Konzock O, Zaghen S, Norbeck J. Tolerance of Yarrowia lipolytica to inhibitors commonly found in lignocellulosic hydrolysates. *BMC Microbiol.* (2021) 21:77. doi: 10.1186/s12866-021-02126-0
97. Chen X, Li Z, Zhang X, Hu F, Ryu DD, Bao J. Screening of oleaginous yeast strains tolerant to lignocellulose degradation compounds. *Appl Biochem Biotechnol.* (2009) 159:591–604. doi: 10.1007/s12010-008-8491-x
98. Intasit R, Cheirsilp B, Louhasakul Y, Boonsawang P. Consolidated bioprocesses for efficient bioconversion of palm biomass wastes into biodiesel feedstocks by oleaginous fungi and yeasts. *Bioresour Technol.* (2020) 315:123893. doi: 10.1016/j.biortech.2020.123893
99. Hughes SR, Qureshi N, López-Núñez JC, Jones MA, Jarodsky JM, Galindo-Leva LÁ, et al. Utilization of inulin-containing waste in commercial fermentations to produce biofuels and bio-based chemicals. *World J Microbiol Biotechnol.* (2017) 33:78. doi: 10.1007/s11274-017-2241-6
100. Zhao CH, Cui W, Liu XY, Chi ZM, Madzak C. Expression of inulinase gene in the oleaginous yeast *Yarrowia lipolytica* and single cell oil production from inulin-containing materials. *Metab Eng.* (2010) 12:510–7. doi: 10.1016/j.ymben.2010.09.001
101. Bao R, Wu X, Liu S, Xie T, Yu C, Lin X. Efficient Conversion of Fructose-Based Biomass into Lipids with *Trichosporon fermentans* Under Phosphate-Limited Conditions. *Appl Biochem Biotechnol.* (2018) 184:113–23. doi: 10.1007/s12010-017-2536-y
102. Wang G, Liu L, Liang W. Single Cell Oil Production from Hydrolysates of Inulin by a Newly Isolated Yeast *Papiliotrema laurentii* AM113 for Biodiesel Making. *Appl Biochem Biotechnol.* (2018) 184:168–81. doi: 10.1007/s12010-017-2538-9
103. Wang GY, Chi Z, Song B, Wang ZP, Chi ZM. High level lipid production by a novel inulinase-producing yeast Pichia guilliermondii Pcla22. *Biores Technol.* (2012) 124:77–82. doi: 10.1016/j.biortech.2012.08.024
104. Cho HU, Park JM. Biodiesel production by various oleaginous microorganisms from organic wastes. *Bioresour Technol.* (2018) 256:502–8. doi: 10.1016/j.biortech.2018.02.010
105. Diwan B, Parkhey P, Gupta P. From agro-commercial wastes to single cell oils: a step towards prospective biorefinery. *Folia Microbiol (Praha).* (2018) 63:547–68. doi: 10.1007/s12223-018-0602-7
106. Wang ZP, Wang PK, Ma Y, Lin JX, Wang CL, Zhao YX, et al. Laminaria japonica hydrolysate promotes fucoxanthin accumulation in *Phaeodactylum tricornutum*. *Bioresour Technol.* (2022) 344:126117. doi: 10.1016/j.biortech.2021.126117
107. Zhang L, Loh KC, Kuroki A, Dai Y, Tong YW. Microbial biodiesel production from commercial organic wastes by oleaginous microorganisms: Current status and prospects. *J Hazard Mater.* (2021) 402:123543. doi: 10.1016/j.jhazmat.2020.123543
108. Tang W, Zhang SF, Wang Q, Tan HD, Zhao ZK. The isocitrate dehydrogenase gene of oleaginous yeast *Lipomyces starkeyi* is linked to lipid accumulation. Can J Microbiol (2009) 55: 1062-1069. doi: 10.1139/W09-063
109. Yang J, Khan MAK, Zhang H, Zhang Y, Certik M, Garre V, et al. Mitochondrial citrate transport system in the fungus mucor circinelloides: identification, phylogenetic analysis, and expression profiling during growth and lipid accumulation. *Curr Microbiol.* (2020) 77:220–31. doi: 10.1007/s00284-019-01822-5
110. Zhao L, Cánovas-Márquez JT, Tang X, Chen H, Chen YQ, Chen W, et al. Role of malate transporter in lipid accumulation of oleaginous fungus *Mucor circinelloides*. *Appl Microbiol Biotechnol.* (2016) 100:1297–305. doi: 10.1007/s00253-015-7079-y
111. Wang X, Mohamed H, Bao Y, Wu C, Shi W, Song Y, et al. Heterologous expression of two malate transporters from an oleaginous fungus *Mucor circinelloides* improved the lipid accumulation in *Mucor lusitanicus*. *Front Microbiol.* (2021) 12:774825. doi: 10.3389/fmicb.2021.774825
112. Arhar S, Gogg-Fassolter G, Ogrizović M, Pačnik K, Schwaiger K, Žganjar M, et al. Engineering of *Saccharomyces cerevisiae* for the accumulation of high amounts of triacylglycerol. *Microb Cell Fact.* (2021) 20:147. doi: 10.1186/s12934-021-01640-0
113. Katja K Dove, Malika F Kadirova, Sara M Nowinski, Yeyun Ouyang, Jon G Van Vranken, Jared Rutter. Exploring the functional role of an ancient mitochondrial fatty acid synthesis pathway. The FASEB Journal (2019) 33: 660.5-660.5.
114. Nosheen S, Yang J, Naz T, Nazir Y, Ahmad MI, Fazili ABA Li S, et al. Annotation of AMP-activated protein kinase genes and its comparative transcriptional analysis between high and low lipid producing strains of *Mucor circinelloides*. *Biotechnol Lett.* (2021) 43:193–202. doi: 10.1007/s10529-020-02990-2
115. Schaub AJ, Moreno GO, Zhao S, Truong HV, Luo R, Tsai SC. Computational structural enzymology methodologies for the study and engineering of fatty acid synthases, polyketide synthases and nonribosomal peptide synthetases. *Methods Enzymol.* (2019) 622:375–409. doi: 10.1016/bs.mie.2019.03.001
116. Chen X, Xu M, Feng C, Hu C. Progress in fungal polyketide biosynthesis. *Sheng Wu Gong Cheng Xue Bao.* (2018) 34:151–64. doi: 10.13345/j.cjb.170219
117. Smith S, Tsai SC. The type I fatty acid and polyketide synthases: a tale of two megasynthases. *Nat Prod Rep.* (2007) 24:1041–72. doi: 10.1039/b603600g
118. Nicholson TP, Rudd BA, Dawson M, Lazarus CM, Simpson TJ, Cox RJ. Design and utility of oligonucleotide gene probes for fungal polyketide synthases. *Chem Biol.* (2001) 8:157–78. doi: 10.1016/S1074-5521(00)90064-4
119. Morabito C, Bournaud C, Maës C, Schuler M, Aiese Cigliano R, Dellero Y, et al. The lipid metabolism in thraustochytrids. *Prog Lipid Res.* (2019) 76:101007. doi: 10.1016/j.plipres.2019.101007
120. Navarro-Muñoz JC, Collemare J. Evolutionary histories of type III polyketide synthases in fungi. *Front Microbiol.* (2020) 10:3018. doi: 10.3389/fmicb.2019.03018
121. Larsen JS, Pearson LA, Neilan BA. Genome Mining and Evolutionary Analysis Reveal Diverse Type III Polyketide Synthase Pathways in *Cyanobacteria*. *Genome Biol Evol.* (2021) 13:*evab*056. doi: 10.1093/gbe/evab056
122. Manoharan G, Sairam T, Thangamani R, Ramakrishnan D. K Tiwari M, Lee JK, Marimuthu J. Identification and characterization

of type III polyketide synthase genes from culturable endophytes of ethnomedicinal plants. *Enzyme Microb Technol.* (2019) 131:109396. doi: 10.1016/j.enzmictec.2019.109396
123. Wang J, Ledesma-Amaro R, Wei Y, Ji B, Ji XJ. Metabolic engineering for increased lipid accumulation in Yarrowia lipolytica—a Review. *Bioresour Technol.* (2020) 313:123707. doi: 10.1016/j.biortech.2020.123707
124. Zoni V, Khaddaj R, Campomanes P, Thiam AR, Schneiter R, Vanni S. Pre-existing bilayer stresses modulate triglyceride accumulation in the ER versus lipid droplets. *Elife*. (2021) 10:e62886. doi: 10.7554/eLife.62886
125. Ledesma-Amaro R, Nicaud JM. *Yarrowia lipolytica* as a biotechnological chassis to produce usual and unusual fatty acids. *Prog Lipid Res.* (2016) 61:40–50. doi: 10.1016/j.plipres.2015.12.001
126. Rogers S, Henne WM. Analysis of Neutral Lipid Synthesis in *Saccharomyces cerevisiae* by Metabolic Labeling and Thin Layer Chromatography. *J Vis Exp*. (2021). doi: 10.3791/62201. [Epub ahead of print].
127. Papanikolaou S, Aggelis G. Modeling lipid accumulation and degradation in Y*arrowia lipolytica* cultivated on commercial fats. Curr Microbiol. (2003) 46 :0398-0402. doi: 10.1007/s00284-002-3907-2
128. Beopoulos A, Mrozova Z, Thevenieau F, Le Dall MT, Hapala I, Papanikolaou S, et al. Control of lipid accumulation in the yeast *Yarrowia lipolytica*. *Appl Environ Microbiol.* (2008) 74:7779–89. doi: 10.1128/AEM.01412-08
129. Silverman AM, Qiao K, Xu P, Stephanopoulos G. Functional overexpression and characterization of lipogenesis-related genes in the oleaginous yeast *Yarrowia lipolytica*. Appl. *Microbiol Biotechnol.* (2016) 100:3781–98. doi: 10.1007/s00253-016-7376-0
130. Tai M, Stephanopoulos G. Engineering the push and pull of lipid biosynthesis in oleaginous yeast *Yarrowia lipolytica* for biofuel production. *Metab Eng.* (2013) 15:1–9. doi: 10.1016/j.ymben.2012.08.007
131. Beopoulos A, Chardot T, Nicaud J-M. *Yarrowia lipolytica*: a model and a tool to understand the mechanisms implicated in lipid accumulation. *Biochimie.* (2009) 91:692–6. doi: 10.1016/j.biochi.2009.02.004
132. Dulermo T, Tréton B, Beopoulos A, Kabran Gnankon AP, Haddouche R, Nicaud JM. Characterization of the two intracellular lipases of Y. lipolytica encoded by TGL3 and TGL4 genes: new insights into the role of intracellular lipases and lipid body organisation. *Biochim Biophys Acta Mol Cell Biol Lipids.* (2013) 1831:1486–95. doi: 10.1016/j.bbalip.2013.07.001
133. Dulermo R, Gamboa-Meléndez H, Ledesma-Amaro R, Thévenieau F, Nicaud JM. Unraveling fatty acid transport and activation mechanisms in *Yarrowia lipolytica*. *Biochim Biophys Acta Mol Cell Biol Lipids.* (2015) 1851:1202–17. doi: 10.1016/j.bbalip.2015.04.004
134. Dulermo R, Gamboa-Meléndez H, Ledesma-Amaro R, Thevenieau F, Nicaud JM. Yarrowia lipolytica AAL genes are involved in peroxisomal fatty acid activation. *Biochim Biophys Acta Mol Cell Biol Lipids.* (2016) 1861:555–65. doi: 10.1016/j.bbalip.2016.04.002
135. Zhu X, Li S, Liu L, Li S, Luo Y, Lv C, et al. Genome Sequencing and Analysis of *Thraustochytriidae* sp. SZU445 provides novel insights into the polyunsaturated fatty acid biosynthesis pathway. *Mar Drugs.* (2020) 18:118. doi: 10.3390/md18020118
136. Abdel-Mawgoud AM, Markham KA, Palmer CM, Liu N, Stephanopoulos G, Alper HS. Metabolic engineering in the host *Yarrowia lipolytica*. *Metab Eng.* (2018) 50:192–208. doi: 10.1016/j.ymben.2018.07.016
137. Nosheen S, Naz T, Yang J, Hussain SA, Fazili ABA, Nazir Y, et al. Role of Snf-β in lipid accumulation in the high lipid-producing fungus *Mucor circinelloides* WJ11. *Microb Cell Fact.* (2021) 20:52. doi: 10.1186/s12934-021-01545-y
138. Tang X, Chen H, Gu Z, Zhang H, Chen YQ, Song Y, et al. Role of *g6pdh* and *leuB* on lipid accumulation in mucor circinelloides. *J Agric Food Chem.* (2020) 68:4245–51. doi: 10.1021/acs.jafc.9b08155
139. Yang W, Dong S, Yang J, Mohamed H, Shah AM, Nazir Y, et al. Molecular Mechanism of Citrate Efflux by the Mitochondrial Citrate Transporter CT in Filamentous Fungus *Mucor circinelloides* WJ11. *Front Microbiol.* (2021) 12:673881. doi: 10.3389/fmicb.2021.673881
140. Yan FX, Dong GR, Qiang S, Niu YJ, Hu CY, Meng YH. Overexpression of Δ12, Δ15-Desaturases for Enhanced Lipids Synthesis in *Yarrowia lipolytica*. Front. Microbiol. (2020) 11: 289. doi: 10.3389/fmicb.2020.00289
141. Blazeck J, Hill A, Liu L, Knight R, Miller J, Pan A, et al. Harnessing *Yarrowia lipolytica* lipogenesis to create a platform for lipid and biofuel production. *Nat Commun.* (2014) 5:3131. doi: 10.1038/ncomms4131
142. Ruenwai R, Cheevadhanarak S, Laoteng K. Overexpression of acetyl-CoA carboxylase gene of Mucor rouxii enhanced fatty acid content in Hansenula polymorpha. *Mol Biotechnol.* (2009) 42:327–32. doi: 10.1007/s12033-009-9155-y
143. Wang S, Chen H, Tang X, Zhang H, Hao G, Chen W, et al. The role of glyceraldehyde-3-phosphate dehydrogenases in NADPH supply in the oleaginous filamentous fungus *Mortierella alpina*. *Front Microbiol.* (2020) 11:818. doi: 10.3389/fmicb.2020.00818
144. Bhutada G, Kavscek M, Ledesma-Amaro R, Thomas S, Rechberger GN, Nicaud JM, et al. Sugar versus fat: elimination of glycogen storage improves lipid accumulation in Yarrowia lipolytica. *FEMS Yeast Res*. (2017) 17:fox020. doi: 10.1093/femsle/fox020
145. Tang X, Sun X, Wang X, Zhang H, Chen YQ, Zhao J, et al. Characterization of NAD+/NADP+-specific isocitrate dehydrogenases from Oleaginous Fungus *Mortierella alpina* involved in lipid accumulation. *Front Nutr.* (2021) 8:746342. doi: 10.3389/fnut.2021.746342
146. Ling X, Zhou H, Yang Q, Yu S, Li J, Li Z, et al. Functions of Enyolreductase (ER) Domains of PKS Cluster in Lipid Synthesis and Enhancement of PUFAs Accumulation in Schizochytrium limacinum SR21 Using Triclosan as a Regulator of ER. *Microorganisms.* (2020) 8:300. doi: 10.3390/microorganisms8020300
147. Han X, Zhao Z, Wen Y, Chen Z. Enhancement of docosahexaenoic acid production by overexpression of ATP-citrate lyase and acetyl-CoA carboxylase in *Schizochytrium* sp. *Biotechnol Biofuels.* (2020) 13:131. doi: 10.1186/s13068-020-01767-z
148. Wang F, Bi Y, Diao J, Lv M, Cui J, Chen L, et al. Metabolic engineering to enhance biosynthesis of both docosahexaenoic acid and odd-chain fatty acids in *Schizochytrium* sp. *S31 Biotechnol Biofuels.* (2019) 12:141. doi: 10.1186/s13068-019-1484-x
149. Yang J, Cánovas-Márquez JT Li P, Li S, Niu J, Wang X, Nazir Y, et al. Deletion of Plasma Membrane Malate Transporters Increased Lipid Accumulation in the Oleaginous Fungus *Mucor circinelloides* WJ11. *J Agric Food Chem.* (2021) 69:9632–41. doi: 10.1021/acs.jafc.1c03307
150. Satoh S, Ozaki M, Matsumoto S, Nabatame T, Kaku M, Shudo T, et al. Enhancement of fatty acid biosynthesis by exogenous acetyl-CoA carboxylase and pantothenate kinase in *Escherichia coli*. *Biotechnol Lett.* (2020) 42:2595–605. doi: 10.1007/s10529-020-02996-w
151. Wang J, Xu R, Wang R, Haque ME, Liu A. Overexpression of ACC gene from oleaginous yeast *Lipomyces starkeyi* enhanced the lipid accumulation in *Saccharomyces cerevisiae* with increased levels of glycerol 3-phosphate substrates. *Biosci Biotechnol Biochem.* (2016) 80:1214–22. doi: 10.1080/09168451.2015.1136883
152. Qiao K, Imam Abidi SH, Liu H, Zhang H, Chakraborty S, Watson N, Kumaran Ajikumar P, Stephanopoulos G. Engineering lipid overproduction in the oleaginous yeast *Yarrowia lipolytica*. Metab. Eng. (2015) 29: 56-65. doi: 10.1016/j.ymben.2015.02.005
153. Hardie DG, Pan DA. Regulation of fatty acid synthesis and oxidation by the AMP-activated protein kinase. *Biochem Soc Trans.* (2002) 30:1064–70. doi: 10.1042/bst0301064
154. Xu Y, Caldo KMP, Pal-Nath D, Ozga J, Lemieux MJ, Weselake RJ, et al. Properties and Biotechnological Applications of Acyl-CoA: diacylglycerol acyltransferase and phospholipid: diacylglycerol acyltransferase from terrestrial plants and microalgae. *Lipids.* (2018) 53:663–88. doi: 10.1002/lipd.12081
155. Friedlander J, Tsakraklides V, Kamineni A, Greenhagen EH, Consiglio AL, MacEwen K, et al. Engineering of a high lipid producing Yarrowia lipolytica strain. *Biotechnol Biofuels.* (2016) 9:77. doi: 10.1186/s13068-016-0492-3
156. Guo ZP, Robin J, Duquesne S, O'Donohue MJ, Marty A, Bordes F. Developing cellulolytic *Yarrowia lipolytica* as a platform for the production of valuable products in consolidated bioprocessing of cellulose. *Biotechnol Biofuels.* (2018) 11:141. doi: 10.1186/s13068-018-1144-6
157. Hao G, Chen H, Gu Z, Zhang H, Chen W, Chen YQ. Metabolic engineering of mortierella alpina for enhanced arachidonic acid production through the NADPH-supplying strategy. *Appl Environ Microbiol.* (2016) 82:3280–8. doi: 10.1128/AEM.00572-16
158. Dulermo R, Dulermo T, Gamboa-Meléndez H, Thevenieau F, Nicaud JM. Role of Pex11p in lipid homeostasis in *Yarrowia lipolytica*. Eukaryot Cell. (2015) 14 :511-525. doi: 10.1128/EC.00051-15

159. Xie D, Jackson EN, Zhu Q. Sustainable source of omega-3 eicosapentaenoic acid from metabolically engineered *Yarrowia lipolytica*: from fundamental research to commercial production. *Appl Microbiol Biotechnol.* (2015) 99:1599–610. doi: 10.1007/s00253-014-6318-y
160. Lazar Z, Liu N, Stephanopoulos G. Holistic approaches in lipid production by *Yarrowia lipolytica*. *Trends Biotechnol.* (2018) 36:1157–70. doi: 10.1016/j.tibtech.2018.06.007
161. Yang RL, Lu N, Zhang H, Zhou SN, Zhang Q, Xue CH, Tang QJ. Improvement of lipid metabolism by DHA liposomes. Modern Food Science and Technology. (2021) 37: 11-20.
162. Lazzarin N, Vaquero E, Exacoustos C, Bertonotti E, Romanini ME, Arduini D. Low-dose aspirin and omega-3 fatty acids improve uterine artery blood flow velocity in women with recurrent miscarriage due to impaired uterine perfusion. Fertil. Steril. (2009) 92, 296-300. doi: 10.1016/j.fertnstert.2008.05.045
163. Swanson D, Block R, Mousa S. Omega-3 fatty acids EPA and DHA: Health benefits throughout life. *Adv Nutr An Int Rev J.* (2012) 3:1–7. doi: 10.3945/an.111.000893
164. Calder PC. Very long-chain n-3 fatty acids and human health: fact, fiction and the future. *Proc Nutr Soc.* (2018) 77:52–72. doi: 10.1017/S0029665117003950
165. Abdelhamid AS, Brown TJ, Brainard JS, Biswas P, Thorpe GC, Moore HJ, Deane KH, AlAbdulghafoor FK, Summerbell CD, Worthington HV, Song F, Hooper L. Omega-3 fatty acids for the primary and secondary prevention of cardiovascular disease. *Cochrane Database Syst Rev*. (2018) 7:*CD*003177. doi: 10.1002/14651858.CD003177.pub4
166. Zhang XM, Zhao L, Hu XW. Progress on Nutritional Value of *Schizochytrium limacinum* and its application in animal production. *J Henan Agricult Sci.* (2021) 50:1–10. doi: 10.15933/j.cnki.1004-3268.2021.03.001
167. Peng Z, Zhang C, Yan L, Zhang Y, Yang Z, Wang J, et al. is More effective than DHA to improve depression-like behavior, glia cell dysfunction and hippcampal apoptosis signaling in a chronic stress-induced rat model of depression. *Int J Mol Sci.* (2020) 21:1769. doi: 10.3390/ijms21051769
168. Leger T, Jouve C, Hininger-Favier I, Rigaudiere JP, Capel F, Sapin V, et al. is Cardioprotective in male rats subjected to sepsis, but ALA is not beneficial. *Antioxidants (Basel).* (2020) 9:371. doi: 10.3390/antiox9050371
169. Riediger ND, Othman RA, Suh M, Moghadasian MH. A systemic review of the roles of n-3 fatty acids in health and disease. *J Am Dietetic Assoc*. (2009) 109: 668–79. doi: 10.1016/j.jada.2008.12.022
170. Byelashov OA, Sinclair AJ, Kaur G. Dietarysources, current intakesand nutritional role of omega-3 docosapentaenoic acid. Lipid Technology. (2015) 27: 79-82. doi: 10.1002/lite.201500013
171. Qin SY. Analysis of patent application of EPA in infant milk powder. *Guangdong Chem*. (2020) 17:261–3.
172. Tounian P, Bellaïche M, Legrand P, ARA. or no ARA in infant formulae, that is the question. *Arch Pediatr.* (2021) 28:69–74. doi: 10.1016/j.arcped.2020.10.001
173. Cao G, Guan Z, Liu FG, Liao X, Cai Y. Arachidonic acid production by *Mortierella alpina* using raw crop materials. *Acta Sci Pol Technol Aliment.* (2015) 14:133–43. doi: 10.17306/J.AFS.15
174. Salem N Jr, Wegher B, Mena P, Uauy R. Arachidonic and docosahexaenoic acids are biosynthesized from their 18-carbon precursors in human infants. *Proc Natl Acad Sci USA.* (1996) 93:49–54. doi: 10.1073/pnas.93.1.49
175. Bieren J. Esser-von. Immune-regulation and functions of eicosanoid lipid mediators. *Biol Chem.* (2017) 398:1177–91. doi: 10.1515/hsz-2017-0146
176. Tallima H, Hadley K, Ridi RE. Praziquantel and arachidonic acid combination. Innovative approach to the treatment of Schistosomiasis. *Intech Opens*. (2015) 145–72. doi: 10.5772/61185
177. Markworth JF, Mitchell CJ, D'Souza RF, Aasen KMM, Durainayagam BR, Mitchell SM, et al. Arachidonic acid supplementation modulates blood and skeletal muscle lipid profile with no effect on basal inflammation in resistance exercise trained men. *Prostaglandins Leukot Essent Fatty Acids*. (2018) l:74–86. doi: 10.1016/j.plefa.2017.12.003
178. Certik M,Adamechova Z,Laoteng K. Microbial production of gamma-linolenic acid: Submerged versus solid-state fermentations. *Food Sci Biotechno*. (2012) 21:921–6. doi: 10.1007/s10068-012-0121-2
179. Mohamed H, El-Shanawany AR, Shah AM, Nazir Y, Naz T, Ullah S, et al. Comparative analysis of different isolated oleaginous mucoromycota fungi for their γ-linolenic acid and carotenoid production. *Biomed Res Int.* (2020) 2020:3621543. doi: 10.1155/2020/3621543
180. Zhang Y, Luan X, Zhang H, Garre V, Song Y, Ratledge C. Improved γ-linolenic acid production in *Mucor circinelloides* by homologous overexpressing of delta-12 and delta-6 desaturases. *Microb Cell Fact.* (2017) 16:113. doi: 10.1186/s12934-017-0723-8
181. Del Gobbo LC, Imamura F, Aslibekyan S, Marklund M, Virtanen JK, Wennberg M, et al. ω-3 polyunsaturated fatty acid biomarkers and coronary heart disease: pooling project of 19 cohort studies. JAMA internal medicine (2016) 176: 1155-1166. doi: 10.1001/jamainternmed.2016.2925
182. Aasen IM, Ertesvåg H, Heggeset TM, Liu B, Brautaset T, Vadstein O, et al. Thraustochytrids as production organisms for docosahexaenoic acid (DHA), squalene, and carotenoids. *Appl Microbiol Biotechnol.* (2016) 100:4309–21. doi: 10.1007/s00253-016-7498-4
183. Tegenge MA, Von Tungeln LS, Mitkus RJ, Anderson SA, Vanlandingham MM, Forshee RA, et al. Pharmacokinetics and biodistribution of squalene-containing emulsion adjuvant following intramuscular injection of H5N1 influenza vaccine in mice. *Regul Toxicol Pharmacol.* (2016) 81:113–9. doi: 10.1016/j.yrtph.2016.08.003
184. Gohil N, Bhattacharjee G, Khambhati K, Braddick D, Singh V. Engineering strategies in microorganisms for the enhanced production of squalene: advances, challenges and opportunities. *Front Bioeng Biotechnol.* (2019) 7:50. doi: 10.3389/fbioe.2019.00050
185. Shakeri S, Amoozyan N, Fekrat F, Maleki M. Antigastric cancer bioactive Aurantiochytrium oil rich in docosahexaenoic acid: from media optimization to cancer cells cytotoxicity assessment. *J Food Sci.* (2017) 82:2706–18. doi: 10.1111/1750-3841.13925
186. Patel A, Liefeldt S, Rova U, Christakopoulos P, Matsakas L. Co-production of DHA and squalene by thraustochytrid from forest biomass. *Sci Rep.* (2020) 10:1992. doi: 10.1038/s41598-020-58728-7

Conflict of Interest: PW was employed by company Linyang Group.

The remaining authors declare that the research was conducted in the absence of any commercial or financial relationships that could be construed as a potential conflict of interest.

Publisher's Note: All claims expressed in this article are solely those of the authors and do not necessarily represent those of their affiliated organizations, or those of the publisher, the editors and the reviewers. Any product that may be evaluated in this article, or claim that may be made by its manufacturer, is not guaranteed or endorsed by the publisher.

Advantages of publishing in Frontiers

OPEN ACCESS
Articles are free to read for greatest visibility and readership

FAST PUBLICATION
Around 90 days from submission to decision

HIGH QUALITY PEER-REVIEW
Rigorous, collaborative, and constructive peer-review

TRANSPARENT PEER-REVIEW
Editors and reviewers acknowledged by name on published articles

Frontiers
Avenue du Tribunal-Fédéral 34
1005 Lausanne | Switzerland

Visit us: www.frontiersin.org
Contact us: frontiersin.org/about/contact

REPRODUCIBILITY OF RESEARCH
Support open data and methods to enhance research reproducibility

DIGITAL PUBLISHING
Articles designed for optimal readership across devices

FOLLOW US
@frontiersin

IMPACT METRICS
Advanced article metrics track visibility across digital media

EXTENSIVE PROMOTION
Marketing and promotion of impactful research

LOOP RESEARCH NETWORK
Our network increases your article's readership